Doctoral Thesis

Response of marine microbial communities to natural fertilization events

Clàudia Pérez Barrancos

Surface microbial communities are essential to the functioning of marine ecosystems. Phytoplankton and bacteria drive key ecological and biogeochemical processes in the upper ocean, including carbon fixation, nutrient cycling and organic matter transformation. These processes are strongly modulated by nutrient availability, which varies across oceanic regions and over different time scales. In the subtropical Northeast Atlantic, natural fertilization events–such as Saharan dust deposition and shallow submarine hydrothermal emissions–release pulses of nutrients and trace elements to surface waters. Although these inputs influence surface chemistry and productivity, their effects on microbial ecology remain underexplored. This thesis combines experimental bioassays with long-term field observations to study how such geochemical perturbations influence phytoplankton and bacterial communities, focusing on changes in cell abundance, metabolic activity and community structure.

Response of marine microbial communities to natural fertilization events

ULPGC

ULPGC
Universidad de Las Palmas de Gran Canaria

Doctorado en Oceanografía y Cambio Global
Santa Cruz de Tenerife
Septiembre 2025

Dª Juana Magdalena Santana Casiano coordinadora del programa de doctorado en Oceanografía y Cambio Global de la Universidad de Las Palmas de Gran Canaria

INFORMA,

De que la Comisión Académica del Programa de Doctorado, en su sesión de fecha tomó el acuerdo de dar el consentimiento para su tramitación, a la tesis doctoral titulada *"Response of marine microbial communities to natural fertilization events"* presentada por la doctoranda **Clàudia Pérez Barrancos**, dirigida por el **Doctor Jesús M. Arrieta López de Uralde** y codirigida por el **Doctor Eugenio Fraile Nuez**.

Y para que así conste, y a efectos de lo previsto en el Artº 11 del Reglamento de Estudios de Doctorado (BOULPGC, 04/03/2019) de la Universidad de Las Palmas de Gran Canaria, firmo la presente en Las Palmas de Gran Canaria,

Response of marine microbial communities to natural fertilization events

Respuesta de las Comunidades Microbianas Marinas a Eventos de Fertilización Natural

Tesis doctoral realizada por Clàudia Pérez Barrancos dentro del Programa de Doctorado en Oceanografía y Cambio Global de la Universidad de Las Palmas de Gran Canaria con la financiación del Ministerio de Universidades (PRE2018-083800)

Dirigida por el Dr. Jesús M. Arrieta López de Uralde
y codirigida por el Dr. Eugenio Fraile Nuez

Santa Cruz de Tenerife

Septiembre de 2025

This thesis has been carried out at the Oceanographic Center of the Canary Islands of the Spanish Institute of Oceanography and the Spanish National Research Council (IEO-CSIC). It is a contribution to the research projects FLUXES (CTM2015-69392-C3), POSEIDON (CTM2017-84735-R), VULCANA-II-III-IV (IEO-CSIC-2015-2026), FAMOUS (PID2021-125368NB-I00) and PROTECCION (2022CLISA30). During her PhD, Clàudia Pérez Barrancos has been supported by an FPI PhD fellowship funded by the Spanish Ministry of Universities (PRE2018-083800). The author has actively participated in multiple oceanographic cruises and experiments linked to the research projects, has completed a research stay at the Oceanographic Center of A Coruña (Spain) and has participated in seven scientific meetings.

Als meus pares,
pel seu suport incondicional.

Acknowledgements

Esta tesis ha sido una apuesta constante por desarrollar una línea de investigación novedosa y útil. Es un trabajo del que me siento profundamente orgullosa porque refleja el esfuerzo, la perseverancia, la resiliencia, la curiosidad y la capacidad de adaptación de quienes hemos formado parte de este camino. Ha sido un trayecto lleno de aprendizajes personales, académicos y profesionales, pero, sobre todo, lleno de personas que me acompañarán para siempre. A todos y cada uno de vosotros, gracias.

A Txetxu, gracias por la libertad y la confianza, por fomentar mi curiosidad hasta niveles estratosféricos y por compartir conmigo tus conocimientos e inquietudes. Gracias por descubrirme el mundo de la microbiología, por tantas horas compartidas de muestreo, laboratorio y análisis de datos, pero también por las charlas que me enseñaron mucho más que ciencia. A Eugenio, gracias por tu apoyo, por empujarme al fascinante mundo de la vulcanología submarina y por mantener la puerta siempre abierta. A los dos, gracias por acompañarme en este camino, por darme espacio para aprender y crecer. Habéis sido un ejemplo de dedicación y compromiso por la ciencia, demostrándome que, aunque haya momentos donde todo parezca ponerse en nuestra contra (como cuando no había recursos ni para papel de laboratorio), el trabajo y la constancia siempre dan sus frutos.

A los/as compañeros/as del Centro Oceanográfico de Canarias. Gracias por vuestra generosidad, vuestros conocimientos y, en mayor importancia, vuestro tiempo. Me siento muy afortunada por haber tenido la oportunidad de coincidir con muchísimas personas de ámbitos muy diferentes a lo largo de mi paso por este centro de investigación, a todos gracias por haber formado parte de este camino. En especial, a Alba, Alberto, Ángela, Carmen, Juan Pablo, Marisa, Pedro, Pepe, José Antonio, Marijn y Zoraida. A los mejores regalos que me brindó este centro, Naiara y Deiene, que allanaron las malditas cuestas con su compañía y las convirtieron en oportunidades para crecer y disfrutar. No sé qué hubiera hecho sin vosotras. A los/as muchos/as compañeros/as de laboratorio, pasillo, comedor, café y tardeos, por las palabras de apoyo a lo largo de estos años. También una mención especial al Grupo de Divulgación, a Marisa, Marta, Vanessa y Alberto, por su altruismo y amor a la ciencia, por infundir en mí confianza y creatividad.

A los/as compañeros/as del Centro Oceanográfico de A Coruña. Un soplo de aire fresco que me recordó el por qué empecé con esto e hizo que valorara y echara de menos aguas más calientes. En especial, a Mar Nieto, gracias por abrirme las puertas de tu laboratorio con los brazos bien abiertos, compartir conmigo tus conocimientos y darme la oportunidad de crecer no solo como profesional sino también como persona. También gracias a Marta Álvarez por su generosidad y sus enseñanzas, y por permitirme compartir espacio y tiempo con el gran equipo que la rodea. Alba, Lucía, Lisandro, Nacho y Rubén, hicisteis de mi estancia un mar de risas. Graciñas a todos/as. También a mí familia gallega, quienes me acompañaron en esta aventura.

A los/as compañeros/as del Grupo de Oceanografía Biológica (GOB) y del Grupo de Tecnologías, Gestión y Biogeoquímica Ambiental (TGBA), ambos de la Universidad de Las Palmas de Gran Canaria (ULPGC), con los que compartí muchos momentos y en el que su trabajo y su apoyo se ve reflejado en el primer capítulo de esta tesis doctoral. De todos ellos aprendí una infinidad y asentaron las bases de mis siguientes etapas formativas. En especial, gracias a Javier Arístegui, por sus consejos y sus enseñanzas.

De hecho, fue en la ULPGC y en su *resi* donde encontré un hogar lejos de casa lleno de personas únicas que, tras 10 años en tierras canarias, siguen acompañándome de una forma u otra. En especial, gracias a Felipe y a Eugenio, por seguir compartiendo nuestros mares como el primer día. Me inspiráis con vuestros ideales y vuestra lucha en defensa del lugar que nos unió y tanto amamos: las aguas y tierras canarias. A Abi y a Tania, por ser los mejores y más generosos compañeros, por los dulces, los chismes y los eco-valores que nos unen. A Maria, por enseñarme que, incluso cuando todo se complica, hay que *seguir nadando*. Te sigo encontrando en nuestra barra de Las Canteras y allí donde *los peces son amigos*. A Markel, eskerrik asko, por ser un ejemplo de dedicación y humildad.

A Agustín, a los *guiris* (Arash–y Baloo–, Chus, Dominique, Edu, Javi, Marijn, María y Nai), a mis pilateras y yoguis de Omtrivi, quienes, con su amistad, buen rollo y muchos *oooooommmmm,* hacen más ligero el día a día.

A la Judit, l'*Hér*, per ensenyar-me que la valentia és una qüestió de decisió i per ser, en tot moment, aquella germana amb qui sempre hi puc comptar. Als Mugrons divers (Cris, Òscar, Quim, Miquel, Mireia, Ona i Lluc), a sa meua família menorquina (Fay, Juana & co.), a la família barcelonina (Marta i Jordi). Gràcies a tots/es per ser nius on compartir caliu, collir forces i agafar impuls

abans de tornar a volar. Soc molt afortunada que els meus pares us posessin a la meva vida.

Als meus pares, l'Albert i la Cèlia, per la llibertat i alhora la protecció. Heu estat presents en tot el camí i aquesta dedicació que heu tingut amb mi m'acompanyarà sempre. Estic molt orgullosa de vosaltres i us estimo amb tot el meu cor. Al meu pare, gràcies per la teva protecció, saviesa i bondat, i per encomanar-me del teu amor i admiració per la mar. A la meva mare, per la teva fortalesa i generositat, per compartir la teva destresa i saber fer, per ser la meva millor consellera. Al meu avi Antonio, per la teva ànima protectora, per les arrels mediterrànies, per ser-hi sempre i per sempre. A les meves àvies, que són unes lluitadores, per transmetre'm la vostra noblesa i recordar-me que, encara que els camins siguin pedregosos, col·leccionem records que valen or. A la meva família, que encara no sap ben bé a què em dedico, però que sempre em dedica paraules de comprensió i alè.

A Alberto, gracias por tu cariño, paciencia y generosidad. Gracias por cuidarme durante todo este periodo y por acompañarme en los altos y en los bajos. Por infundirme confianza, ayudarme a ser más amable conmigo misma y empujarme a mirar siempre un poco más allá. Podría nombrar tantas cosas… pero me quedo con lo esencial: gracias por ser el recordatorio diario de que lo mejor y más importante en mi vida está lejos de una pantalla o un laboratorio. Sin duda, esta tesis no hubiera sido posible sin ti. Gracias también por descubrirme las comidas reconfortantes de tu padre y los abrazos de tu madre. Sois casa.

A la *Mar*, per ser el refugi on em retrobo constantment i em sento plena, i on em trobo amb els meus. Per haver posat a la meva vida totes i cadascuna de les persones que he anomenat, perquè, d'una manera o altra, amb totes elles comparteixo un bonic vincle vora el mar.

I ara, com diu en Juanico:

"Peuades damunt s'arena.

Si vens em trobaràs

ballant de puntes damunt d'aquesta roca".

Contents

Summary

Surface microbial communities are essential to the functioning of marine ecosystems. Phytoplankton and bacteria drive key ecological and biogeochemical processes in the upper ocean, including carbon fixation, nutrient cycling and organic matter transformation. These processes are strongly modulated by nutrient availability, which varies across oceanic regions and over different time scales. In the subtropical Northeast Atlantic, natural fertilization events–such as Saharan dust deposition and shallow submarine hydrothermal emissions–release pulses of nutrients and trace elements to surface waters. Although these inputs influence surface chemistry and productivity, their effects on microbial ecology remain underexplored. This thesis combines experimental bioassays with long-term field observations to study how such geochemical perturbations influence phytoplankton and bacterial communities, focusing on changes in cell abundance, metabolic activity and community structure. Microbial responses were assessed under diverse environmental conditions, including surface productivity gradients and seasonal variability, to understand how these responses are also shaped by broader oceanographic processes and climate variability at local and regional scales. The effects of Saharan dust deposition on surface microbial communities were examined in the Mauritanian-Senegalese coastal transition zone, an area subject to frequent dust intrusions and strong surface productivity gradients. Dust-enrichment experiments revealed increased microbial metabolic activity, particularly bacterial production relative to primary production, especially under low-nutrient, oligotrophic conditions. Dust additions increased the concentrations of bioavailable nutrients in seawater, such as nitrate, phosphate and, to a lesser extent, silicate, which selectively favored the growth of specific microbial groups based on their distinct metabolic requirements and ecological traits. Future increases in atmospheric dust deposition, combined with a projected weakening in the intensity of the Mauritanian-Senegalese upwelling, could thus favor heterotrophic processes and potentially reduce the efficiency of this region for carbon sequestration. Meanwhile, the influence of shallow-sea hydrothermal activity on microbial communities was examined at the Tagoro submarine volcano (Canary Islands, Spain), where persistent diffuse emissions of nutrient-rich, low-temperature and low-pH fluids often reach sunlit surface waters. Using over a decade of hydrographic data, we assessed the spatial extent and temporal evolution of these hydrothermal inputs, characterized by silicate and phosphate among

other compounds, and their effects on microbial dynamics. Experimental simulations of natural dilutions of hydrothermal fluids showed that these nutrient-rich inputs promoted primary production, particularly favoring small eukaryotic phytoplankton, as well as photo- and chemoautotrophic bacteria. Seasonal variations influenced the magnitude of microbial responses, highlighting the importance of background environmental variability when assessing microbial responses to natural geochemical perturbations. Furthermore, field observations revealed distinct microbial community structures across hydrothermally influenced epipelagic and benthic habitats, dominated by specialized microbial taxa associated with nitrogen, iron, sulfur and methane cycling. These findings reveal broader biogeochemical processes than previously recognized in the area, along with notable novel microbial diversity with potential biotechnological applications, underscoring the need for further research into these often overlooked, geochemically dynamic shallow hydrothermal systems. Altogether, this thesis demonstrates that distinct natural geochemical fertilization events can significantly alter surface marine microbial communities, with implications for nutrient cycling, carbon export, productivity and biodiversity in the subtropical Northeast Atlantic, particularly under future climate scenarios of increasing environmental variability.

CHAPTER 1
INTRODUCTION

1.1 Microbial roles in surface ocean productivity

Microorganisms are ubiquitous in the ocean and represent one of the most abundant and diverse components of marine life (Sunagawa et al., 2015; Bar-On and Milo, 2019). These microscopic assemblages include a wide range of organisms, such as bacteria, archaea, protists, fungi and viruses, collectively accounting for approximately 68% of total marine biomass (Bar-On et al., 2018; Bar-On and Milo, 2019). The majority of this biomass is planktonic, transported by ocean currents, and contributes substantially to key biogeochemical processes, including carbon fixation, organic matter degradation and nutrient cycling. Together, these processes promote the export and long-term sequestration of carbon in deep ocean waters and sediments through the biological pump (**Figure 1**), ultimately influencing Earth's climate.

In the sunlit upper layer of the ocean, known as the epipelagic zone (0–200 m), phytoplankton act as the main primary producers, shaping the structure and productivity of marine ecosystems. This diverse group of unicellular, photosynthetic organisms includes both eukaryotic algae (such as dinoflagellates and diatoms) and photoautotrophic prokaryotes like *Synechococcus* and *Prochlorococcus* cyanobacteria. Despite accounting for less than 1% of the total autotrophic biomass on Earth (Field et al., 1998; Bar-On et al., 2018), phytoplankton are responsible for nearly half of the global net primary production, estimated at ~50 Gt C $year^{-1}$ (Falkowski et al., 1998; Field et al., 1998). Their ecological success is largely attributed to their small cell size (~0.2–200 μm) and high surface-to-volume ratio, which facilitate nutrient uptake,

particularly in oligotrophic environments where nutrient availability is limited (Litchman et al., 2010; Marañón, 2015; Hillebrand et al., 2022).

Through the release of organic compounds and predation by zooplankton grazers, phytoplankton not only sustain higher trophic levels but also fuel the activity of heterotrophic bacteria and archaea (Azam et al., 1983; Ducklow et al., 2001; Pomeroy et al., 2015) (**Figure 1**). As primary producers, phytoplankton drive the marine carbon cycle by converting CO_2 into biomass through photosynthesis. However, most of this fixed carbon is rapidly utilized and recycled by microbial consumers. Heterotrophic microbes play a crucial role in the degradation and remineralization of the organic matter pool, breaking it down into its inorganic constituents like carbon, nitrogen and phosphorous. By utilizing particulate and dissolved organic matter (POM and DOM, respectively) as sources of energy and carbon (Azam and Malfatti, 2007; Buchan et al., 2014), these microbes recycle essential nutrients that support autotrophic growth in surface waters (Levitus et al., 1993) and maintain productivity in regions with limited new nutrient inputs. Additionally, a portion of organic matter is converted into microbial biomass, which is then returned into marine food webs through grazing processes (Azam et al., 1983; Kirchman, 1994). This trophic pathway, known as the microbial loop (Pomeroy et al., 2015), plays a critical role in epipelagic seawaters, especially in oligotrophic environments, by retaining energy and nutrients within the surface ocean and supporting the overall ecosystem function.

Marine microbial diversity encompasses multiple domains of life and comprises thousands of taxonomic groups with distinct metabolic strategies, ecological roles and environmental niches. Despite significant advancements in sequencing techniques and global sampling efforts, a large proportion of marine microbial diversity remains uncultured or undescribed (Giovannoni and Stingl, 2005). This hidden diversity holds a vast ecological and biotechnological potential, with novel enzymes and biochemical compounds (Paoli et al., 2022). Conservative estimates suggest that only about 1% of marine prokaryotic taxa have been formally identified, assuming a total diversity of $\sim 2 \times 10^6$ species (Curtis et al., 2002). However, more recent estimates indicate that prokaryotic diversity in the oceans may reach $\sim 10^{10}$ species (Lennon and Locey, 2020), meaning that the number of described marine prokaryotic taxa represents just 0.0002% of the total. Nevertheless, both estimates underscore the extent to which microbial life has been underestimated or overlooked in global biodiversity assessments, especially in extreme environments (Shu and Huang,

2022). Broader taxonomic studies further suggest that between one-third and two-thirds of all marine species remain undescribed (Appeltans et al., 2012). Understanding microbial diversity and function is therefore essential for assessing microbial responses and ecosystem resilience under ongoing climate change and anthropogenic pressures (Doney et al., 2012).

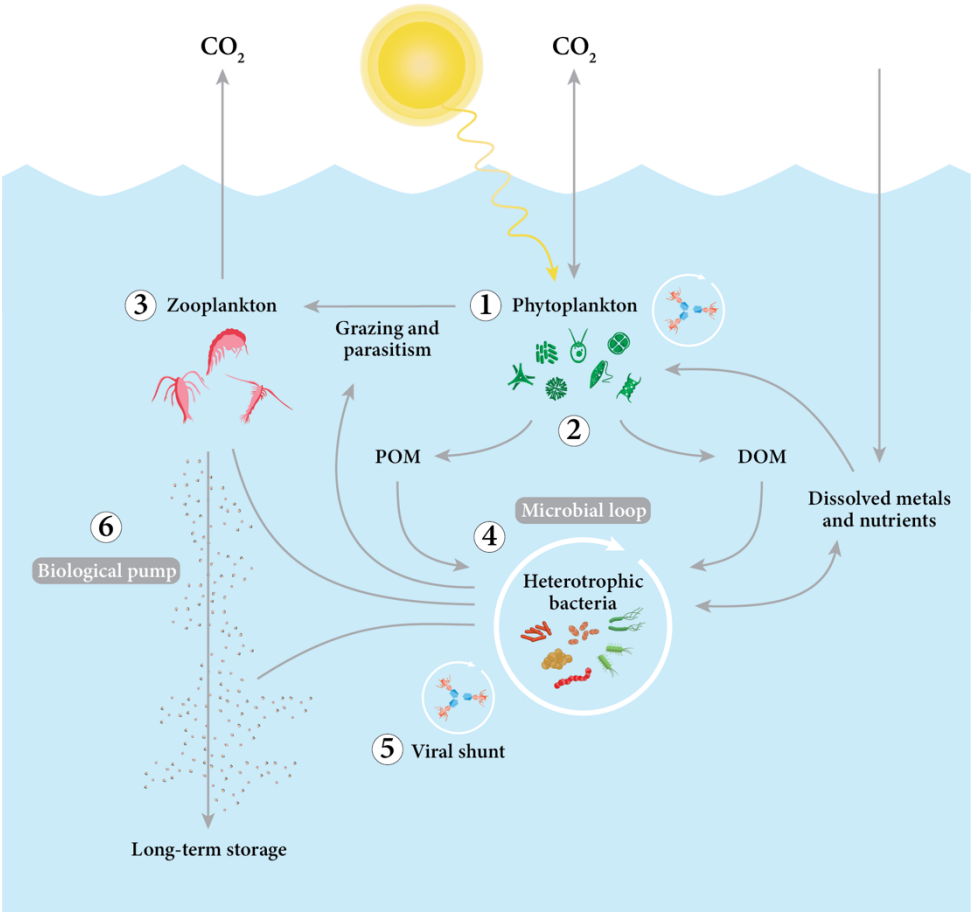

Figure 1. Microbial processes driving the marine carbon cycle. Photosynthetic phytoplankton convert inorganic carbon (such as CO_2) into organic matter (**step 1**), which is subsequently released as particulate and dissolved organic matter (POM and DOM, respectively) (**step 2**). A portion of this organic matter is incorporated into microbial biomass and transferred through marine food webs via zooplankton grazing on phytoplankton and other planktonic organisms (**step 3**). Heterotrophic bacteria consume organic material and remineralize nutrients into inorganic forms (a process known as the microbial loop), which then become available to phytoplankton (**step 4**). Viral-mediated cell lysis releases organic matter from both phytoplankton and bacterial pools (**step 5**). Finally, the biological pump (**step 6**) refers to the export of microbial-derived organic matter from surface waters to the deep ocean, resulting in long-term carbon sequestration. Modified from Buchan et al. (2014).

1.2 Nutrient availability limits microbial growth

Microbial growth and productivity in the surface ocean are shaped by a complex interplay of physical, chemical and biological factors, including light availability, seasonal stratification, nutrient pulses, competition and trophic interactions (Moreno and Martiny, 2018). Among these many drivers, nutrient availability plays a central role, as most oceanic surface waters are depleted in inorganic nitrogen, phosphorus, iron and/or silicon (Bristow et al., 2017).

Marine microorganisms require a broad range of chemical elements to sustain cellular growth and function (Arrigo, 2005; Moore et al., 2013; Bristow et al., 2017). Macronutrients, such as nitrogen (N), phosphorous (P) and silicon (Si), are needed in relatively high concentrations, as they are structural components of proteins, nucleic acids and membrane structures, for example, silicon is essential for diatoms, silica frustules. Micronutrients like iron (Fe), cobalt (Co) and zinc (Zn), among others, are often required in smaller concentrations but are essential for enzymatic activity, electron transport and photosynthesis. For instance, iron is a key cofactor in the formation of proteins involved in nitrogen fixation, respiration and electron transfer.

The availability of these nutrients varies across spatial and temporal scales, leading to contrasting surface productivity across oceanic regions (**Figure 2**). A key determinant of this variability is the balance between nutrient supply and biological demand, which is captured by the stoichiometric requirements of microbial communities (Moore et al., 2013). Plankton elemental stoichiometric ratios can vary considerably among taxa and environments from the Redfield ratio (106C:16N:1P) (Redfield, 1934; Martiny et al., 2014; Moreno and Martiny, 2018), resulting in diverse patterns of nutrient limitation. According to Liebig's Law of the Minimum, growth is determined by the nutrient in least supply relative to demand. However, recent studies emphasize the importance of co-limitation, in which multiple nutrients limit microbial growth (Browning and Moore, 2023). For instance, the availability of nitrogen tends to limit productivity throughout much of the surface low-latitude ocean and stratified subtropical gyres, while iron is more often limiting in the main oceanic upwelling systems (**Figure 2**). Phosphorous and silicon, as well as vitamins and micronutrients other than iron, may also co-limit microbial growth under specific ecological conditions. Additionally, Moreno and Martiny (2018) observed that physiological traits strongly influence plankton

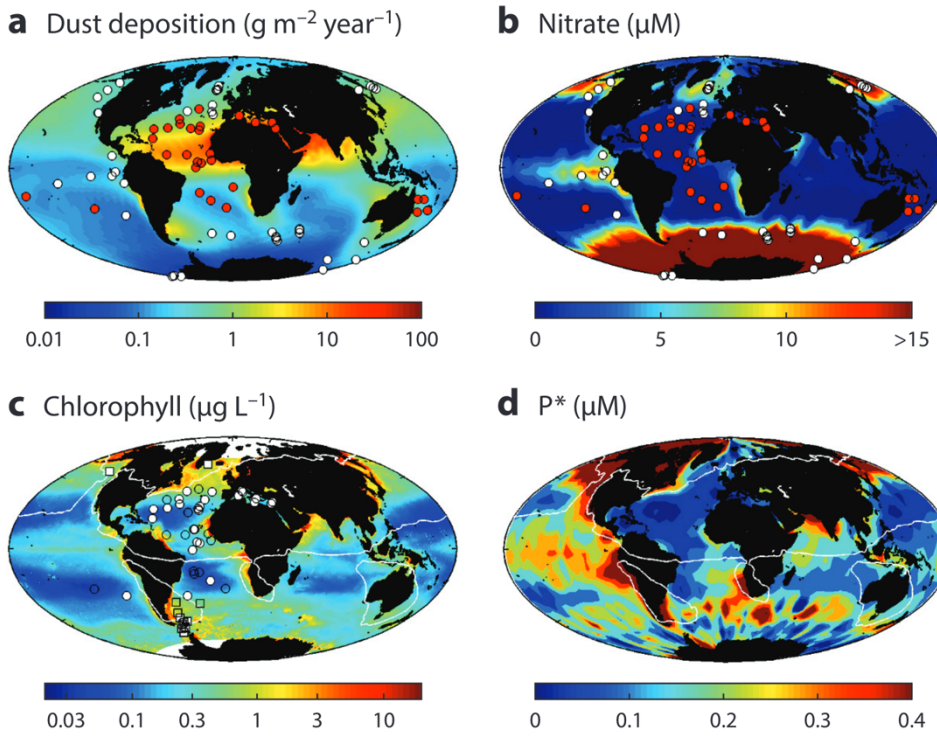

Figure 2. Relationships between dust deposition, surface water nutrient concentrations and nutrient limitation. **(a)** Dust deposition, **(b)** nitrate concentration, **(c)** chlorophyll concentration and **(d)** P* are shown. P* indicates an excess of phosphorus relative to nitrogen (as quantified through P*=P–N/16, the relative proportion compared with the Redfield ratio; P, phosphorous; N, nitrogen). Regions where iron (white dots) and nitrogen (red dots) are limiting for primary production are indicated in panels **a** and **b** (Moore et al., 2013). In panel **c**, the dots represent locations of dust (circles) or ash (squares) addition experiments, and white shapes indicate a significant response by phytoplankton (Achterberg et al., 2013; Moore et al., 2013; Browning et al., 2014; Mélançon et al., 2014). Contours in panels **c** and **d** are 0.5 mg m^{-2} $year^{-1}$ dust deposition. Taken from Jickells and Moore (2015).

community stoichiometry in nutrient-rich conditions, while in oligotrophic gyres, broader biogeochemical interactions play a more dominant role.

Surface primary production relies substantially on the introduction of nutrients through vertical mixing of nutrient-rich deep waters and through remineralization of organic matter by microbial decomposers. However, external nutrient inputs are essential for sustaining long-term primary production and carbon sequestration in the deep ocean (Bristow et al., 2017). The external supply of nutrients like phosphorus, iron, and silicon is often limited to atmospheric deposition and/or coastal and riverine inputs. Meanwhile, nitrogen can also be supplied biologically through microbial

fixation of atmospheric nitrogen. These alternative inputs, though less thoroughly described, play a significant role in modulating surface productivity, especially in dynamic oceanic regions like the Northeast Atlantic Ocean where external inputs like atmospheric deposition are prominent (Jickells et al., 2016). In this region, emergent areas of study are also emphasizing submarine volcanic and hydrothermal emissions as nutrient-rich inputs capable of influencing microbial productivity in surface waters (e.g., Santana-Casiano et al., 2013; González-Vega et al., 2020). Together, these nutrient pathways, spanning atmospheric, terrestrial, oceanic and biological reservoirs, drive biological production and shapes biogeochemical dynamics in the surface ocean (Arrigo, 2005). Yet, understanding the relationship between microbial processes and nutrient cycling remains a key challenge in ocean biogeochemistry.

1.3 Prospective nutrient sources in the subtropical Northeast Atlantic Ocean

1.3.1 Atmospheric dust deposition

The subtropical Northeast Atlantic Ocean is among the highest receivers of atmospheric dust inputs in the world (**Figure 2**). Due to its proximity to vast North African arid regions, the Atlantic Ocean receives approximately 43% of the estimated 450 Tg $year^{-1}$ of global atmospheric dust deposited in surface oceans (Jickells, 2005). Transported westward by the Saharan Air Layer, mainly from the Sahara and Sahel (Prospero and Lamb, 2003; Jickells, 2005), these mineral aerosols constitute a major source of phosphate, iron, and other trace elements to surface waters (Guieu et al., 2002; Jickells et al., 2016). As discussed in **Section 1.2**, these nutrients can impact the overall marine productivity by influencing microbial growth and nitrogen fixation rates (Jickells and Moore, 2015), especially in oligotrophic waters where nutrient supply is otherwise limited (Mills et al., 2008; Moore et al., 2008) (**Figure 2**).

While the significance of dust inputs in this region has long been recognized, recent studies highlight unprecedented increases in both the frequency and intensity of Saharan dust deposition events. Between 2020 and 2022, massive dust plumes were transported from northwest Africa to the Atlantic and Europe, with particulate matter concentrations in some cases exceeding 6000 $\mu m\ m^{-3}$ (Rodríguez and López-Darias, 2024). Addressing dust deposition trends in this region is crucial, as climate projections suggest a northwestward

expansion of North African drylands and an associated increase in dust aerosol loading (Liu et al., 2024).

These intense dust events are particularly relevant for marine systems, as they may trigger short-term increases in surface productivity and enhanced vertical particle export (Neuer et al., 2004). However, interpreting microbial and biogeochemical responses in this region remains challenging due to high lateral transport and mesoscale variability, which are common in eastern boundary upwelling ecosystems (Chavez and Messié, 2009; Nowald et al., 2015).

1.3.2 Volcanic and hydrothermal activity

In addition to atmospheric inputs, volcanic and hydrothermal activity represents another important source of nutrients in this region. Approximately 85% of global volcanic activity takes place beneath the ocean surface (Crisp, 1984), with ~75% associated with mid-ocean ridge systems (**Figure 3**). While deep-sea hydrothermalism has historically received more attention, shallow submarine volcanism and intra-plate hydrothermal systems have recently emerged as key areas of scientific interest (e.g., Buck et al., 2018; Esposito et al., 2018; Bellec et al., 2020; Rizzo et al., 2022; Barosa et al., 2023). Unlike deep-sea hydrothermal systems, typically located at depths of 1–4 km, shallow-sea hydrothermal systems occur above ~200 m, allowing direct interaction with sunlight, surface waters and microbial communities (Price and Giovannelli, 2017). These environments combine chemical energy from reduced compounds with light availability, supporting diverse microbial metabolisms, including both phototrophic and chemotrophic pathways (Tarasov et al., 2005; Price and Giovannelli, 2017). The emission of bioavailable macro- and micronutrients–such as ammonium, silicate and iron–from shallow hydrothermal systems likely stimulates microbial growth and influences community composition (e.g., Ardyna et al., 2019; Bonnet et al., 2023; Tilliette et al., 2023).

The subtropical Northeast Atlantic hosts several volcanic island chains, including the Canary Islands and Cape Verde, as well as potentially thousands of unrecognized seamounts (Gevorgian et al., 2023), suggesting widespread potential for underwater hydrothermal activity. A notable example is the 2011–2012 submarine eruption off El Hierro island, which led to the formation of the Tagoro submarine volcano and its associated shallow hydrothermal system at depths between 88 and 127 m. This site offers a unique natural laboratory

for investigating shallow-sea hydrothermal processes and their influence on microbial communities, which likely harbor a vast diversity of microbes with significant ecological and biotechnological potential (e.g., García-Davis et al., 2021; Rizzo et al., 2022).

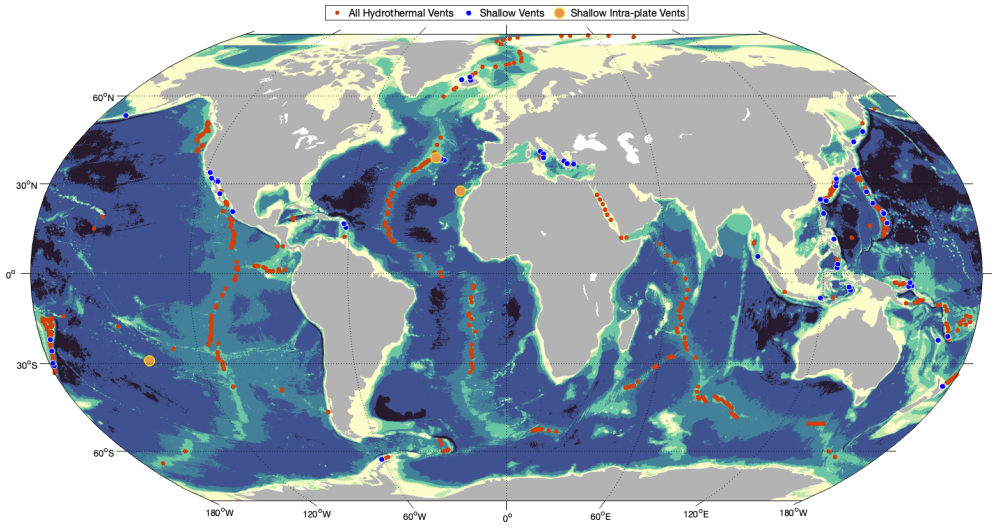

Figure 3. Global distribution of hydrothermal vents included in the InterRidge Hydrothermal Vents Dataset v3.4 (http://vents-data.interridge.org). Shallow vents located at ≤200 m depth (blue dots) and shallow intra-plate vents (orange dots) are highlighted among all identified vents (red dots).

1.4 Aim of the thesis

This thesis aims to investigate the responses of surface marine microbial communities, specifically phytoplankton and bacteria, to natural geochemical fertilization events in the subtropical Northeast Atlantic Ocean. In particular, it focuses on the effects of nutrient inputs derived from Saharan dust deposition and shallow submarine hydrothermal activity on microbial ecology (**Figure 4**). This research is guided by the following hypotheses:

- Natural fertilization events, including Saharan dust deposition and shallow submarine hydrothermal activity, provide essential nutrients and trace elements to surface waters that can significantly enhance microbial productivity in marine ecosystems.
- These nutrient inputs promote distinct responses among microbial taxa, leading to changes in cell abundance, metabolic activity and community structure.

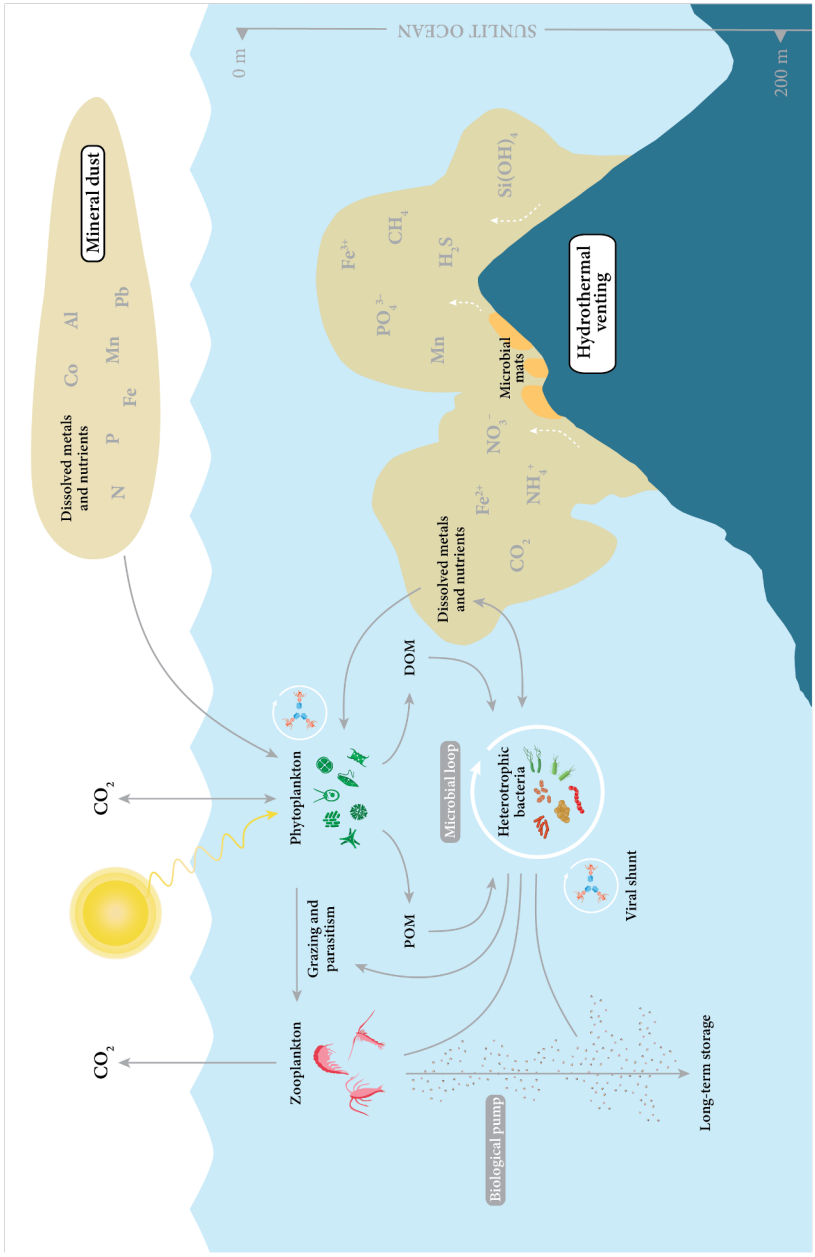

Figure 4. Diagram illustrating the main hypotheses of this thesis: that natural fertilization events, including Saharan dust deposition and shallow submarine hydrothermal activity, provide essential nutrients and trace elements to surface waters that can significantly enhance microbial productivity in marine ecosystems; and that these nutrient inputs promote distinct responses among microbial taxa, leading to changes in cell abundance, metabolic activity and community structure.

To assess the ecological impact of these often-overlooked natural fertilization processes under varying oceanographic conditions and within the broader context of climate change, the research was designed to encompass a range of scenarios reflecting the natural variability of the marine environment. These include differences in surface productivity, seasonal patterns, and variations in the magnitude and frequency of atmospheric deposition events and hydrothermal emissions.

Within the overarching framework provided by the two main hypotheses, this thesis aims to address the following research questions:

i. How do nutrient inputs from dust deposition and hydrothermal activity influence surface marine microbial communities in terms of cell abundance and metabolic activity?

ii. To what extent do trophic gradients or seasonal variability modulate microbial production?

iii. Do these nutrient inputs differentially affect autotrophic and heterotrophic components of the microbial food web?

iv. Do these inputs stimulate specific microbial taxa with key ecological and biogeochemical traits, potentially reshaping microbial diversity across habitats?

v. Can the observed microbial responses impact local or regional biogeochemical cycles and surface productivity?

These questions were explored through a combination of experimental bioassays and field observations, presented across three core research chapters.

Chapter 2 addresses the first four research questions by examining the effects of Saharan dust deposition on surface microbial communities in the Mauritanian-Senegalese coastal transition zone. Dust-enrichment experiments were conducted along a surface productivity gradient to evaluate changes in microbial cell abundances, metabolic rates and community composition under varying environmental conditions. In addition, this chapter incorporates an analysis of over 20 years of aerosol dust deposition monitoring in the Canary Islands (Spain), including aerosol gravimetry, chemical composition and source tracking analyses. These data provide a broader context for understanding the influence of dust on microbial productivity and regional biogeochemical cycles, thereby also contributing to the fifth research question.

Chapters 3 and 4 focus on the influence of diffuse hydrothermal emissions from the Tagoro submarine volcano (Canary Islands) on microbial communities. These studies integrate more than a decade of environmental monitoring, collected from the eruption of Tagoro in 2011 to its current degassing phase, to provide insights into the spatial and temporal extent of hydrothermal influence on the water column and adjacent benthic habitats.

Chapter 3 explores the response of phytoplankton and bacteria in pelagic waters through experimental bioassays simulating natural dilution gradients of hydrothermal fluids. Changes in microbial cell abundance, metabolism and community composition were evaluated alongside hydrographic profiles and dissolved silicate concentrations, a known tracer of hydrothermal activity in the region. Additionally, the potential influence of seasonal variation in surface waters was considered based on hydrographic data from the last decade. This chapter primarily contributes to research questions i, ii, iii and v, while also laying the groundwork for the microbial community characterization developed in more detail in the following chapter.

Chapter 4 thus focuses on identifying key prokaryotic taxa inhabiting distinct hydrothermal habitats at Tagoro, including pelagic and benthic environments. Special attention is given to their potential contributions to local biogeochemical processes. This final research chapter directly addresses the last three research questions.

Chapter 5 synthesizes the main findings of the thesis and discusses their broader implications, offering perspectives for future research directions.

Together, this thesis provides a multidisciplinary understanding of how distinct natural fertilization events shape microbial community dynamics and biogeochemical processes in a climatically sensitive and ecologically important region of the global ocean: the subtropical Northeast Atlantic Ocean.

References

Achterberg, E. P., Moore, C. M., Henson, S. A., Steigenberger, S., Stohl, A., Eckhardt, S., et al. (2013). Natural iron fertilization by the Eyjafjallajökull volcanic eruption. *Geophysical Research Letters* 40, 921–926. doi: 10.1002/grl.50221

Appeltans, W., Ahyong, S. T., Anderson, G., Angel, M. V., Artois, T., Bailly, N., et al. (2012). The Magnitude of Global Marine Species Diversity. *Current Biology* 22, 2189–2202. doi: 10.1016/j.cub.2012.09.036

Ardyna, M., Lacour, L., Sergi, S., d'Ovidio, F., Sallée, J.-B., Rembauville, M., et al. (2019). Hydrothermal vents trigger massive phytoplankton blooms in the Southern Ocean. *Nat Commun* 10, 2451. doi: 10.1038/s41467-019-09973-6

Arrigo, K. R. (2005). Marine microorganisms and global nutrient cycles. *Nature* 437, 349–355. doi: 10.1038/nature04159

Azam, F., Fenchel, T., Field, J. G., Gray, J. S., Meyer-Reil, L. A., and Thingstad, F. (1983). The Ecological Role of Water-Column Microbes in the Sea. *Marine Ecology Progress Series* 10, 257–263.

Azam, F., and Malfatti, F. (2007). Microbial structuring of marine ecosystems. *Nat Rev Microbiol* 5, 782–791. doi: 10.1038/nrmicro1747

Bar-On, Y. M., and Milo, R. (2019). The Biomass Composition of the Oceans: A Blueprint of Our Blue Planet. *Cell* 179, 1451–1454. doi: 10.1016/j.cell.2019.11.018

Bar-On, Y. M., Phillips, R., and Milo, R. (2018). The biomass distribution on Earth. *Proceedings of the National Academy of Sciences* 115, 6506–6511. doi: 10.1073/pnas.1711842115

Barosa, B., Ferrillo, A., Selci, M., Giardina, M., Bastianoni, A., Correggia, M., et al. (2023). Mapping the microbial diversity associated with different geochemical regimes in the shallow-water hydrothermal vents of the Aeolian archipelago, Italy. *Front. Microbiol.* 14. doi: 10.3389/fmicb.2023.1134114

Bellec, L., Cambon-Bonavita, M.-A., Durand, L., Aube, J., Gayet, N., Sandulli, R., et al. (2020). Microbial Communities of the Shallow-Water Hydrothermal Vent Near Naples, Italy, and Chemosynthetic Symbionts Associated With a Free-Living Marine Nematode. *Front. Microbiol.* 11. doi: 10.3389/fmicb.2020.02023

Bonnet, S., Benavides, M., Le Moigne, F. A. C., Camps, M., Torremocha, A., Grosso, O., et al. (2023). Diazotrophs are overlooked contributors to carbon and nitrogen export to the deep ocean. *ISME J* 17, 47–58. doi: 10.1038/s41396-022-01319-3

Bristow, L. A., Mohr, W., Ahmerkamp, S., and Kuypers, M. M. M. (2017). Nutrients that limit growth in the ocean. *Current Biology* 27, R474–R478. doi: 10.1016/j.cub.2017.03.030

Browning, T. J., Bouman, H. A., Henderson, G. M., Mather, T. A., Pyle, D. M., Schlosser, C., et al. (2014). Strong responses of Southern Ocean phytoplankton communities to volcanic ash. *Geophysical Research Letters* 41, 2851–2857. doi: 10.1002/2014GL059364

Browning, T. J., and Moore, C. M. (2023). Global analysis of ocean phytoplankton nutrient limitation reveals high prevalence of co-limitation. *Nat Commun* 14, 5014. doi: 10.1038/s41467-023-40774-0

Buchan, A., LeCleir, G. R., Gulvik, C. A., and González, J. M. (2014). Master recyclers: features and functions of bacteria associated with phytoplankton blooms. *Nat Rev Microbiol* 12, 686–698. doi: 10.1038/nrmicro3326

Buck, N. J., Resing, J. A., Baker, E. T., and Lupton, J. E. (2018). Chemical Fluxes From a Recently Erupted Shallow Submarine Volcano on the Mariana Arc. *Geochemistry, Geophysics, Geosystems* 19, 1660–1673. doi: 10.1029/2018GC007470

Chavez, F. P., and Messié, M. (2009). A comparison of Eastern Boundary Upwelling Ecosystems. *Progress in Oceanography* 83, 80–96. doi: 10.1016/j.pocean.2009.07.032

Crisp, J. A. (1984). Rates of magma emplacement and volcanic output. *Journal of Volcanology and Geothermal Research* 20, 177–211. doi: 10.1016/0377-0273(84)90039-8

Curtis, T. P., Sloan, W. T., and Scannell, J. W. (2002). Estimating prokaryotic diversity and its limits. *Proceedings of the National Academy of Sciences* 99, 10494–10499. doi: 10.1073/pnas.142680199

Doney, S. C., Ruckelshaus, M., Duffy, J. E., Barry, J. P., Chan, F., English, C. A., et al. (2012). Climate change impacts on marine ecosystems. *Ann Rev Mar Sci* 4, 11–37. doi: 10.1146/annurev-marine-041911-111611

Ducklow, H., Steinberg, D., and Buesseler, K. (2001). Upper Ocean Carbon Export and the Biological Pump. *oceanog* 14, 50–58. doi: 10.5670/oceanog.2001.06

Esposito, V., Andaloro, F., Canese, S., Bortoluzzi, G., Bo, M., Bella, M. D., et al. (2018). Exceptional discovery of a shallow-water hydrothermal site in the SW area of Basiluzzo islet (Aeolian archipelago, South Tyrrhenian Sea): An environment to preserve. *PLOS ONE* 13, e0190710. doi: 10.1371/journal.pone.0190710

Falkowski, P. G., Barber, R. T., and Smetacek, V. (1998). Biogeochemical Controls and Feedbacks on Ocean Primary Production. *Science* 281, 200–206. doi: 10.1126/science.281.5374.200

Field, C. B., Behrenfeld, M. J., Randerson, J. T., and Falkowski, P. (1998). Primary Production of the Biosphere: Integrating Terrestrial and Oceanic Components. *Science* 281, 237–240. doi: 10.1126/science.281.5374.237

García-Davis, S., Reyes, C. P., Lagunes, I., Padrón, J. M., Fraile-Nuez, E., Fernández, J. J., et al. (2021). Bioprospecting Antiproliferative Marine Microbiota From Submarine Volcano Tagoro. *Frontiers in Marine Science* 8. Available at: https://www.frontiersin.org/articles/10.3389/fmars.2021.687701 (Accessed November 3, 2022).

Gevorgian, J., Sandwell, D. T., Yu, Y., Kim, S.-S., and Wessel, P. (2023). Global Distribution and Morphology of Small Seamounts. *Earth and Space Science* 10, e2022EA002331. doi: 10.1029/2022EA002331

Giovannoni, S. J., and Stingl, U. (2005). Molecular diversity and ecology of microbial plankton. *Nature* 437, 343–348. doi: 10.1038/nature04158

González-Vega, A., Fraile-Nuez, E., Santana-Casiano, J. M., González-Dávila, M., Escánez-Pérez, J., Gómez-Ballesteros, M., et al. (2020). Significant Release of Dissolved Inorganic Nutrients From the Shallow Submarine Volcano Tagoro (Canary Islands) Based on Seven-Year Monitoring. *Frontiers in Marine Science* 6, 829. doi: 10.3389/fmars.2019.00829

Guieu, C., Loÿe-Pilot, M.-D., Ridame, C., and Thomas, C. (2002). Chemical characterization of the Saharan dust end-member: Some biogeochemical implications for the western Mediterranean Sea. *Journal of Geophysical Research: Atmospheres* 107, ACH 5-1-ACH 5-11. doi: 10.1029/2001JD000582

Hillebrand, H., Acevedo-Trejos, E., Moorthi, S. D., Ryabov, A., Striebel, M., Thomas, P. K., et al. (2022). Cell size as driver and sentinel of phytoplankton community structure and functioning. *Functional Ecology* 36, 276–293. doi: 10.1111/1365-2435.13986

Jickells, T. D. (2005). Global Iron Connections Between Desert Dust, Ocean Biogeochemistry, and Climate. *Science* 308, 67–71. doi: 10.1126/science.1105959

Jickells, T. D., Baker, A. R., and Chance, R. (2016). Atmospheric transport of trace elements and nutrients to the oceans. *Phil. Trans. R. Soc. A* 374, 20150286. doi: 10.1098/rsta.2015.0286

Jickells, T., and Moore, C. M. (2015). The Importance of Atmospheric Deposition for Ocean Productivity. *Annual Review of Ecology, Evolution, and Systematics* 46, 481–501. doi: 10.1146/annurev-ecolsys-112414-054118

Kirchman, D. L. (1994). The uptake of inorganic nutrients by heterotrophic bacteria. *Microb Ecol* 28, 255–271. doi: 10.1007/BF00166816

Lennon, J. T., and Locey, K. J. (2020). More support for Earth's massive microbiome. *Biology Direct* 15, 5. doi: 10.1186/s13062-020-00261-8

Levitus, S., Conkright, M. E., Reid, J. L., Najjar, R. G., and Mantyla, A. (1993). Distribution of nitrate, phosphate and silicate in the world oceans. *Progress in Oceanography* 31, 245–273. doi: 10.1016/0079-6611(93)90003-V

Litchman, E., de Tezanos Pinto, P., Klausmeier, C. A., Thomas, M. K., and Yoshiyama, K. (2010). Linking traits to species diversity and community structure in phytoplankton. *Hydrobiologia* 653, 15–28. doi: 10.1007/s10750-010-0341-5

Liu, J., Wang, X., Wu, D., Wei, H., Li, Y., and Ji, M. (2024). Historical footprints and future projections of global dust burden from bias-corrected CMIP6 models. *npj Clim Atmos Sci* 7, 1. doi: 10.1038/s41612-023-00550-9

Marañón, E. (2015). Cell size as a key determinant of phytoplankton metabolism and community structure. *Ann Rev Mar Sci* 7, 241–264. doi: 10.1146/annurev-marine-010814-015955

Martiny, A. C., Vrugt, J. A., and Lomas, M. W. (2014). Concentrations and ratios of particulate organic carbon, nitrogen, and phosphorus in the global ocean. *Sci Data* 1, 140048. doi: 10.1038/sdata.2014.48

Mélançon, J., Levasseur, M., Lizotte, M., Delmelle, P., Cullen, J., Hamme, R. C., et al. (2014). Early response of the northeast subarctic Pacific plankton assemblage to volcanic ash fertilization. *Limnology and Oceanography* 59, 55–67. doi: 10.4319/lo.2014.59.1.0055

Mills, M. M., Moore, C. M., Langlois, R., Milne, A., Achterberg, E., Nachtigall, K., et al. (2008). Nitrogen and phosphorus co-limitation of bacterial productivity and growth in the oligotrophic subtropical North Atlantic. *Limnol. Oceanogr.* 53, 824–834. doi: 10.4319/lo.2008.53.2.0824

Moore, C. M., Mills, M. M., Arrigo, K. R., Berman-Frank, I., Bopp, L., Boyd, P. W., et al. (2013). Processes and patterns of oceanic nutrient limitation. *Nature Geosci* 6, 701–710. doi: 10.1038/ngeo1765

Moore, C. M., Mills, M. M., Langlois, R., Milne, A., Achterberg, E. P., La Roche, J., et al. (2008). Relative influence of nitrogen and phosphorous availability on phytoplankton physiology and productivity in the oligotrophic sub-tropical North Atlantic Ocean. *Limnol. Oceanogr.* 53, 291–305. doi: 10.4319/lo.2008.53.1.0291

Moreno, A. R., and Martiny, A. C. (2018). Ecological Stoichiometry of Ocean Plankton. *Ann. Rev. Mar. Sci.* 10, 43–69. doi: 10.1146/annurev-marine-121916-063126

Neuer, S., Torres-Padrón, M. E., Gelado-Caballero, M. D., Rueda, M. J., Hernández-Brito, J., Davenport, R., et al. (2004). Dust deposition pulses to the eastern subtropical North Atlantic gyre: Does ocean's biogeochemistry respond?: Dust deposition in the eastern subtropic. *Global Biogeochem. Cycles* 18, n/a-n/a. doi: 10.1029/2004GB002228

Nowald, N., Iversen, M. H., Fischer, G., Ratmeyer, V., and Wefer, G. (2015). Time series of in-situ particle properties and sediment trap fluxes in the coastal upwelling filament off Cape Blanc, Mauritania. *Prog. Oceanogr.* 137, 1–11. doi: 10.1016/j.pocean.2014.12.015

Paoli, L., Ruscheweyh, H.-J., Forneris, C. C., Hubrich, F., Kautsar, S., Bhushan, A., et al. (2022). Biosynthetic potential of the global ocean microbiome. *Nature* 607, 111–118. doi: 10.1038/s41586-022-04862-3

Pomeroy, L. R., Williams, P. J. leB, Azam, F., and Hobbie, J. E. (2015). The Microbial Loop. *Oceanography* 20, 28–33. doi: 10.5670/oceanog.2007.45

Price, R. E., and Giovannelli, D. (2017). "A Review of the Geochemistry and Microbiology of Marine Shallow-Water Hydrothermal Vents," in *Reference Module in Earth Systems and Environmental Sciences*, (Elsevier). doi: 10.1016/B978-0-12-409548-9.09523-3

Prospero, J. M., and Lamb, P. J. (2003). African Droughts and Dust Transport to the Caribbean: Climate Change Implications. *Science* 302, 1024–1027. doi: 10.1126/science.1089915

Redfield, A. C. (1934). *On the Proportions of Organic Derivatives in Sea Water and Their Relation to the Composition of Plankton*. James Johnstone Memorial Volume, University Press of Liverpool.

Rizzo, C., Arcadi, E., Calogero, R., Sciutteri, V., Consoli, P., Esposito, V., et al. (2022). Ecological and Biotechnological Relevance of Mediterranean Hydrothermal Vent Systems. *Minerals* 12, 251. doi: 10.3390/min12020251

Rodríguez, S., and López-Darias, J. (2024). Extreme Saharan dust events expand northward over the Atlantic and Europe, prompting record-breaking PM_{10} and $PM_{2.5}$ episodes. *Atmospheric Chemistry and Physics* 24, 12031–12053. doi: 10.5194/acp-24-12031-2024

Santana-Casiano, J. M., González-Dávila, M., Fraile-Nuez, E., de Armas, D., González, A. G., Domínguez-Yanes, J. F., et al. (2013). The natural ocean acidification and fertilization event caused by the submarine eruption of El Hierro. *Sci Rep* 3, 1140. doi: 10.1038/srep01140

Shu, W.-S., and Huang, L.-N. (2022). Microbial diversity in extreme environments. *Nat Rev Microbiol* 20, 219–235. doi: 10.1038/s41579-021-00648-y

Sunagawa, S., Coelho, L. P., Chaffron, S., Kultima, J. R., Labadie, K., Salazar, G., et al. (2015). Structure and function of the global ocean microbiome. *Science* 348, 1261359. doi: 10.1126/science.1261359

Tarasov, V. G., Gebruk, A. V., Mironov, A. N., and Moskalev, L. I. (2005). Deep-sea and shallow-water hydrothermal vent communities: Two different phenomena? *Chemical Geology* 224, 5–39. doi: 10.1016/j.chemgeo.2005.07.021

Tilliette, C., Gazeau, F., Portlock, G., Benavides, M., Bonnet, S., Guigue, C., et al. (2023). Influence of shallow hydrothermal fluid release on the functioning of phytoplankton communities. *Frontiers in Marine Science* 10. doi: 10.3389/fmars.2023.1082077

CHAPTER 2

UNEVEN RESPONSE OF MICROBIAL COMMUNITIES TO INTENSE DUST DEPOSITION ACROSS THE COASTAL TRANSITION ZONE OFF MAURITANIA

Pérez-Barrancos, C., Gelado-Caballero, M. D., Hernández-Hernández, N., Baños, I., Gómez-Letona, M., Montero, M. F., Arrieta, J.M., and Arístegui, J. (2022). Uneven response of microbial communities to intense dust deposition across the coastal transition zone off Mauritania. *Front. Mar. Sci.* 9, 999729. doi: 10.3389/fmars.2022.999729

The eastern North Atlantic region receives large Saharan dust deposition inputs, providing nutrients and trace metals to the surface waters. We assessed the effects of intense dust deposition on phytoplankton and bacteria cell abundances, metabolic activity and community structure, along a surface productivity gradient in the Mauritanian-Senegalese upwelling system. Dust concentrations above 4 mg L^{-1} were added to triplicate microcosms in four bioassay experiments, each lasting three days, increasing nitrate, phosphate and, to a lesser extent, silicate seawater concentrations. Even though dust deposition enhanced both heterotrophic and photosynthetic activity, bacterial production responded faster and stronger than primary production, especially as oligotrophic conditions increased. Bacterial production rates in oligotrophic waters almost tripled one day after the enrichment. However, such favorable response could not be observed on the total organic carbon production until a lag phase of 2 days and whilst under moderate eutrophic conditions. Dust enrichment benefited the presence of certain planktonic groups over others according to their nutrient requirements. Indicator species analysis revealed that our dust-treated microcosms were

consistently characterized by Raphid-pennate diatoms, as well as by *Hyphomonas* genus of Alphaproteobacteria and several species of *Alteromonas* Gammaproteobacteria. Yet, changes in microbial community structure and composition were primarily shaped by the starting conditions of each experiment. These findings indicate that increasing dust deposition events and the weakening of the Mauritanian-Senegalese upwelling system under climate change may result in a more heterotrophic system, particularly in oligotrophic waters, reducing its potential to function as an atmospheric carbon sink.

2.1 Introduction

Every year about 450 teragrams of atmospheric dust are deposited on the world's oceans, of which 43% reaches the Atlantic Ocean (Jickells, 2005). Almost half of the global dust production arrives from North Africa, where the arid regions of the Sahara and the Sahel make up the largest sources of mineral dust (Prospero and Lamb, 2003). Although dust deposition provides the surface ocean with new inorganic nutrients, trace metals and organic carbon (Guieu et al., 2002; Pulido-Villena et al., 2008; Jickells et al., 2016), the bioavailability of these and the extent of their fertilizing effect on microbial communities remains uncertain (e.g., Chien et al., 2016).

Past studies on the role of dust inputs on ocean biogeochemistry have focused on the impact on autotrophic productivity, given their potential to enhance the efficiency of the biological pump and hence ocean carbon sequestration. Some bioassay studies have shown that phytoplankton biomass, primary production and N_2 fixation may increase after dust additions (Bonnet et al., 2005; Herut et al., 2005, 2016; Duarte et al., 2006; Ridame et al., 2011; Rahav et al., 2018). However, further studies combining field and experimental approaches also denoted a significant increase in bacterial abundance and metabolic rates following dust additions (Herut et al., 2005, 2016; Pulido-Villena et al., 2008, 2014; Lekunberri et al., 2010; Marañón et al., 2010; Guieu et al., 2014; Rahav et al., 2018; Gazeau et al., 2021). Indeed, under suitable conditions bacteria can outcompete phytoplankton for inorganic nutrients (Joint et al., 2002; Mills et al., 2008; Hale et al., 2017). Yet, the potential uptake of inorganic nutrients and organic carbon by heterotrophic bacteria during dust bioassays may be masked under the impact of grazing exerted by predators such as heterotrophic flagellates, ciliates and dinoflagellates (Pitta et al., 2017) and, to a lesser extent, by viral lysis (Tsiola et al., 2017).

Although the Northeast Atlantic Ocean is among the highest receivers of Saharan dust fluxes in the world, few bioassay studies on dust fertilization have been conducted in the region (Blain et al., 2004; Duarte et al., 2006; Hill et al., 2010; Marañón et al., 2010; Langlois et al., 2012). Most of these studies focused on the response of microbial community abundance and metabolic activity without considering the shifts in community structure. Only Marañón et al. (2010) addressed the concurrent effects of dust inputs on phytoplankton and bacteria using conventional molecular techniques along a latitudinal transect in the central Atlantic Ocean.

In our study, we assessed the effects of intense dust deposition on surface-ocean microbial communities (phytoplankton and bacteria) in the Mauritanian-Senegalese area, characterized by recurrent dust intrusions (Jickells, 2005) and high particle export rates (Nowald et al., 2015). Four dust bioassays were conducted at four stations along a zonal trophic gradient stretching from the eutrophic coastal upwelling region to the oligotrophic open ocean. The differential effects of dust-derived nutrients on phytoplankton and bacteria were assessed in terms of cell abundances, autotrophic and heterotrophic production and community structure.

2.2 Material and methods

2.2.1 Aerosol collection

Total suspended particles were sampled at Pico de la Gorra (1930 m above sea level; 27° 56'N, 15° 33'W), as part of a long-term aerosol monitoring program in the Canary Islands (Torres-Padrón et al., 2002; Gelado-Caballero et al., 2012; López-García et al., 2013). High-volume aerosol collectors (60 m^3 h^{-1}, 24 h; MCV, model CAV-A/M) were used to collect dry material for (1) chemical composition analyses on acid-washed cellulose filters (Whatman 41) and (2) measuring gravimetrically total suspended particles concentrations on glass-fiber filters (Whatman GF/A). Several Whatman GF/A filters were also collected on board the FLUXES I cruise (CAV-A/mb model; MCV). Trace-metal clean techniques were strictly followed throughout the aerosol collection and manipulation (**Supplementary Methods**).

2.2.2 Microcosms setup

Four dust addition experiments were performed at four stations during the FLUXES I cruise on board the R/V *Sarmiento de Gamboa* (**Table 1**, **Figure 1**). The sampling locations were distributed along the coastal transition zone from the open-ocean Atlantic waters to the upwelling off Mauritania. Surface seawater samples (10–20 m depth) were collected using acid-cleaned Niskin bottles with external closure mounted on a SBE 38 rosette sampler equipped with a Sea-Bird 911+ CTD system. At each station, the surface seawater samples were homogenized, prefiltered through a 250 μm mesh size and transferred to 15-L acid-cleaned microcosms (made of polyvinylchloride) before the start of the experiment (**Table 1**). Prior to dust addition, seawater was sampled for all measured parameters (0 h of sampling time) using an acid-washed silicone tube. Each experiment comprised three replicate control microcosms (C1, C2 and C3) and three replicate dust-treated microcosms (D1, D2 and D3) placed in an on-deck incubator. The dust treatment consisted in a single addition of a dust stock solution (**Supplementary Methods**) that resulted in concentrations between 4.2 and 6.7 mg dust L^{-1} (**Table 2**). The amendment provided an average of 0.16, 0.02 and 0.01 μmol of nitrate, phosphate and silicate per mg of dust, as estimated from fluxes already reported through the Canary Region (López-García et al., 2021). These conditions simulate a cumulative event of intense dust deposition (~5500 μg TSP m^{-3}, Gelado-Caballero et al., 2012) over 20 days in the upper 30 m mixed layer in the Northeast Atlantic Ocean. Likewise, a control stock solution (without dust) was poured into the control microcosms. During the experiments, each lasting three days, the microcosms were attached to a weight, covered with a three-layer neutral-density mesh lid (~48.6%) and subjected to a continuous flow of surface seawater (25 ± 1.5 ºC) to reproduce natural conditions. Most parameters were sampled 24 and 72 h after the addition of dust, although depending on the parameter an additional sampling after 48 h was performed.

2.2.3 Nutrient analysis

Samples (15 mL) were collected in polypropylene tubes and frozen upright at –20°C until analyzed. Concentrations were determined using a 4-channel Skalar San^{++} continuous flow autoanalyzer for nitrate and nitrite (NO_x) (Cd reduction method), phosphate (PO_4^{3-}) and silicate ($Si(OH)_4$) (molybdate blue method). The instrumental limit of quantification was 0.001 μM.

Table 1. Station properties and initial characteristics of the surface waters used to conduct each experiment.

	Experiment name			
	FL01	FL02	FL03	FL04
Experiment duration (2017)	21-24 July	2-5 August	17-20 July	6-9 August
Sampling station	12	26	5	33
Longitude	25° 59.46'	20° 48.02'	20° 9.03'	18° 34.19'
Latitude	23° 00.01'	17° 20.01'	23° 0.03'	20° 41.99'
Sampling depth	10 m	20 m	10 m	12 m
Mixed layer depth	40 m	25 m	25 m	20 m
Temperature	24.6 °C	24.0 °C	23.1 °C	21.1 °C
Salinity	36.97	35.99	35.90	36.05
Nitrate (μmol L^{-1})	0.01	0.80	0.15	3.09
Phosphate (μmol L^{-1})	0.10	0.32	0.12	0.45
Silicate (μmol L^{-1})	0.53	0.55	0.50	0.87
Nitrate/Phosphate	0.10	2.50	1.25	6.87
Nitrate/Silicate	0.02	1.45	0.30	3.55
Phosphate/Silicate	0.19	0.58	0.24	0.52
Chlorophyll *a* (μg L^{-1})	0.02	0.78	1.33	7.96
Microphytoplankton abundance (cells mL^{-1})	10	384	405	959
Nanophytoplankton abundance (cells mL^{-1})	24	175	424	738
Picophytoplankton abundance (10^5 cells mL^{-1})	1.09	1.40	4.72	0.51
Bacterial abundance (10^5 cells mL^{-1})	4.49	8.60	25.65	15.72
Total primary production (μg C L^{-1} h^{-1})	0.06	1.13	2.36	7.64
Bacterial production (μg C L^{-1} h^{-1})	0.04	0.19	0.76	2.44

Table 2. Dust microcosm concentration (mg dust L^{-1}) and released soluble inorganic nutrient concentrations (μmol L^{-1}) in each experiment.

	Experiment name			
	FL01	FL02	FL03	FL04
Dust (mg L^{-1})	4.2	4.6	6.7	4.8
Nitrate (μmol L^{-1})	0.692	0.758	1.104	0.791
Phosphate (μmol L^{-1})	0.084	0.092	0.134	0.096
Silicate (μmol L^{-1})	0.046	0.051	0.074	0.053

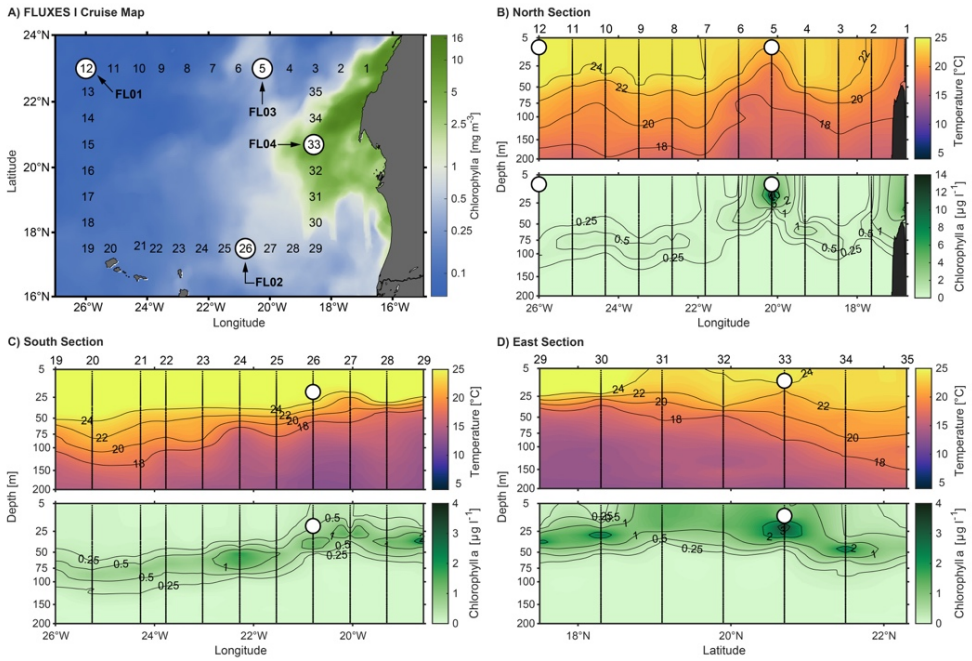

Figure 1. (A) Eight-day mean Chl *a* concentration (mg m^{-3}) during FLUXES I cruise. Data provided by The Copernicus Marine Environment Monitoring Service (http://marine.copernicus.eu/). White points show the sampled stations to conduct each experiment. **(B)** Vertical sections (0–200 m) of temperature (°C) and Chl *a* (μg L^{-1}) for the northern, **(C)** southern and **(D)** eastern cruise transects. Stations are indicated at the top of the upper panels. White points show the depths sampled to perform each numbered experiment (see **Table 1**).

2.2.4 Chlorophyll *a*

Samples (500 mL) were filtered on board through 25 mm diameter, 0.7 μm pore size Whatman GF/F glass-fiber filters. Pigments were extracted overnight in cold acetone (90% v/v) at –20°C in the dark. Chlorophyll *a* (Chl *a*) concentration was estimated fluorometrically by means of a Turner Designs bench fluorometer (Holm-Hansen et al., 1965).

2.2.5 Microbial abundance

Samples (125 mL) were fixed and preserved in acidic Lugol solution to 1% final concentration and settled in sedimentation chambers for 24-48 hours. Large phytoplankton (>20 μm) was identified and enumerated by inverted microscopy (Utermöhl, 1958) at 20× magnification.

Heterotrophic bacteria, nano- and picoeukaryotes and *Prochlorococcus* sp. and *Synechococcus* sp. type of cyanobacteria, were enumerated using a FACScalibur (Becton and Dickinson) flow cytometer. Samples for microbial abundance (2 mL) were fixed with paraformaldehyde to a final concentration of 2%, refrigerated 30 minutes at 4°C, frozen in liquid nitrogen (–190°C) and stored at –80°C until analysis. Subsamples (400 μL) were stained with 4 μL of SYBR Green I, Molecular Probes Inc. (final concentration 1000× dilution of the commercial product) for bacteria analysis. High nucleic-acid content (HNA) bacteria and low nucleic-acid content (LNA) bacteria were identified in bivariate scatter plots of side scatter versus green fluorescence. Cyanobacteria and eukaryotes were discriminated in plots of orange fluorescence versus red fluorescence.

2.2.6 Microbial community structure

Samples for amplicon sequencing were collected from each microcosm at time zero and at the end of the experiments. Approximately 2-L of seawater were filtered through a 0.22 μm pore-size Sterivex filter (Millipore), immediately frozen into liquid nitrogen and stored at –80°C.

DNA extracts were obtained using the standard phenol-chloroform method (Sambrook and Russell, 2001). The V4 region of the prokaryotic 16S rDNA genes (~390 bp) was amplified by PCR using the 515F (5'-GTGYCAGCMGCCGCGGTAA-3') and 806R (5'-GGACTACNVGGGTWTCTAAT-3') primer pair sequences (Apprill et al.,

2015; Parada et al., 2016). The same DNA extracts were used to amplify the V9 region of the eukaryotic 18S rDNA genes (~260 ± 50 bp) using primers 1391F (5'-GTACACACCGCCCGTC-3') and 1510R (5'-TGATCCTTCTGCAGGTTCACCTAC-3') (Amaral-Zettler et al., 2009; Stoeck et al., 2010). Sample processing, library preparation and sequencing were performed by the Earth Microbiome Project (Thompson et al., 2017; https://earthmicrobiome.org/) at Argonne National Laboratory (Lemont, IL, USA; https://www.anl.gov/). Sequencing raw datasets are deposited at NCBI (https://www.ncbi.nlm.nih.gov/) under accession number PRJNA862364.

In both V4 and V9 amplicon datasets, raw reads were filtered and trimmed to remove amplification primers with cutadapt v1.18 (Martin, 2011) and processed using the software package *DADA2* v1.24 (Callahan et al., 2016) with the parameters *truncQ* 2, *truncLen* 140,130 and *maxEE* 4,5. Sequences from all samples were pooled together for sample inference and bimera identification. For each dataset, an amplicon sequence variant (ASV) table was generated. After the taxonomic assignation of prokaryotes according to Silva SSU version 138.1, sequences classified as eukaryote, mitochondria and chloroplast were removed from the V4 dataset. Eukaryotic taxonomy was then assigned using the PR^2 database (Guillou et al., 2013), from which bacterial and archaeal sequences were removed. In this occasion, those sequences belonging to the Opisthokonta supergroup of eukaryotes were also excluded from the V9 dataset since were considered non-relevant for the purpose of our study. To avoid library size differences, each amplicon dataset was rarefied using the function *rarefy_even_depth* (phyloseq package v1.40; McMurdie and Holmes, 2013). Species richness (Chao 1 index) and diversity (Shannon index) were estimated using phyloseq.

2.2.7 ^{14}C-Based primary production

Primary production (PP) was determined by the ^{14}C method. Three culture flasks per microcosm (50 mL) were inoculated with 5 μCi of ^{14}C-labeled $NaH^{14}CO_3$ solution. Labelled samples were incubated for 24 hours in the same deck incubator as the microcosms, remaining one of the three under complete darkness to measure the dark carbon uptake. At the end of the incubations, 5 mL of the water sample were filtered through 0.2 μm pore size polycarbonate filters under low vacuum pressure. To measure the particulate organic carbon production (PP_{POC}), filters were placed in 6 mL scintillation vials, after exposure to concentrated HCl fumes overnight to remove inorganic carbon. A volume

of 5 mL of the filtrate was transferred to a 20 mL scintillation vial to determine the amount of fixed ^{14}C released into the dissolved organic carbon fraction (PP_{DOC}). Liquid samples were acidified with 100 μL of HCl 6 N and placed in an orbital oscillator for 24 hours. Finally, scintillation cocktail was added to every sample to quantify the remaining radioactivity using a Liquid Scintillation Counter. The total primary production (PP_{TOC}) was determined from the sum of the two size fractions considering the isotopic dilution of the tracer.

2.2.8 Bacterial production

Bacterial production (BP) was estimated from rates of protein synthesis determined by the incorporation of tritiated leucine [^3H] using the centrifugation method (Smith and Azam, 1992). For each microcosm, four replicated seawater samples (1 mL) were inoculated with 20 nM warm leucine of final concentration. Two trichloroacetic acid (TCA)-killed controls were established by adding 100 μL of 50% TCA. Samples, including controls, were incubated in the dark for 4–7 h at the same deck incubator as the microcosms and terminated by adding 100 μL of 50% TCA. Centrifugation was carried out at 12000 rpm for 20 minutes, followed by aspiration of the supernatant. Then, 1 mL of 5% TCA was added to each sample and centrifuged again. Once removed the supernatant, 1 mL of scintillation cocktail was placed in each sample. Leucine incorporation rates were then estimated from the mean disintegrations per minute (DPM) of the samples after subtracting the DPM of the TCA-killed controls from the corresponding samples. BP was calculated by leucine incorporation rates (Kirchman and Ducklow, 1993), assuming no isotopic dilution and using a carbon conversion factor of 1.5 kg C mol leucine^{-1} (Simon and Azam, 1989).

2.2.9 Statistical analyses

Analyses were conducted in *R* v4.2.1 (R Core Team, 2021) and mostly performed using tidyverse v1.3.2 (Wickham et al., 2019).

Shapiro-Wilk test of normality and Levene's test for homogeneity of variance were checked across all variables by groups of treatment and/or experiments (rstatix package v.0.7; Kassambara, 2021). Single tailed, non-parametric Mann-Whitney-Wilcoxon tests were computed by applying *alternative = "less"* to test whether the treatment effect was greater on dust than control microcosms at each sampling time. Pairwise comparisons between all dust-treated microcosms

were assessed with Kruskal-Wallis test and Conover-Iman *post-hoc* analyses (conover.test package v.1.1.5; Dinno, 2017). Two-way ANOVA tests were performed on microbial richness and diversity estimates to assess the interaction between treatment and experiment variables at the end of the incubations (rstatix package v.0.7; Kassambara, 2021). One-way ANOVA and Tukey *post-hoc* analyses were computed to determine the differences between experiments, being displayed with ggpubr v.0.4 (Kassambara, 2020).

A non-metric multidimensional scaling (NMDS) was performed from Bray-Curtis dissimilarities (phyloseq package v1.40; McMurdie and Holmes, 2013). PERMANOVA tests were then computed on treatment and experiment variables at the end of the incubations, as well as its interaction (vegan package v2.6.2; Oksanen et al., 2019). To assess the uncertainty in hierarchical cluster analyses, a multiscale bootstrap resampling was performed on the Bray-Curtis dissimilarity data matrix (pvclust package v.2.2; Suzuki et al., 2019) and displayed as a dendrogram with ggtree v.3.4.2 (Yu, 2020). Finally, an indicator species analysis was computed to determine which species characterized certain treatments (indicspecies package v.1.7.12; De Cáceres and Legendre, 2009).

2.3 Results

2.3.1 Initial characteristics of surface waters

Table 1 and **Figure 1** illustrate the variable biogeochemical conditions of the surface waters collected to carry out the experiments. The surface water used to fill the FL01 microcosms was characterized by being typically oligotrophic (Chl *a* < 0.5 μg L^{-1}, NO_x < 0.2 μM), whereas the remaining experiments displayed a range of increasing eutrophic properties (FL02, FL03 and FL04, lowest to highest), as indicated by Chl *a* and productivity rates.

Temperature, salinity, oxygen and Chl *a* concentration at the sampling site from 0 to 200 m (**Figure 1**) showed that the northern section (23ºN) was influenced by a coastal meandering westward Cape Blanc (station 5) separating the nutrient-rich upwelled water from the warmer, stratified offshore water. While the Cape Blanc coastal upwelling was the principal supplier of nitrate in the FL03 experiment (station 5), total inorganic nitrogen was almost depleted in FL01 (station 12). Thus, the offshore PP and BP might be limited by nitrate concentration among other variables (**Table 1**). Similar initial phosphate and silicate concentrations were found in both stations. Surface Chl *a* concentration

(~10 m) presented an abrupt drop from values above 1-2 μg L^{-1} near the coast to 0.02 μg L^{-1} in the open-ocean following the decrease in phytoplankton abundances with increasing oligotrophy (from 4.72×10^5 cells mL^{-1} to 1×10^5 cells mL^{-1}). Picophytoplankton (<2 μm) always showed the highest abundances, although micro (>20 μm) and nano (2-20 μm) phytoplankton size fractions were also abundant in the most productive waters. Among the photosynthetic picophytoplankton (**Supplementary Figure 1**), *Synechococcus* was always numerically dominant, except in the oligotrophic experiment in which *Prochlorococcus* were the most abundant cyanobacteria. Diatoms were the dominant microphytoplankton group in coastal waters, while dinoflagellates dominated the FL01 experiment (**Supplementary Figure 2**). Bacterial abundance was one order of magnitude lower at FL01 compared with the coastal stations.

The southern transect (17ºN), where the FL02 experiment was performed (station 26), also presented some variability throughout the large offshore extension (**Figure 1**). Waters with high Chl *a* deepened at stations 26–27 until station 19, as colder waters persisted along the water column. Inorganic nutrients were higher than those observed in the northern section, with nitrate concentrations of about 0.80 μM (**Table 1**). The community structure remained similar to that in FL03, although with lower values of microbial abundance and production.

The last experiment FL04 (station 33) was conducted in the eastern section (18ºW), where the greatest influence by upwelled waters occurred (**Figure 1**). The highest inorganic nutrient concentrations were found on this eutrophic area, along with the greatest Chl *a* concentration (above 7 μg L^{-1}) and metabolic activity rates (PP_{TOC}, 7.64 μg C L^{-1} h^{-1}; BP, 2.44 μg C L^{-1} h^{-1}) (**Table 1**). Nanophytoplankton and diatom abundance were highest compared with the rest of stations (**Table 1; Figure S2**).

2.3.2 Nutrient dynamics

Dust addition increased an average of +0.8 μM of nitrate and +0.1 μM of phosphate seawater concentrations in all incubations (**Table 2; Figure S3**). FL01 and FL02 took 48 to 71 hours after dust addition to drive nitrate concentrations back to control levels (NO_x < 0.05 μM). FL03 and FL04 exhibited a sharp decline following dust addition albeit similar between control and dust-treated microcosms. The same pattern was observed in phosphate

concentrations since the decrease was consistent between treatments and experiments.

By contrast, the addition of silicate through dust was minor (+0.06 μM). FL04 silicate concentrations decreased over the experimental time, reaching lower concentrations than those of the control 71 hours after the addition (~0.6 μM). In the remaining experiments, dust-treated microcosms had on average silicate concentrations significantly higher than control values (about +0.3 μM of $Si(OH)_4$ above the control) for the most part of the experiments (**Table S1**).

2.3.3 Phytoplankton abundance and production

The abundance of microphytoplankton in the dust-treated microcosms significantly increased over 5-fold in FL01 (from 10 to 50 cells mL^{-1}) and about 1.5-fold in FL04 (from 900 to 1,500 cells mL^{-1}) 24 hours after dust addition (**Figure 2A**). However, no significant differences were observed in the remaining experiments until 71 hours of incubation. The enhancement in FL01 was associated with the increase of dinoflagellates, while in FL02, FL03 and FL04 with diatoms (**Figure S2**). Dust addition also induced an increase on nanophytoplankton abundance throughout the incubation period, which was significantly larger in dust-treated microcosms of FL01 (+116 cells mL^{-1}) and FL03 (+160 cells mL^{-1}) when compared to control (**Figure 2B**). In addition to the micro- and nanophytoplankton size fractions, picophytoplankton response also differed among experiments and groups of organisms (**Figure 2C; Figure S1**). *Synechococcus* and picoeukaryotes abundance increased through the dust-treated microcosms of FL01 (2,309 to 6,705 and 1,117 to 1,898 cells mL^{-1}, respectively), while *Prochlorococcus* decreased regardless of the treatment (105,944 to 40,913 cells mL^{-1} in dust-treated microcosms and to 40,054 cells mL^{-1} in controls). *Synechococcus* abundance was also significantly greater in FL02 towards 48 hours after dust addition (+44,983 cells mL^{-1}, 1.4-fold versus the control). Lastly, significant variances in picoeukaryotes abundance were noticed in FL03 and FL04 towards the end of the experiments (about +1,262 and +38,070 cells mL^{-1}, respectively, in dust-treated microcosms).

No early responses could be observed in Chl *a* concentration or PP_{TOC} during the first 24 hours in most incubations (**Figure 3A and 3C**), yet both were significantly enhanced by dust 48 hours onwards. The FL03 experiment displayed the most significant responses precisely at that time, in which Chl *a* was 2.3-fold greater than control (1.49 versus 0.65 $\mu g\ L^{-1}$) and PP_{TOC} rates were

1.3-fold above (3.51 versus 2.73 μg C L^{-1} h^{-1}). The overall hourly-integrated PP_{TOC} rates over the entire duration of the incubations evidenced that phytoplankton tend to thrive in the presence of dust. Other than a modest change of 2% in FL02, dust induced an increase in the whole hourly-integrated total primary production rates of 23% to 28% with respect to the control. Lastly, pair-wise comparisons among all dust-treated microcosms confirmed the substantial variation in the response of phytoplankton to dust addition according to the initial hydrographic conditions (**Table S2**). The differences in phytoplankton stocks, Chl *a* concentration and metabolic rates were statistically significant between the eutrophic experiments and when compared to the oligotrophic experiment.

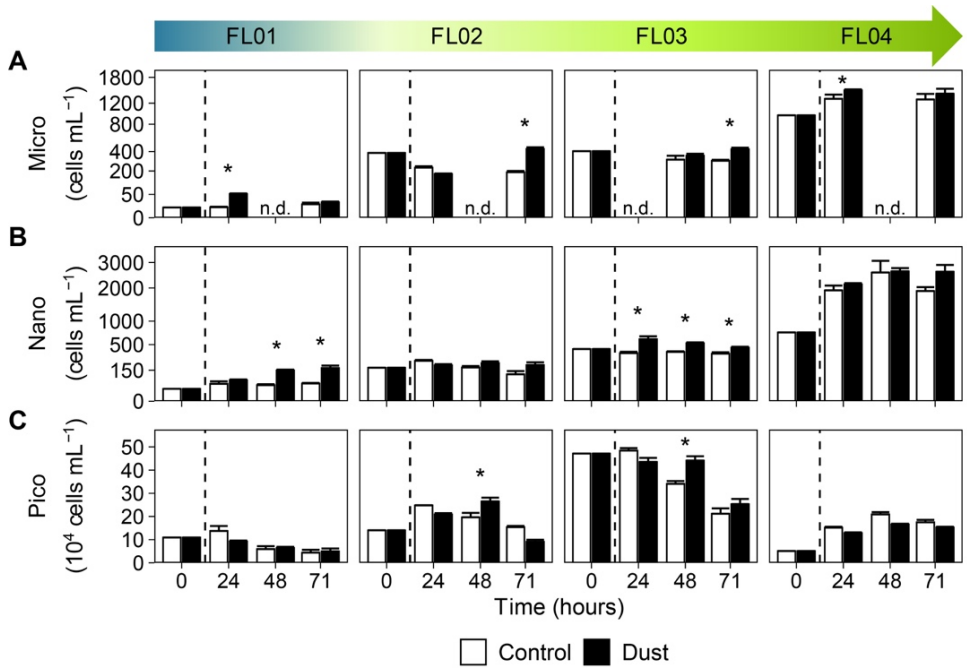

Figure 2. Phytoplankton abundance (cells mL^{-1}) by size fraction: **(A)** microphytoplankton (>20 μm), **(B)** nanophytoplankton (2–20 μm), and **(C)** picophytoplankton (<2 μm), in the control (white bars) and dust-treated microcosms (black bars). The vertical line indicates the dust addition time. Each data point represents the average and standard deviation of three replicated microcosms. The asterisk denotes where the value of dust triplicates was significantly greater than control ($p < 0.05$, Wilcoxon test). The abbreviation n.d. (no-data) indicate the absence of data at that time of the experimental incubation. Note that different scales were used.

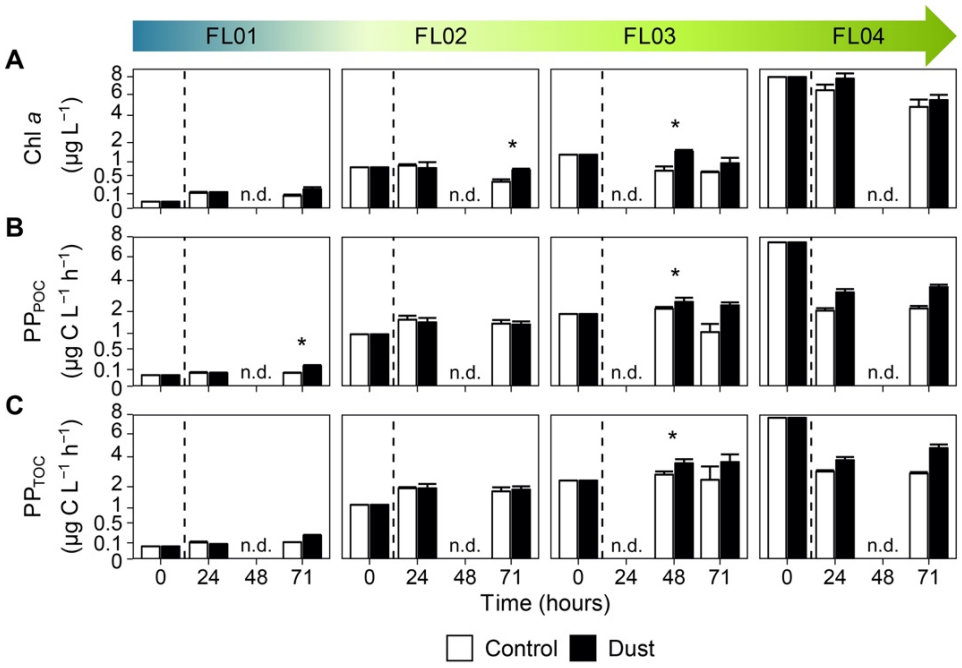

Figure 3. Time evolution of **(A)** Chl *a* concentration (μg L^{-1}), **(B)** primary production (μg C L^{-1} h^{-1}) in the total particulate fraction (PP_{POC}), and **(C)** total organic fraction (PP_{TOC}), in the control (white bars) and dust-treated microcosms (black bars). The vertical line indicates the dust addition time. Each data point represents the average and standard deviation of three replicated microcosms. The asterisk denotes where the value of dust triplicates was significantly greater than control ($p < 0.05$, Wilcoxon test). The abbreviation n.d. (no-data) indicate the absence of data at that time of the experimental incubation. Note that different scales were used.

2.3.4 Bacterial abundance and production

The dynamics of total bacterial abundance (**Figure 4A**) and the proportion of HNA and LNA cells (**Figure 4B**) over the course of the experiments remained similar between control and dust-treated microcosms, supported by the general absence of statistical differences (**Table S1**). Conversely, the metabolic rates of bacteria displayed major changes upon dust addition as the trophic gradient decreased (**Figure 4C**). BP in FL01 displayed a sharp increase 24 hours after the enrichment (from 0.045 to 2.39 μg C L^{-1} h^{-1}), nearly tripling the rates observed in the control. At the same time, FL02 and FL04 were stimulated 14-fold (from 0.19 to 2.85 μg C L^{-1} h^{-1}) and 1.4-fold (from 2.45 to 3.23 μg C L^{-1} h^{-1}), respectively. However, no statistical differences were observed between treatments apart from the FL01 experiment.

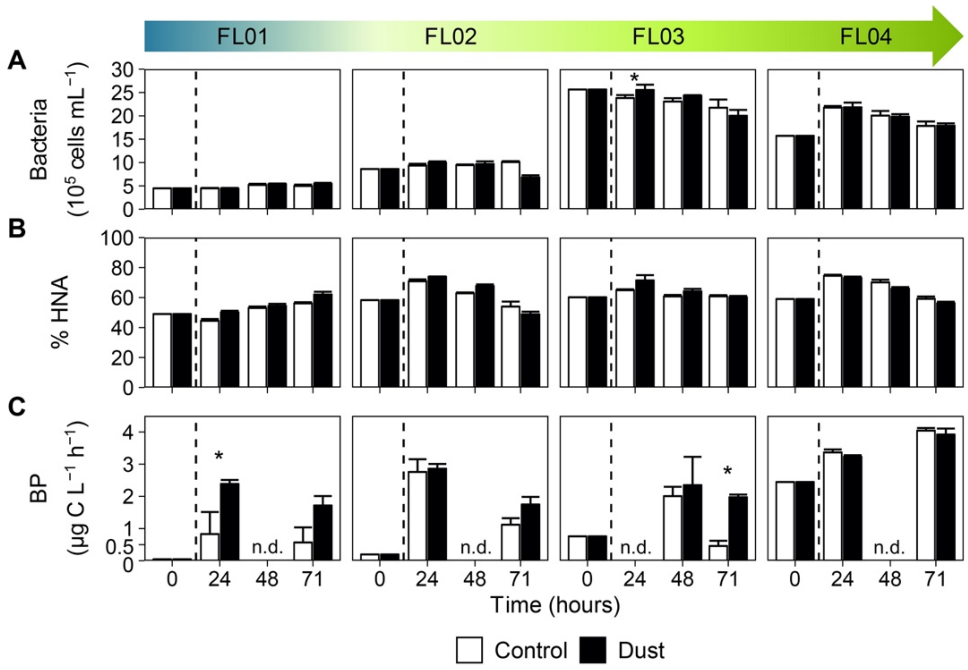

Figure 4. Time evolution of **(A)** bacterial abundance (cells mL^{-1}), **(B)** percentage of HNA bacteria, and **(C)** production (μg C L^{-1} h^{-1}) over the incubation time. in the control (white bars) and dust-treated microcosms (black bars). The vertical line indicates the dust addition time. Each data point represents the average and standard deviation of three replicated microcosms. The asterisk denotes where the value of dust triplicates was significantly greater than control ($p < 0.05$, Wilcoxon test). The abbreviation n.d. (no-data) indicate the absence of data at that time of the experimental incubation. Note that different scales were used.

The overall metabolic rates at the end of the incubations were greater than the initial ones, suggesting a positive reaction not only in magnitude but also in duration. Indeed, hourly-integrated BP over the entire incubation period evidenced dust as one of the main factors fueling heterotrophic activity. Specifically, dust induced an enhancement of about 190% compared to control in FL01, yet between 14% and 31% in FL02 and FL03, respectively. Non-significant shifts were observed in integrated BP rates in FL04 (-3% relative to the control).

Pair-wise comparisons among all dust-treated microcosms (**Table S2**) showed that the highest differences in bacterial abundance and production were found between the experiments FL01 and FL03, as compared to the differences between FL02 and FL04.

2.3.5 Microbial community structure and diversity

Eukaryotic 18S samples counted for a total of 422,390 reads by 1,026 ASVs, in which 73 class-level taxa and 216 family-level taxa was determined. Meanwhile, prokaryotic 16S samples contained 446,856 reads by 1,275 ASVs, and comprised 36 class-level and 132 family-level taxa.

Two major clusters were distinguished in both eukaryotic and prokaryotic taxonomic composition according to experiment location (**Figure 5**). The microbial composition of the oligotrophic FL01 experiment clearly differed from those most eutrophic (FL02, FL03 and FL04). In turn, the FL03 and FL04 experiments clustered together and were distant from the FL02 experiment. NMDS plots confirmed not only the clear separation between experiments' microbial composition but also between treatments regardless of the incubation time (**Figure S4 and S5**). The dissimilarities between control and dust-treated microcosms three days after the enrichment were smaller as eutrophic conditions increased. Almost 60% of the eukaryotic community variance recorded at the end of the experimental period was explained by the experiment physicochemical characteristics (df = 3, r^2 = 0.594; F = 14.68, p < 0.001, PERMANOVA test), followed by the differences in treatment (6%; df = 1, r^2 = 0.061; F = 4.5, p < 0.01, PERMANOVA). Prokaryotic test results also revealed the variable 'experiment' as the main community structuring parameter rather than 'treatment', explaining 61.5% and 8.8% of the variance (Experiment: df = 3, r^2 = 0.615; F = 11.3, p < 0.001; Treatment: df = 1, r^2 = 0.088; F = 4.81, p < 0.001, PERMANOVA), respectively. In addition, the interaction between 'treatment' and 'experiment' variables played a key role, as defined 15% of the eukaryotic variance (df = 3, r^2 = 0.15; F = 3.84, p < 0.001, PERMANOVA) and a marginal 6% of the prokaryotic differences (df = 2, r^2 = 0.06; F = 1.68, p < 0.1, PERMANOVA).

The relative abundance of each taxonomic group also displayed a distinct distribution between experiments and dust-treated microcosms (**Figure 5**). The natural eukaryotic communities under eutrophic conditions were dominated by Bacillariophyta (diatoms), ranging from 51% to 78% of relative abundance (**Figure S6A**). The family Polar-centric-Mediophyceae accounted for more than 50% of diatom abundances and showed little changes in response to dust addition (**Figure 5A**). As opposed to the control microcosms (**Table S3**), the indicator species analysis revealed a significant association of the Raphid-pennate diatom's family with the overall dust-treated microcosms

(p = 0.01, *stat* = 0.79) (**Table S4**), reaching no more than 15% at the end of all incubations. Other eukaryotic groups, such as Dinophyceae and Syndiniales (dinoflagellates), and Prymnesiophyceae (haptophytes), showed higher relative abundances (37%, 10% and 8% respectively) under natural oligotrophic conditions. While dinoflagellates consistently decreased regardless of the treatment and experiment, several members of marine stramenopiles, haptophytes and ciliates thrived upon dust addition under oligotrophic conditions. Particularly, *Chrysochromulina rotalis* (p = 0.02, *stat* = 0.80) and *Labyrinthulomycetes* sp. (p = 0.03, *stat* = 0.82) species were significantly related to the dust treatment, accounting for less than 1% of eukaryotic relative abundances. On the other hand, natural prokaryotic communities were almost similar at class-level among the four experiments (**Figure S6B**). Alpha- and gamma-Proteobacteria showed the highest relative abundances (>30%), followed by Cyanobacteria (>20%) and Bacteroidia (<15%). Changes in the bacterial community structure among experiments or following dust addition were observed at family-level (**Figure 5B**). The *Cyanobiaceae* family was responsible for most of the natural cyanobacterial populations, in which *Synechococcus* relative abundance was higher under eutrophic conditions (~22-27%) and *Prochlorococcus* genus under the oligotrophic one (~30%). Overall, the former cyanobacterial group increased towards dust addition, while the latter decreased. However, the most striking responses were found in *Alteromonadaceae* family of Gammaproteobacteria, since several members of this family significantly increased in dust-treated microcosms (p < 0.05, *stat* > 0.75; **Table S4**). The indicator species analysis also indicated several families of Alphaproteobacteria, such as *Hyphomonadaceae*, *Sphingomonadaceae* and *Rhodobacteraceae*, as organisms significantly related to dust (p < 0.05, *stat* > 0.75). Particularly, *Alteromonas* and *Hyphomonas* genera were always present after dust addition, with relative abundances ranging from 6% to 20% and 0.4% to 14%, respectively.

The association between microbial richness (Chao 1 index) and local productivity in natural samples displayed a hump-shaped relationship and peaked at intermediate productivity levels (**Figure 6A**). The diversity (Shannon index) of eukaryotes declined with increasing productivity, and that of prokaryotes was similar albeit highest between eutrophic conditions (**Figure 6B**). The relationship between alpha diversity and productivity showed little change throughout the experimental incubations (**Figure 6C and 6D; Figure S7**).

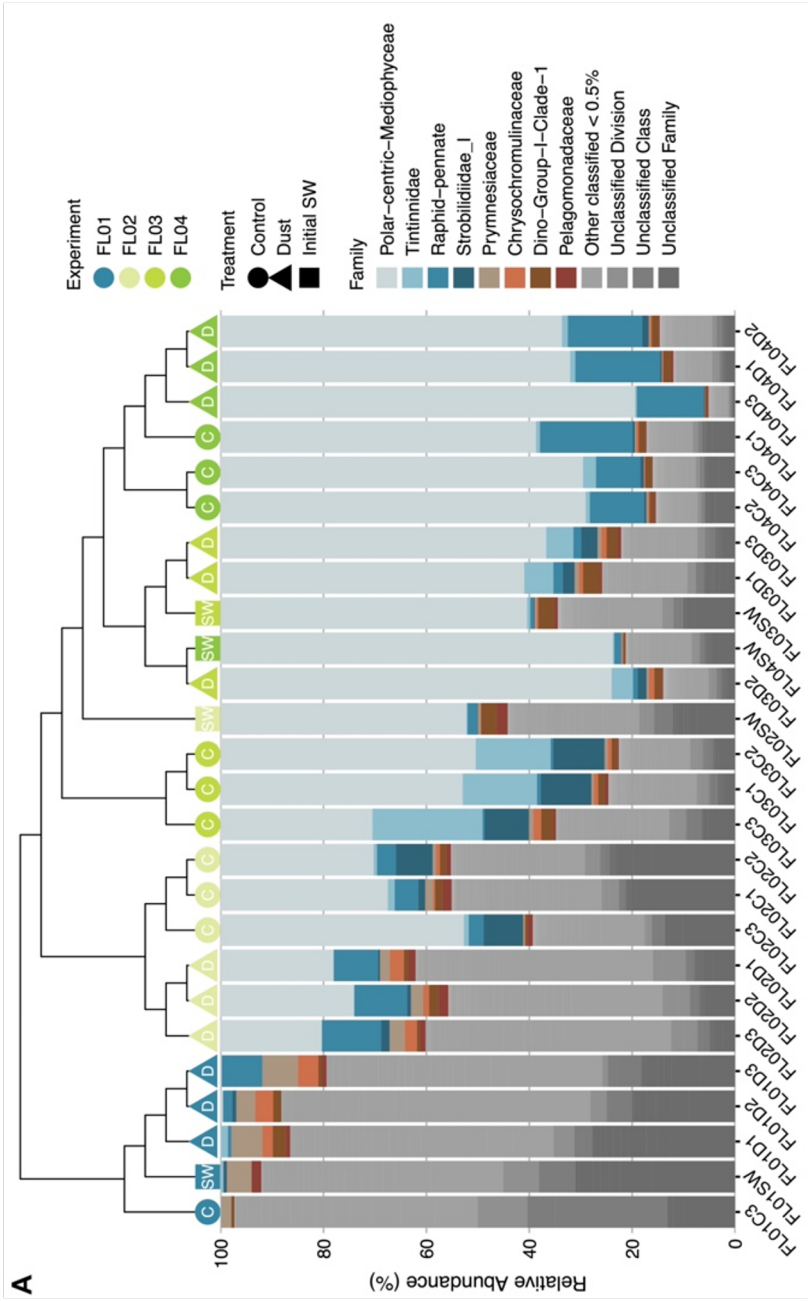

Figure 5. Hierarchical clustering and relative abundance of family-classified **(A)** eukaryotes and **(B)** prokaryotes. Groups are ordered by decreasing median relative abundances. Histograms colours were assigned for all phyla detected with a relative abundance ≥0.5% and/or ≥2%. Data represent the initial time (SW) of the incubations, and control (C) and dust-treated (D) triplicate microcosms at the end of the experiments.

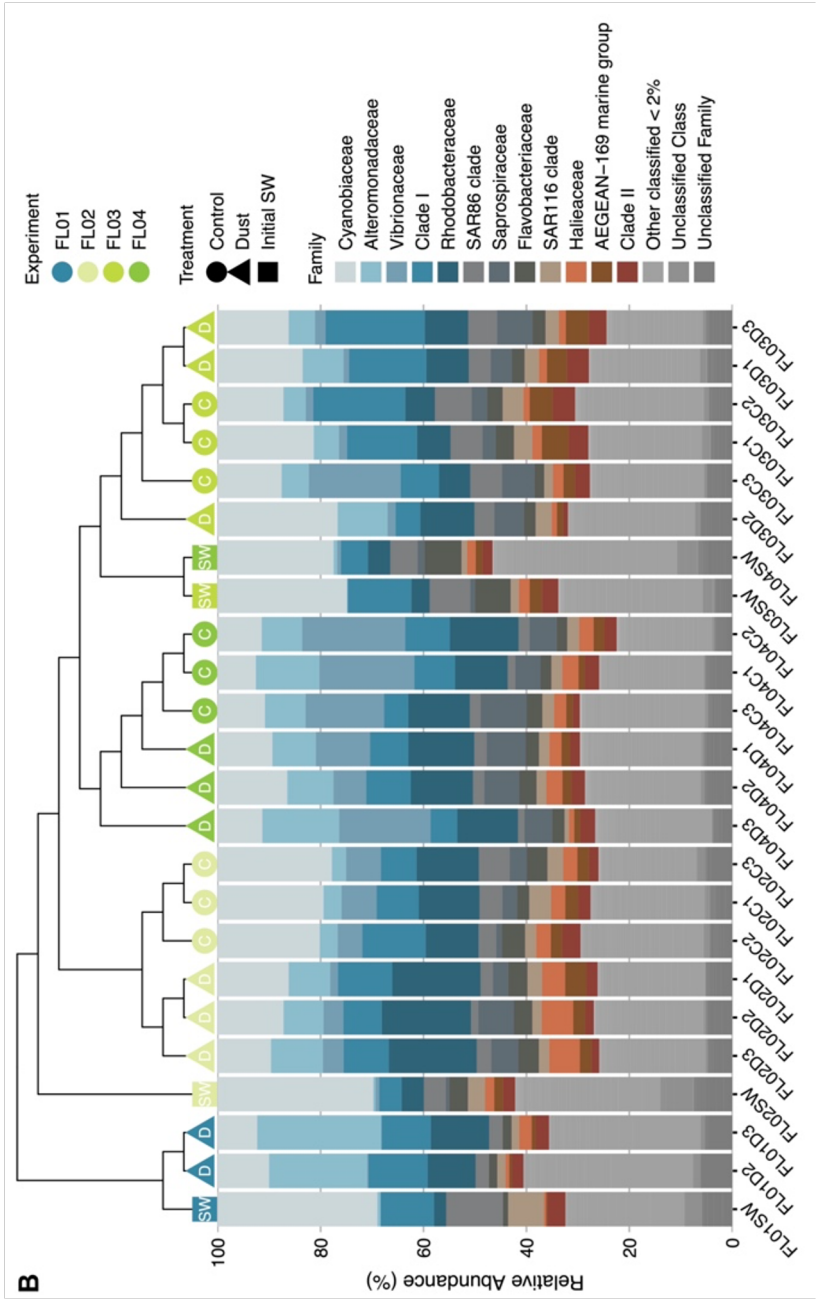

Figure 5. Continued.

No responses to dust addition were observed in prokaryotic alpha diversity when compared to the controls (ΔChao1 and ΔShannon). In this context, dust specially benefited eukaryotic alpha diversity under oligotrophic conditions, and strongly stimulated BP over PP_{TOC}. Yet, in the dust-treated microcosms, greater microbial richness was observed with increasing eutrophic conditions, as opposed to the diversity estimates (**Figure S7**). Therefore, dust inputs unevenly altered microbial alpha diversity among experiments ($p < 0.001$, One-way ANOVA; **Figure S7**). The greatest variations in the response of microbial alpha diversity were found between the oligotrophic experiment and the most eutrophic. Two-way ANOVA results underlined that microbial richness and diversity were primarily modulated by the starting conditions of the incubations ($p < 0.005$, Two-way ANOVA; **Table S5**). Nonetheless, the interaction between dust addition and each experiment singularity had a significant impact on the diversity of eukaryotes ($p < 0.05$, Two-way ANOVA).

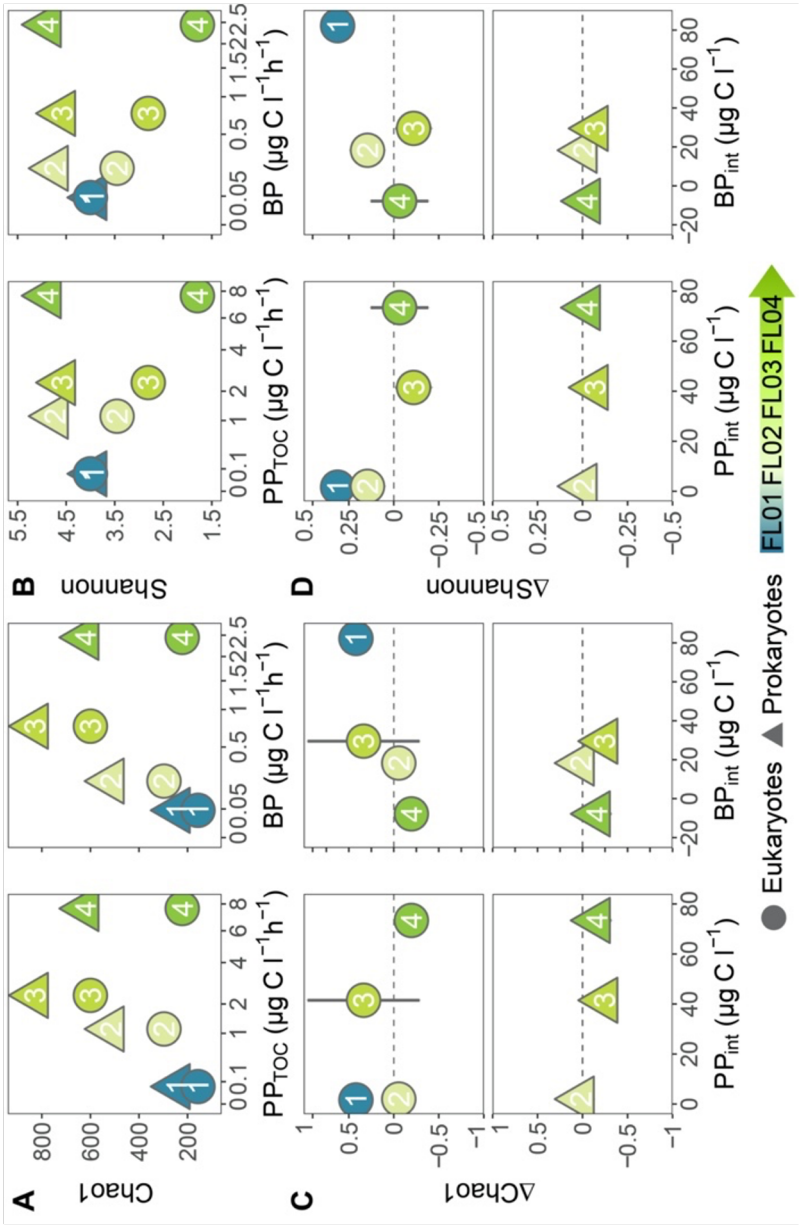

Figure 6. (A) Estimated richness (Chao 1) and **(B)** diversity (Shannon) versus primary production (PP_{TOC}; μg C L^{-1} h^{-1}) and bacterial production (BP; μg C L^{-1} h^{-1}) at the beginning of the incubations. Difference between control and dust-treated microcosms in **(C)** richness and **(D)** diversity estimates at the end of the experiments against the hourly-integrated primary and bacterial production rates (μg C L^{-1}). Each point colour represents an experiment whereas the shape indicates the eukaryotes (circle) and prokaryotes (triangle) datasets. Note that different scales were used.

2.4 Discussion

2.4.1 Metabolic rates

Microbial metabolic rates showed greater changes in response to dust addition than total microbial cell abundances. The uncoupling between cell abundances and metabolic processes was most evident in oligotrophic waters, which was consistent with earlier findings during nutrient (Martínez-García et al., 2010) and dust bioassays (Marañón et al., 2010) along latitudinal transects in the central Atlantic Ocean.

Marañón et al. (2010) presented evidence that the predominant type of metabolic response following dust deposition in the central Atlantic Ocean depended on the ecosystem's degree of oligotrophy and was modulated by the competition for nutrients between microbial communities. The authors observed that primary production response to dust tended to decrease with increasing oligotrophy, whereas the response of bacterial production showed the opposite pattern. Our results agree with their observations in terms of a greater stimulation of bacterial production as oligotrophy increases but differ on the response of phytoplankton metabolism based on the initial environmental conditions. Primary production rates in our experiments showed a lag phase as short as 2 days under moderate and low levels of nutrient concentrations, which was consistent with observations in other oligotrophic areas worldwide (Gazeau et al., 2021; Maki et al., 2021). We assumed that changes in primary production were mediated by a stimulation in the relative contribution of larger phytoplankton cells and picoeukaryotic and picocyanobacterial communities to total abundance and production, as well as by the interactions across microbial communities. Dust bioassays conducted on the Mediterranean Sea underlined the importance of the composition and metabolic state of the initial microbial community on the potential positive effect of dust deposition on microbial metabolism (Dinasquet et al., 2021; Gazeau et al., 2021). While it is true that intense dust deposition induced a favorable effect on the overall autotrophic productivity in our experiments, bacterial production response to dust treatment was sharper than that of primary production. Integrated PP_{TOC} rates in dust-treated microcosms increased between 2% to 28% above the controls, while the ones of BP ranged from ≤31% in the eutrophic experiments to 190% in the oligotrophic experiment. Given the current trend of increased dust deposition (Jickells et al.,

2005) and weakening of the Mauritanian-Senegalese upwelling system under climate change (Sylla et al., 2019), future dust deposition in the region may result in a more heterotrophic system and the decrease in carbon sequestration.

Several nutrient bioassays revealed that autotrophic productivity over the Atlantic Ocean was primarily limited by nitrogen concentration over short timescales (Mills et al., 2004, 2008; Davey et al., 2008; Moore et al., 2008), while heterotrophic productivity was likewise limited by available phosphate and carbon substrates (Mills et al., 2008; Martínez-García et al., 2010). Because Saharan dust deposition provides simultaneous additions of nutrients, such as nitrate, phosphate, iron and organic carbon (Guieu, 2002; Pulido-Villena et al., 2008; this study), one might speculate that the plausible metabolic response would be dependent on the C:N and C:P ratios of dust inputs in the Atlantic Ocean. In this context, integrated PP_{POC} rates in our experiments converted to P (using a 6.6 C:P molar ratio; Martiny et al., 2014) showed that phosphate addition through dust (+0.1 μmol L^{-1}) exceeded phytoplankton P requirements in the oligotrophic incubation (~0.004 μmol P L^{-1}) and barely covered those under eutrophic conditions (~0.1 μmol P L^{-1}, on average). These estimations suggest that the decrease in phosphate seawater concentration right after dust addition was primarily driven by heterotrophic bacteria, particularly under low nutrient concentrations. Nutrient input in the context of an intense dust deposition event would therefore not be sufficient to sustain both the fast response of heterotrophic bacteria and the delayed one of primary producers, which lends support to previous findings in the Mediterranean Sea (Gazeau et al., 2021). Earlier studies found that the apparent success of these bacteria was also related to sources of organic carbon derived from dust deposition (Pulido-Villena et al., 2008). Their smaller cells showing larger surface-to-volume ratios, among other mechanisms, help bacteria access nutrients more efficiently under low nutrient concentrations (Young, 2006). The extent to which phytoplankton was benefited from our pulse of dust deposition was hence influenced by the competition for nutrients between microbial communities.

2.4.2 Cell abundances, structure and composition of microbial communities

Dust enrichment favored the presence of certain planktonic groups over others, even though phytoplankton and bacteria total abundances barely changed compared to controls. This result correlates favorably with previous observations in the Atlantic Ocean (Marañón et al., 2010; Chien et al., 2016).

The release of nutrients through dust enhanced larger phytoplankton cells, associated with either the abundance of diatoms under eutrophic conditions or dinoflagellates in oligotrophic conditions. While the relative abundance of Dinophyceae and Syndiniales (dinoflagellates) decreased throughout the experiments, Bacillariophyta (diatoms) benefited from the dust input. Previous bioassay studies had already underlined the role of diatoms as the main contributors in total phytoplankton biomass (and primary production) following dust deposition, even under oligotrophic conditions where diatoms initially had minor populations (Duarte et al., 2006; Maki et al., 2021). The diatom community in our experiments was dominated by the family Polar-centric-Mediophyceae, who commonly describes phytoplankton functional assemblages (Medlin and Kaczmarska, 2004). However, it was the Raphid-pennate family who took advantage from the dust addition, with a consistent increase of almost 15% of relative abundance throughout the incubations. Although the two families are closely related, Raphid-pennate differs in its high motility and ability to glide over surfaces and through sediment (Adl et al., 2019). The large proportion of soluble nitrate in aerosols in this region (López-García et al., 2021; this study) might have supported the growth of these microphytoplankton organisms, especially under low nutrient environments. The apparent utilization of nitrate by diatoms could explain the observed decline in nitrate seawater concentrations, which was faster with increasing eutrophic conditions. Previous findings in the literature showed that members of the Raphid-pennate family could display a widespread symbiosis with marine diazotroph organisms under persistent nitrate depletion (Schvarcz et al., 2022). Shifts in dissolved silicate concentrations in our dust-treated microcosms could be related to this diatom assemblage, but also to other identified siliceous protists (such as radiolarians and silicoflagellates) and potentially *Synechococcus* cyanobacteria (Baines et al., 2012). Certain bacteria could also accelerate silica dissolution in seawater by enzymatically degrading diatom organic matter, like *Flavobacteriaceae*, *Alteromonadaceae* and *Vibrionaceae* groups (Bidle and Azam, 2001). Therewithal, our approach evidenced that intense dust deposition could not only sustain the proliferation of diatoms (consistent with previous findings, e.g., Maki et al., (2021)) but could also regulate their community structure and composition no matter the initial trophic conditions.

Other members of marine stramenopiles also thrived in our dust-treated microcosms, including heterotrophic protists and several MAST lineages comprising heterotrophic nanoflagellates (such as MAST-1 and -7) (Massana et

al., 2004, 2006). This would imply that total bacteria and/or picophytoplankton abundances in our experiments may be limited by grazing pressure. Nonetheless, our results suggest that changes in total picophytoplankton abundance were driven primarily by picocyanobacterial responses. *Synechococcus* cell abundance increased over the experimental time, being especially significant after 2-3 days, whereas *Prochlorococcus* decreased. Hill et al. (2010) presented evidence that the metabolic activity of *Prochlorococcus* strains in the tropical Northeast Atlantic Ocean was inhibited in the presence of either natural dust or dust-leachate additions. This cyanobacterial genus did not respond strongly to neither nutrient nor dust amendments in the oligotrophic ocean off Barbados (Chien et al., 2016), yet the authors identified that the length of time some *Prochlorococcus* strains stayed in stationary phase was a function of the N:P ratio. Their study suggests that the high atmospheric deposition rates and high N:P ratios sustain P limitation in low-nutrient low-chlorophyll areas and favor phytoplankton with low P requirements and efficient P acquisition mechanisms, such as *Prochlorococcus*. The inability of *Prochlorococcus* to assimilate nitrate is in fact an important factor underlying its distribution (Martiny et al., 2009), which could explain the low abundance of these cyanobacteria in our study region. Since the oligotrophic waters off the Mauritanian-Senegalese region were not only depleted in P but more severely in N, it seems unlikely that *Prochlorococcus* would benefit from elevated dust-leached nutrient concentrations considering that these high quantities of nutrients and dust may be toxic to this microorganism (Paytan et al., 2009). The lack of many regulatory proteins for nutrient uptake in *Prochlorococcus* (Martiny et al., 2009) may also prevent this population to outcompete more abundant picocyanobacterial organisms in the area, like *Synechococcus*. In a time-series study in the western Atlantic, Borchardt et al. (2020) observed an increase in picoeukaryote cellular abundance preceded by a picocyanobacterial peak upon highly processed dust deposition. In contrast, Marañón et al. (2010) reported the concurrent decrease of both cyanobacteria populations following dust deposition in the central North Atlantic while picoeukaryotes abundance increased. Our results confirm those of earlier nutrient bioassays conducted in the tropical North Atlantic Ocean (Davey et al., 2008; Moore et al., 2008), where not only both picocyanobacterial populations but also picoeukaryotes increased after combined N and P or N and Fe additions.

Furthermore, smaller cells reached higher responses to dust addition under low levels of nutrient concentrations. Experiments conducted in the Mediterranean

Sea highlighted haptophytes in the response of active picoeukaryotes to the addition of Saharan dust or European aerosols (Wu et al., 2018). In line with this observation, the relative abundance of Haptophyta (mostly *Prymnesiophyceae*) increased throughout our dust-treated microcosms (<12% of relative abundance), where the species *Chrysochromulina rotalis* was found to be indicative of dust treatment (<0.5% in dust-treated microcosms). Interestingly, the *Chrysochromulina* genus has been previously identified as one of the most abundant grazers of *Prochlorococcus* cyanobacteria in the upper euphotic zone (Li et al., 2022). However, since their abundance was markedly low in our treated microcosms (<3%), their potential effect on *Prochlorococcus* population would be minimal. Likewise, the protist *Labyrinthulomycetes*, who plays an important role in mineralization of marine plankton detritus (Raghukumar, 2002), was found associated with our dust-treated microcosms (<1%).

Total heterotrophic bacteria cell abundances showed minor changes upon dust addition despite the high variability in bacterial community structure. The *Alteromonadaceae* family, which comprises widespread marine bacteria (López-Pérez and Rodriguez-Valera, 2014), benefited the most from the addition of dust in all our experiments albeit especially under oligotrophic conditions. In particular, the presence of the *Alteromonas* genus in our dust-treated microcosms was significant, with increases ranging from 6 to 20% of relative abundance at the end of the experiments. Ecologically, *Alteromonas* are typical *r* strategists that bloom under conditions of sudden increase in the availability of resources (Allers et al., 2007; López-Pérez and Rodriguez-Valera, 2014) hence the likely release of organic matter (and phosphate) from our dust pulse may have triggered its growth. This reproduces previous observations in which *Alteromonadaceae* abundance increased induced by additions of organic matter through aerosol inputs under oligotrophic and nutrient-sufficient seawater conditions (Dinasquet et al., 2021; Maki et al., 2021). This fast-responding strategy upon dust inputs had been also observed on the Vibrio genus (Westrich et al., 2018), in contrast to our results as Vibrio increased regardless of the dust treatment (~10% and ~4% in control and dust-treated microcosms, respectively). Denitrifying bacteria such as *Hyphomonas* were also distinguished at the end of our dust microcosms and especially in the oligotrophic experiment. Another aspect that could have promoted some of these copiotrophic taxa was the release of organic matter by phytoplankton. Previous literature indeed suggests that at least the family of marine *Rhodobacteraceae* was

associated with blooms of diatoms (Grossart et al., 2005), which would explain its presence in our oligotrophic and more notably in eutrophic experiments.

Alpha diversity of the investigated microbial communities was primarily determined by the unique initial characteristics of each experiment (intrinsic local productivity and nutrient availability). Initially, seawater samples exhibited a hump-shaped relationship between productivity and species richness. However, the underlying mechanisms of this widely accepted relationship remain unclear (Mittelbach et al., 2001; Horner-Devine et al., 2003). Earlier studies proposed that increasing productivity may amplify the importance of competition and predation on microbial community composition (Bohannan and Lenski, 2000; Vallina et al., 2014). The strongest competitors were favored at low levels of productivity, while those more resistant to predation thrived at higher productivity levels. Eukaryotic diversity estimates in natural surface seawaters were lower as eutrophic conditions increased, which was explained by the relative increase of sequences related to diatoms. The diversity of prokaryotes was similar albeit highest under natural eutrophic conditions as observed when comparing coastal against open sea diversity. Dust addition in our experiments showed little effect on the above-mentioned alpha diversity patterns and displayed the most significant variations between the oligotrophic experiment versus the most eutrophic one. Despite the trophic gradient was one of the main factors sustaining microbial alpha diversity across the Mauritanian-Senegalese region, intense dust deposition exerted a significant influence on the diversity of eukaryotes on a local scale.

2.5 Conclusions

This study provides a detailed description of the complex response of marine microbial communities to intense dust deposition along a trophic gradient in the coastal transition zone of the subtropical Northeast Atlantic. We show that certain groups of organisms thrived better than others in response to dust addition according to their nutrient requirements. Our dust-treated microcosms were typically characterized by Raphid-pennate diatoms, and by copiotrophic bacteria like *Hyphomonas* (Alphaproteobacteria) and *Alteromonas* (Gammaproteobacteria). However, smaller phytoplankton cells showed larger responses to dust addition as initial nutrient concentrations declined. Picoeukaryote cellular abundance increased, followed by a subsequent peak in *Synechococcus* cell abundance along with a decrease in *Prochlorococcus*. The

dissimilarities between picocyanobacteria populations were related to the N and P co-limitation identified in the region of study. Likewise, intense dust deposition emerges as a key determinant of microbial diversity only when the singularity of the environment (i.e., nutrient bioavailability and productivity conditions) is considered. Dust treatments increased microbial alpha diversity under low nutrient concentrations, as well as promoted bacterial production over primary production. These findings suggest that increasing dust deposition events and weakening of the Mauritanian-Senegalese upwelling system under climate change may result in greater stimulation of bacterial metabolism rather than enhancing primary production, leading to a more heterotrophic system and reducing its potential to function as an atmospheric carbon sink.

Supplementary material

Supplementary methods

Aerosol collection

Aerosols – in the form of total suspended particles (TSP) – were sampled in Pico de la Gorra (Canary Islands; 1930 m above sea level; 27º 56'N, 15º 33'W) and onboard the FLUXES I cruise (Mauritanian-Senegalese upwelling; 17-23º N, 18-25º W). TSP concentrations were estimated a few days before and during the FLUXES I cruise by a dust deposition model predictor (provided by AEMET Barcelona Dust Forecast Center). As not enough TSP concentration was predicted to arrive on board, aerosol filter samples from Pico de la Gorra were used for the microcosm experiments.

At Pico de la Gorra, a time-series record of TSP concentration has been recorded from 1 December 1996 to 31 December 1998 (Torres-Padrón et al., 2002) and 1 December 2001 to the present (Gelado-Caballero et al., 2012; unpublished data). Thereby, glass fiber filters (Whatman GF/A) were loaded on high-volume aerosol samplers to obtain a continuous data set of daily gravimetric measurements over each 7-day period. Simultaneous acid-washed cellulose filters (Whatman 41) for chemical composition analysis were collected one day per week. Filters were selected based on TSP concentrations and the forecast presence of African dust intrusions (see Aerosol Classification). In-detail, aerosol samples from Pico de la Gorra were collected on different seasons between July 11th (2014) and March 09th (2017), while FLUXES I filters were sampled from July 15th to 17th (2017).

Trace metals (Al, Co, Fe, Cu and Mn) and ions (nitrate, phosphate and silicate) concentrations on Pico de la Gorra aerosol filters have been previously published at Gelado-Caballero et al. (2012), while element and nutrient solubility values at López-García et al. (2017). Trace-metal clean techniques were strictly followed throughout the aerosol collection and manipulation.

Aerosol classification

The origin and route of the air masses contributing to each dust sample were tracked by calculating 5-day isentropic back trajectories at 6:00 p.m. UTC using the NOAA HYSPLIT model (Stein et al., 2015) and GDAS meteorological dataset. The chosen altitude levels for the interpretation were 200, 750, 1500, 2000 and 2500 m in 6 h steps. According to Gelado-Caballero et al. (2012),

three geographic sectors were identified based on source region mineralogy aerosol type: AD (African dust, trajectories over the African continent), MAR (maritime aerosol, trajectories over the Atlantic Ocean) and EUR (European and maritime aerosol, trajectories that cross the European continent and the Atlantic Ocean). Differences between African sectors were not taken into account since chemical variability found in previous studies across the region remains negligible (López-García et al., 2017). As the average of the filters exceeded 300 μg TSP m^{-3}, AD was taken as the main source of dust in the present study.

Dust stock solution preparation

A dust stock solution was prepared a few hours before the start of each experiment to preserve the concentration of nutrients. Under a laminar flow cabinet, dry deposited material was extracted from a 1/4 Whatman 41 filter piece into 100 mL of aged, low nutrient surface seawater by sonication for 2 x 15 min in an ultrasonic bath. Aerosol extractions were performed on different Whatman 41 filter pieces and transferred together. At each experiment, the number of filter samples was selected to obtain a dust stock solution of average ~525 mg L^{-1} concentration. The same procedure was performed on identical acid washed blank Whatman 41 filters to assess contamination and/or fertilization effects due to the filter themselves. No particles were detected in this blank solution.

Particle flux simulation

Dust concentrations used to enrich our bioassays were determined based on a maximum dust deposition of ~5500 μg TSP m^{-3} in the Canary Islands (Gelado-Caballero et al., 2012), an average residence time of 20-days and a 30-m mixed layer depth in the region of study. The maximum dust particle concentration was then estimated in 6336 mg m^{-3}, categorized as intense dust deposition. Our dust additions ranged between 4.2 and 6.7 mg of dust per liter of seawater, thus in agreement with the previously simulated intense event.

Supplementary figures

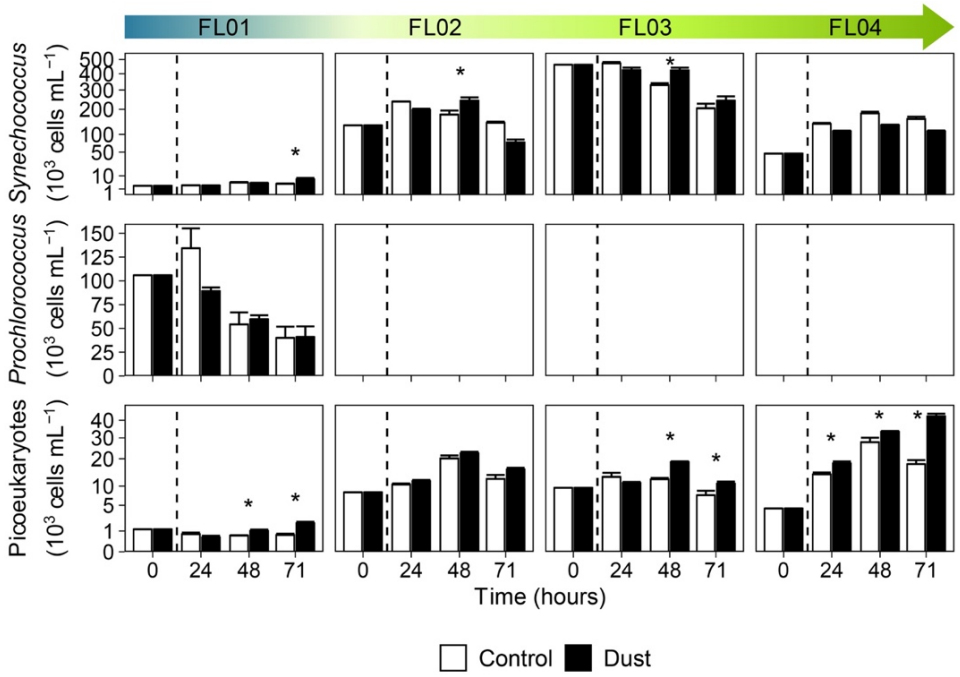

Figure S1. Picophytoplankton abundance (cells mL^{-1}) by identified groups: *Synechococcus* and *Prochlorococcus* cyanobacteria, and picoeukaryotes, in the control (white bars) and dust-treated microcosms (black bars). The vertical line indicates the dust addition time. Each data point represents the average and standard deviation of three replicated microcosms. The asterisk denotes where the value of dust triplicates was significantly greater than control ($p < 0.05$, Wilcoxon test). Note that different scales were used.

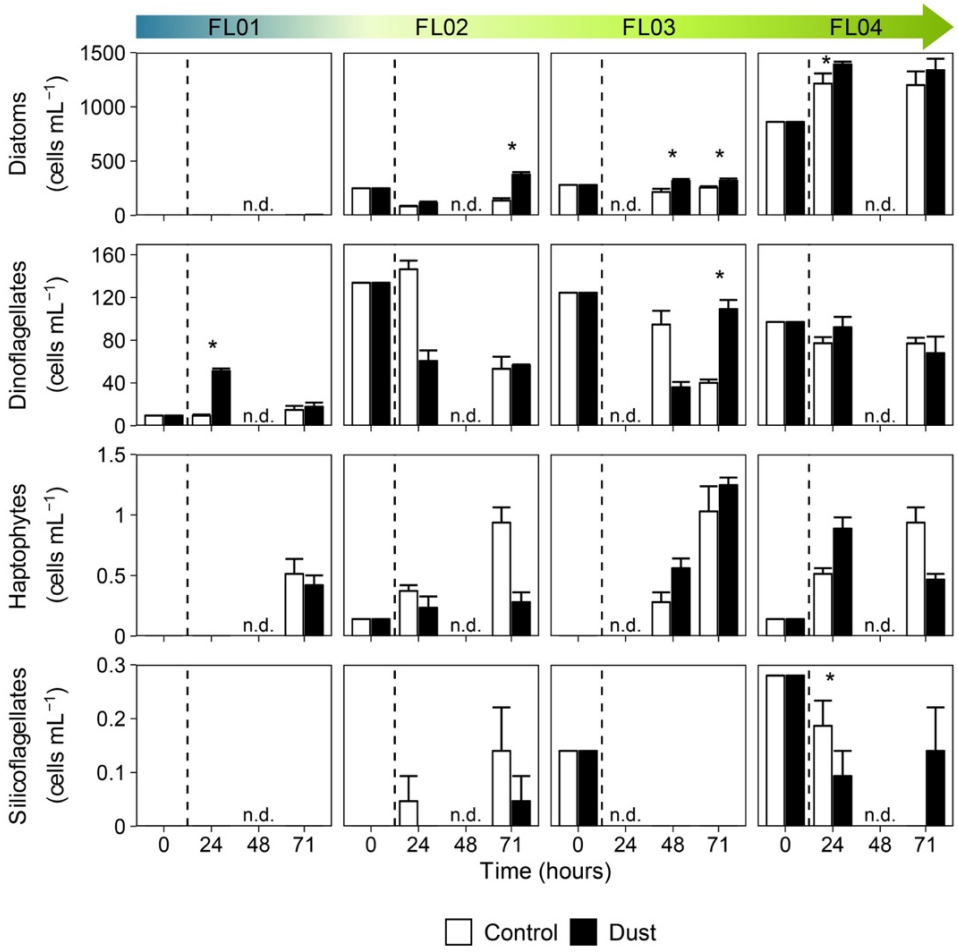

Figure S2. Microphytoplankton abundance (cells mL^{-1}) by groups: diatoms, dinoflagellates, haptophytes and silicoflagellates, in the control (white bars) and dust-treated microcosms (black bars). The vertical line indicates the dust addition time. Each data point represents the average and standard deviation of three replicated microcosms. The asterisk denotes where the value of dust triplicates was significantly greater than control ($p < 0.05$, Wilcoxon test). The abbreviation n.d. (no-data) indicate the absence of data at that time of the experimental incubation. Note that different scales were used.

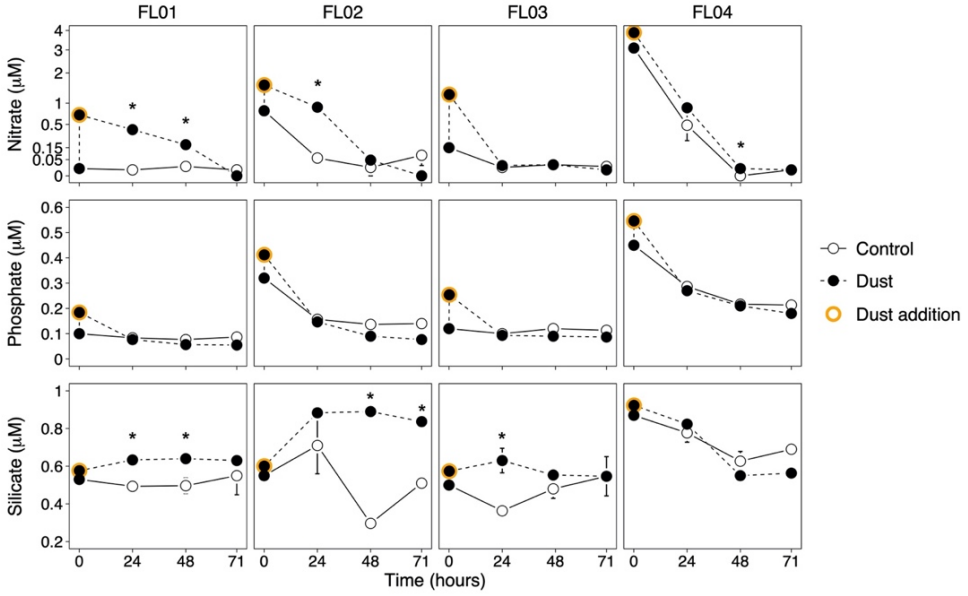

Figure S3. Inorganic nutrient concentration (μmol L^{-1}) in the control (white points) and dust-treated microcosms (black points). The orange circle indicates the dust addition time. Each data point represents the average and standard deviation of three replicated microcosms. The asterisk denotes where the value of dust triplicates was significantly greater than control ($p < 0.05$, Wilcoxon test). Note that different scales were used.

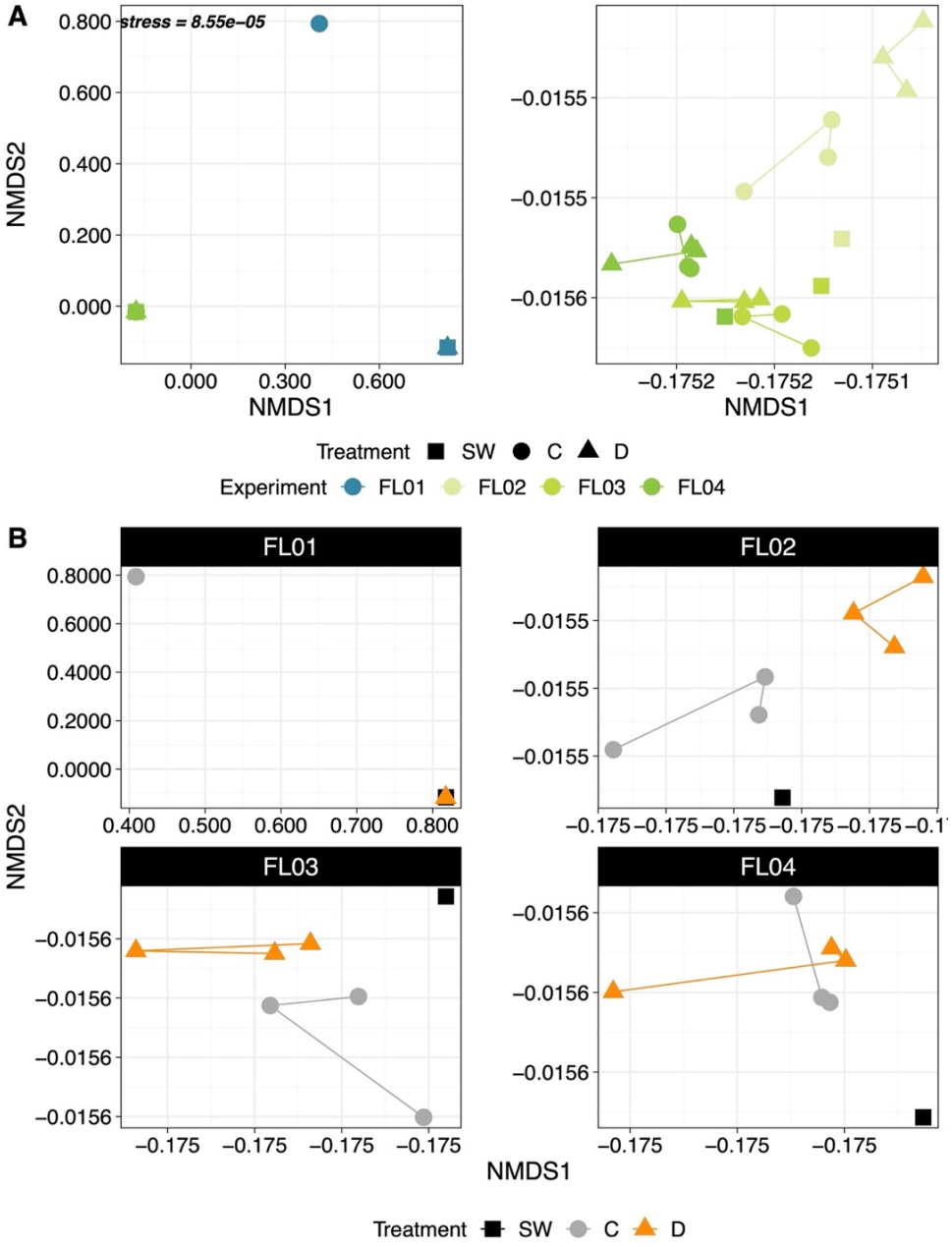

Figure S4. NMDS (Non-metric Multidimensional scaling) plots based on Bray-Curtis dissimilarities of eukaryotic diversity samples from FLUXES experiments. Point colors were assigned by **(A)** experiment and **(B)** treatment.

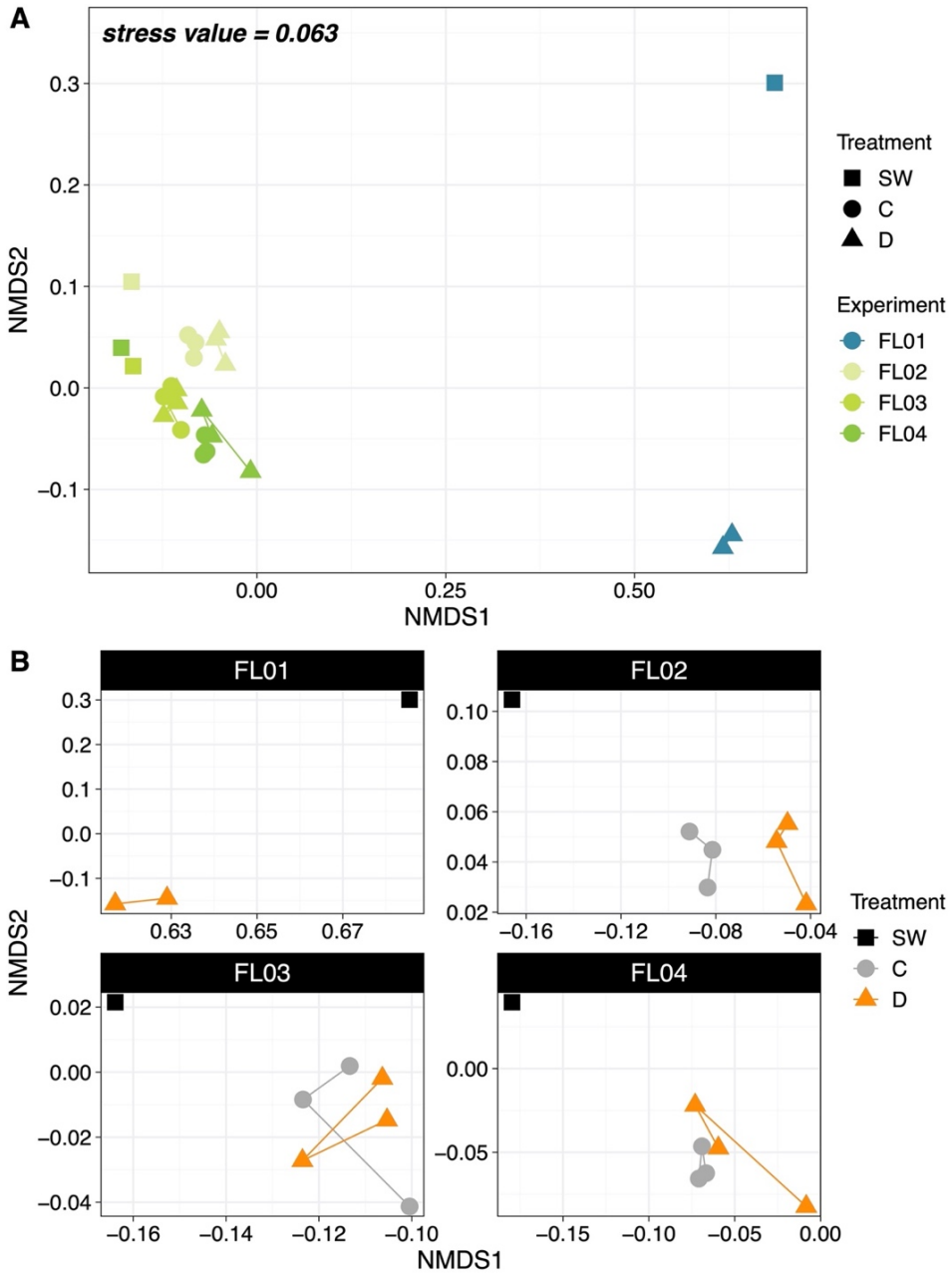

Figure S5. NMDS (Non-metric Multidimensional scaling) plots based on Bray-Curtis dissimilarities of prokaryotic diversity samples from FLUXES experiments. Point colors were assigned by **(A)** experiment and **(B)** treatment.

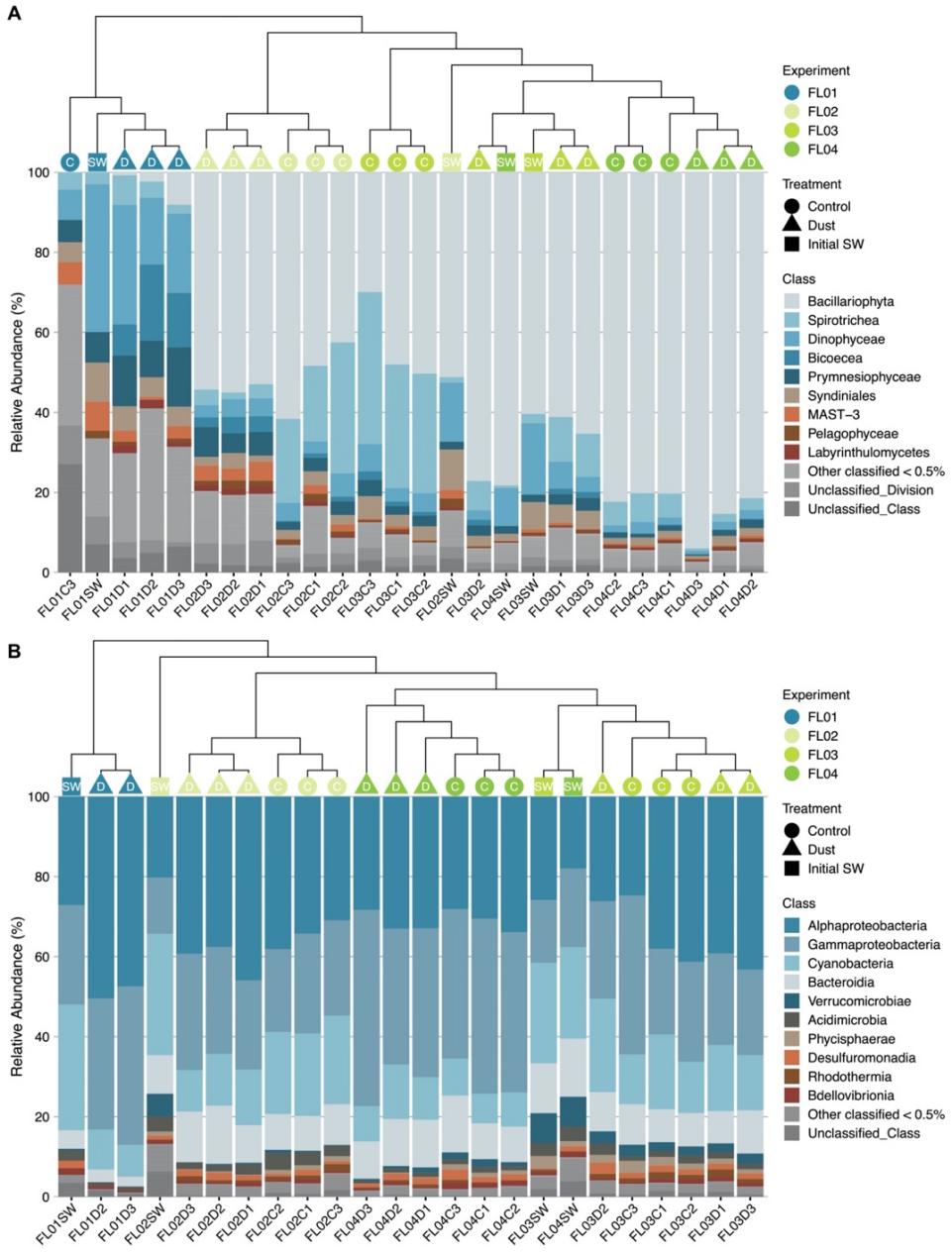

Figure S6. Hierarchical clustering and relative abundance of class-classified **(A)** eukaryotes and **(B)** prokaryotes. Groups are ordered by decreasing median relative abundances. Histograms colours were assigned for all phyla detected with a relative abundance ≥ 0.5%. Data represent the initial time (SW) of the incubations, and control (C) and dust-treated (D) triplicate microcosms at the end of the experiments.

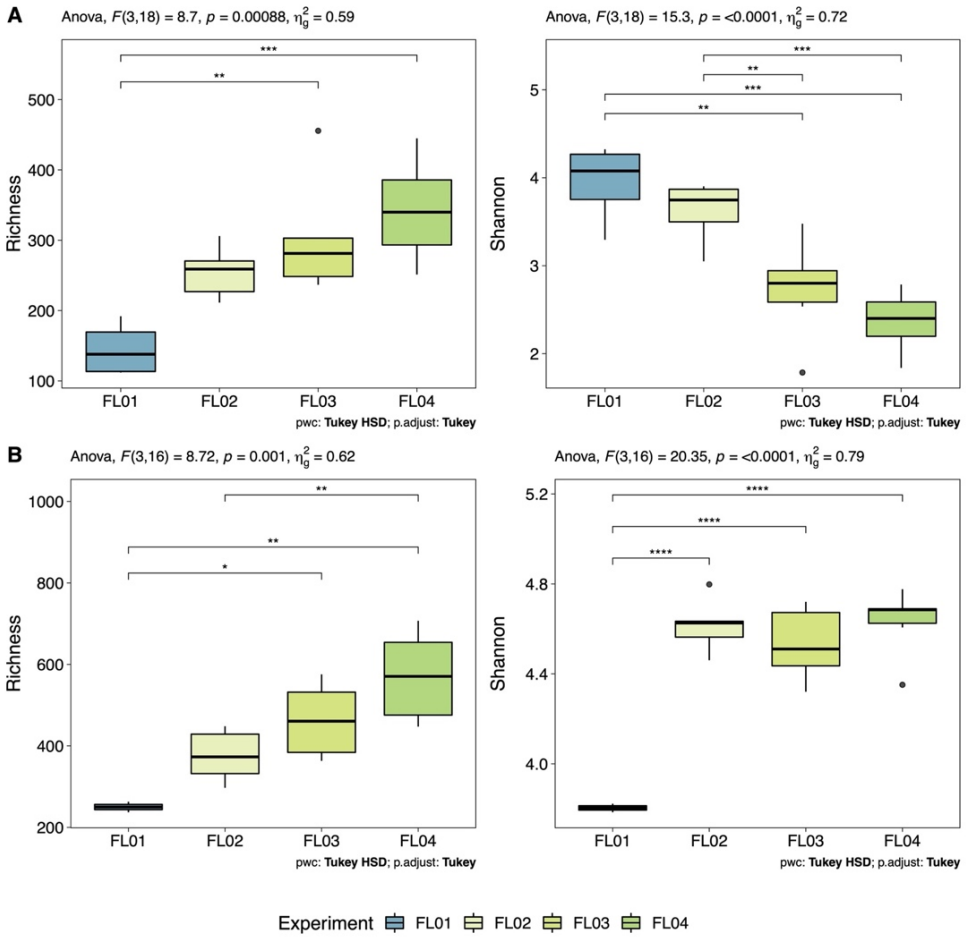

Figure S7. One-way ANOVA and *post-hoc* Tukey HSD test comparing **(A)** eukaryotic and **(B)** prokaryotic Chao1 richness and Shannon diversity estimates across the four experiments. Data correspond to the end of the experiments. Significance level of 0.05 (*), 0.01 (**), 0.001 (***) and 0.0001 (****).

Supplementary tables

Table S1. Results from Wilcoxon Signed-Rank test on inorganic nutrients, phytoplankton size-groups and bacteria abundance and production differences between control and dust-treated microcosms for each experiment. The abbreviation n.d. (no-data) indicate the absence of data at that time of the experimental incubation. Significance level of 0.05 (*), 0.005 (**) and 0.001 (***).

		Wilcoxon Signed-Rank test (*p* value)											
Exp	Time	Nit	Phos	Sil	Chl *a*	Micro	Nano	Pico	PP_{DOC}	PP_{POC}	PP_{TOC}	Bact	BP
FL01	24	0.04*	0.94	0.04*	0.33	0.04*	0.09	0.98	0.98	0.81	0.98	0.67	0.04*
	48	0.04*	0.99	0.04*	n.d.	n.d.	0.04*	0.33	n.d.	n.d.	n.d.	0.5	n.d.
	71	0.89	0.98	0.39	0.09	0.19	0.04*	0.5	0.27	0.04*	0.27	0.19	0.19
FL02	24	0.04*	0.91	0.33	0.5	0.99	0.99	0.98	0.61	0.81	0.39	0.09	0.33
	48	0.13	0.99	0.03*	n.d.	n.d.	0.19	0.04*	n.d.	n.d.	n.d.	0.5	n.d.
	71	0.99	0.99	0.04*	0.04*	0.04*	0.09	0.98	0.04*	0.67	0.5	0.98	0.09

Notes. Exp: Experiment; Nir: Nitrate; Phos: Phosphate; Sil: Silicate; Chl *a*: Chlorophyll *a*; Micro: Microphytoplankton abundance; Nano: Nanophytoplankton abundance; Pico: Picophytoplankton abundance; PP_{DOC}: Dissolved Organic Carbon Primary Production; PP_{POC}: Particulate Organic Carbon Primary Production; PP_{TOC}: Total Organic Carbon Primary Production; Bact: Bacterial abundance; BP: Bacterial Production.

Table S1. Continued.

		Wilcoxon Signed-Rank test (*p* value)											
Exp	Time	Nit	Phos	Sil	Chl *a*	Micro	Nano	Pico	PP_{DOC}	PP_{POC}	PP_{TOC}	Bact	BP
FL03	24	0.33	0.88	0.04*	n.d.	n.d.	0.04*	0.98	n.d.	n.d.	n.d.	0.09	n.d.
	47	0.68	0.99	0.19	0.04*	0.33	0.04*	0.04*	0.04*	0.04*	0.04*	0.04*	0.33
	71	0.91	0.99	0.5	0.33	0.04*	0.04*	0.19	0.88	0.12	0.12	0.81	0.04*
FL04	24	0.19	0.82	0.33	0.19	0.04*	0.33	0.98	0. 98	0.07	0.07	0.33	0.90
	48	0.02*	0.87	0.94	n.d.	n.d.	0.81	0.98	n.d.	n.d.	n.d.	0.67	n.d.
	71	0.68	0.96	0.99	0.19	0.33	0.09	0.98	0.04*	0.07	0.07	0.5	0.81

Notes. Exp: Experiment; Nir: Nitrate; Phos: Phosphate; Sil: Silicate; Chl *a*: Chlorophyll *a*; Micro: Microphytoplankton abundance; Nano: Nanophytoplankton abundance; Pico: Picophytoplankton abundance; PP_{DOC}: Dissolved Organic Carbon Primary Production; PP_{POC}: Particulate Organic Carbon Primary Production; PP_{TOC}: Total Organic Carbon Primary Production; Bact: Bacterial abundance; BP: Bacterial Production.

Table S2. Results from Kruskal-Wallis and *post-hoc* Conover tests inorganic nutrients, and phytoplankton and bacterial abundance and production differences between the dust-treated microcosms of all four experiments at 24-hour sampling time. The abbreviation n.d. (no-data) indicate the absence of data at that time of the experimental incubation. Bonferroni adjusted *p* values. Significance level of 0.05 (*), 0.005 (**) and 0.001 (***).

	Kruskal-Wallis test (*p* value)	*Post-hoc* Conover test (*p* value)					
	Sampling time	Experiment pair					
	24 h	1 – 2	1 – 3	2 – 3	1 – 4	2 – 4	3 – 4
Nitrate	0.02*	0.02*	0.15	0.001**	0.04*	1	0.002**
Phosphate	0.01*	2.97e-05***	0.0036**	0.004**	1.35e-06***	0.0036**	2.97e-05***
Silicate	0.02*	0.0007***	1	0.002**	0.01*	0.14	0.04*
Chl *a*	0.03*	0.01*	n.d.	n.d.	0.0005***	0.01*	n.d.
Microphytoplankton abundance	n.d.	n.d.	n.d.	n.d.	n.d.	n.d.	n.d.
Nanophytoplankton abundance	0.01*	0.02*	2.40e-04***	0.02*	1.22e-05***	2.40e-04***	0.02*
Picophytoplankton abundance	0.01*	2.40e-04***	1.22e-05***	0.02*	0.02*	0.02*	2.40e-04***
Phytoplankton production (PP_{DOC})	0.04*	0.02*	n.d.	n.d.	0.002**	0.05	n.d.
Phytoplankton production (PP_{POC})	0.04*	0.02*	n.d.	n.d.	0.002**	0.05	n.d.
Phytoplankton production (PP_{TOC})	0.04*	0.02*	n.d.	n.d.	0.002**	0.05	n.d.
Bacterial abundance	0.01*	0.02*	1.22e-05***	2.40e-04***	2.40e-04***	0.02*	0.02*
Bacterial production	0.04*	0.12	n.d.	n.d.	0.003**	0.04*	n.d.

Table S3. Eukaryote and bacteria indicator species ($p < 0.05$ and $stat > 0.75$) for the control microcosms. The parameter *str* indicates the strength of the association between a species and the site-group (seawater used to fill the microcosms, SW; control microcosms, C; dust-treated microcosms, D). The abbreviation *stat* indicates the association value and *p* the degree of statistical significance of the association (*p* values are based on 999 permutations). Significance level of 0.05 (*), 0.005 (**) and 0.001 (***). The dash symbol (–) indicates unclassified taxa.

OTU	Kingdom	Supergroup	Division	Class	Order	Family	Genus	Species	str_{SW}	str_{C}	str_{D}	*stat*	*p*
ASV_35	Eukaryota	Alveolata	Ciliophora	Spirotrichea	Tintinnida	Tintinnidae	–	–	0.161	0.827	0.307	0.83	0.008*
ASV_17	Eukaryota	Alveolata	Ciliophora	Spirotrichea	Choreotrichida	Strobilidiidae_I	–	–	0	0.825	0.319	0.82	0.01*
ASV_73	Eukaryota	Alveolata	Ciliophora	Spirotrichea	Choreotrichida	Strobilidiidae_I	*Pelagostrobilidium*	*Pelagostrobilidium paraepacrum*	0.084	0.752	0.069	0.75	0.04*
ASV_10	Eukaryota	Alveolata	Ciliophora	Spirotrichea	Tintinnida	Tintinnidae	–	–	0.223	0.836	0.341	0.84	0.05*
ASV_47	Bacteria	–	Proteobacteria	Gammaproteobacteria	Enterobacterales	*Alteromonadaceae*	*Salinimonas*	–	0.168	0.798	0.486	0.80	0.001***
ASV_266	Bacteria	–	Bacteroidota	Bacteroidia	Flavobacteriales	*NS7 marine group*	–	–	0.285	0.865	0.155	0.86	0.001***

Table S3. Continued.

OTU	Kingdom	Supergroup	Division	Class	Order	Family	Genus	Species	str_{SW}	str_{C}	str_{D}	*stat*	*p*
ASV_88	Bacteria	–	Planctomycetota	Phycisphaerae	Phycisphaerales	*Phycisphaeraceae*	*Urania-1B-19 marine sediment group*	–	0.468	0.789	0.198	0.79	0.004**
ASV_3	Bacteria	–	Proteobacteria	Gammaproteobacteria	Enterobacterales	*Vibrionaceae*	*Vibrio*	*artabrorum/atlanticus/…*	0.04	0.824	0.535	0.82	0.005**
ASV_469	Bacteria	–	Planctomycetota	Phycisphaerae	Phycisphaerales	*Phycisphaeraceae*	*CL500-3*	–	0.226	0.787	0	0.79	0.009**
ASV_185	Bacteria	–	Proteobacteria	Alphaproteobacteria	Puniceispirillales	*SAR116 clade*	–	–	0.308	0.782	0.403	0.78	0.01*
ASV_258	Bacteria	–	Proteobacteria	Alphaproteobacteria	SAR11 clade	*Clade IV*	–	–	0.161	0.783	0.274	0.78	0.02*
ASV_144	Bacteria	–	Proteobacteria	Alphaproteobacteria	Rhizobiales	*Stappiaceae*	*Labrenzia*	*marina*	0	0.762	0.617	0.76	0.02*
ASV_410	Bacteria	–	Bacteroidota	Bacteroidia	Flavobacteriales	*Flavobacteriaceae*	*Aureicoccus*	*marinus*	0	0.771	0.327	0.77	0.03*

Table S4. Eukaryote and bacteria indicator species ($p < 0.05$ and $stat > 0.75$) for the dust-treated microcosms. The parameter *str* indicates the strength of the association between a species and the site-group (seawater used to fill the microcosms, SW; control microcosms, C; dust-treated microcosms, D). The abbreviation *stat* indicates the association value and *p* the degree of statistical significance of the association (*p* values are based on 999 permutations). Significance level of 0.05 (*), 0.005 (**) and 0.001 (***). The dash symbol (–) indicates unclassified taxa.

OTU	Kingdom	Supergroup	Division	Class	Order	Family	Genus	Species	str_{SW}	str_{C}	str_{D}	*stat*	*p*
ASV_5	Eukaryota	Stramenopiles	Ochrophyta	Bacillariophyta	Bacillariophyta_X	Raphid-pennate	–	–	0.231	0.529	0.786	0.79	0.01*
ASV_258	Eukaryota	Hacrobia	Haptophyta	Prymnesiophyceae	Prymnesiales	Chrysochromulinaceae	*Chrysochromulina*	*Chrysochromulina_rotalis*	0	0.302	0.798	0.80	0.02*
ASV_57	Eukaryota	Stramenopiles	Sagenista	Labyrinthulomycetes	Labyrinthulomycetes_X	Labyrinthulomycetes_X_LAB7	*Labyrinthulomycetes_X_LAB7_X*	*Labyrinthulomycetes_X_LAB7_X_sp.*	0.22	0.317	0.821	0.82	0.03*
ASV_118	Eukaryota	Stramenopiles	–	–	–	–	–	–	0	0.07	0.754	0.75	0.04*
ASV_5	Bacteria	–	Proteobacteria	Gammaproteobacteria	Enterobacterales	*Alteromonadaceae*	*Alteromonas*	*alvinellae/australica/…*	0.163	0.5	0.85	0.85	0.001***
ASV_13	Bacteria	–	Proteobacteria	Alphaproteobacteria	Caulobacterales	*Hyphomonadaceae*	*Hyphomonas*	*atlantica/johnsonii*	0	0.18	0.979	0.98	0.001***

Table S4. Continued.

OTU	Kingdom	Supergroup	Division	Class	Order	Family	Genus	Species	str_{SW}	str_{C}	str_{D}	*stat*	*p*
ASV_109	Bacteria	–	Proteobacteria	Gammaproteobacteria	Enterobacterales	*Alteromonadaceae*	*Alteromonas*	–	0.15	0.573	0.801	0.80	0.005**
ASV_43	Bacteria	–	Proteobacteria	Gammaproteobacteria	Enterobacterales	*Alteromonadaceae*	–	–	0.03	0.531	0.824	0.82	0.01*
ASV_254	Bacteria	–	Proteobacteria	Alphaproteobacteria	Sphingomonadales	*Sphingomonadaceae*	*Erythrobacter*	*citreus*	0	0.146	0.875	0.87	0.01*
ASV_269	Bacteria	–	Proteobacteria	Gammaproteobacteria	Enterobacterales	*Colwelliaceae*	*Colwellia*	–	0.232	0.261	0.777	0.78	0.03*
ASV_16	Bacteria	–	Proteobacteria	Gammaproteobacteria	Enterobacterales	*Alteromonadaceae*	*Alteromonas*	*australica*	0.019	0.627	0.778	0.78	0.03*
ASV_444	Bacteria	–	Proteobacteria	Gammaproteobacteria	Enterobacterales	*Alteromonadaceae*	*Aestuariibacter*	–	0	0.328	0.766	0.77	0.03*
ASV_76	Bacteria	–	Proteobacteria	Alphaproteobacteria	Rhodobacterales	*Rhodobacteraceae*	*Thalassobius*	–	0	0.439	0.801	0.80	0.05*

Table S5. Two-way ANOVA test comparing eukaryotic and prokaryotic Chao1 richness and Shannon diversity estimates on the interaction between Treatment and Experiment. Data correspond to the end of the experiments. Significance level of 0.05 (*), 0.005 (**) and 0.001 (***).

	Dataset	Eukaryotic			Prokaryotic		
	Effect	Experiment	Treatment	Experiment:Treatment	Experiment	Treatment	Experiment:Treatment
Chao1 richness	DFn	3	1	3	3	1	2
	DFd	14	14	14	13	13	13
	F	8.778	0.004	1.588	7.829	1.059	1.053
	p	0.002**	0.949	0.237	0.003**	0.322	0.377
	ges	0.653	0.0003	0.254	0.644	0.075	0.139
Shannon diversity	DFn	3	1	3	3	1	2
	DFd	14	14	14	13	13	13
	F	24.485	0.019	5.116	17.296	1.871	0.884
	p	7.85e-06***	0.892	0.013*	0.00008***	0.195	0.436
	ges	0.840	0.001	0.523	0.800	0.126	0.120

References

Amaral-Zettler, L. A., McCliment, E. A., Ducklow, H. W., and Huse, S. M. (2009). A Method for Studying Protistan Diversity Using Massively Parallel Sequencing of V9 Hypervariable Regions of Small-Subunit Ribosomal RNA Genes. PLOS ONE 4, e6372. doi: 10.1371/journal.pone.0006372

Apprill, A., McNally, S., Parsons, R., and Weber, L. (2015). Minor revision to V4 region SSU rRNA 806R gene primer greatly increases detection of SAR11 bacterioplankton. Aquat. Microb. Ecol. 75, 129–137. doi: 10.3354/ame01753

Blain, S., Guieu, C., Claustre, H., Leblanc, K., Moutin, T., Quèguiner, B., et al. (2004). Availability of iron and major nutrients for phytoplankton in the northeast Atlantic Ocean. Limnol. Oceanogr. 49, 2095–2104. doi: 10.4319/lo.2004.49.6.2095

Bonnet, S., Guieu, C., Chiaverini, J., Ras, J., and Stock, A. (2005). Effect of atmospheric nutrients on the autotrophic communities in a low nutrient, low chlorophyll system. Limnol. Oceanogr. 50, 1810–1819. doi: 10.4319/lo.2005.50.6.1810

Callahan, B. J., McMurdie, P. J., Rosen, M. J., Han, A. W., Johnson, A. J. A., and Holmes, S. P. (2016). DADA2: High-resolution sample inference from Illumina amplicon data. Nat Methods 13, 581–583. doi: 10.1038/nmeth.3869

Chien, C.-T., Mackey, K. R. M., Dutkiewicz, S., Mahowald, N. M., Prospero, J. M., and Paytan, A. (2016). Effects of African dust deposition on phytoplankton in the western tropical Atlantic Ocean off Barbados: Dust Deposition and Phytoplankton Growth. Global Biogeochem. Cycles 30, 716–734. doi: 10.1002/2015GB005334

De Cáceres, M., and Legendre, P. (2009). Associations between species and groups of sites: indices and statistical inference. Ecology 90, 3566–3574. doi: 10.1890/08-1823.1

Dinno, A. (2017). conover.test: Conover-Iman test of multiple comparisons using rank sums. R software package. Available at: https://alexisdinno.com/stata/conovertest.html

Duarte, C. M., Dachs, J., Llabrés, M., Alonso-Laita, P., Gasol, J. M., Tovar-Sánchez, A., et al. (2006). Aerosol inputs enhance new production in the subtropical northeast Atlantic. J. Geophys. Res. 111. doi: 10.1029/2005JG000140

Gazeau, F., Van Wambeke, F., Marañón, E., Pérez-Lorenzo, M., Alliouane, S., Stolpe, C., et al. (2021). Impact of dust addition on the metabolism of Mediterranean plankton communities and carbon export under present and future conditions of pH and temperature. Biogeosciences 18, 5423–5446. doi: 10.5194/bg-18-5423-2021

Gelado-Caballero, M. D., López-García, P., Prieto, S., Patey, M. D., Collado, C., and Hérnández-Brito, J. J. (2012). Long-term aerosol measurements in Gran Canaria, Canary Islands: Particle concentration, sources and elemental composition. J. Geophys. Res. 117, n/a-n/a. doi: 10.1029/2011JD016646

Guieu, C., Loÿe-Pilot, M.-D., Ridame, C., and Thomas, C. (2002). Chemical characterization of the Saharan dust end-member: Some biogeochemical implications for the western

Mediterranean Sea. Journal of Geophysical Research: Atmospheres 107, ACH 5-1-ACH 5-11. doi: 10.1029/2001JD000582

Guieu, C., Ridame, C., Pulido-Villena, E., Bressac, M., Desboeufs, K., and Dulac, F. (2014). Impact of dust deposition on carbon budget: a tentative assessment from a mesocosm approach. Biogeosciences 11, 5621–5635. doi: 10.5194/bg-11-5621-2014

Guillou, L., Bachar, D., Audic, S., Bass, D., Berney, C., Bittner, L., et al. (2013). The Protist Ribosomal Reference database (PR2): a catalog of unicellular eukaryote small sub-unit rRNA sequences with curated taxonomy. Nucleic Acids Research 41, D597-604. doi: 10.1093/nar/gks1160

Hale, M. S., Li, W. K. W., and Rivkin, R. B. (2017). Meridional patterns of inorganic nutrient limitation and co-limitation of bacterial growth in the Atlantic Ocean. Prog. Oceanogr. 158, 90–98. doi: 10.1016/j.pocean.2016.11.007

Herut, B., Rahav, E., Tsagaraki, T. M., Giannakourou, A., Tsiola, A., Psarra, S., et al. (2016). The Potential Impact of Saharan Dust and Polluted Aerosols on Microbial Populations in the East Mediterranean Sea, an Overview of a Mesocosm Experimental Approach. Front. Mar. Sci. 3. doi: 10.3389/fmars.2016.00226

Herut, B., Zohary, T., Krom, M. D., Mantoura, R. F. C., Pitta, P., Psarra, S., et al. (2005). Response of East Mediterranean surface water to Saharan dust: On-board microcosm experiment and field observations. Deep Sea Research Part II: Topical Studies in Oceanography 52, 3024–3040. doi: 10.1016/j.dsr2.2005.09.003

Hill, P. G., Zubkov, M. V., and Purdie, D. A. (2010). Differential responses of Prochlorococcus and SAR11-dominated bacterioplankton groups to atmospheric dust inputs in the tropical Northeast Atlantic Ocean. FEMS Microbiology Letters 306, 82–89. doi: 10.1111/j.1574-6968.2010.01940.x

Holm-Hansen, O., Lorenzen, C. J., Holmes, R. W., and Strickland, J. D. H. (1965). Fluorometric determination of chlorophyll. J. Cons. perm. int. Explor. Mer 30, 3–15. doi: 10.1093/icesjms/30.1.3

Jickells, T. D. (2005). Global Iron Connections Between Desert Dust, Ocean Biogeochemistry, and Climate. Science 308, 67–71. doi: 10.1126/science.1105959

Jickells, T. D., Baker, A. R., and Chance, R. (2016). Atmospheric transport of trace elements and nutrients to the oceans. Phil. Trans. R. Soc. A 374, 20150286. doi: 10.1098/rsta.2015.0286

Joint, I., Henriksen, P., Fonnes, G., Bourne, D., Thingstad, T., and Riemann, B. (2002). Competition for inorganic nutrients between phytoplankton and bacterioplankton in nutrient manipulated mesocosms. Aquat. Microb. Ecol. 29, 145–159. doi: 10.3354/ame029145

Kassambara, A. (2020). ggpubr: "ggplot2" Based Publication Ready Plots. R package version 0.4.0. Available at: https://CRAN.R-project.org/package=ggpubr

Kassambara, A. (2021). rstatix: Pipe-Friendly Framework for Basic Statistical Tests. R package version 0.7.0. Available at: https://CRAN.R-project.org/package=rstatix

Kirchman, D., and Ducklow, H. (1993). "Estimating conversion factors for the Thymidine and Leucine methods for measuring bacterial production," in Handbook of Methods in Aquatic Microbial Ecology., (Lewis Publishers, Boca Raton, FL), 513–517.

Langlois, R. J., Mills, M. M., Ridame, C., Croot, P., and LaRoche, J. (2012). Diazotrophic bacteria respond to Saharan dust additions. Mar. Ecol. Prog. Ser. 470, 1–14. doi: 10.3354/meps10109

Lekunberri, I., Lefort, T., Romero, E., Vázquez-Domínguez, E., Romera-Castillo, C., Marrasé, C., et al. (2010). Effects of a dust deposition event on coastal marine microbial abundance and activity, bacterial community structure and ecosystem function. J. Plankton Res. 32, 381–396. doi: 10.1093/plankt/fbp137

López-García, P., Gelado-Caballero, M. D., Patey, M. D., and Hernández-Brito, J. J. (2021). Atmospheric fluxes of soluble nutrients and Fe: More than three years of wet and dry deposition measurements at Gran Canaria (Canary Islands). Atmos. Environ. 246, 118090. doi: 10.1016/j.atmosenv.2020.118090

López-García, P., Gelado-Caballero, M. D., Collado-Sánchez, C., and Hernández-Brito, J. J. (2017). Solubility of aerosol trace elements: Sources and deposition fluxes in the Canary Region. Atmos. Environ. 148, 167–174. doi: 10.1016/j.atmosenv.2016.10.035

López-García, P., Gelado-Caballero, M. D., Santana-Castellano, D., Suárez de Tangil, M., Collado-Sánchez, C., and Hernández-Brito, J. J. (2013). A three-year time-series of dust deposition flux measurements in Gran Canaria, Spain: A comparison of wet and dry surface deposition samplers. Atmos. Environ. 79, 689–694. doi: 10.1016/j.atmosenv.2013.07.044

Marañón, E., Fernández, A., Mouriño-Carballido, B., MartÍnez-GarcÍa, S., Teira, E., Cermeño, P., et al. (2010). Degree of oligotrophy controls the response of microbial plankton to Saharan dust. Limnol. Oceanogr. 55, 2339–2352. doi: 10.4319/lo.2010.55.6.2339

Martin, M. (2011). Cutadapt removes adapter sequences from high-throughput sequencing reads. EMBnet.journal 17, 10–12. doi: 10.14806/ej.17.1.200

McMurdie, P. J., and Holmes, S. (2013). phyloseq: An R Package for Reproducible Interactive Analysis and Graphics of Microbiome Census Data. PLOS ONE 8, e61217. doi: 10.1371/journal.pone.0061217

Mills, M. M., Moore, C. M., Langlois, R., Milne, A., Achterberg, E., Nachtigall, K., et al. (2008). Nitrogen and phosphorus co-limitation of bacterial productivity and growth in the oligotrophic subtropical North Atlantic. Limnol. Oceanogr. 53, 824–834. doi: 10.4319/lo.2008.53.2.0824

Nowald, N., Iversen, M. H., Fischer, G., Ratmeyer, V., and Wefer, G. (2015). Time series of in-situ particle properties and sediment trap fluxes in the coastal upwelling filament off Cape Blanc, Mauritania. Prog. Oceanogr. 137, 1–11. doi: 10.1016/j.pocean.2014.12.015

Oksanen, J., Blanchet, F. G., Friendly, M., Kindt, R., Legendre, P., McGlinn, D., et al. (2019). vegan: Community Ecology Package. Available at: https://CRAN.R-project.org/package=vegan

Parada, A. E., Needham, D. M., and Fuhrman, J. A. (2016). Every base matters: assessing small subunit rRNA primers for marine microbiomes with mock communities, time series and global field samples. Environ. Microbiol. 18, 1403–1414. doi: 10.1111/1462-2920.13023

Pitta, P., Kanakidou, M., Mihalopoulos, N., Christodoulaki, S., Dimitriou, P. D., Frangoulis, C., et al. (2017). Saharan Dust Deposition Effects on the Microbial Food Web in the Eastern Mediterranean: A Study Based on a Mesocosm Experiment. Front. Mar. Sci. 4, 117. doi: 10.3389/fmars.2017.00117

Prospero, J. M., and Lamb, P. J. (2003). African Droughts and Dust Transport to the Caribbean: Climate Change Implications. Science 302, 1024–1027. doi: 10.1126/science.1089915

Pulido-Villena, E., Baudoux, A.-C., Obernosterer, I., Landa, M., Caparros, J., Catala, P., et al. (2014). Microbial food web dynamics in response to a Saharan dust event: results from a mesocosm study in the oligotrophic Mediterranean Sea. Biogeosciences 11, 5607–5619. doi: 10.5194/bg-11-5607-2014

Pulido-Villena, E., Wagener, T., and Guieu, C. (2008). Bacterial response to dust pulses in the western Mediterranean: Implications for carbon cycling in the oligotrophic ocean: Bacterial response to dust pulses. Global Biogeochem. Cycles 22, n/a-n/a. doi: 10.1029/2007GB003091

R Core Team (2021). R: A language and environment for statistical computing. R Foundation for Statistical Computing, Vienna, Austria. Available at: https://www.R-project.org/

Rahav, E., Belkin, N., Paytan, A., and Herut, B. (2018). Phytoplankton and Bacterial Response to Desert Dust Deposition in the Coastal Waters of the Southeastern Mediterranean Sea: A Four-Year In Situ Survey. Atmosphere 9, 305. doi: 10.3390/atmos9080305

Ridame, C., Le Moal, M., Guieu, C., Ternon, E., Biegala, I. C., L'Helguen, S., et al. (2011). Nutrient control of N2 fixation in the oligotrophic Mediterranean Sea and the impact of Saharan dust events. Biogeosciences 8, 2773–2783. doi: 10.5194/bg-8-2773-2011

Sambrook, J., and Russell, D. W. (2001). Molecular Cloning: A Laboratory Manual., 3rd Edn. Cold Spring Harbor Laboratory Press.

Simon, M., and Azam, F. (1989). Protein content and protein synthesis rates of planktonic marine bacteria. Marine Ecology Progress Series 51, 201–213. doi: 10.3354/meps051201

Smith, D. C., and Azam, F. (1992). A simple, economical method for measuring bacterial protein synthesis rates in seawater using 3H-leucine. Mar. microb. food webs 6, 107–114.

Stein, A. F., Draxler, R. R., Rolph, G. D., Stunder, B. J. B., Cohen, M. D., and Ngan, F. (2015). Noaa's hysplit atmospheric transport and dispersion modeling system. Bull. Amer. Meteor. Soc. 96, 2059–2077. doi: 10.1175/BAMS-D-14-00110.1

Stoeck, T., Bass, D., Nebel, M., Christen, R., Jones, M. D. M., Breiner, H.-W., et al. (2010). Multiple marker parallel tag environmental DNA sequencing reveals a highly complex eukaryotic community in marine anoxic water. Molecular Ecology 19, 21–31. doi: 10.1111/j.1365-294X.2009.04480.x

Suzuki, R., Terada, Y., and Shimodaira, H. (2019). pvclust: Hierarchical Clustering with P-Values via Multiscale Bootstrap Resampling. Available at: https://CRAN.R-project.org/package=pvclust

Thompson, L. R., Sanders, J. G., McDonald, D., Amir, A., Ladau, J., Locey, K. J., et al. (2017). A communal catalogue reveals Earth's multiscale microbial diversity. Nature 551, 457–463. doi: 10.1038/nature24621

Torres-Padrón, M. E., Gelado-Caballero, M. D., Collado-Sánchez, C., Siruela-Matos, V. F., Cardona-Castellano, P. J., and Hernández-Brito, J. J. (2002). Variability of dust inputs to the CANIGO zone. Deep Sea Research Part II: Topical Studies in Oceanography 49, 3455–3464. doi: 10.1016/S0967-0645(02)00091-7

Tsiola, A., Tsagaraki, T. M., Giannakourou, A., Nikolioudakis, N., Yücel, N., Herut, B., et al. (2017). Bacterial Growth and Mortality after Deposition of Saharan Dust and Mixed Aerosols in the Eastern Mediterranean Sea: A Mesocosm Experiment. Front. Mar. Sci. 3. doi: 10.3389/fmars.2016.00281

Utermöhl, H. (1958). Methods of collecting plankton for various purposes are discussed. SIL Communications, 1953-1996 9, 1–38. doi: 10.1080/05384680.1958.11904091

Wickham, H., Averick, M., Bryan, J., Chang, W., McGowan, L., François, R., et al. (2019). Welcome to the Tidyverse. JOSS 4, 1686. doi: 10.21105/joss.01686

Yu, G. (2020). Using ggtree to Visualize Data on Tree-Like Structures. Current Protocols in Bioinformatics 69, e96. doi: 10.1002/cpbi.96

CHAPTER 3

SHALLOW HYDROTHERMAL FLUIDS SHAPE MICROBIAL DYNAMICS AT THE TAGORO SUBMARINE VOLCANO (CANARY ISLANDS, SPAIN)

Pérez-Barrancos, C., Fraile-Nuez, E., Martín-Díaz, J.P., González-Vega, A., Escánez-Pérez, J., Díaz-Durán, M.I., Presas-Navarro, C., Nieto-Cid, M., and Arrieta, J.M. (2025). Shallow hydrothermal fluids shape microbial dynamics at the Tagoro submarine volcano (Canary Islands, Spain). *Environmental Microbiology* 27, e70052. doi: 10.1111/1462-2920.70052

Shallow underwater hydrothermal systems are often overlooked despite their potential contribution to marine diversity and biogeochemistry. Over a decade after its eruption, the Tagoro submarine volcano continues to emit heat, reduced compounds and nutrients into shallow waters, serving as a model system for studying the effects of diffuse hydrothermal fluids on surface microbial communities. The impact on both phytoplankton and bacterial communities was examined through experimental manipulations mimicking dilution levels up to ~100 m from the primary crater of Tagoro. Chlorophyll a concentration doubled in the presence of hydrothermal products, with peak levels detected about a day earlier than in controls. Picoeukaryotes and *Synechococcus* cell abundances moderately increased, yet small eukaryotic phytoplankton (≤ 5 μm) predominated in the hydrothermally enriched bottles. Dinoflagellates, diatoms, small green algae and radiolarians particularly benefited from the hydrothermal inputs, along with phototrophic and chemoautotrophic bacteria. Our results indicate that hydrothermal products in shallow waters enhance primary production driven by phototrophic microbes, potentially triggering a secondary response

associated with increased organic matter availability. Additionally, protistan grazing and parasitism emerged as key factors modulating local planktonic communities. Our findings highlight the role of shallow submarine hydrothermal systems in enhancing local primary production and element cycling.

3.1 Introduction

Shallow hydrothermal vents represent unique ecosystems where primary productivity is particularly supported by both chemosynthesis and photosynthesis. These vents are distributed worldwide but have not received as much attention as their deep-sea counterparts (Price and Giovannelli 2017). The availability of light, together with the enrichment of nutrients and reduced chemical compounds through buoyant hydrothermal fluids, sustain intense microbial activity in surface seawaters capable of supporting higher trophic levels (Caramanna, Sievert, and Bühring 2021). However, the development of microbial communities is frequently subject to substantial variability due to tides, wind forcing and abrupt geodynamic events (Yücel et al. 2013). Previous studies have shown that shallow-water hydrothermal habitats often foster the growth of indigenous microorganisms, compared with deep-sea vents, which tend to host vent-specific taxa (Tarasov et al. 2005). Still, the activity of seawater and vent-derived microbes and their influence on geochemical fluxes is not well understood, especially in low-temperature diffuse vents (Wankel et al. 2011; Olins et al. 2013). Recent studies highlight shallow diffuse vents as important contributors to the total thermal and chemical flux entering the ocean (Martín-Díaz et al. 2024). These lower-temperature vents (< 100°C) display a mixture of oxygen-rich seawater with reduced chemicals from hydrothermal inputs, resulting in a wide range of microbial habitats. This diversity likely supports higher rates of primary productivity and biological biomass compared to high-temperature vents (Tarasov et al. 2005; Olins et al. 2013). Nonetheless, the specific environmental factors that influence the abundance and activity of microbes in these habitats require further investigation.

The Tagoro submarine volcano, located only 1.8 km off the southern coast of El Hierro island (Canary Islands, Spain) and with a summit 89 m below the sea surface (Fraile-Nuez et al. 2012, 2018), represents a unique opportunity to expand our understanding of the impacts of shallow underwater eruptive and degassing processes on the marine environment. It has indeed been monitored

by the Spanish Institute of Oceanography (IEO-CSIC) for over a decade, with more than 30 multidisciplinary oceanographic cruises conducted since the early eruptive phase in October 2011 to the current active venting phase. Fieldwork strategies for the detection and monitoring of active hydrothermal sources in the area have been most recently detailed in González (2023). Major efforts have been focused on the geomorphological characterisation of its volcanic structure (Álvarez-Valero et al. 2023; Vázquez et al. 2023), as well as on the physical–chemical perturbations near the bottom and throughout the adjacent water column (Fraile-Nuez et al. 2012, 2018, 2023; Santana-Casiano et al. 2013, 2016; González-Vega et al. 2020, 2022, 2023; Martín-Díaz et al. 2024). Currently, the hydrothermal field covers an area of 7600 m^2, extending from the main hydrothermal crater at 127 m depth to the summit (Martín-Díaz et al. 2024). Thousands of small and diverse hydrothermal vents, irregularly dispersed across the venting field, inject warm waters, reduced compounds, trace metals and inorganic nutrients (Santana-Casiano et al. 2013; Martín-Díaz et al. 2024). The waters surrounding Tagoro exhibit significant physical–chemical anomalies, with an increase in potential temperature of 2.55°C, a decrease in salinity of 1.02 units, a decrease in density of 1.43 kg m^{-3} and a decrease in pH of 1.25 units (Fraile-Nuez et al. 2018), yet anomalies in oxygen profiles are no longer found (González-Vega et al. 2022). Significant enrichments of dissolved inorganic nutrient concentrations persist in the vicinity of Tagoro (González-Vega et al. 2020, 2023; Martín-Díaz et al. 2024), with large amounts of hydrothermal iron ores depositing in the sediments (González et al. 2020), while large concentrations of reduced iron also remain dissolved and bioavailable (Santana-González et al. 2017).

The progressive recovery of the ecosystem after the devastating eruptive process of Tagoro (October 2011–March 2012) was particularly noticeable in benthic and pelagic communities (Ariza et al. 2014; Danovaro et al. 2017; González et al. 2020; Sotomayor-García et al. 2023). The post-eruptive phase offered more hospitable conditions for marine organisms to thrive, in which microorganisms involved in iron, sulfur and methane metabolism were able to grow (González et al. 2020; Sotomayor-García et al. 2020), including novel microbes such as *Candidatus* Thiolava veneris (Danovaro et al. 2017). The recuperation also involved early colonisers such as small hydrozoan colonies with a high diversity of annelids, arthropods, cnidarians and molluscs, together with some sponges and echinoderms (Sotomayor-García et al. 2023).

Few studies have yet investigated the ecological impact of Tagoro on surface planktonic communities, particularly during the current degassing stage (Ferrera et al. 2015; Gómez-Letona et al. 2018; Fernández de Puelles et al. 2021). Higher abundances of zooplankton in waters affected by the volcano have been described (Fernández de Puelles et al. 2021). Researchers especially observed a higher presence of non-calanoid copepods, along with a decline in the diversity of the copepod community. High concentrations of inorganic nutrients and iron injected from Tagoro into the water column are expected to favour the proliferation of photosynthetic communities in Tagoro (Santana-Casiano, González-Dávila, and Fraile-Nuez 2017; González-Vega et al. 2020), as it has been often observed in other shallow-water systems around the world (e.g., Tarasov 2006; Ardyna et al. 2019; Schine et al. 2021). However, so far no clear evidence of fertilisation (i.e., the enhancement of primary productivity due to nutrient enrichment) has been found around Tagoro (Gómez-Letona et al. 2018). This is possibly due to the difficulty in distinguishing hydrothermally enriched water masses from unaffected background seawater, which makes it challenging to detect a potential fertilisation signal.

In this study, an experimental approach was employed to assess the potential effects of diffuse hydrothermal emissions on surface marine microbial communities (phytoplankton and bacteria) at the Tagoro submarine volcano. Microbial responses to proportional increases of hydrothermally enriched seawater and vent fluids were assessed in terms of cell abundances, diversity and community structure. The experimental treatments were designed to replicate the natural dilution of vent fluids in the vicinity of Tagoro. Dilution levels simulated in situ observations obtained over 9 years using dissolved inorganic silicate as a proxy for hydrothermal emissions in the area. The potential dispersion of hydrothermal fluids to the illuminated surface waters was assessed by examining mixed layer depth (MLD) estimates derived from in situ hydrographic data collected over the past decade. Together, our research enhances our understanding of the dynamics of surface marine microbial communities, their potential interactions with higher trophic levels and their implications for local productivity, nutrient cycling and carbon sequestration around shallow hydrothermal venting areas.

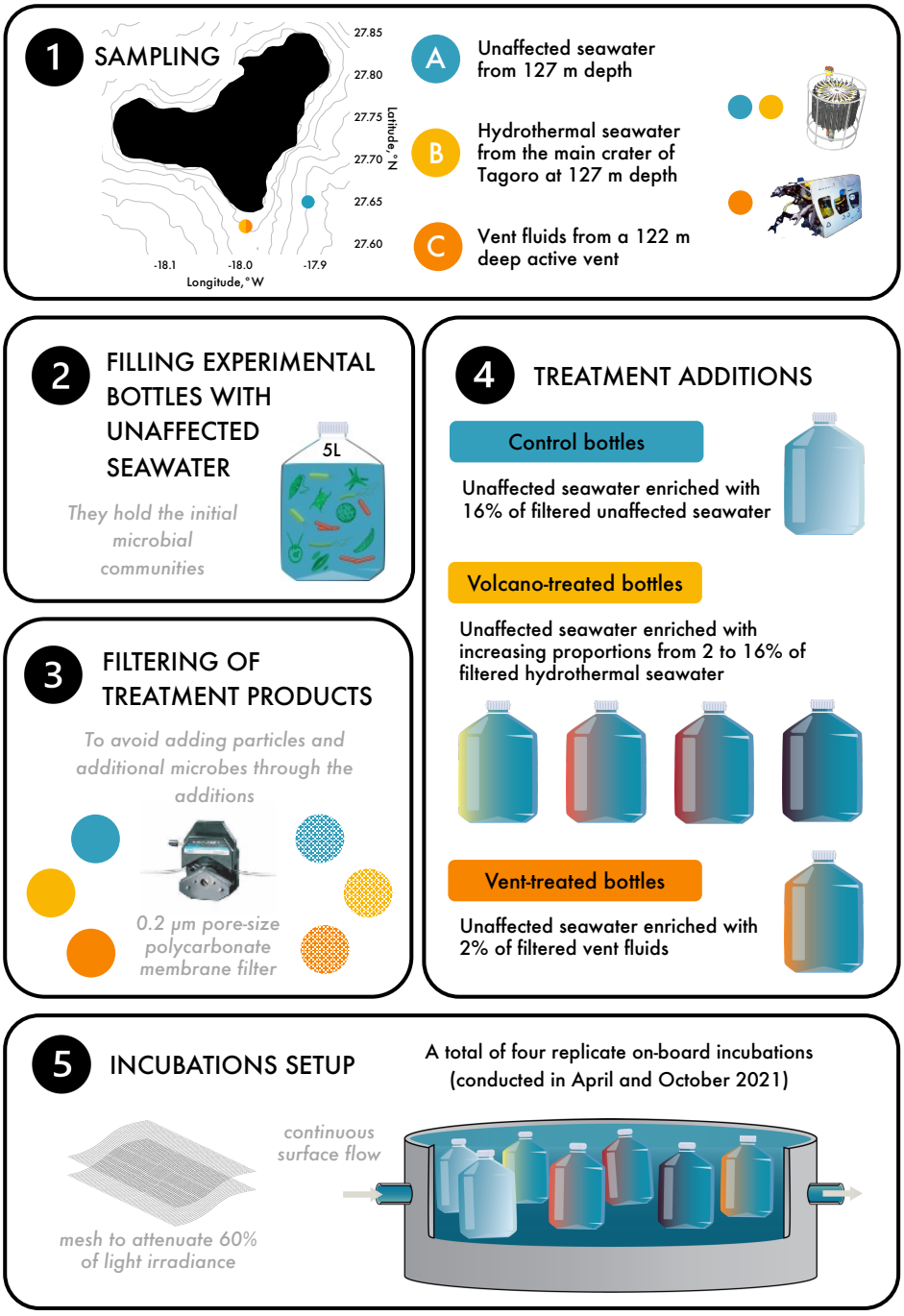

Figure 1. Overview of the setup used to test the effect of hydrothermal fluid additions at Tagoro submarine volcano (El Hierro, Spain).

3.2 Material and methods

3.2.1 Experimental addition of hydrothermal fluids

This research was developed as part of the VULCANA monitoring program from the Spanish Institute of Oceanography (IEO-CSIC). Two hydrothermal fluid addition experiments were conducted in April (spring) and two more in October (autumn) 2021, each lasting 8–10 days, on board the R/V *Ángeles Alvariño* at the Tagoro submarine volcano (El Hierro, Spain).

Seawater samples were collected at two vertical hydrographic stations using a rosette frame equipped with 24 Niskin bottles, each with a 12-L capacity, a dissolved oxygen sensor, a pH/oxidation–reduction potential (ORP) sensor, a fluorometer and two turbidimeters, coupled to an SBE 911-plus (Sea-Bird Electronics) CTD sensor (conductivity, temperature and depth). Calibration of all sensors was conducted before and after each oceanographic cruise. An outline of the experiments is provided in **Figure 1**. Briefly, unaffected seawater was collected at a reference station located outside the area of influence of Tagoro (~127 m depth; 27°39.000' N, 17°54.587' W; **Figure 2A**) and was used to fill the 5-L polycarbonate bottles designated as experimental bottles. All plasticwares were acid-washed with 0.12 N HCl for 30 min and rinsed three times with sample water. A few hours later, hydrothermally enriched seawater samples were collected from the primary crater of Tagoro (~127 m depth; 27°37.184' N, 17°59.184' W; **Figure 2B**) at locations where simultaneous decreases in pH and increases in temperature were detected compared to the surrounding waters. Hydrothermal samples were then filtered through 47 mm diameter, 0.2 μm pore-size polycarbonate membrane filters using a peristaltic pump and homogenised in a 20-L polycarbonate bottle before being added to the experimental bottles. Each experiment consisted of two replicate control bottles filled with unaffected seawater and four bottles filled with unaffected seawater enriched with increasing volumes of filtered hydrothermal seawater (from 2% to 16% of the total volume), hereafter referred to as 'volcano-treated'. Controls were also subjected to an addition of 16% filtered unaffected seawater to account for any artefacts introduced by the handling of hydrothermal water samples.

An additional treatment, labelled as 'vent-treated', was introduced during the October 2021 cruise using vent fluids collected directly from an active hydrothermal vent near the primary crater (~122 m depth; 27°37.1832' N,

17°59.5712' W; **Figure 2B**). Sampling was performed using a remotely operated vehicle (ROV, *Liropus 2000*) equipped with a piston-driven suction system and with a HOBO TidbiT water temperature data logger (Onset Computer Corp.). Vent fluids were filtered (0.2 μm pore-size polycarbonate membrane filter) and homogenised in a 20-L polycarbonate bottle prior to the addition. In this instance, two replicate bottles filled with unaffected seawater were enriched with filtered vent fluids to 2% of the total volume. These vent-treated bottles were then incubated with the rest of experimental bottles for 9 days. Throughout the manuscript we will use the term 'treated' to refer to both volcano and vent-treated bottles.

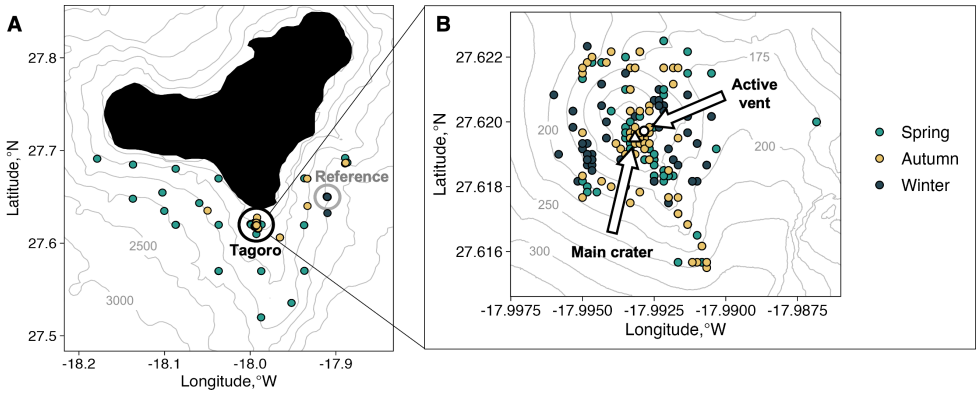

Figure 2. (A) Hydrographic stations sampled south of El Hierro during VULCANA cruises from 2013 to 2023. Point colours indicate the season of sampling: Spring (green), autumn (yellow) and winter (blue). Circled areas highlight the reference station (grey) and the Tagoro hydrothermal field (black). Contours are displayed with an interval of 500 m. **(B)** Map of the hydrothermal field, with contour intervals of 25 m, showing the location of the main crater of Tagoro (white triangle) and the active vent sampled (white circle).

The ratios of dilution were determined based on previous reports of dissolved silicate concentrations in the area of influence of Tagoro (González-Vega et al. 2020), where this nutrient was found to be a tracer of hydrothermal activity. These authors reported median and maximum enrichments of 4.6-and 16.3-fold, respectively, in the water column during the degassing stage compared to unaffected waters. We designed our experiments to cover a range from 2% to 16% of hydrothermal fluid addition, corresponding to the dissolved silicate concentrations in seawater previously observed adjacent to the main hydrothermal sources of Tagoro. In the case of vent fluids, previous studies observed a median 243.4-fold enrichment compared to unaffected waters (González-Vega et al. 2020). Thus, we simulated an addition of at least 2% of

vent fluids, expected to result in the ~4-fold enrichment levels found in the water column.

The experimental bottles were incubated in 600 L high-density polyethylene tanks on-deck. Each tank was subjected to a continuous flow of surface seawater to provide sea surface temperature conditions and was covered with a double layer of optically neutral wire mesh reducing light intensity by 60%. Seawater temperature and light intensity were continuously monitored using a HOBO Pendant Temp/Light data logger (Onset Computer Corp.). Sampling was mostly performed at the beginning and end of experiments, although some parameters like chlorophyll *a* concentration and microbial abundances were sampled daily.

3.2.2 Estimation of dilution levels

The dilution levels reproduced in our experiments were estimated from the exponential decay of dissolved silicate concentrations with increasing distance to the primary crater. This was determined using 145 water column samples collected at depths of approximately 120 and 130 m between March 2014 and February 2023 (**Figure 4B and Table S1**). A nonlinear regression using the least-squares fitting method was applied, resulting in an exponential decay equation that best described the observed data at Tagoro (**Figure 4B**). This equation was then used to compute the corresponding distances (i.e., dilution levels) for each experimental treatment based on their dissolved silicate concentrations. The uncertainty of the model was evaluated using the standard error and 95% confidence intervals. This data compilation represents the largest dataset published to date on the continuous silicate enrichment at the active Tagoro hydrothermal field throughout its degassing phase.

3.2.3 Estimation of the seasonal mixed layer depth

The potential of hydrothermal fluids from Tagoro to reach shallower layers throughout the euphotic zone was assessed through seasonal MLD estimates. Hydrographic profiles of temperature, salinity and pressure collected between March 2013 and February 2023 as part of the VULCANA research project were used to derive the MLD south of El Hierro (latitudes between 27.46983º N and 27.69200º N). Most profiles were acquired using an SBE 911-plus CTD, with an average vertical resolution of 1 dbar, a temperature precision of 0.001ºC and a conductivity precision of 0.0003 S m^{-1}.

Only profiles extending to depths below 100 m were used, resulting in a total of 1070 profiles in our study region. About 485 of the profiles were collected in spring (March–June), 154 in autumn (September–November) and 431 in winter. Moreover, about 75% of the profiles were acquired above the Tagoro hydrothermal field (**Figure 2B**) and another 12% were collected at the reference station southeast of El Hierro (**Figure 2A**). Examples of typical spring, autumn and winter profiles at both sites are shown in Figure S1, along with their seasonal median MLD estimates. Given the differences in sampling frequency across seasons and the large variability in MLD estimates, we chose to represent seasonal median values to provide a more accurate representation of the central tendency for each season (**Figures 2A and 3**).

The MLD was defined as the depth at which the maximum difference in the potential density profile was observed. Potential density is a valuable parameter for estimating the vertically homogeneous mixed layer, as it depends on both temperature and salinity and includes a correction for pressure effects (de Boyer Montégut et al. 2004). Based on the method of Lorbacher et al. (2006), we identified the maximum potential density gradient in each profile. This approach enabled the identification of the maximum depth reached by recent mixing events.

3.2.4 Dissolved inorganic nutrient concentrations

Seawater samples (12 mL per duplicate) were collected in polypropylene tubes and frozen at −20ºC until analysis. Nutrient concentrations were analysed by colorimetric determination using a four-channel automatised air-segmented continuous flow system SEAL AA3 AutoAnalyzer. Nitrate plus nitrite (NO_3^-+ NO_2^-) were determined by the copper–cadmium reduction method, whereas phosphate (PO_4^{3-}) and silicate ($Si(OH)_4$) were determined by the molybdate blue method (Aminot and Kérouel 2007). The instrumental limit of quantification was 0.02 μM for NO_3^-+ NO_2^-, 0.01 μM for PO_4^{3-} and 0.04 μM for $Si(OH)_4$.

3.2.5 Dissolved organic carbon and nitrogen concentrations

Seawater samples (30 mL per duplicate) were collected in combusted (450ºC for 12 h) amber glass vials at the beginning and end of the October 2021 incubations and preserved at −20ºC until analysis. After acidification with H_3PO_4 to pH < 2, dissolved organic carbon (DOC) and total dissolved nitrogen

(TDN) were measured using a Shimadzu TOC-V organic carbon analyser coupled to a TNM-1 total nitrogen unit. The system was standardised daily with a mixture of potassium hydrogen phthalate and glycine.

3.2.6 Chlorophyll *a* concentrations and phytoplankton growth estimates

Seawater samples for chlorophyll *a* (250 mL) were filtered on-board through 25 mm diameter, 0.7 μm pore size Whatman GF/F glass fibre filters and stored at −20ºC until analysis. Pigments were extracted overnight in 90% acetone at −20ºC in the dark (Holm-Hansen et al. 1965). Chlorophyll *a* concentrations were determined fluorometrically on an Aquafluor (Turner Designs) handheld fluorometer.

The apparent phytoplankton growth rates (μ) were estimated from changes in chlorophyll *a* concentration, assuming an exponential growth model

$$N_t = N_0 e^{\mu t}$$

where N_0 is the population size at the beginning of a time interval, N_t is the population size at the end of the time interval and μ is the proportional rate of change expressed per unit time (t^{-1}). Note that losses incurred through viral lysis, grazing or other factors were not accounted for. Consequently, the actual growth rates of phytoplankton in our experiments are expected to be higher than the estimates provided in this study.

3.2.7 Picophytoplankton and heterotrophic bacteria abundances

Seawater samples for microbial abundance (1 mL per duplicate) were preserved with paraformaldehyde (1% final concentration), fixed for 30 min in the dark at 4ºC, flash frozen in liquid nitrogen and stored at −80ºC until processed. Once in the laboratory, samples were thawed, diluted in Tris-EDTA 1× buffer (pH 8) and 200 μL aliquots were stained in the dark for 10 min with SYBR Green I prior to analysis. Picophytoplankton and heterotrophic bacteria (≤ 2 μm) were counted using a CytoFLEX flow cytometer (Beckman Coulter) fitted with 405, 488 and 561 nm lasers. Autotrophic cells were readily detected in seawater samples by the fluorescence of their photosynthetic pigments. Specifically, *Synechococcus* were differentiated from *Prochlorococcus* by their emission of orange fluorescence and generally larger cell size, whereas picoeukaryotes were detected by their larger side scatter and red fluorescence

and absence of orange fluorescence (Marie et al. 1997). Heterotrophic bacteria were detected in SYBR Green I–stained samples and characterised by the presence of green fluorescence and lack of red or orange fluorescence.

3.2.8 Microbial community structure

Seawater samples for 16S and 18S rRNA gene sequencing (~1 L) were filtered through a 0.20-μm pore-size filter using a peristaltic pump and stored at −80ºC.

The isolation of genomic DNA and the preparation of sequencing libraries were performed at the Canary Islands Oceanographic Center (IEO-CSIC) research facilities. DNA was extracted following the phenol–chloroform method (Sambrook and Russell 2001). Primers 515F (GTGYCAGCMGCCGCGGTAA) (Parada, Needham, and Fuhrman 2016) and 806R (GGACTACNVGGGTWTCTAAT) (Apprill et al. 2015) were used to target the V4 region of the prokaryotic 16S rRNA (~390 bp). Each PCR reaction (20 μL) contained 10 μL of AccuStart II PCR SuperMix (2×), 0.6 μL of each 20 μM primer stock, 3.8 μL of water and 5 μL of DNA template. The PCR program comprised an initial denaturation step at 94ºC during 3 min, 35 amplification cycles, each consisting of 94ºC for 45 s, 50ºC for 60 s and 72ºC for 90 s, a final elongation step at 72ºC for 10 min and cooling to 4ºC. On the other hand, the V4 region of the eukaryotic 18S rRNA (~260 ± 50 bp) was targeted using TAReuk454FWD1 (CCAGCASCYGCGGTAATTC) and TAReukREV3 (ACTTTCGTTCTTGATYRA) primer set (Stoeck et al. 2010). PCR reactions were set up as previously described for the 16S rRNA gene. On this occasion, the PCR program consisted of an initial denaturation step at 94ºC for 3 min, 15 amplification cycles of 94ºC for 45 s, 53ºC for 30 s and 72ºC for 30 s, followed by 20 additional amplification cycles, each consisting of 94ºC for 45 s, 48ºC for 30 s and 72ºC for 30 s, a final elongation step at 72ºC for 10 min and cooling to 4ºC. For each library, amplified PCR products were cleaned, indexed and quantified following the Illumina 16S metagenomic sequencing library preparation protocol. Equimolar amounts of cleaned-up indexed samples were pooled and paired-end sequenced (2 × 300) on an Illumina MiSeq platform (Macrogen, Korea). Sequence data (demultiplexed sequences with primers and adapters) is available at NCBI (https://www.ncbi.nlm.nih.gov/sra) under ID Number PRJNA1098582.

After primer removal with cutadapt v1.18, amplicon datasets were processed using the DADA2 v1.28 pipeline (Callahan et al. 2016) with trimming and

filtering parameters estimated through FIGARO (Weinstein et al. 2019). The obtained combinations were *truncLen* 216,143 and *maxEE* 1 for the prokaryotic 16S rRNA dataset, and *truncLen* 230,200 and *maxEE* 2 for the eukaryotic 18S rRNA dataset. Sample inference was performed by pooling together sequences from all samples. An amplicon sequence variant (ASV) table was obtained for each dataset, with chimera removal using the consensus approach. Prokaryotic taxonomic assignment was performed according to Silva SSU Version 138.1, and sequences classified as eukaryote, mitochondria or chloroplast were discarded from the 16S rRNA dataset. Eukaryotic taxonomy was determined using the PR_2 database (Guillou et al. 2013), and any bacterial and archaeal sequences were excluded from the 18S rRNA dataset. Opisthokonta sequences, comprising 1.5% of the eukaryotic 18S rRNA dataset, were also removed from the analysis. They were predominantly classified within the Metazoa and Pseudofungi divisions, including a broad group of animals and heterokonts not relevant to the purpose of our study, with median abundances too low ($\leq 0.5\%$) to support robust interpretations. Both amplicon datasets were rarefied to avoid library size differences using phyloseq v.1.44 (McMurdie and Holmes 2013).

Chao1 and Shannon diversity metrics were estimated using phyloseq v.1.44, and the individual and combined effects of hydrothermal treatment and environmental conditions on species alpha diversity were analysed through two-way ANOVA with rstatix v.0.7.2 (Kassambara 2021). An additional grouping variable called 'environmental conditions' was included in the analysis to account for seasonal differences in the initial sample. To assess the uncertainty in hierarchical clustering based on Bray–Curtis dissimilarities, multiscale bootstrap resampling was performed using pvclust v2.2 (Suzuki, Terada, and Shimodaira 2019) to obtain unbiased probabilities (au) for each cluster, which were later plotted with ggtree v3.8.2 (Yu 2020). PERMANOVA tests were then conducted to evaluate the relative contribution of hydrothermal treatment and environmental conditions, along with their interaction, to prokaryotic and eukaryotic community structure using vegan v2.6.4 (Oksanen et al. 2019). Additionally, indicator species analyses were computed using indicspecies v1.7.12 (De Cáceres and Legendre 2009) to identify microbial species most strongly associated with hydrothermally enriched environments, based on their occurrence and abundance in the treated incubations. We only considered those phylotypes most often found in surface waters affected by hydrothermal emissions, with an indicator value greater than 85% ($stat > 0.85$),

a statistical significance $p \leq 0.001$ and mostly absent from controls ($str_C \leq 0.5$). All analyses were computed in R v4.3.1 (R Core Team 2021) and processed using tidyverse v2.0 (Wickham et al. 2019).

3.3 Results

3.3.1 Physical–chemical characterisation of vent fluids and waters affected by Tagoro

Seawater above the primary crater of Tagoro submarine volcano exhibited higher temperatures, increased acidity and greater $Si(OH)_4$ concentrations, as compared to unaffected seawater (**Table S2**). Thermal anomalies were larger in autumn (+0.37ºC) than in spring (+0.09ºC), whereas a consistent pH anomaly of −0.1 was observed across seasons. $Si(OH)_4$ concentrations ranged from 2.67 to 5.84 μmol kg^{-1}, reflecting a 3–6-fold increase compared to unaffected seawaters, with maximum concentrations observed in spring. Vent fluids were ~9ºC warmer than the water column and exhibited the highest concentrations of dissolved inorganic nutrients, particularly $Si(OH)_4$ at 18.3 ± 1.2 μmol kg^{-1} and PO_4^{3-} at 15.6 ± 4.8 μmol kg^{-1} (**Table S2**).

The MLD south of El Hierro showed seasonal variations (**Figure 3**). Median MLD estimates were deepest in spring, reaching depths of ~121 m, followed by winter at ~96 m and autumn at ~70 m. MLD estimates varied largely as expected; however, the mixed layer often extended below the summit of Tagoro (≥ 89 m depth) throughout the year and occasionally below its primary crater (≥ 127 m), particularly in spring and winter (**Figure 3**). Nevertheless, mixing events deeper than the primary crater also occurred in autumn.

3.3.2 Dissolved inorganic and organic compounds throughout the incubations

The treatment strategy resulted in proportional enrichments of $Si(OH)_4$ in the treated bottles, ranging from 0.9 to 2 μmol kg^{-1} (**Figure 4A**). No measurable changes were observed in the concentration of NO_2^- + NO_3^- and PO_4^{3-} following the enrichment (**Figure 4A**). Both the hydrothermally enriched seawater and the vent fluids had concentrations in the lower range of the concentrations measured in previous studies. Thus, instead of the 4–16-fold nutrient enrichment expected, our initial conditions corresponded to a range between 0.97- and 1.83-fold enrichment in $Si(OH)_4$.

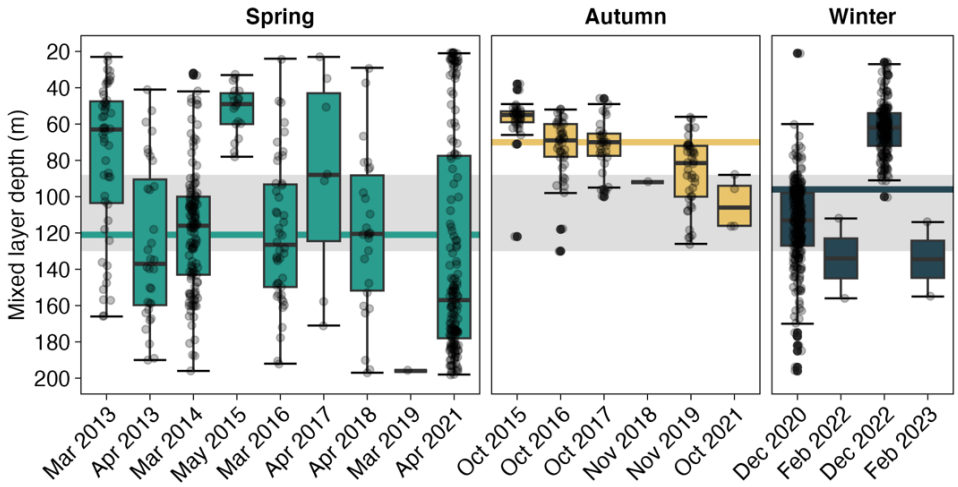

Figure 3. Mixed layer depth (MLD, m) estimates per cruise conducted south of El Hierro. Grey dots show the actual observations and boxplots show the median, and first (upper) and third (lower) quartiles. Outliers are marked as black dots. Horizontal bold lines indicate the median MLD for spring (n = 485 profiles), autumn (n = 154) and winter (n = 431). Grey shaded areas indicate the depth of active hydrothermal venting at Tagoro following Martín-Díaz et al. (2024).

These additions mimicked mixing conditions observed between 41 and 95 m away from the primary crater of Tagoro (**Figure 4B**). Since $Si(OH)_4$ concentrations were higher in the spring experiments, in this season the volcano-treated bottles corresponded to those observed at distances ranging from 41 to 63 m from the active sources of hydrothermal activity in Tagoro. In autumn, the volcano-treated bottles represented more distant waters, about 67–88 m. The vent-treated bottles resulted in the lowest hydrothermal additions, with $Si(OH)_4$ concentrations corresponding to about 95 m. The concentrations of dissolved inorganic nutrients were nearly depleted by the end of all treated incubations. Conversely, DOC and DON concentrations increased in the volcano-treated bottles, whereas they slightly decreased in the vent-treated bottles (**Table S3**).

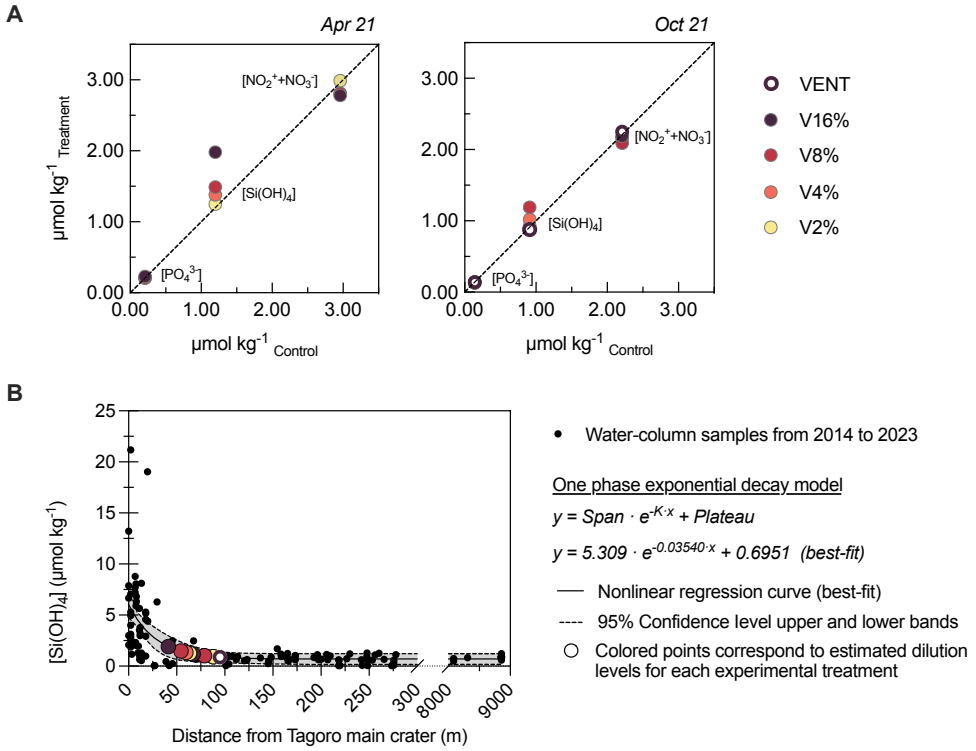

Figure 4. (A) Initial dissolved inorganic nutrient concentrations (*µ*mol kg^{-1}) in control versus volcano-and vent-treated bottles in April and October 2021 experiments. Data are also reported in **Table S3**. **(B)** Exponential decay fitting of dissolved inorganic silicate (*µ*mol kg^{-1}) versus distance from the main crater of Tagoro (m), based on a decade of in situ measurements at seawater depths of 120–130 m. The exponential decay equation, 95% confidence intervals and estimated dilution levels (distance to the main crater) for each experimental treatment (see **Section 3.2.2**).

3.3.3 Microbial growth

Regardless of the season, hydrothermal additions led to higher phytoplankton biomass (assessed through chlorophyll *a* concentration) and faster apparent growth rates compared to controls (**Figure 5**). Phytoplankton biomass in the volcano-treated bottles peaked at 2.5–7.8 μg Chl *a* L^{-1} after 5–7 days of incubation, occurring a day earlier than in the controls. Afterwards, a gradual decrease in biomass was observed until the end of the incubations. The vent-treated bottles, on the other hand, required an additional 2 days to achieve phytoplankton biomasses between 2.0 and 2.8 μg Chl *a* L^{-1}.

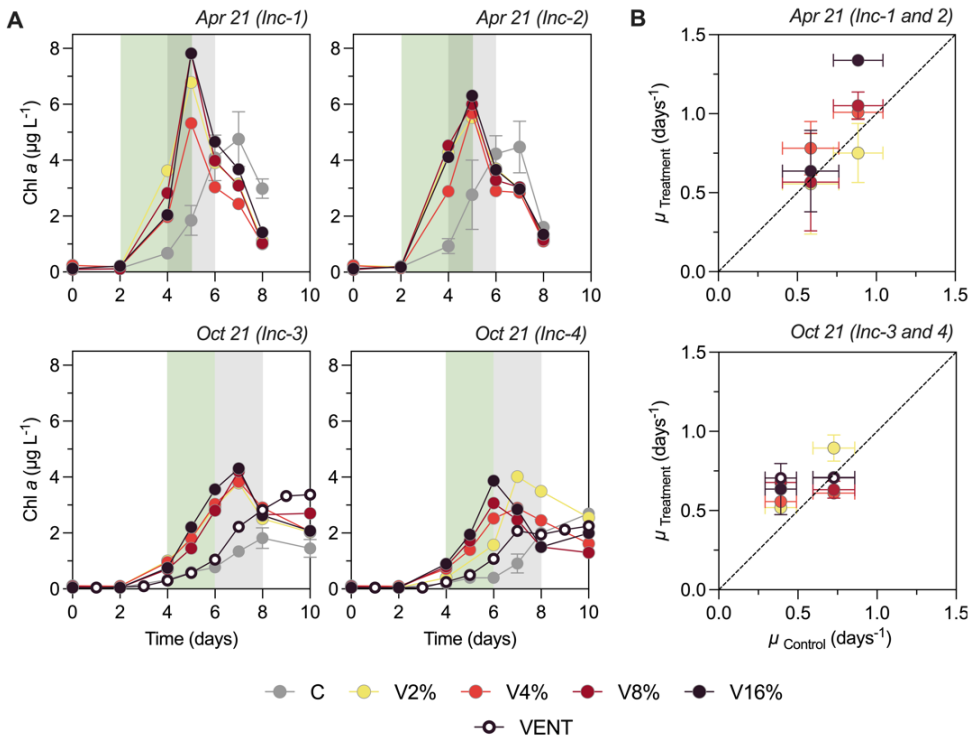

Figure 5. (A) Chlorophyll a concentration (μg Chl *a* L^{-1}) in April and October 2021 incubations. Control (grey) dots represent the average and standard deviation from two replicate control bottles placed in each incubator (Inc). In contrast, volcano- (colour gradient) and vent-treated (white) dots represent individual bottles, each enriched with a proportion of filtered hydrothermal seawater (ranging from 2% to 16% of the total volume) or with 2% of vent fluids. Shaded areas indicate the exponential growth phase in control (grey) versus volcano-and vent-treated (green) bottles. **(B)** Apparent phytoplankton growth rates ($days^{-1}$) estimated from the exponential growth phases.

Flow cytometric analyses (**Figures S2 and S3**) showed that picoeukaryotes and *Synechococcus* populations (0.2–2 μm) benefited from hydrothermal enrichments. The cell abundance of picoeukaryotes increased exponentially in both volcano-treated and control bottles until Days 5 and 6 (**Figures S2A and S3A**). Despite the obvious differences between the autumn and spring samples, picoeukaryotes reached their maximum abundance earlier in the hydrothermally enriched treatments as compared to the corresponding controls. *Synechococcus* populations also exhibited earlier and faster increases in cell abundances in the presence of hydrothermal products (**Figures S2B and S3B**), with maximum values 3-fold higher than the controls. Interestingly, *Synechococcus* continued exponential growth in the controls after the collapse of their treated counterparts during the spring incubations, suggesting a top-down control in the volcano-treated bottles that did not happen in the controls. Although differences between control and vent-treated bottles were small for both populations (**Figure S3A, B**), Incubations 3 and 4 displayed *Synechococcus* abundances that were 3-to 4-fold higher 6 days after the vent enrichment, and these populations predominated thereafter. In contrast, *Prochlorococcus* populations grew regardless of the treatment throughout all incubations, although usually reached higher final cell abundances in treated bottles than in controls (**Figures S2C and S3C**). Heterotrophic bacteria showed little difference in cell abundances between treated bottles and controls, even though some stimulation of growth was detectable in all cases after the collapse of the phytoplankton populations (**Figure S4**).

In addition, molecular analyses revealed that all treated bottles were primarily composed of small photosynthetic eukaryotes ($\leq$ 5 μm) belonging to the divisions Dinoflagellata (dinoflagellates), Ochrophyta (photosynthetic stramenopiles), Chlorophyta (small green algae) and Radiolaria (protists) (**Figure 6**), rather than Cyanobacteria, which accounted for a low proportion of sequences ($\leq$ 1%) in most cases (**Figure 7**). The initial eukaryotic and prokaryotic microbial communities in our incubations were similar to those found in situ in seawater adjacent to the primary active sources of Tagoro (**Figure S5**), including the photo- and chemoautotrophic organisms later found in the incubations.

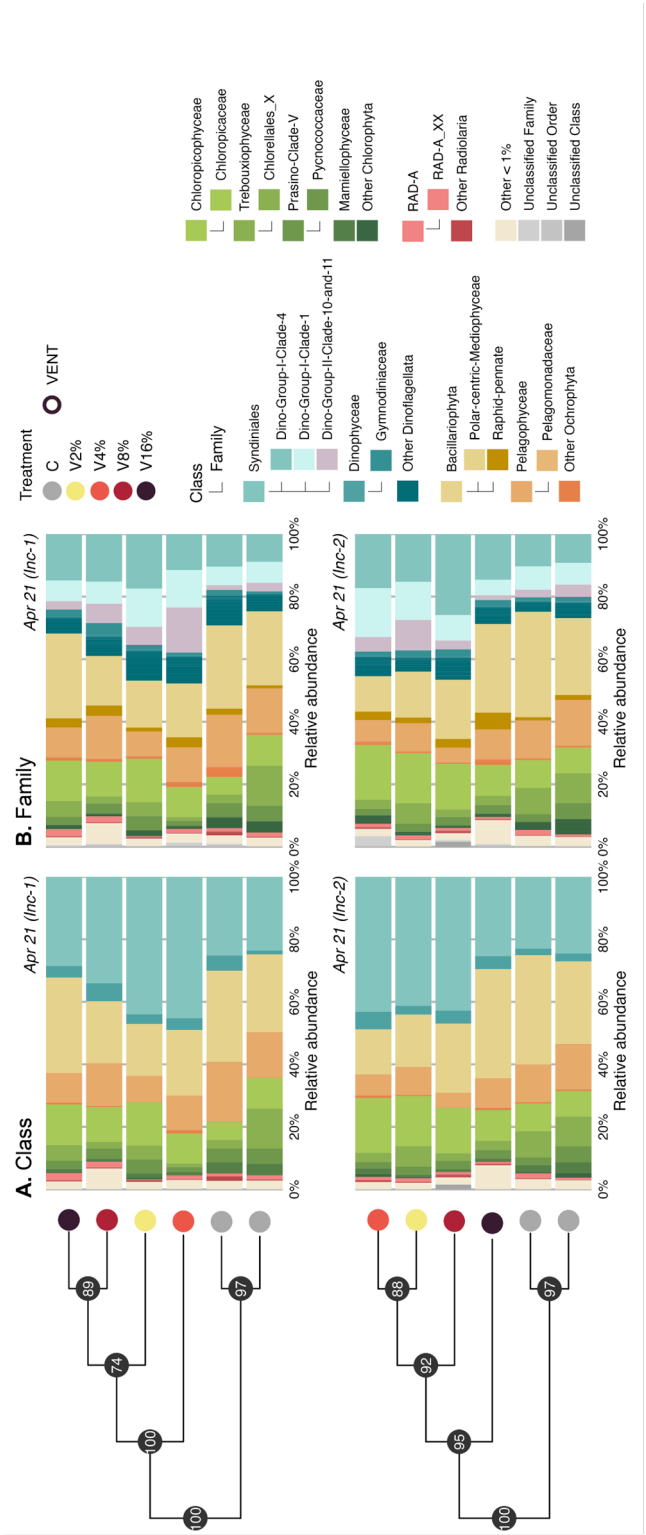

Figure 6. Hierarchical clustering and relative abundance of eukaryotic 18S rRNA sequences classified down to **(A)** class and **(B)** family level for each incubation (Inc). Coloured dots represent the control (grey), volcano-treated (colour gradient) and vent-treated (white) bottles at the end of the April and October 2021 incubations. Volcano bottles were enriched with filtered hydrothermal seawater at concentrations ranging from 2% to 16% of the total volume, whereas vent bottles were treated with a 2% addition of vent fluids. Black points in the dendrogram represent the approximately unbiased *p* value (au) for each cluster. Taxa are ordered by decreasing relative abundance greater than 1% and grouped by the highest division groups.

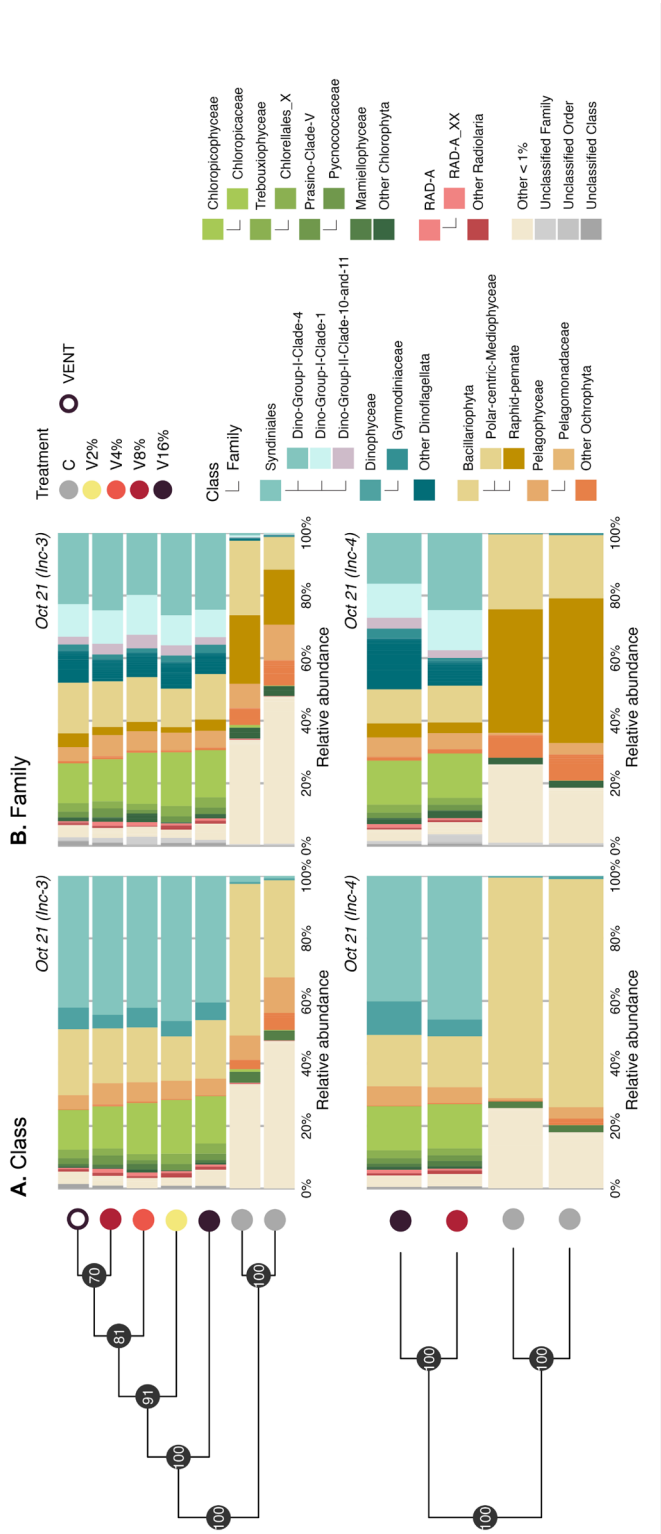

Figure 6. Continued.

Dinoflagellates were the prevailing group in the treated bottles as opposed to the controls, often accounting for half of the eukaryotic community at the end of the incubations (**Figure 6**). The class Syndiniales dominated with median relative abundances of 42% in the treated bottles (**Figure 6A**) and was mostly composed of parasitic dinoflagellates (**Figure 6B**), including Dino-Group I Clades 1 and 4 (> 10%) and Dino-Group II Clades 10 and 11 (2%–3%). A total of 24 ASVs belonging to these families were indeed significantly associated with the hydrothermal additions according to the indicator species analyses ($stat \geq 0.85$, $p \leq 0.001$ and $str_C \leq 0.4$; **Table S4**), comprising 19% of the relative abundance of species (**Figure S6**). Regarding the Dinophyceae class, it comprised about 5%–7% of Dinoflagellata at the end of the treated incubations (**Figure 6A**), with approximately 2% of the sequences belonging to the Gymnodiniaceae family (**Figure 6B**). However, it was a member of the Blastodiniaceae family (≤ 1%) that showed a significant association with the treatment ($stat = 0.95$, $p \leq 0.001$ and $str_C = 0.14$; **Table S4**), being the only one among the Dinophyceae class.

Meanwhile, photosynthetic stramenopiles were the second most abundant division throughout the treated incubations (**Figure 6**). Although their relative abundances increased 2-fold higher in control bottles, where they ended up comprising half of the eukaryotic community, the stramenopiles assemblage was generally composed of diatoms (Bacillariophyta, 17%–33% of relative abundance) and other heterokonts (Pelagophyceae, 4%–12%) in all incubations (**Figure 6A**). Diatoms were primarily composed of polar centric Mediophyceae diatoms (16%–24%), which included a diverse range of low-abundance diatoms, and to a lesser extent, raphid pennate diatoms (3%–10%) (**Figure 6B**). Despite these observations, the pico-and nano-sized (2–20 μm) planktonic polar-centric species *Chaetoceros tenuissimus*, *Arcocellulus cornucervis* and *Minutocellus polymorphus* showed significant associations with the treated bottles ($stat \geq 0.91$, $p \leq 0.001$ and $str_C \leq 0.3$; **Table S4**), even though most of them exhibited abundances below 1% (**Figure S6**). Pelagomonadaceae (4%–12%) predominated among Pelagophyceae at the end of all incubations (**Figure 6B**), and especially those identified as *Pelagomonas* (4%–9%), with *Pelagomonas calceolata* (3.5%–9%) as the primary species. However, only one ASV within this family could be significantly associated with the hydrothermal treatment ($stat = 0.91$, $p \leq 0.001$ and $str_C = 0.3$; **Table S4**).

Small green algae were the third most abundant division at the end of all incubations, even though they appeared to be the most enriched by the

hydrothermal treatments (19%–21% of relative abundance), generally doubling the increases observed in control bottles (**Figure 6**). The family Chloropicaceae, belonging to the Chloropicophyceae class, particularly benefited from the treatments (**Figure 6B**), holding median relative abundances up to 9% at the end of the volcano- and vent-treated bottles. Since it was majorly composed of *Chloropicon* (~9%) and a few *Chloroparvula* (< 1%), the indicator species analyses pointed to *Chloropicon roscoffensis* as the species most closely related to the hydrothermal treatments ($stat \geq 0.87$, $p \leq 0.001$ and $str_C \leq 0.4$; **Table S4**). A total of 10 ASVs of *C. roscoffensis* were, in fact, significantly associated with the treated incubations, accounting for 12% of the relative abundance at the end (**Figure S6**). Other classes of Chlorophyta also had higher relative abundances compared to controls, such as Trebouxiophyceae, Prasino Clade V and Mamiellophyceae (**Figure 6A**), yet exhibited median relative abundances below 3%.

Lastly, analyses showed that the Radiolaria division was enriched, with low relative abundances (1%–2%) and primarily composed of RAD-A protozoa, in the bottles treated with hydrothermal products (**Figure 6**).

These differences in the taxonomic composition of the eukaryotic community between controls and treatments were also evidenced by hierarchical clustering analyses, as replicate control bottles clustered together and apart from treated bottles with high bootstrap probabilities (**Figure 6**). Treatment accounted for 28% of the variance in eukaryotic composition recorded at the end of the experimental period (df = 1, $r^2 = 0.277$; $F = 10.4$, $p < 0.001$, PERMANOVA), whereas about 24% was explained by the environmental conditions (i.e., minor variations related to seasonal differences in the initial sample) (df = 3, $r^2 = 0.245$; $F = 3.07$, $p < 0.01$, PERMANOVA test). Fewer significant differences were observed in the composition of the prokaryotic community relative to the treatment (**Figure 7**), consistent with the small differences observed in heterotrophic bacterial cell abundances (**Figure S4**). Nonetheless, the treatment was responsible for 20% of the prokaryotic variance (df = 1, $r^2 = 0.201$; $F = 13.18$, $p < 0.001$, PERMANOVA test), whereas environmental conditions explained 39% of the variance (df = 3, $r^2 = 0.386$; $F = 8.45$, $p < 0.001$, PERMANOVA test).

Regarding the prokaryotic community composition, most treated bottles consisted of the phyla Proteobacteria, Bacteroidota and Actinobacteriota, followed by Crenarchaeota (**Figure 7**).

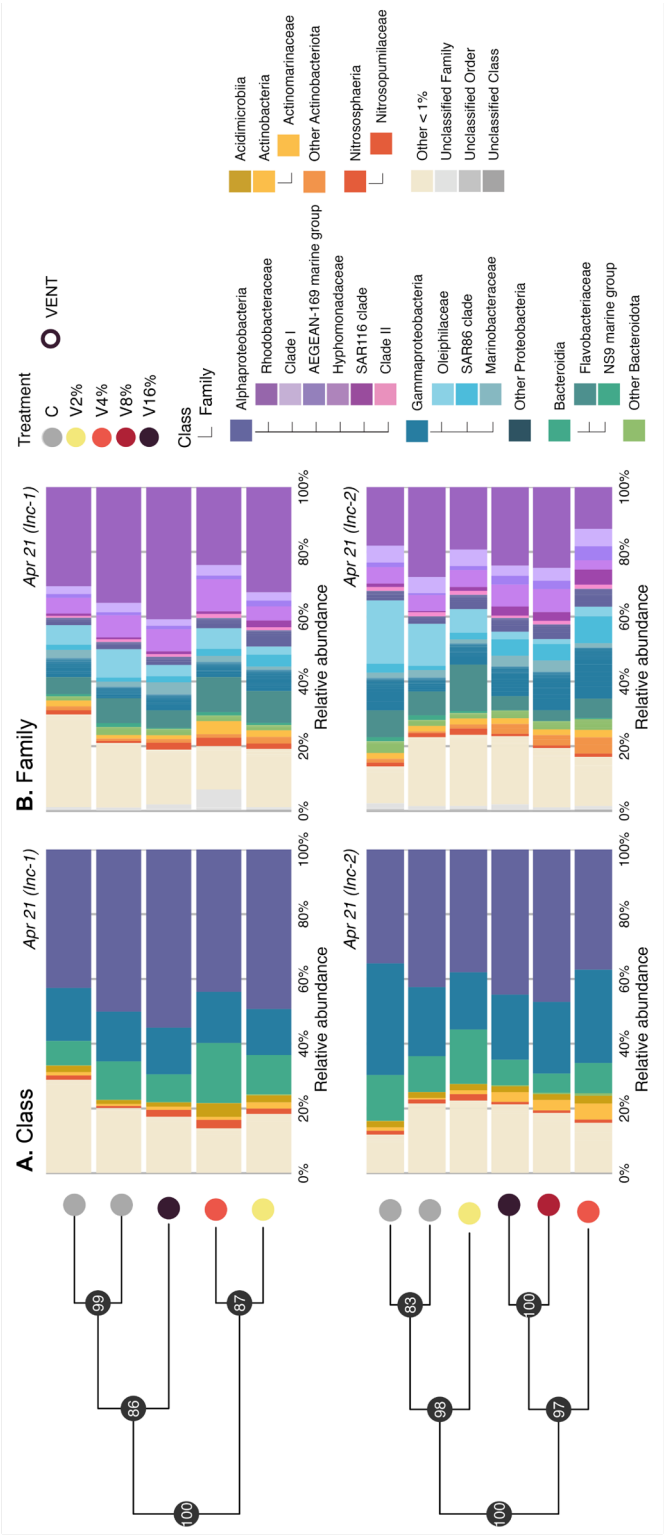

Figure 7. Hierarchical clustering and relative abundance of prokaryotic 16S rRNA sequences classified down to **(A)** class and **(B)** family level for each incubation (Inc). Coloured dots represent the control (grey), volcano (colour gradient) and vent-treated (white) bottles at the end of the April and October 2021 incubations. Volcano bottles were enriched with filtered hydrothermal seawater at concentrations ranging from 2% to 16% of the total volume, whereas vent bottles were treated with a 2% addition of vent fluids. Black points in the dendrogram represent the approximately unbiased p value (au) for each cluster. Taxa are ordered by decreasing relative abundance greater than 1% and grouped by the highest phylum groups.

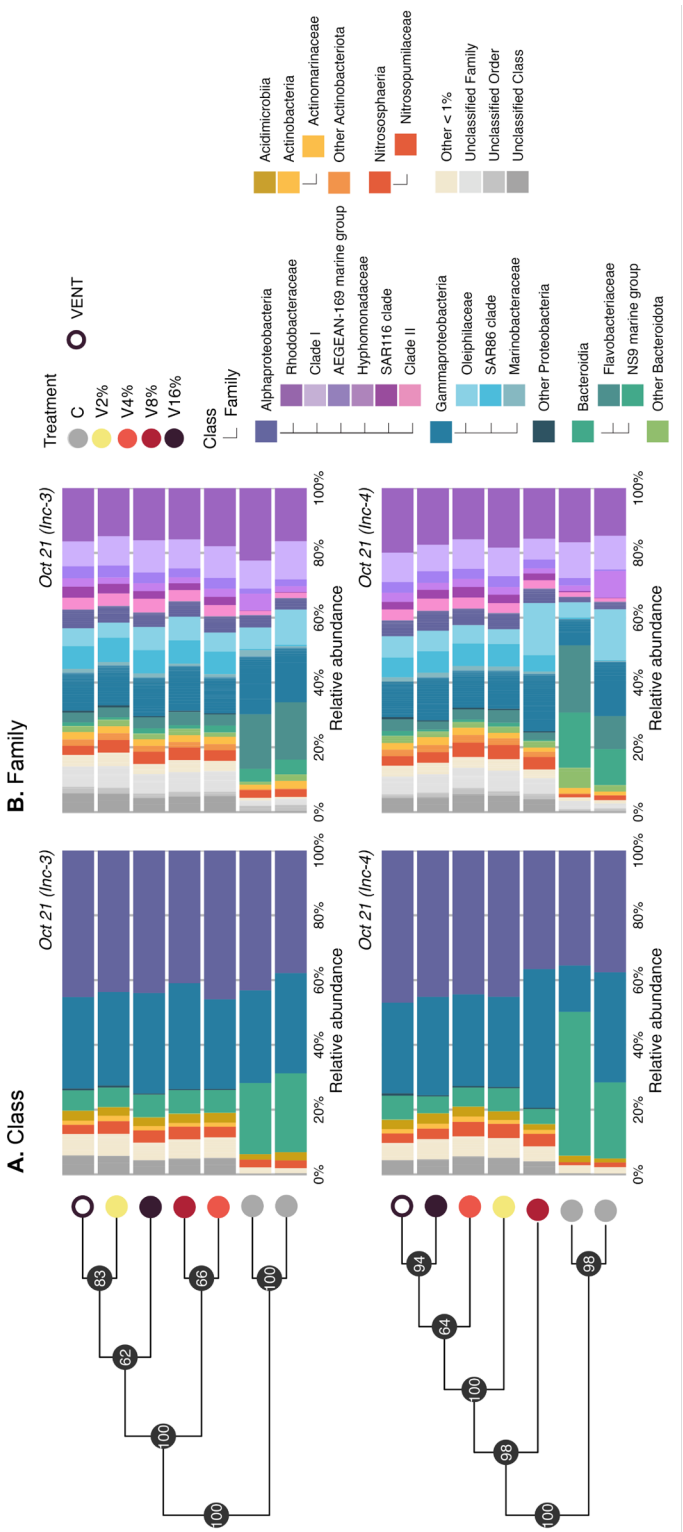

Figure 7. Continued.

Proteobacteria (67%–75%) was the most abundant phylum, comprising the classes Alphaproteobacteria (40%–46%) and Gammaproteobacteria (25%–28%). The Proteobacteria displayed some differences between control and treated bottles at the end of the incubations (**Figure 7A**) and contained the majority of the ASVs associated with the hydrothermal treatments (**Table S5**). *Rhodobacteraceae* (18%), *Clade I* (6%–8%), *AEGEAN-169 marine group* (3%–3.5%) and *Clade II* (2.5%–3.5%) families of Alphaproteobacteria predominated throughout the volcano- and vent-treated bottles (**Figure 7B**). Additionally, *Hyphomonadaceae* (2.5%–3%) and *SAR116 clade* (2.5%–3%) were some of the most benefited by the addition of hydrothermal products. A total of 31 alphaproteobacterial ASVs were associated with the treated bottles (*stat* > 0.85, $p \leq 0.001$ and $str_C \leq 0.5$; **Table S5**). Among these, many classified as *SAR116 clade*, *AEGEAN-169 marine group*, *Clade II* and *Rhodobacteraceae* stood out in terms of relative abundance (≤ 2%) (**Figure S7**). The diverse clade *SAR86* (Gammaproteobacteria) was also favoured by the additions (6.5%–7%) and contributed 14 out of 40 gammaproteobacterial ASVs (≤ 4%) indicative of hydrothermal treatment (*stat* > 0.85, $p \leq 0.001$ and $str_C < 0.5$; **Table S5 and Figure S7**). The remaining ASVs included several genera of phototrophic and chemotrophic Gammaproteobacteria, each below < 1% (**Table S5 and Figure S7**), such as *Litoricola*, *Pseudomonas*, the *OM60 (NOR5) clade*, the *SUP05 cluster* and *Pseudoalteromonas*.

Indicator species analyses identified another 25 ASVs, belonging to the phyla Actinobacteriota, Bacteroidota, Firmicutes, Desulfobacterota and Marinimicrobia (SAR406 clade), as treatment indicators (*stat* > 0.85, $p \leq 0.001$ and $str_C < 0.5$; **Table S5**). This group included around 14 genera and 9 species of low-abundance (≤ 0.5%) bacteria (**Table S5**), such as the free-living photoheterotrophs *Candidatus* Actinomarina (Actinobacteriota) and *NS5 marine group* (Bacteroidota), the chemoorganotrophic *Fabibacter* (Bacteroidota) and several human pathogens.

Lastly, the Crenarchaeota archaeal lineage was exclusively composed of the chemolithoautotrophic ammonia oxidisers *Nitrosopumilaceae* in all incubations (**Figure 7**). Despite a consistent decrease in their abundance across all treatments, their final relative abundances were higher in the treated bottles (~3%) than in the controls (~1%).

The treated bottles exhibited the largest prokaryotic richness and diversity of ASVs (**Figure 8A, B**). Statistical analyses identified the hydrothermal treatment

as the primary factor significantly influencing prokaryotic alpha diversity (p < 0.01, two-way ANOVA), followed by other factors related to the environmental conditions (including seasonal variations) (p < 0.05, two-way ANOVA). Meanwhile, the number of eukaryotic ASVs (richness) at the end of the treated incubations was generally higher relative to controls (**Figure 8A**), but exhibited some variability primarily influenced by the environmental conditions (p < 0.05, two-way ANOVA) rather than the treatment (p > 0.05, two-way ANOVA). In contrast, eukaryotic diversity was significantly modulated by the treatment (p ≤ 0.001, two-way ANOVA), with hydrothermally enriched waters displaying higher diversity estimates compared to controls (**Figure 8B**). Moreover, the alpha diversity estimates of prokaryotes at the end of the treated incubations surpassed those of eukaryotes (**Figure 8A and 8B**).

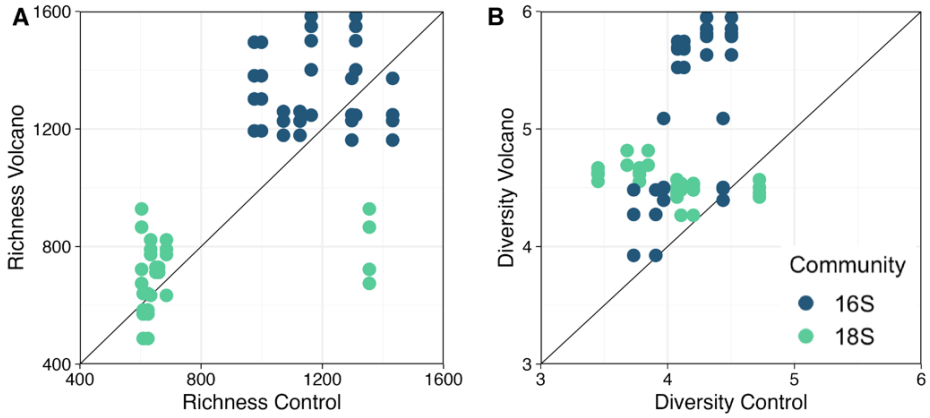

Figure 8. Control versus volcano and vent-treated **(A)** Chao1 richness and **(B)** Shannon diversity estimates at the end of the incubations. Volcano bottles were enriched with filtered hydrothermal seawater at concentrations ranging from 2% to 16% of the total volume, whereas vent bottles were treated with a 2% addition of vent fluids.

3.4 Discussion

Shallow-water hydrothermal vents constitute unique ecosystems rich in nutrients and reduced compounds, where primary production is often sustained by both photosynthesis and chemosynthesis (e.g., Tarasov et al. 2005; Maugeri et al. 2010). Using an experimental approach, we assessed for the first time the effects of diffusive hydrothermal emissions on microbial community abundance, structure and diversity at the Tagoro shallow submarine volcano in El Hierro (Canary Islands, Spain).

3.4.1 Effects of shallow hydrothermal fluids on the growth of marine microbes

Phytoplankton biomass and growth estimates, assessed by means of chlorophyll *a* concentration, exhibited the greatest increases in the volcano-treated bottles. Although the vent-treated bottles received the lowest hydrothermal enrichment, as indicated by $Si(OH)_4$ concentrations, they still exceeded control estimates. However, the increase in phytoplankton biomass in the vent-treated bottles was observed 2 days later than those in the volcano-treated bottles, possibly due to the small amount of nutrients added and/or the presence of toxic constituents that may have affected phytoplankton growth. These findings clearly show that hydrothermal fluids from Tagoro stimulate phytoplankton growth in shallow waters (i.e., primary production), inducing a fertilisation effect that may be detectable even up to a 100 m away from the active source and despite seasonal variations. This is consistent with in situ and experimental evidence across hydrothermal systems worldwide, where inorganic nutrients such as bioavailable Fe provided by hydrothermal inputs enhance primary productivity in the surface layer (e.g., Buck et al. 2018; Guieu et al. 2018; Bonnet et al. 2023; Tilliette et al. 2023). In a similar experiment carried out in the Western Tropical South Pacific Ocean, Tilliette et al. (2023) observed a clear stimulation of net community production following the addition of hydrothermal fluids to indigenous phytoplankton communities.

The enhancement in phytoplankton biomass likely led to high dissolved organic matter production in our treated incubations, thereby driving microbial utilisation of organic material. Besides introducing trace metals like Fe that serve as micronutrients for plankton communities (Guieu et al. 2018; Ardyna et al. 2019; Schine et al. 2021; Bonnet et al. 2023; Mériguet et al. 2023), hydrothermal fluids also contain essential metals that may become harmful at

the high concentrations found near vents (e.g., Cu and As) (Lilley, Feely, and Trefry 1995; Price et al. 2013). In this context, vent microorganisms have been shown to produce organic ligands to either enhance the bioavailability of some essential metals or decrease their toxicity at high levels (Klevenz et al. 2012). Recently, some *Synechococcus* ecotypes have been observed to produce strong binding ligands, especially thiols, proving their ability to detoxify the environment and thus favour phytoplankton growth (Tilliette et al. 2023). These findings raise concerns about the potential impact of toxic metals on plankton communities near Tagoro and suggest that common surface microbes may possess mechanisms to overcome these extreme conditions. Despite the absence of direct measurements, significant amounts of heavy metals have been observed in cephalopods captured in the vicinity of this submarine volcano (Lozano-Bilbao et al. 2022), supporting the idea that vent fluids from Tagoro contain relevant concentrations of toxic elements. However, both auto-and heterotrophic microbes grew equally well or better in the presence of hydrothermal fluids as compared to controls. This indicates that, even if some toxic metals may have been present, their effect on productivity was small as compared to the stimulation caused by the other components of hydrothermal fluids.

The stimulation of primary production in the incubations enriched with hydrothermal fluids was coupled with increases in cell abundances of certain photosynthetic picoplankton (0.2–2 μm) populations. Picoeukaryotes and *Synechococcus* picocyanobacteria reached cell abundances that were 3- to 5-fold higher than those in controls, evidencing their ability to thrive in hydrothermally enriched habitats. Despite the lower hydrothermal enrichment in the vent-treated bottles, some *Synechococcus* populations managed to increase their cell abundances up to 4-fold higher than in controls. *Prochlorococcus* picocyanobacteria and heterotrophic bacteria, on the other hand, grew similarly well across all treatments, albeit they reached higher cell abundances in the presence of hydrothermal fluids. Other experimental studies have shown similar results, where picocyanobacterial growth (mainly *Synechococcus*) was sustained by dissolved Fe concentrations provided by hydrothermal inputs (Tilliette et al. 2023).

Molecular analyses further revealed a strong presence of small photosynthetic eukaryotes ($\leq$ 5 μm) in the treated bottles, including dinoflagellates, photosynthetic stramenopiles, small green algae and radiolarians, which likely supported the enhancement in chlorophyll *a* levels. The treated bottles also

supported the growth of ecologically and metabolically diverse prokaryotes, comprising chemosynthetic and photosynthetic bacteria, as well as a few ammonia-oxidising archaea. It is relevant to emphasise that, despite the enhancement of phytoplankton growth, hydrothermal inputs from Tagoro did not result in harmful, disruptive events such as the proliferation of harmful algal species. Instead, they sustained the enhanced growth of many microbial populations already present in the area, as discussed in **Section 3.4.2**. Remarkably, the natural communities collected at a depth of 127 m, both around the crater and in unaffected waters, already contained a large proportion of the photoautotrophic microbes that benefited from hydrothermal fluid additions. This indicates that enhanced photosynthesis may occur not only when hydrothermal fluids mix with surface waters but also in deeper waters around the main crater. Our estimates of the MLD and in situ dissolved silicate concentrations further confirm that, especially in spring, hydrothermal, nutrient-rich products often reach photosynthetic organisms near the Tagoro submarine volcano, a scenario we aimed to replicate in our experiments.

3.4.2 Effects of shallow hydrothermal fluids on the composition and diversity of marine microbes

The taxonomic composition of the eukaryotic community differed between controls and treated bottles, with volcano- and vent-treated bottles developing characteristic communities, as evidenced by hierarchical clustering analyses. Statistical analyses further indicated that, despite variations in environmental conditions (i.e., seasonal or minor variations in physical–chemical properties of the water column), hydrothermal inputs from the Tagoro submarine volcano induced a clear response in the eukaryotic community structure.

Photosynthetic stramenopiles, primarily comprising diatoms (Bacillariophyta), along with other heterokonts (Pelagophyceae), exhibited a significant presence across all incubations. However, their relative abundance was twice as high in the control samples compared to the treated bottles, and they consistently maintained the second highest representation within the treated incubations. Among the predominant and varied diatom community, the less abundant (≤ 1%) pico-and nanoplanktonic polar-centric species, including *C. tenuissimus*, *A. cornucervis* and *M. polymorphus*, demonstrated a robust association with hydrothermal inputs, as they were predominantly observed in treated bottles. Diatoms, unlike other major phytoplankton groups, strictly depend on dissolved silicon, along with sufficient light, inorganic nutrients and trace

elements, to sustain their fast growth rates (Morel and Price 2003). Although the surface waters affected by Tagoro may provide favourable conditions for diatom proliferation, as evidenced by nutrient depletion at the end of the treated incubations, our findings suggest that factors such as resource competition, selective grazing and viral activity may control the extent of their response. Centric diatoms in the planktonic realm have the ability to adjust their buoyancy, allowing them to move vertically within the water column. This capability may provide these species with advantages in resource competition and predator evasion (Armbrust 2009). Our findings emphasise the ability of certain diatom species to benefit from changing ambient conditions and thus contribute to the overall productivity of the system (Benoiston et al. 2017; Serôdio and Lavaud 2020). Recent evidence has demonstrated that the small pico-and nanoplanktonic diatom cells, often overlooked, may not only fuel the microbial loop but also contribute to sustaining higher trophic levels and facilitating carbon export (Leblanc et al. 2018). Therefore, small planktonic diatoms (mostly centric forms) may exert a significant impact on the productivity, nutrient cycling and carbon sequestration in Tagoro. Other high-abundance heterokont species, such as *P. calceolata*, were largely unaffected by the addition of hydrothermal fluids. The persistence of this specific species throughout the incubations underscored its adaptative capacities, as *P. calceolata* is known to thrive under the high temperature, low light and low iron conditions (Guérin et al. 2022) typical of the deep, unaffected waters at the sampling location. These traits might explain its low diversity compared to that of diatoms in the context of a shallow hydrothermal system characterised by $Si(OH)_4$, NO_2^- + NO_3^-, and presumably Fe-rich seawaters, which are quite different from those conditions where *Pelagomonas* may be a strong competitor.

Small green algae emerged as a key contributor to local primary production, doubling the increases in relative abundances observed in controls. The hydrothermal additions notably benefited the Chloropicophyceae prasinophyte lineage, particularly the Chloropicaceae family. The Prasino Clade V and Mamiellophyceae prasinophyte lineages, together with the Trebouxiophyceae class (core Chlorophyta), also exhibited higher relative abundances compared to controls. These independent prasinophyte lineages comprise small-sized coccoid species that play a key role in marine phytoplankton communities, especially in moderately oligotrophic waters (Lopes dos Santos et al. 2017). Their higher surface area-to-volume ratio enhances nutrient uptake efficiency and thus improves their competitiveness in nutrient-poor environments,

facilitates their escape from predators and promotes buoyancy (Lemieux et al. 2019). These traits may grant Chloropicophyceae, and particularly the species *C. roscoffensis*, with the necessary advantages to outcompete other planktonic algae under the moderate nutrient concentrations in our hydrothermal additions. *Chloropicon* presence is ubiquitous across the globe, known for its ability to recycle propionate for carbon and energy sources, as well as synthesise scarce vitamins, among other traits (Lemieux et al. 2019). The indicator species analysis underscored the responsiveness of this particular species, with 10 ASVs identified as treatment indicators.

Our study also revealed the important role of protists, mostly dinoflagellates, in modulating the marine plankton dynamics within the Tagoro ecosystem. Contrary to the controls, dinoflagellates constituted half of the eukaryotic community at the end of the treated incubations. Syndiniales, a diverse group of unicellular parasites, emerged as the dominant class, with several families being linked to the presence of hydrothermal fluids, including Dino-Group I Clades 1 and 4, and Dino-Group II Clades 10 and 11. Interestingly, these groups are common inhabitants of deep-sea hydrothermal vents (Hu et al. 2023), emphasising the importance of parasitic protists in the ecology of submarine hydrothermal vents. As already observed in deep sea hydrothermal vent ecosystems, the enhanced biological activity associated with diffusive vent fluids increases host and prey biomass and thereby parasitic encounters and infection. Syndiniales display putative parasite–host relationships with a wide range of hosts, such as other dinoflagellates and protist groups (e.g., ciliates, radiolarians, diatoms and copepods) (Anderson and Harvey 2020), yet these relationships remain poorly understood. Recent studies have shown that Syndiniales are often associated with Dinophyceae and Arthropoda (mainly copepods) in surface oligotrophic waters (Anderson et al. 2024). In our treated bottles, hydrothermal inputs indeed favoured the less abundant Dinophyceae class, with relatively large contributions of family Gymnodiniaceae, a recognised putative host of Syndiniales (Guillou et al. 2008). In addition, the less abundant species *Blastodinium mangini* within Dinophyceae exhibited a significant association with the treated bottles. *Blastodinium* is known to inhabit the gut of planktonic copepods, especially in warm temperate to tropical waters (Skovgaard, Karpov, and Guillou 2012), which aligns with previous observations of enhanced zooplankton growth in waters affected by degassing emissions at Tagoro (Fernández de Puelles et al. 2021). Indeed, those authors observed a significant presence of Oncaea non-calanoid copepods, which are

frequently infected by *B. mangini* (Skovgaard, Karpov, and Guillou 2012). Mixotrophic protists like Radiolaria, known for their phagotrophic feeding (Biard 2022), also benefited from the presence of hydrothermal products in our incubations, despite their relatively low representation. Their prey includes bacteria, small autotrophs (like diatoms and dinoflagellates), other protists (mostly ciliates and tintinnids) and even multicellular heterotrophs (like copepods). These findings suggest an important top-down pressure exerted by protist marine phagotrophy and parasitism on the local plankton community at Tagoro. Protistan grazing thus not only represents an important ecological link in food webs by transferring organic carbon from primary producers to higher trophic levels (Hu et al. 2021) but also to the microbial loop (Park, Yih, and Coats 2004). Recent studies have indicated that Syndiniales in particular may contribute to attenuating the particulate carbon flux through remineralisation of host carbon that in the end may fuel bacterial production (Anderson et al. 2024). However, the contribution of parasitism to pools of dissolved organic matter in the ocean is uncertain. Contrarily, Radiolaria are active players in the biogeochemical cycles of silica, carbon and strontium, depending on their main skeletal chemical component (Biard 2022). These findings indicate that protistan activity will not only influence the planktonic community structure but also the local cycling of nutrients.

Alpha diversity estimates, encompassing richness and diversity, indicated the pronounced dominance of a select few eukaryotic populations within the overall assemblage observed in the treated bottles. This finding, supported by robust statistical significance, highlights a marked specialisation within the eukaryotic community in response to the hydrothermally enriched conditions, in contrast to the prokaryotic community.

Conversely, the differences in prokaryotic community structure between control and treated bottles were mostly driven by the environmental conditions, such as seasonal variations in the properties of the water column. Although hydrothermal inputs did have a significant effect on shaping the prokaryotic community, their overall impact was minor. As mentioned in **Section 3.4.1**, a great diversity of ecologically and metabolically diverse prokaryotes was observed at the end of the treated incubations. Yet, the predominant Alphaproteobacteria and Gammaproteobacteria classes displayed some of the greatest differences throughout the incubations. Among the alphaproteobacterial ASVs significantly associated with the hydrothermal additions, the *SAR116 clade*, *AEGEAN-169 marine group*, *Clade II* and

Rhodobacteraceae stood out in terms of relative abundance. Their presence in the treated bottles was likely related to their ability to utilise phytoplankton-derived organic matter and/or form symbiotic associations with marine eukaryotes to obtain carbon and other nutrients at hydrothermal vents. Moreover, many harbour distinct metabolic capacities that potentially allow them to adapt and thrive at particular habitat conditions, like those at hydrothermal vents. For instance, *SAR116* have genes for proteorhodopsin-based photoheterotrophy, carbon monoxide dehydrogenase and dimethylsulfoniopropionate demethylase, which at the same time evidence the biogeochemical importance of this clade, especially in the marine sulfur cycle (Roda-Garcia et al. 2021). The *AEGEAN-169 marine group*, likewise, is known for its potential to transport and utilise a wide spectrum of sugars, trace metals and vitamins (Getz et al. 2023). Within the gammaproteobacteria, different ASVs belonging to the *SAR86 clade* were strongly linked to hydrothermal inputs. *SAR86* is recognised as an aerobic chemoheterotroph with the potential for energy generation through proteorhodopsin (Dupont et al. 2012). Given its vast genetic diversity, distinct *SAR86* subgroups have demonstrated a unique geographic distribution closely associated with specific environmental characteristics (Hoarfrost et al. 2020), such as hydrothermal plumes (Zhou et al. 2020), consistent with our previous findings regarding other proteobacterial groups. Despite the clear dominance of Proteobacteria, several low-abundance bacteria species (≤ 0.5%) belonging to Actinobacteriota, Bacteroidota, Firmicutes, Desulfobacterota and Marinimicrobia (SAR406 clade) phyla were also identified as treatment indicators. Interestingly, members of Desulfobacterota appear as strong indicators of hydrothermal activity, indicating that sulfur oxidation may be an important microbial process in the water column around the Tagoro volcano. Moreover, the ubiquitous persistence of chemosynthetic microbes related to the oxidation of sulfur and ammonia throughout the treatments and controls highlights the potential for rapid dispersal of these organisms among different hydrothermal sites. Overall, our study indicates that the current hydrothermal fluids from Tagoro influence the prokaryotic community, directly by fuelling chemosynthetic processes but also indirectly by supporting higher phototrophic production, as has been observed.

3.5 Conclusions

Our findings confirm that hydrothermal processes affect surface microbial communities surrounding the Tagoro underwater volcano even a decade after its eruption. Phytoplankton biomass and growth increased in response to hydrothermal additions, demonstrating the potential of hydrothermal fluids to enhance primary production. This increase in primary production was accompanied by shifts in the structure and composition of the local marine microbial community, with notable contributions from small green algae (Chlorophyta) and diatoms (Bacillariophyta). Our analyses identified certain species within these groups as highly adapted to the new environmental conditions associated with the hydrothermal treatment. The results also indicated that parasitism by Syndiniales (Dinoflagellata) and protistan grazing may play a crucial role in modulating local plankton dynamics, ultimately shaping nutrient cycling and carbon export in the area. Phototrophic and chemotrophic bacteria also thrived in the treated bottles, although heterotrophic prokaryotes in the Tagoro hydrothermal ecosystem were the major drivers of prokaryotic growth. Overall, our findings support recent observations that shallow diffusive hydrothermal vent systems, such as the Tagoro submarine volcano, may enhance primary production rates locally by both phototrophic and chemoautotrophic processes. Our study demonstrates that shallow hydrothermal fluxes can serve as local drivers of microbial productivity, an aspect previously overlooked, highlighting the need for further research in this area.

Supplementary material

Supplementary figures

(A) Reference

Spring
April 2021

Autumn
October 2021

Winter
February 2023

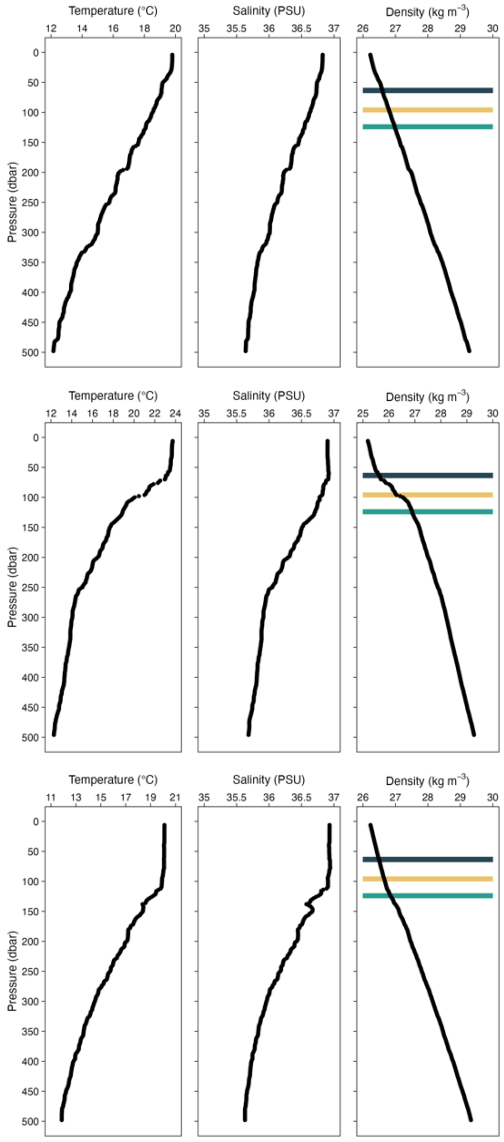

Figure S1. Example of temperature, salinity and potential density profiles from vertical hydrographic profiles during seasonal VULCANA cruises at **(A)** the reference station 901 and **(B)** above the main crater of Tagoro (stations 31 and 61). Note that vertical and horizontal scales differ between stations. Horizontal bold solid lines indicate the median MLD estimates for spring (green), autumn (yellow) and winter (blue) seasons based on the maximum potential density gradient approach.

(B) Main crater of Tagoro

Spring
April 2021

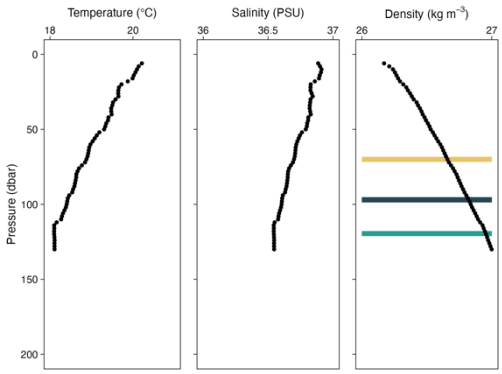

Autumn
November 2019

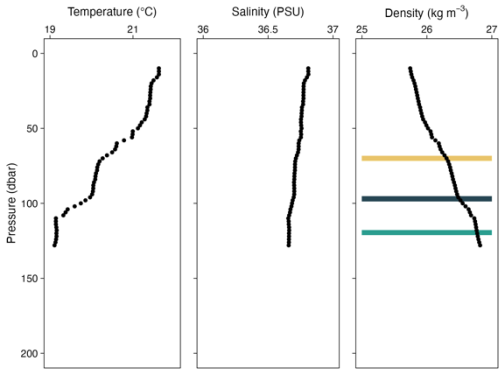

Winter
December 2020

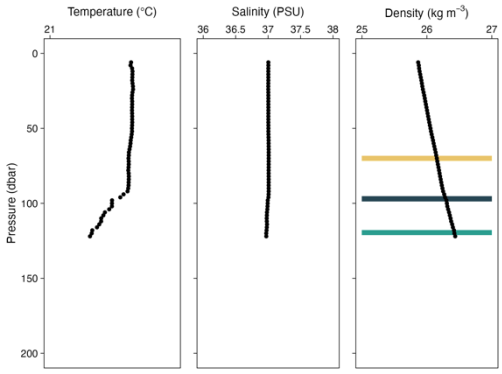

Figure S1. Continued.

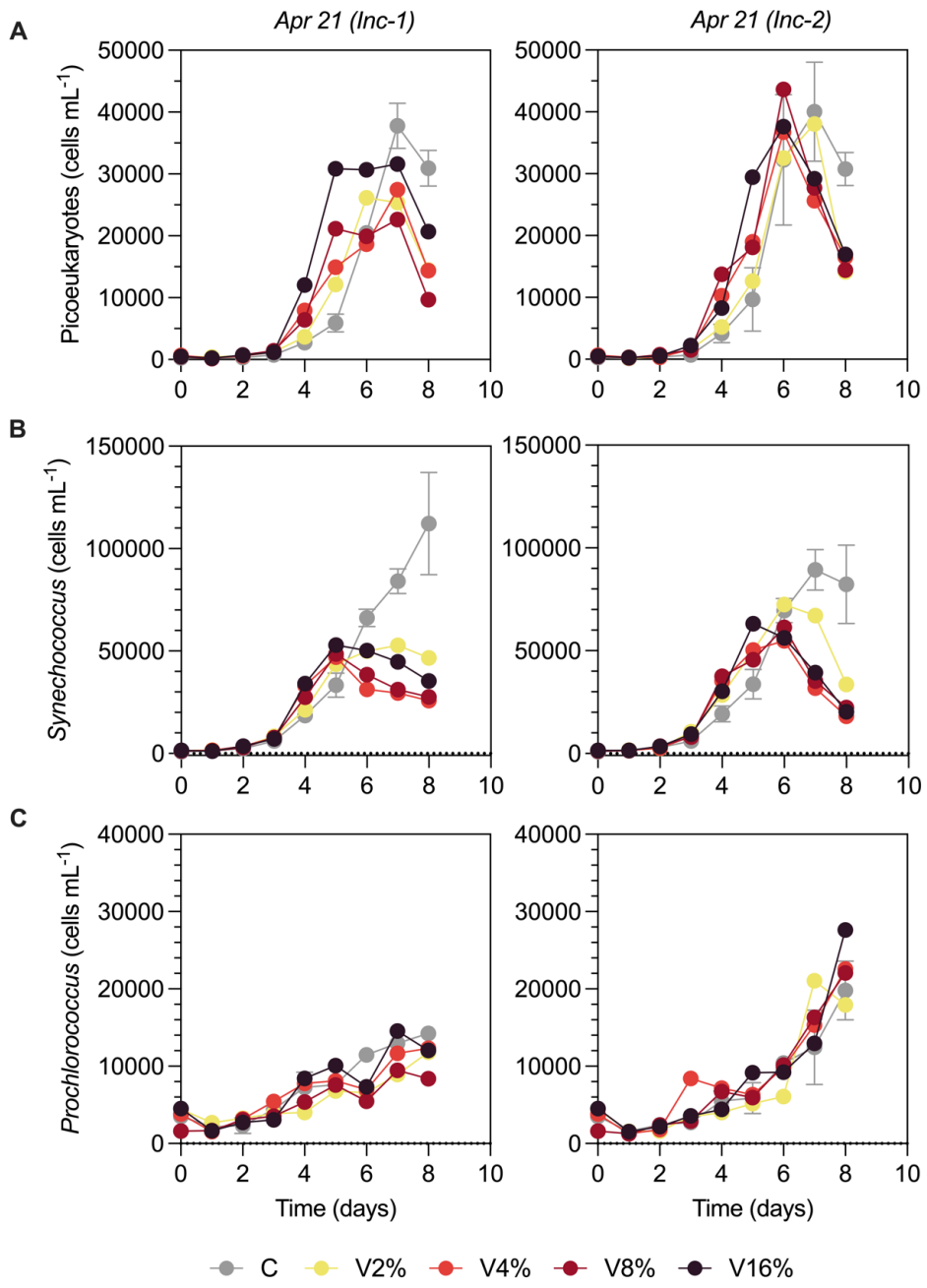

Figure S2. Picophytoplankton cell abundances (cells mL^{-1}) in April 2021 incubations of **(A)** picoeukaryotes, **(B)** *Synechococcus* and **(C)** *Prochlorococcus* populations. Control (grey) dots represent the average and standard deviation from two replicate control bottles placed in each incubator (Inc). In contrast, volcano-treated (color gradient) dots represent individual bottles, each enriched with a proportion of filtered hydrothermal seawater (ranging from 2% to 16% of the total volume).

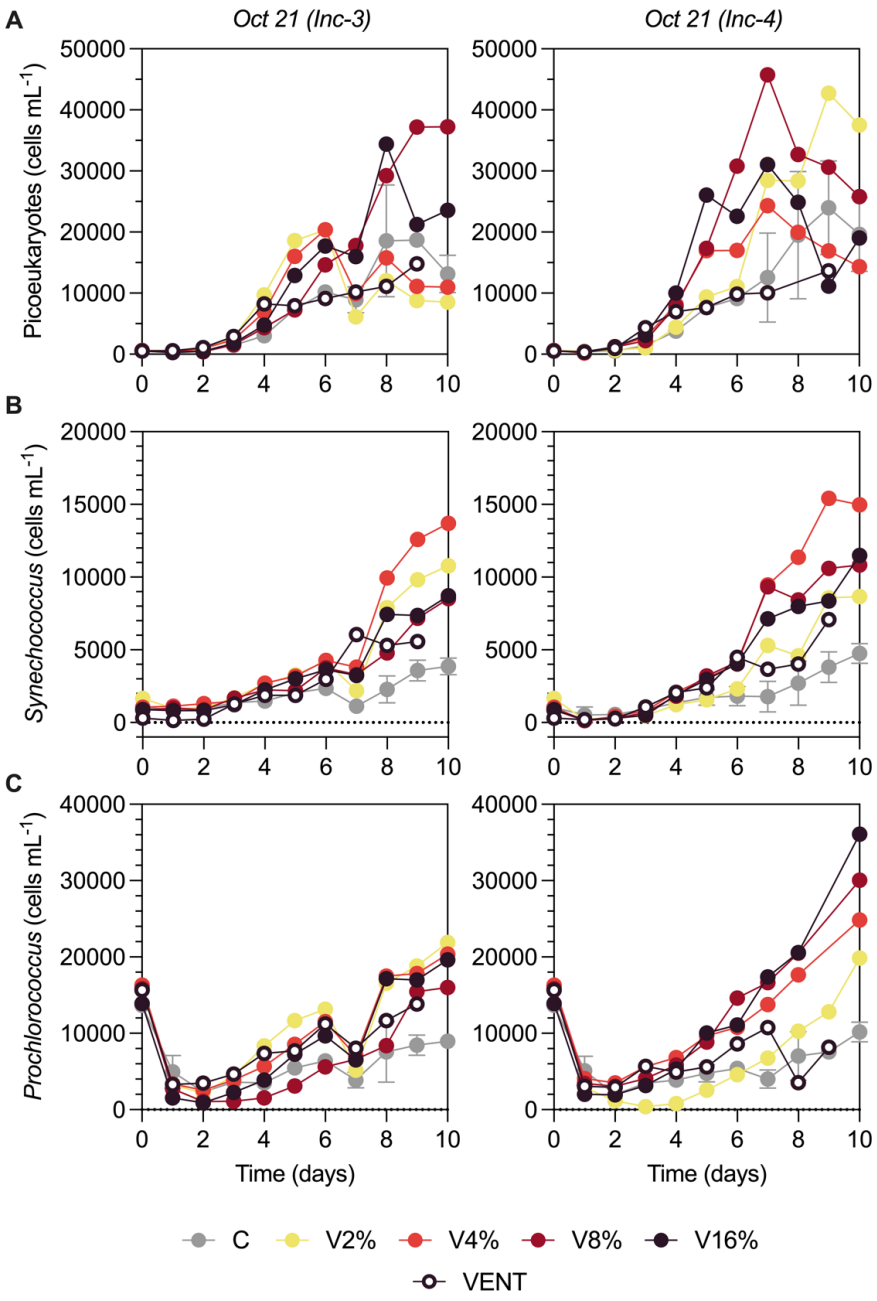

Figure S3. Picophytoplankton cell abundances (cells mL^{-1}) in October 2021 incubations of **(A)** picoeukaryotes, **(B)** *Synechococcus* and **(C)** *Prochlorococcus* populations. Control (grey) dots represent the average and standard deviation from two replicate control bottles placed in each incubator (Inc). In contrast, volcano (color gradient) and vent-treated (white) dots represent individual bottles, each enriched with a proportion of filtered hydrothermal seawater (ranging from 2% to 16% of the total volume) or with 2% of vent fluids.

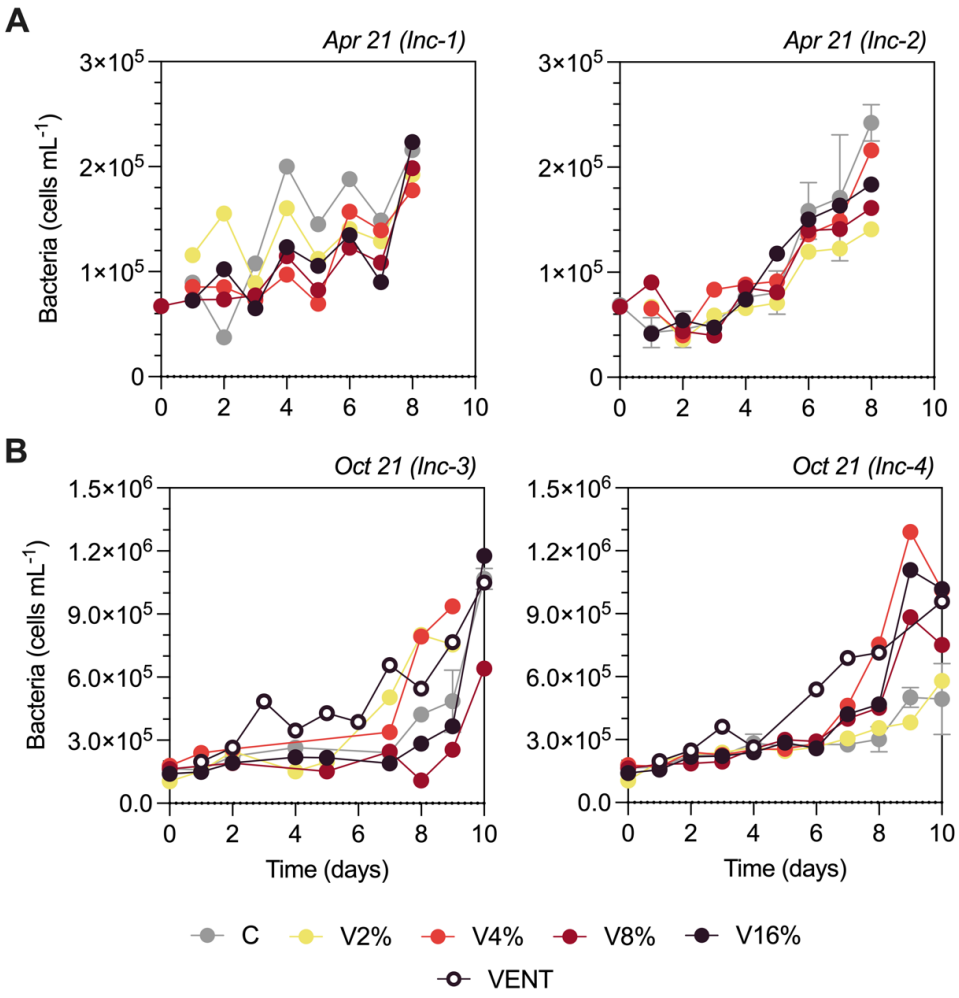

Figure S4. Heterotrophic bacteria cell abundances (cells mL^{-1}) in **(A)** April and **(B)** October 2021 incubations. Control (grey) dots represent the average and standard deviation from two replicate control bottles placed in each incubator (Inc). In contrast, volcano (color gradient) and vent-treated (white) dots represent individual bottles, each enriched with a proportion of filtered hydrothermal seawater (ranging from 2% to 16% of the total volume) or with 2% of vent fluids.

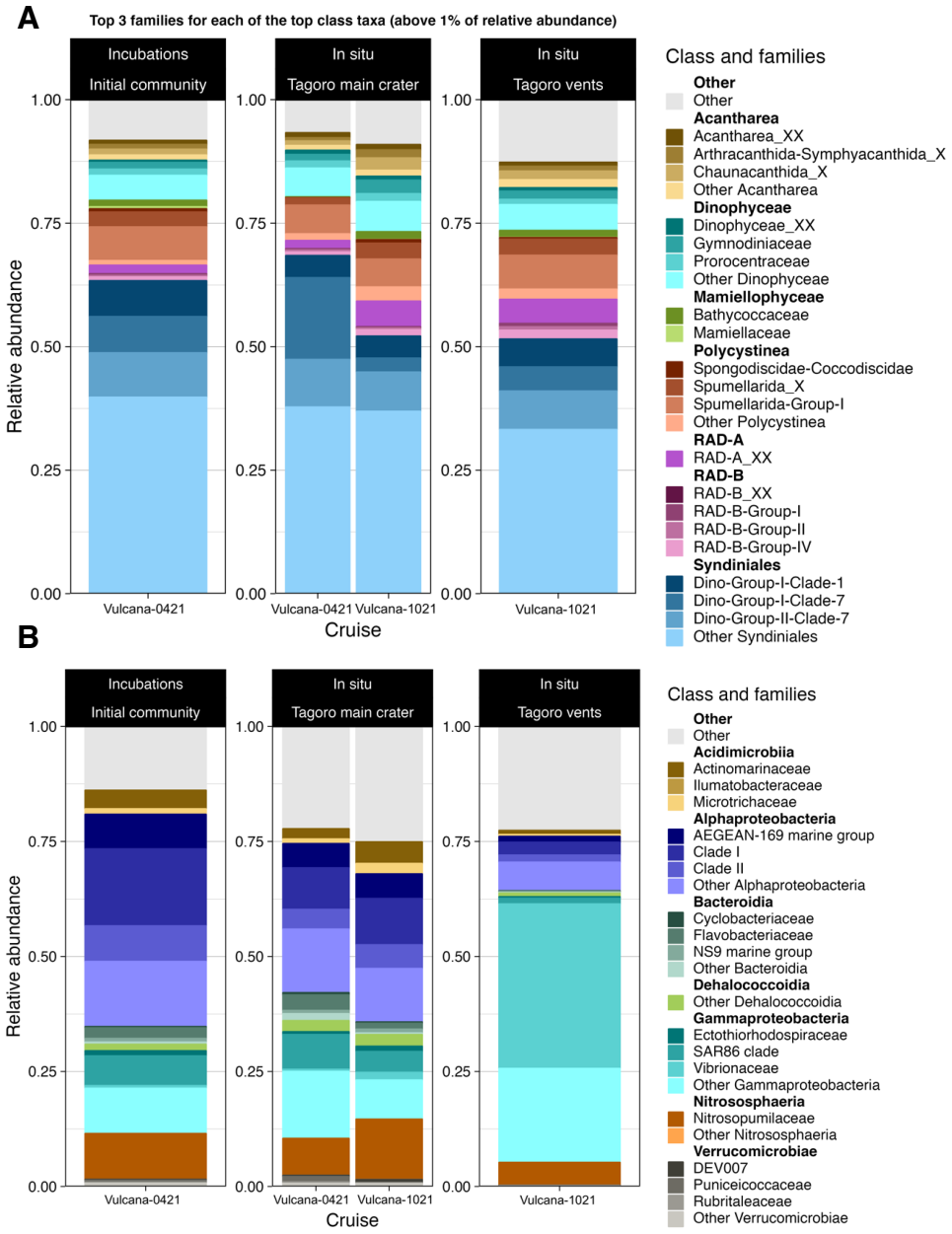

Figure S5. Relative abundance of family-classified **(A)** eukaryotes and **(B)** prokaryotes at the start of the April 2021 incubations, alongside seawater samples collected in situ from the Tagoro main crater (~127 m depth) and active vent (~122 m depth) during the April and October 2021 VULCANA cruises. Taxa displaying more than 1% of relative abundance are grouped by class.

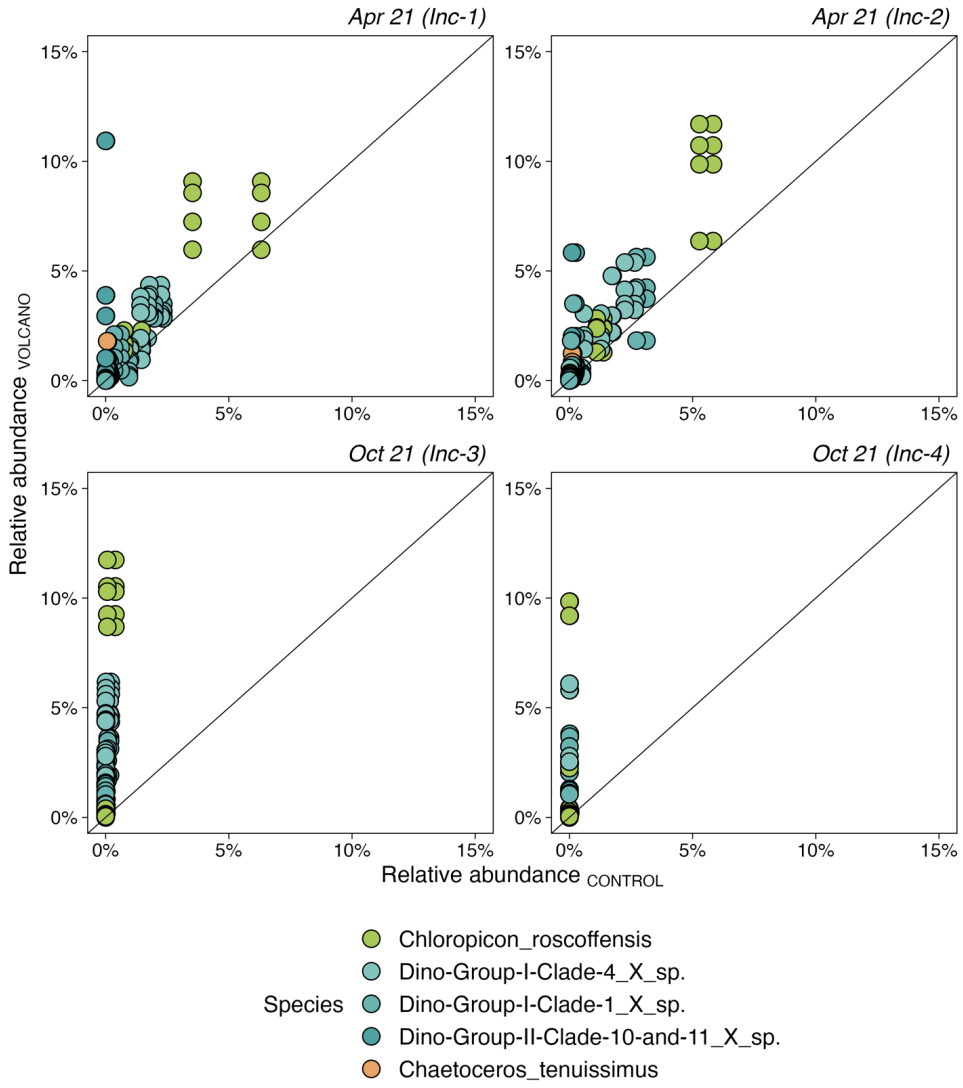

Figure S6. Eukaryotic ASVs significantly associated with both volcano and vent treatments (*stat* > 0.85, $p = 0.001$ and $str_C < 0.5$), and with median relative abundances ≥ 1% at the end of the April and October incubations. Results related to **Table S4**.

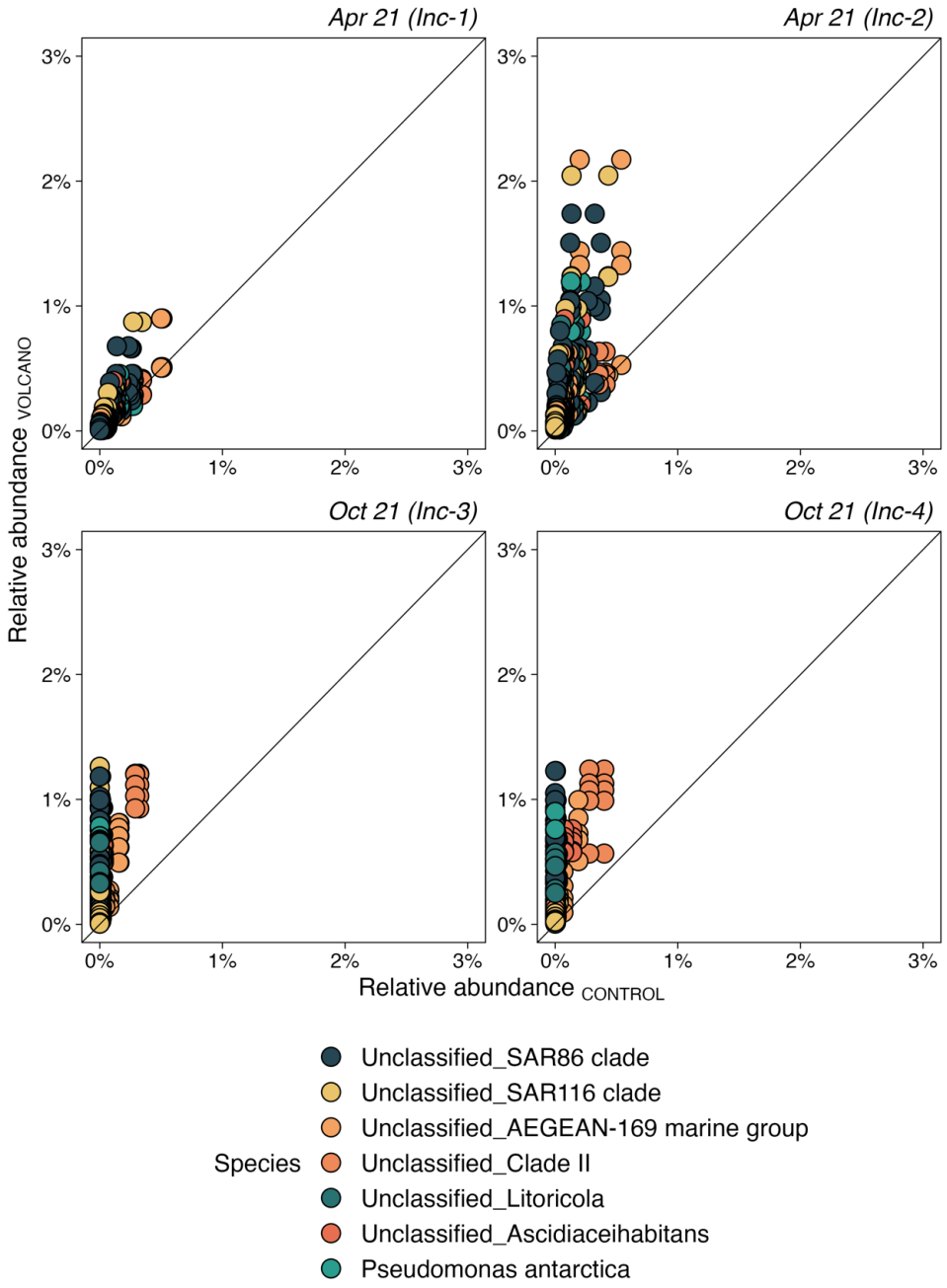

Figure S7. Prokaryotic ASVs significantly associated with both volcano and vent treatments (*stat* > 0.85, $p = 0.001$ and $str_C < 0.5$), and with median relative abundances ≥ 0.5% at the end of the April and October incubations. Results related to **Table S5**.

Supplementary tables

Table S1. $Si(OH)_4$ concentrations (μmol kg^{-1}) from water column samples (120–130 m depth) collected over the last 9 years of VULCANA cruises (2014–2023) in vertical hydrographic stations above and around the main crater of Tagoro (station 31; ~127 m). Reference station 901 is also included. Average from duplicate nutrient analysis ± standard deviation is shown. NA (not applicable) indicates single unreplicated measurements.

Cruise date	Station	Distance to main crater (m)	Latitude	Longitude	Pressure (dbar)	$Si(OH)_4$ (μmol kg^{-1})
Feb-23	901	8846.71	27.64992	-17.90986	127.287	0.88±0.00
Nov-22	901	8852.81	27.65000	-17.90983	126.965	0.88±0.00
Nov-22	902	8310.83	27.63250	-17.90983	126.6	0.82±0.01
Nov-22	01	247.73	27.61817	-17.99117	125.224	0.95±0.00
Nov-22	04	196.25	27.61900	-17.99483	120.294	1.12±0.00
Nov-22	11	229.86	27.61983	-17.99533	120.485	1.20±0.01
Nov-22	14	44.39	27.61933	-17.99317	125.213	1.75±0.00
Nov-22	16	256.37	27.61867	-17.99067	125.208	1.10±0.00
Nov-22	19	67.53	27.61983	-17.99233	128.67	2.48±0.00
Nov-22	21	158.27	27.62050	-17.99433	125.314	1.18±0.01
Nov-22	22	4892.47	27.62100	-17.94333	121.088	1.08±0.01
Nov-22	27	158.81	27.62100	-17.99233	128.094	0.95±0.01
Nov-22	28	205.98	27.62150	-17.99350	121.004	1.15±0.00
Nov-22	31	3.33	27.61967	-17.99300	123.294	1.16±0.02
Nov-22	34	260.27	27.62200	-17.99350	120.875	1.26±0.00
Feb-22	901	8857.37	27.65000	-17.90978	127.436	0.58±NA
Feb-22	901	8857.37	27.65000	-17.90978	127.436	0.74±NA
Oct-21	61	17.71	27.61960	-17.99286	128.075	0.98±0.08
Oct-21	61	12.02	27.61972	-17.99288	129.428	3.18±0.02
Oct-21	61	11.81	27.61970	-17.99288	127.196	2.99±0.01
Oct-21	61	12.02	27.61972	-17.99288	128.963	3.78±0.03
Oct-21	901	8859.19	27.65000	-17.90976	127.275	0.89±0.07

Table S1. Continued.

Cruise date	Station	Distance to main crater (m)	Latitude	Longitude	Pressure (dbar)	$Si(OH)_4$ (μmol kg^{-1})
Oct-21	61	10.32	27.61964	-17.99292	127.742	1.95±0.05
Oct-21	61	8.18	27.61968	-17.99292	129.436	2.02±0.21
Oct-21	61	8.18	27.61968	-17.99292	129.345	6.83±0.05
Oct-21	61	8.18	27.61968	-17.99292	129.135	6.32±0.86
Oct-21	61	11.29	27.61980	-17.99302	127.818	3.53±1.57
Oct-21	61	17.89	27.61986	-17.99302	123.882	2.93±0.93
Oct-21	61	17.89	27.61986	-17.99302	124.416	4.58±0.51
Oct-21	61	17.89	27.61986	-17.99302	124.397	5.17±0.36
Apr-21	01	241.86	27.61820	-17.99122	121.910	0.63±0.01
Apr-21	02	265.61	27.61748	-17.99200	128.306	0.67±0.01
Apr-21	03	197.36	27.61798	-17.99350	121.116	0.63±0.04
Apr-21	06	120.35	27.61880	-17.99368	122.175	0.52±0.01
Apr-21	10	123.04	27.61946	-17.99422	123.343	0.64±0.00
Apr-21	11	226.84	27.61982	-17.99530	120.521	0.72±0.00
Apr-21	17	200.45	27.61928	-17.99102	123.535	0.69±0.00
Apr-21	19	69.81	27.61980	-17.99230	121.363	0.67±0.00
Apr-21	21	154.58	27.62048	-17.99430	127.056	1.69±0.00
Apr-21	23	113.23	27.62048	-17.99226	124.690	0.94±0.00
Apr-21	29	209.61	27.62118	-17.99432	124.796	1.00±0.00
Apr-21	901	8856.39	27.65002	-17.90980	128.333	1.22±0.00
Apr-21	710	173.25	27.61820	-17.99252	129.476	1.05±0.01
Apr-21	720	173.25	27.61820	-17.99252	129.765	1.00±0.00
Apr-21	740	173.25	27.61820	-17.99252	129.941	0.64±0.01
Dec-20	07	171.73	27.61820	-17.99258	129.641	0.70±NA
Dec-20	14	61.16	27.61916	-17.99312	120.826	1.16±NA
Dec-20	21	165.23	27.62052	-17.99440	124.204	1.25±NA

Table S1. Continued.

Cruise date	Station	Distance to main crater (m)	Latitude	Longitude	Pressure (dbar)	$Si(OH)_4$ (μmol kg^{-1})
Dec-20	23	111.92	27.62052	-17.99234	129.917	0.65±NA
Dec-20	23	107.53	27.62052	-17.99242	129.951	0.96±NA
Dec-20	28	206.96	27.62150	-17.99354	129.775	0.63±NA
Dec-20	31	13.48	27.61958	-17.99298	123.854	1.28±NA
Dec-20	31	13.33	27.61958	-17.99300	121.805	8.11±NA
Dec-20	31	11.29	27.61960	-17.99302	121.593	5.64±NA
Dec-20	31	7.74	27.61964	-17.99304	120.383	8.05±NA
Dec-20	31	6.95	27.61964	-17.99302	120.297	8.78±NA
Dec-20	31	6.95	27.61964	-17.99302	120.382	7.69±NA
Dec-20	31	6.81	27.61965	-17.99304	122.570	7.22±NA
Dec-20	31	7.74	27.61964	-17.99304	122.935	5.90±NA
Dec-20	27	192.57	27.62138	-17.99252	124.385	0.84±NA
Dec-20	31	13.33	27.61958	-17.99300	121.402	0.55±NA
Dec-20	31	9.72	27.61962	-17.99304	121.472	1.31±NA
Dec-20	31	7.24	27.61968	-17.99307	121.217	2.32±NA
Dec-20	31	20.00	27.61952	-17.99300	123.328	4.40±NA
Dec-20	31	17.78	27.61954	-17.99300	123.322	5.30±NA
Dec-20	22	137.02	27.62090	-17.99332	123.108	0.80±NA
Nov-19	01	3115.14	27.60622	-17.96526	120.867	1.05±NA
Nov-19	01	3117.28	27.60618	-17.96526	125.501	0.87±NA
Nov-19	01	3115.55	27.60618	-17.96528	120.864	0.71±NA
Mar-18	02	8082.83	27.66968	-17.93334	125.388	0.74±NA
Mar-18	02	8082.83	27.66968	-17.93334	125.520	0.50±NA
Mar-18	51	357.37	27.61684	-17.99134	124.814	0.04±NA
Mar-18	52	248.41	27.61764	-17.99202	125.954	0.04±NA
Mar-18	54	101.26	27.61884	-17.99266	124.444	0.04±NA

Table S1. Continued.

Cruise date	Station	Distance to main crater (m)	Latitude	Longitude	Pressure (dbar)	$Si(OH)_4$ (μmol kg^{-1})
Mar-18	58	218.36	27.62166	-17.99316	124.929	0.04±NA
Mar-18	59	273.36	27.62216	-17.99300	124.440	0.04±NA
Mar-18	60	26.72	27.61952	-17.99318	120.623	0.05±NA
Oct-17	03	6314.14	27.64024	-17.93320	125.901	0.11±NA
Oct-17	50	504.59	27.61566	-17.99066	125.102	0.09±NA
Oct-17	51	358.27	27.61684	-17.99132	125.438	0.48±NA
Oct-17	52	247.93	27.61766	-17.99198	125.801	0.60±NA
Oct-17	53	164.86	27.61851	-17.99200	123.705	0.80±NA
Oct-17	54	104.01	27.61882	-17.99264	124.615	0.96±NA
Oct-17	58	218.36	27.62166	-17.99316	125.876	0.62±NA
Oct-17	59	275.58	27.62218	-17.99298	126.015	0.36±NA
Oct-17	60	2.22	27.61968	-17.99300	125.325	2.67±NA
Oct-17	60	2.22	27.61968	-17.99300	125.519	2.91±NA
Oct-17	60	2.22	27.61968	-17.99300	126.525	4.01±NA
Oct-17	60	0.00	27.61970	-17.99300	126.313	7.87±NA
Oct-17	60	0.00	27.61970	-17.99300	126.937	2.07±NA
Oct-17	60	2.22	27.61968	-17.99300	126.743	2.30±NA
Oct-17	60	0.00	27.61970	-17.99300	127.109	6.67±NA
Oct-17	60	2.22	27.61968	-17.99300	126.884	1.88±NA
Oct-17	60	0.00	27.61970	-17.99300	127.532	2.99±NA
Oct-17	60	2.22	27.61968	-17.99300	127.014	3.13±NA
Oct-17	60	2.22	27.61968	-17.99300	127.462	4.95±NA
Oct-17	60	2.22	27.61968	-17.99300	127.041	7.06±NA
Oct-17	60	2.22	27.61968	-17.99300	127.796	5.30±NA
Oct-17	60	0.00	27.61970	-17.99300	127.771	13.22±NA
Oct-17	60	2.22	27.61968	-17.99300	127.750	21.17±NA

Table S1. Continued.

Cruise date	Station	Distance to main crater (m)	Latitude	Longitude	Pressure (dbar)	$Si(OH)_4$ (μmol kg^{-1})
Apr-17	50	517.61	27.61552	-17.99068	125.761	0.12±NA
Apr-17	54	100.60	27.61882	-17.99276	123.748	0.36±NA
Apr-17	57	145.04	27.62094	-17.99346	125.125	0.24±NA
Apr-17	62	45.51	27.61974	-17.99346	124.580	2.5±NA
Apr-17	62	45.51	27.61974	-17.99346	124.124	0.24±NA
Oct-16	50	510.76	27.61558	-17.99070	125.624	0.49±NA
Oct-16	51	357.37	27.61684	-17.99134	125.595	1.65±NA
Oct-16	52	247.93	27.61766	-17.99198	125.719	1.28±NA
Oct-16	53	165.75	27.61850	-17.99200	124.310	0.72±NA
Oct-16	54	101.26	27.61884	-17.99266	126.882	0.84±NA
Oct-16	55	38.89	27.61935	-17.99300	125.956	0.45±NA
Oct-16	57	148.28	27.62100	-17.99334	122.458	0.88±NA
Oct-16	58	219.62	27.62167	-17.99318	125.030	0.04±NA
Oct-16	59	275.58	27.62218	-17.99300	126.445	0.08±NA
Oct-16	60	11.79	27.61960	-17.99296	124.611	0.67±NA
Oct-16	60	11.79	27.61960	-17.99296	122.296	1.07±NA
Oct-16	60	11.79	27.61960	-17.99296	121.744	0.64±NA
Oct-16	60	11.79	27.61960	-17.99296	122.743	0.98±NA
Mar-16	50	500.64	27.61570	-17.99066	124.996	0.06±NA
Mar-16	52	242.79	27.61768	-17.99206	126.163	0.06±NA
Mar-16	53	166.37	27.61852	-17.99196	122.766	0.54±NA
Mar-16	54	104.28	27.61880	-17.99270	126.054	0.20±NA
Mar-16	55	42.27	27.61932	-17.99298	122.929	0.04±NA
Mar-16	58	218.68	27.62166	-17.99320	126.300	0.55±NA
Mar-16	59	275.58	27.62218	-17.99300	126.214	0.58±NA
Mar-16	61	27.24	27.61950	-17.99316	129.625	0.04±NA

Table S1. Continued.

Cruise date	Station	Distance to main crater (m)	Latitude	Longitude	Pressure (dbar)	$Si(OH)_4$ (μmol kg^{-1})
Mar-14	06	7864.09	27.67000	-17.93680	124.317	0.75±NA
Mar-14	08	5493.96	27.61950	-17.93720	124.986	0.50±NA
Mar-14	09	7802.95	27.57020	-17.93680	125.549	0.78±NA
Mar-14	13	5574.23	27.56980	-17.98720	126.394	1.28±NA
Mar-14	14	611.34	27.62000	-17.98680	125.536	1.63±NA
Mar-14	15	7053.47	27.66980	-18.03700	125.026	0.59±NA
Mar-14	16	4312.44	27.61980	-18.03680	126.066	0.60±NA
Mar-14	17	7025.05	27.56980	-18.03680	125.183	0.52±NA
Mar-14	18	7052.41	27.64330	-18.05950	124.802	0.46±NA
Mar-14	50	498.84	27.61570	-17.99070	125.815	0.80±NA
Mar-14	51	363.12	27.61680	-17.99130	125.813	0.66±NA
Mar-14	52	253.27	27.61760	-17.99200	124.893	0.58±NA
Mar-14	54	104.28	27.61880	-17.99270	123.618	0.99±NA
Mar-14	59	277.80	27.62220	-17.99300	124.314	1.12±NA
Mar-14	60	591.68	27.62000	-17.99900	125.710	1.00±NA
Mar-14	64	145.41	27.62080	-17.99220	125.740	0.49±NA
Mar-14	53	165.75	27.61850	-17.99200	125.141	0.50±NA
Mar-14	61	29.69	27.61950	-17.99320	121.604	6.29±NA
Mar-14	61	19.69	27.61970	-17.99320	125.093	19.04±NA

Table S2. Physicochemical properties of seawater sampled outside the area of influence of Tagoro (station 901), above the main crater of Tagoro (station 31 and 61), and directly from a hydrothermal vent (ROV). Average ± standard deviation from duplicate measurements is shown. NA (not applicable) indicates single unreplicated measurements, while ND stands for no data available.

Cruise	Apr 21		Oct 21		
Station	901	31	901	61	ROV
Latitude	27.65002	27.61978	27.65000	27.61971	27.61972
Longitude	-17.90980	-17.99300	-17.90976	-17.99288	-17.99285
Pressure (dbar)	127.19± 0.08	129.44± 0.67	127.31± 0.11	128.53± 1.18	122.00
θ (°C)	18.19±0.01	18.28±0.05	18.89±0.01	19.26±0.28	27.2
Salinity	36.57±0.00	36.56±0.02	36.70±0.00	36.70±0.02	ND
Dissolved O_2 (μmol kg^{-1})	208.74	158.73	204.84	201.82	ND
pH	8.40±0.00	8.27±0.02	8.30±0.00	8.19±0.01	ND
ORP (mV)	-439.43± 0.47	-443.32± 0.27	-440.20± 0.54	-431.73± 1.39	ND
[NO_2^-+NO_3^-] (μmol kg^{-1})	2.43±0.02	2.91±NA	2.50±0.07	1.78±0.15	3.11±0.08
[PO_4^{3-}] (μmol kg^{-1})	0.15±0.00	0.22±NA	0.11±0.02	0.12±0.01	15.56±4.85
[$Si(OH)_4$] (μmol kg^{-1})	0.95±0.03	5.84±NA	0.86±0.07	2.67±0.03	18.28±1.21

Table S3. Measurements of dissolved inorganic nutrient concentrations ([NO_2^-+NO_3^-], [PO_4^{3-}] and [$Si(OH)_4$]) in μmol kg^{-1}, and dissolved organic carbon ([TOC]) and nitrogen ([DON]) in μM, at the beginning (t0) and end (tf) of the experiments. Average ± standard deviation between duplicate incubators per season is shown. ND (no data) indicates the absence of data.

Cruise	Treatment	$[NO_2^-+NO_3^-]_{t0}$	$[NO_2^-+NO_3^-]_{tf}$	$[PO_4^{3-}]_{t0}$	$[PO_4^{3-}]_{tf}$	$[Si(OH)_4]_{t0}$	$[Si(OH)_4]_{tf}$	$[DOC]_{t0}$	$[DOC]_{tf}$	$[DON]_{t0}$	$[DON]_{tf}$
Apr 21	C-I	2.96	0.19±0.02	0.21	0.05±0.00	1.20	0.05±0.01	ND	ND	ND	ND
	C-II	ND	0.11±0.04	ND	0.05±0.00	ND	0.07±0.02	ND	ND	ND	ND
	V2%	2.99	0.11±0.03	0.21	0.05±0.03	1.25	0.06±0.03	ND	ND	ND	ND
	V4%	2.80	0.19±0.00	0.21	0.05±0.00	1.38	0.12±0.08	ND	ND	ND	ND
	V8%	2.81	0.15±0.04	0.21	0.05±0.01	1.49	0.08±0.04	ND	ND	ND	ND
	V16%	2.78	0.17±0.00	0.23	0.05±0.00	1.98	0.13±0.01	ND	ND	ND	ND
Oct 21	C-I	2.21	0.68±0.38	0.14	0.04±0.00	0.91	0.57±0.19	63.3	ND	ND	ND
	C-II	ND	0.84±0.06	ND	0.03±0.01	ND	0.68±0.02	63.3	ND	ND	ND
	V2%	2.16	0.19±0.07	0.13	0.02±0.00	0.93	0.06±0.01	65.6	ND	ND	ND
	V4%	2.17	0.18±0.04	0.13	0.03±0.00	0.93	0.04±0.04	59.3	ND	ND	ND
	V8%	2.09	0.18±0.01	0.13	0.03±0.01	1.02	0.08±0.02	61.5	ND	ND	ND
	V16%	2.19	0.23±0.01	0.14	0.03±0.01	1.19	0.08±0.01	77.3	ND	ND	ND
	VENT	2.25	0.16±0.01	0.14	0.02±0.01	0.88	0.16±0.08	91.1	76.0±1.7	5.4	4.7±0.4

Table S4. Eukaryotic ASVs significantly associated with both volcano and vent treatments (*stat* > 0.85, $p = 0.001$ and $str_C < 0.5$), based on the Indicator Species Analyses results. The parameter *str* indicates the strength of the association between a species and the treatment group (control, C; volcano and vent-treated, V), *stat* indicates the association value, and *p* the degree of statistical significance of the association (based on 999 permutations). The dash symbol (–) indicates unclassified taxa.

ASV	*stat*	str_C	str_V	Division	Class	Order	Family	Genus	Species
ASV_788	0.94	0.21	0.94	Chlorophyta	Chloropicophyceae	Chloropicales	Chloropicaceae	*Chloropicon*	*Chloropicon roscoffensis*
ASV_771	0.93	0.26	0.93	Chlorophyta	Chloropicophyceae	Chloropicales	Chloropicaceae	*Chloropicon*	*Chloropicon roscoffensis*
ASV_934	0.92	0.28	0.92	Chlorophyta	Chloropicophyceae	Chloropicales	Chloropicaceae	*Chloropicon*	*Chloropicon roscoffensis*
ASV_311	0.90	0.34	0.90	Chlorophyta	Chloropicophyceae	Chloropicales	Chloropicaceae	*Chloropicon*	*Chloropicon roscoffensis*
ASV_957	0.89	0.32	0.89	Chlorophyta	Chloropicophyceae	Chloropicales	Chloropicaceae	*Chloropicon*	*Chloropicon roscoffensis*
ASV_314	0.88	0.37	0.88	Chlorophyta	Chloropicophyceae	Chloropicales	Chloropicaceae	*Chloropicon*	*Chloropicon roscoffensis*
ASV_51	0.88	0.41	0.88	Chlorophyta	Chloropicophyceae	Chloropicales	Chloropicaceae	*Chloropicon*	*Chloropicon roscoffensis*
ASV_5	0.88	0.44	0.88	Chlorophyta	Chloropicophyceae	Chloropicales	Chloropicaceae	*Chloropicon*	*Chloropicon roscoffensis*
ASV_961	0.87	0.39	0.87	Chlorophyta	Chloropicophyceae	Chloropicales	Chloropicaceae	*Chloropicon*	*Chloropicon roscoffensis*
ASV_292	0.87	0.39	0.87	Chlorophyta	Chloropicophyceae	Chloropicales	Chloropicaceae	*Chloropicon*	*Chloropicon roscoffensis*
ASV_438	0.95	0.14	0.95	Dinoflagellata	Dinophyceae	Peridiniales	Blastodiniaceae	*Blastodinium*	*Blastodinium mangini*
ASV_49	0.95	0.22	0.95	Dinoflagellata	Syndiniales	Dino-Group-I	Dino-Group-I-Clade-1	*Dino-Group-I-Clade-1_X*	*Dino-Group-I-Clade-1 X sp.*

Table S4. Continued.

ASV	*stat*	str_C	str_V	Division	Class	Order	Family	Genus	Species
ASV_861	0.94	0.16	0.94	Dinoflagellata	Syndiniales	Dino-Group-I	Dino-Group-I-Clade-1	*Dino-Group-I-Clade-1_X*	*Dino-Group-I-Clade-1 X sp.*
ASV_942	0.94	0.14	0.94	Dinoflagellata	Syndiniales	Dino-Group-I	Dino-Group-I-Clade-1	*Dino-Group-I-Clade-1_X*	*Dino-Group-I-Clade-1 X sp.*
ASV_1035	0.93	0.00	0.93	Dinoflagellata	Syndiniales	Dino-Group-I	Dino-Group-I-Clade-1	*Dino-Group-I-Clade-1_X*	*Dino-Group-I-Clade-1 X sp.*
ASV_92	0.91	0.34	0.91	Dinoflagellata	Syndiniales	Dino-Group-I	Dino-Group-I-Clade-1	*Dino-Group-I-Clade-1_X*	*Dino-Group-I-Clade-1 X sp.*
ASV_668	0.88	0.29	0.88	Dinoflagellata	Syndiniales	Dino-Group-I	Dino-Group-I-Clade-1	*Dino-Group-I-Clade-1_X*	*Dino-Group-I-Clade-1 X sp.*
ASV_308	0.85	0.37	0.85	Dinoflagellata	Syndiniales	Dino-Group-I	Dino-Group-I-Clade-1	*Dino-Group-I-Clade-1_X*	*Dino-Group-I-Clade-1 X sp.*
ASV_49	0.95	0.22	0.95	Dinoflagellata	Syndiniales	Dino-Group-I	Dino-Group-I-Clade-1	*Dino-Group-I-Clade-1_X*	*Dino-Group-I-Clade-1 X sp.*
ASV_1486	0.95	0.19	0.95	Dinoflagellata	Syndiniales	Dino-Group-I	Dino-Group-I-Clade-4	*Dino-Group-I-Clade-4_X*	*Dino-Group-I-Clade-4 X sp.*
ASV_2837	0.93	0.18	0.93	Dinoflagellata	Syndiniales	Dino-Group-I	Dino-Group-I-Clade-4	*Dino-Group-I-Clade-4_X*	*Dino-Group-I-Clade-4 X sp.*

Table S4. Continued.

ASV	*stat*	str_C	str_V	Division	Class	Order	Family	Genus	Species
ASV_486	0.92	0.27	0.92	Dinoflagellata	Syndiniales	Dino-Group-I	Dino-Group-I-Clade-4	*Dino-Group-I-Clade-4_X*	*Dino-Group-I-Clade-4 X sp.*
ASV_268	0.92	0.28	0.92	Dinoflagellata	Syndiniales	Dino-Group-I	Dino-Group-I-Clade-4	*Dino-Group-I-Clade-4_X*	*Dino-Group-I-Clade-4 X sp.*
ASV_462	0.92	0.32	0.92	Dinoflagellata	Syndiniales	Dino-Group-I	Dino-Group-I-Clade-4	*Dino-Group-I-Clade-4_X*	*Dino-Group-I-Clade-4 X sp.*
ASV_16	0.91	0.41	0.91	Dinoflagellata	Syndiniales	Dino-Group-I	Dino-Group-I-Clade-4	*Dino-Group-I-Clade-4_X*	*Dino-Group-I-Clade-4 X sp.*
ASV_1057	0.90	0.31	0.90	Dinoflagellata	Syndiniales	Dino-Group-I	Dino-Group-I-Clade-4	*Dino-Group-I-Clade-4_X*	*Dino-Group-I-Clade-4 X sp.*
ASV_55	0.90	0.35	0.90	Dinoflagellata	Syndiniales	Dino-Group-I	Dino-Group-I-Clade-4	*Dino-Group-I-Clade-4_X*	*Dino-Group-I-Clade-4 X sp.*
ASV_5040	0.90	0.09	0.90	Dinoflagellata	Syndiniales	Dino-Group-I	Dino-Group-I-Clade-4	*Dino-Group-I-Clade-4_X*	*Dino-Group-I-Clade-4 X sp.*
ASV_1573	0.89	0.32	0.90	Dinoflagellata	Syndiniales	Dino-Group-I	Dino-Group-I-Clade-4	*Dino-Group-I-Clade-4_X*	*Dino-Group-I-Clade-4 X sp.*
ASV_18	0.89	0.43	0.89	Dinoflagellata	Syndiniales	Dino-Group-I	Dino-Group-I-Clade-4	*Dino-Group-I-Clade-4_X*	*Dino-Group-I-Clade-4 X sp.*

Table S4. Continued.

ASV	*stat*	str_C	str_V	Division	Class	Order	Family	Genus	Species
ASV_537	0.89	0.37	0.89	Dinoflagellata	Syndiniales	Dino-Group-I	Dino-Group-I-Clade-4	*Dino-Group-I-Clade-4_X*	*Dino-Group-I-Clade-4 X sp.*
ASV_522	0.89	0.37	0.89	Dinoflagellata	Syndiniales	Dino-Group-I	Dino-Group-I-Clade-4	*Dino-Group-I-Clade-4_X*	*Dino-Group-I-Clade-4 X sp.*
ASV_75	0.99	0.10	0.99	Dinoflagellata	Syndiniales	Dino-Group-II	Dino-Group-II-Clade-10-and-11	*Dino-Group-II-Clade-10-and-11_X*	*Dino-Group-II-Clade-10-and-11 X sp.*
ASV_1280	0.98	0.12	0.98	Dinoflagellata	Syndiniales	Dino-Group-II	Dino-Group-II-Clade-10-and-11	*Dino-Group-II-Clade-10-and-11_X*	*Dino-Group-II-Clade-10-and-11 X sp.*
ASV_1405	0.96	0.04	0.96	Dinoflagellata	Syndiniales	Dino-Group-II	Dino-Group-II-Clade-10-and-11	*Dino-Group-II-Clade-10-and-11_X*	*Dino-Group-II-Clade-10-and-11 X sp.*
ASV_178	0.95	0.30	0.96	Ochrophyta	Bacillariophyta	Bacillariophyta_X	Polar-centric-Mediophyceae	*Chaetoceros*	*Chaetoceros tenuissimus*
ASV_1021	0.95	0.22	0.95	Ochrophyta	Bacillariophyta	Bacillariophyta_X	Polar-centric-Mediophyceae	*Minutocellus*	*Minutocellus polymorphus*
ASV_2134	0.94	0.25	0.94	Ochrophyta	Bacillariophyta	Bacillariophyta_X	Polar-centric-Mediophyceae	*Arcocellulus*	*Arcocellulus cornucervis*

Table S4. Continued.

ASV	*stat*	str_C	str_V	Division	Class	Order	Family	Genus	Species
ASV_1202	0.91	0.12	0.91	Ochrophyta	Bacillariophyta	Bacillariophyta_X	Polar-centric-Mediophyceae	*Minutocellus*	*Minutocellus polymorphus*
ASV_520	0.91	0.32	0.91	Ochrophyta	Pelagophyceae	Pelagomonadales	Pelagomonadaceae	–	–
ASV_178	0.95	0.30	0.96	Ochrophyta	Bacillariophyta	Bacillariophyta_X	Polar-centric-Mediophyceae	*Chaetoceros*	*Chaetoceros tenuissimus*
ASV_1021	0.95	0.22	0.95	Ochrophyta	Bacillariophyta	Bacillariophyta_X	Polar-centric-Mediophyceae	*Minutocellus*	*Minutocellus polymorphus*
ASV_2134	0.94	0.25	0.94	Ochrophyta	Bacillariophyta	Bacillariophyta_X	Polar-centric-Mediophyceae	*Arcocellulus*	*Arcocellulus cornucervis*

Table S5. Prokaryotic ASVs significantly associated with both volcano and vent treatments (*stat* > 0.85, $p = 0.001$ and $str_C < 0.5$), based on the Indicator Species Analyses results. The parameter *str* indicates the strength of the association between a species and the treatment group (control, C; volcano and vent-treated, V), *stat* indicates the association value, and *p* the degree of statistical significance of the association (based on 999 permutations). The dash symbol (–) indicates unclassified taxa.

ASV	*stat*	str_C	str_V	Division	Class	Order	Family	Genus	Species
ASV_72	0.87	0.50	0.87	Actinobacteriota	Acidimicrobiia	Actinomarinales	*Actinomarinaceae*	*Candidatus* Actinomarina	–
ASV_314	0.90	0.30	0.90	Actinobacteriota	Actinobacteria	Corynebacteriales	*Corynebacteriaceae*	*Corynebacterium*	*Aurimucosum/ minutissimum*
ASV_231	0.93	0.25	0.93	Actinobacteriota	Actinobacteria	Corynebacteriales	*Corynebacteriaceae*	*Corynebacterium*	*aurimucosum/ pseudogenitalium/…*
ASV_889	0.89	0.25	0.89	Actinobacteriota	Actinobacteria	Corynebacteriales	*Corynebacteriaceae*	*Corynebacterium*	*confusum*
ASV_989	0.89	0.20	0.89	Actinobacteriota	Actinobacteria	Micrococcales	*Micrococcaceae*	*Kocuria*	*arsenatis/ rhizophila/salsicia*
ASV_105	0.91	0.30	0.91	Actinobacteriota	Actinobacteria	Micrococcales	*Micrococcaceae*	*Micrococcus*	*alkanovora/ aloeverae/…*
ASV_258	0.93	0.26	0.93	Proteobacteria	Alpha-proteobacteria	Azospirillales	*Azospirillaceae*	–	–
ASV_96	0.94	0.23	0.95	Proteobacteria	Alpha-proteobacteria	Caulobacterales	*Caulobacteraceae*	*Brevundimonas*	*albigilva/nasdae/ vesicularis*

Table S5. Continued.

ASV	*stat*	str_C	str_V	Division	Class	Order	Family	Genus	Species
ASV_554	0.91	0.30	0.91	Proteobacteria	Alpha-proteobacteria	Caulobacterales	*Caulobacteraceae*	–	–
ASV_446	0.92	0.32	0.92	Proteobacteria	Alpha-proteobacteria	Puniceispirillales	*SAR116 clade*	*Candidatus* Puniceispirillum	–
ASV_620	0.94	0.21	0.94	Proteobacteria	Alpha-proteobacteria	Puniceispirillales	*SAR116 clade*	–	–
ASV_256	0.93	0.25	0.93	Proteobacteria	Alpha-proteobacteria	Puniceispirillales	*SAR116 clade*	–	–
ASV_85	0.93	0.29	0.93	Proteobacteria	Alpha-proteobacteria	Puniceispirillales	*SAR116 clade*	–	–
ASV_35	0.93	0.26	0.93	Proteobacteria	Alpha-proteobacteria	Puniceispirillales	*SAR116 clade*	–	–
ASV_144	0.93	0.26	0.93	Proteobacteria	Alpha-proteobacteria	Puniceispirillales	*SAR116 clade*	–	–
ASV_229	0.92	0.40	0.92	Proteobacteria	Alpha-proteobacteria	Puniceispirillales	*SAR116 clade*	–	–
ASV_338	0.93	0.25	0.93	Proteobacteria	Alpha-proteobacteria	Rhizobiales	*Beijerinckiaceae*	*Methylobacterium-Methylorubrum*	–

Table S5. Continued.

ASV	*stat*	str_C	str_V	Division	Class	Order	Family	Genus	Species
ASV_808	0.92	0.19	0.93	Proteobacteria	Alpha-proteobacteria	Rhizobiales	*Beijerinckiaceae*	*Methylobacterium-Methylorubrum*	–
ASV_515	0.91	0.29	0.91	Proteobacteria	Alpha-proteobacteria	Rhizobiales	*Beijerinckiaceae*	*Methylobacterium-Methylorubrum*	–
ASV_346	0.94	0.24	0.94	Proteobacteria	Alpha-proteobacteria	Rhizobiales	*Rhizobiaceae*	*Ciceribacter*	–
ASV_578	0.96	0.13	0.96	Proteobacteria	Alpha-proteobacteria	Rhizobiales	*Xanthobacteraceae*	*Bradyrhizobium*	–
ASV_221	0.91	0.29	0.91	Proteobacteria	Alpha-proteobacteria	Rhizobiales	*Xanthobacteraceae*	*Bradyrhizobium*	–
ASV_74	0.91	0.41	0.91	Proteobacteria	Alpha-proteobacteria	Rhodobacterales	*Rhodobacteraceae*	*Ascidiaceihabitans*	–
ASV_122	0.92	0.27	0.93	Proteobacteria	Alpha-proteobacteria	Rhodobacterales	*Rhodobacteraceae*	*Epibacterium*	–
ASV_202	0.95	0.23	0.95	Proteobacteria	Alpha-proteobacteria	Rhodobacterales	*Rhodobacteraceae*	*Paracoccus*	–
ASV_173	0.95	0.24	0.95	Proteobacteria	Alpha-proteobacteria	Rhodobacterales	*Rhodobacteraceae*	*Yoonia-Loktanella*	–

Table S5. Continued.

ASV	*stat*	str_C	str_V	Division	Class	Order	Family	Genus	Species
ASV_394	0.95	0.20	0.95	Proteobacteria	Alpha-proteobacteria	Rhodospirillales	*AEGEAN-169 marine group*	–	–
ASV_453	0.93	0.25	0.93	Proteobacteria	Alpha-proteobacteria	Rhodospirillales	*AEGEAN-169 marine group*	–	–
ASV_414	0.91	0.40	0.91	Proteobacteria	Alpha-proteobacteria	Rhodospirillales	*AEGEAN-169 marine group*	–	–
ASV_134	0.90	0.41	0.90	Proteobacteria	Alpha-proteobacteria	Rhodospirillales	*AEGEAN-169 marine group*	–	–
ASV_195	0.89	0.46	0.89	Proteobacteria	Alpha-proteobacteria	Rhodospirillales	*AEGEAN-169 marine group*	–	–
ASV_31	0.87	0.50	0.87	Proteobacteria	Alpha-proteobacteria	Rhodospirillales	*AEGEAN-169 marine group*	–	–
ASV_564	0.95	0.19	0.95	Proteobacteria	Alpha-proteobacteria	Rickettsiales	*S25-593*	–	–
ASV_757	0.92	0.11	0.92	Proteobacteria	Alpha-proteobacteria	Rickettsiales	*S25-593*	–	–
ASV_615	0.89	0.43	0.89	Proteobacteria	Alpha-proteobacteria	SAR11 clade	*Clade I*	*Clade Ia*	–

Table S5. Continued.

ASV	*stat*	str_C	str_V	Division	Class	Order	Family	Genus	Species
ASV_581	0.95	0.25	0.95	Proteobacteria	Alpha-proteobacteria	SAR11 clade	*Clade II*	–	–
ASV_586	0.93	0.20	0.93	Proteobacteria	Alpha-proteobacteria	Sphingomonadales	*Sphingomonadaceae*	*Sphingomonas*	*alpina/echinoides/…*
ASV_119	0.91	0.32	0.91	Firmicutes	Bacilli	Lactobacillales	*Aerococcaceae*	*Aerococcus*	*urinaeequi/viridans*
ASV_332	0.93	0.23	0.93	Firmicutes	Bacilli	Lactobacillales	*Streptococcaceae*	*Streptococcus*	*anginosus/cristatus/…*
ASV_238	0.94	0.24	0.94	Firmicutes	Bacilli	Staphylococcales	*Staphylococcaceae*	*Staphylococcus*	*argenteus/aureus/…*
ASV_504	0.93	0.27	0.93	Bacteroidota	Bacteroidia	Chitinophagales	*Saprospiraceae*	–	–
ASV_400	0.91	0.30	0.91	Bacteroidota	Bacteroidia	Chitinophagales	*Saprospiraceae*	–	–
ASV_584	0.92	0.28	0.92	Bacteroidota	Bacteroidia	Chitinophagales	–	–	–
ASV_430	0.93	0.25	0.93	Bacteroidota	Bacteroidia	Cytophagales	*Amoebophilaceae*	–	–
ASV_203	0.92	0.34	0.92	Bacteroidota	Bacteroidia	Cytophagales	*Cyclobacteriaceae*	*Fabibacter*	*halotolerans*
ASV_455	0.95	0.23	0.95	Bacteroidota	Bacteroidia	Flavobacteriales	*Crocinitomicaceae*	*Crocinitomix*	–
ASV_303	0.92	0.32	0.92	Bacteroidota	Bacteroidia	Flavobacteriales	*Flavobacteriaceae*	*Mesonia*	*mobilis*
ASV_215	0.93	0.27	0.93	Bacteroidota	Bacteroidia	Flavobacteriales	*Flavobacteriaceae*	*NS5 marine group*	–

Table S5. Continued.

ASV	*stat*	str_C	str_V	Division	Class	Order	Family	Genus	Species
ASV_608	0.89	0.28	0.89	Bacteroidota	Bacteroidia	Flavobacteriales	*Flavobacteriaceae*	*NS5 marine group*	–
ASV_626	0.93	0.23	0.93	Bacteroidota	Bacteroidia	Flavobacteriales	*Flavobacteriaceae*	*Polaribacter*	–
ASV_406	0.94	0.25	0.94	Bacteroidota	Bacteroidia	Flavobacteriales	*Flavobacteriaceae*	–	–
ASV_194	0.95	0.22	0.95	Bacteroidota	Bacteroidia	Sphingobacteriales	*NS11-12 marine group*	–	–
ASV_747	0.92	0.22	0.92	Firmicutes	Clostridia	Peptostreptococcales-Tissierellales	*Family XI*	*Anaerococcus*	–
ASV_602	0.96	0.17	0.96	Desulfobacterota	Desulfovibrionia	Desulfovibrionales	*Desulfovibrionaceae*	–	–
ASV_378	0.94	0.25	0.94	Proteobacteria	Gamma-proteobacteria	Burkholderiales	*Burkholderiaceae*	*Ralstonia*	*detusculanense/ insidiosa/…*
ASV_594	0.90	0.27	0.90	Proteobacteria	Gamma-proteobacteria	Burkholderiales	*Burkholderiaceae*	*Ralstonia*	*insidiosa/ pickettii/…*
ASV_887	0.93	0.17	0.93	Proteobacteria	Gamma-proteobacteria	Burkholderiales	*Comamonadaceae*	*Hydrogenophaga*	–
ASV_300	0.92	0.28	0.92	Proteobacteria	Gamma-proteobacteria	Burkholderiales	*Comamonadaceae*	–	–

Table S5. Continued.

ASV	*stat*	str_C	str_V	Division	Class	Order	Family	Genus	Species
ASV_1	0.93	0.26	0.93	Proteobacteria	Gamma-proteobacteria	Enterobacterales	*Enterobacteriaceae*	*Escherichia-Shigella*	–
ASV_107	0.92	0.28	0.92	Proteobacteria	Gamma-proteobacteria	Enterobacterales	*Enterobacteriaceae*	*Klebsiella*	–
ASV_28	0.89	0.42	0.89	Proteobacteria	Gamma-proteobacteria	Enterobacterales	*Pseudoalteromonadaceae*	*Pseudoalteromonas*	*aestuariivivens/ agarivorans/…*
ASV_265	0.94	0.24	0.94	Proteobacteria	Gamma-proteobacteria	Pseudomonadales	*Halieaceae*	*OM60(NOR5) clade*	–
ASV_310	0.93	0.25	0.93	Proteobacteria	Gamma-proteobacteria	Pseudomonadales	*Halieaceae*	*OM60(NOR5) clade*	–
ASV_187	0.92	0.28	0.92	Proteobacteria	Gamma-proteobacteria	Pseudomonadales	*Halomonadaceae*	*Cobetia*	*amphilecti/ litoralis/…*
ASV_222	0.92	0.31	0.92	Proteobacteria	Gamma-proteobacteria	Pseudomonadales	*Halomonadaceae*	*Halomonas*	*alkaliantarctica/…*
ASV_1049	0.92	0.06	0.93	Proteobacteria	Gamma-proteobacteria	Pseudomonadales	*Halomonadaceae*	*Halomonas*	–
ASV_707	0.95	0.16	0.95	Proteobacteria	Gamma-proteobacteria	Pseudomonadales	*Halomonadaceae*	*Salinicola*	–

Table S5. Continued.

ASV	*stat*	str_C	str_V	Division	Class	Order	Family	Genus	Species
ASV_248	0.94	0.24	0.94	Proteobacteria	Gamma-proteobacteria	Pseudomonadales	*KI89A clade*	–	–
ASV_205	0.89	0.45	0.90	Proteobacteria	Gamma-proteobacteria	Pseudomonadales	*KI89A clade*	–	–
ASV_103	0.94	0.24	0.94	Proteobacteria	Gamma-proteobacteria	Pseudomonadales	*Litoricolaceae*	*Litoricola*	–
ASV_92	0.94	0.28	0.94	Proteobacteria	Gamma-proteobacteria	Pseudomonadales	*Litoricolaceae*	*Litoricola*	–
ASV_316	0.92	0.28	0.92	Proteobacteria	Gamma-proteobacteria	Pseudomonadales	*Litoricolaceae*	*Litoricola*	–
ASV_1100	0.91	0.22	0.91	Proteobacteria	Gamma-proteobacteria	Pseudomonadales	*Marinobacteraceae*	*Marinobacter*	–
ASV_444	0.96	0.17	0.96	Proteobacteria	Gamma-proteobacteria	Pseudomonadales	*Moraxellaceae*	*Acinetobacter*	*baumannii/beijerinckii/…*
ASV_528	0.92	0.20	0.92	Proteobacteria	Gamma-proteobacteria	Pseudomonadales	*Moraxellaceae*	*Acinetobacter*	*baumannii/bouvetii/…*
ASV_111	0.93	0.26	0.93	Proteobacteria	Gamma-proteobacteria	Pseudomonadales	*Moraxellaceae*	*Psychrobacter*	*faecalis/pulmonis*

Table S5. Continued.

ASV	*stat*	str_C	str_V	Division	Class	Order	Family	Genus	Species
ASV_63	0.93	0.26	0.93	Proteobacteria	Gamma-proteobacteria	Pseudomonadales	*Pseudomonadaceae*	*Pseudomonas*	*antarctica/auricularis/…*
ASV_365	0.89	0.42	0.89	Proteobacteria	Gamma-proteobacteria	Pseudomonadales	*Saccharospirillaceae*	*Oleibacter*	*marinus*
ASV_567	0.97	0.12	0.97	Proteobacteria	Gamma-proteobacteria	Pseudomonadales	*SAR86 clade*	–	–
ASV_197	0.95	0.26	0.96	Proteobacteria	Gamma-proteobacteria	Pseudomonadales	*SAR86 clade*	–	–
ASV_125	0.94	0.24	0.94	Proteobacteria	Gamma-proteobacteria	Pseudomonadales	*SAR86 clade*	–	–
ASV_44	0.94	0.27	0.94	Proteobacteria	Gamma-proteobacteria	Pseudomonadales	*SAR86 clade*	–	–
ASV_102	0.94	0.25	0.94	Proteobacteria	Gamma-proteobacteria	Pseudomonadales	*SAR86 clade*	–	–
ASV_254	0.94	0.28	0.94	Proteobacteria	Gamma-proteobacteria	Pseudomonadales	*SAR86 clade*	–	–
ASV_87	0.94	0.25	0.94	Proteobacteria	Gamma-proteobacteria	Pseudomonadales	*SAR86 clade*	–	–

Table S5. Continued.

ASV	*stat*	str_C	str_V	Division	Class	Order	Family	Genus	Species
ASV_43	0.94	0.31	0.94	Proteobacteria	Gamma-proteobacteria	Pseudomonadales	*SAR86 clade*	–	–
ASV_269	0.93	0.28	0.93	Proteobacteria	Gamma-proteobacteria	Pseudomonadales	*SAR86 clade*	–	–
ASV_466	0.92	0.31	0.92	Proteobacteria	Gamma-proteobacteria	Pseudomonadales	*SAR86 clade*	–	–
ASV_61	0.91	0.41	0.91	Proteobacteria	Gamma-proteobacteria	Pseudomonadales	*SAR86 clade*	–	–
ASV_589	0.91	0.26	0.91	Proteobacteria	Gamma-proteobacteria	Pseudomonadales	*SAR86 clade*	–	–
ASV_368	0.90	0.30	0.90	Proteobacteria	Gamma-proteobacteria	Pseudomonadales	*SAR86 clade*	–	–
ASV_263	0.90	0.41	0.90	Proteobacteria	Gamma-proteobacteria	Pseudomonadales	*SAR86 clade*	–	–
ASV_214	0.97	0.18	0.97	Proteobacteria	Gamma-proteobacteria	Pseudomonadales	*Thioglobaceae*	*SUP05 cluster*	–
ASV_313	0.91	0.29	0.91	Proteobacteria	Gamma-proteobacteria	Tenderiales	*Tenderiaceae*	*Candidatus* Tenderia	–

Table S5. Continued.

ASV	*stat*	str_C	str_V	Division	Class	Order	Family	Genus	Species
ASV_250	0.90	0.32	0.90	Bacteroidota	Rhodothermia	Balneolales	*Balneolaceae*	*Balneola*	–
ASV_324	0.93	0.37	0.93	Marinimicrobia (SAR406 clade)	–	–	–	–	–

References

Álvarez-Valero, A. M., O. Sánchez-Guillamón, I. Navarro, et al. 2023. "From Magma Source to Volcanic Sink Under Tagoro Volcano (El Hierro, Canary Islands): Petrologic, Geochemical and Physiographic Evolution of the 2011–2012 Submarine Eruption." In El Hierro Island, edited by P. J. González, 61–89. Springer International Publishing.

Aminot, A., and R. Kérouel. 2007. Dosage Automatique des Nutriments Dans les Eaux Marines: Méthodes en Flux Continu. Editions Quae.

Anderson, S. R., L. Blanco-Bercial, C. A. Carlson, and E. L. Harvey. 2024. "The Role of Syndiniales Parasites in Depth-Specific Networks and Carbon Flux in the Oligotrophic Ocean." ISME Communications 4, no. 1. doi: 10.1093/ismeco/ycae014

Anderson, S. R., and E. L. Harvey. 2020. "Temporal Variability and Ecological Interactions of Parasitic Marine Syndiniales in Coastal Protist Communities." mSphere 5, no. 3. doi: 10.1128/msphere.00209-20

Apprill, A., S. McNally, R. Parsons, and L. Weber. 2015. "Minor Revision to V4 Region SSU rRNA 806R Gene Primer Greatly Increases Detection of SAR11 Bacterioplankton." Aquatic Microbial Ecology 75: 129–137. doi: 10.3354/ame01753

Ardyna, M., L. Lacour, S. Sergi, et al. 2019. "Hydrothermal Vents Trigger Massive Phytoplankton Blooms in the Southern Ocean." Nature Communications 10: 2451. doi: 10.1038/s41467-019-09973-6

Ariza, A., S. Kaartvedt, A. Røstad, et al. 2014. "The Submarine Volcano Eruption Off El Hierro Island: Effects on the Scattering Migrant Biota and the Evolution of the Pelagic Communities." PLoS One 9. doi: 10.1371/journal.pone.0102354

Armbrust, E. V. 2009. "The Life of Diatoms in the World's Oceans." Nature 459: 185–192. doi: 10.1038/nature08057

Benoiston, A.-S., F. M. Ibarbalz, L. Bittner, et al. 2017. "The Evolution of Diatoms and Their Biogeochemical Functions." Philosophical Transactions of the Royal Society, B: Biological Sciences 372. doi: 10.1098/rstb.2016.0397

Biard, T. 2022. "Diversity and Ecology of Radiolaria in Modern Oceans." Environmental Microbiology 24: 2179–2200. doi: 10.1111/1462-2920.16004

Bonnet, S., C. Guieu, V. Taillandier, et al. 2023. "Natural Iron Fertilization by Shallow Hydrothermal Sources Fuels Diazotroph Blooms in the Ocean." Science 380: 812–817. doi: 10.1126/science.abq4654

Buck, N. J., J. A. Resing, E. T. Baker, and J. E. Lupton. 2018. "Chemical Fluxes From a Recently Erupted Shallow Submarine Volcano on the Mariana Arc." Geochemistry, Geophysics, Geosystems 19: 1660–1673. doi: 10.1029/2018GC007470

Callahan, B. J., P. J. McMurdie, M. J. Rosen, A. W. Han, A. J. A. Johnson, and S. P. Holmes. 2016. "DADA2: High-Resolution Sample Inference From Illumina Amplicon Data." Nature Methods 13: 581–583. doi: 10.1038/nmeth.3869

Caramanna, G., S. M. Sievert, and S. I. Bühring. 2021. "Submarine Shallow-Water Fluid Emissions and Their Geomicrobiological Imprint: A Global Overview." Frontiers in Marine Science 8. doi: 10.3389/fmars.2021.727199

Danovaro, R., M. Canals, M. Tangherlini, et al. 2017. "A Submarine Volcanic Eruption Leads to a Novel Microbial Habitat." Nature Ecology & Evolution 1: 1–9. doi: 10.1038/s41559-017-0144

de Boyer Montégut, C., G. Madec, A. S. Fischer, A. Lazar, and D. Iudicone. 2004. "Mixed Layer Depth Over the Global Ocean: An Examination of Profile Data and a Profile-Based Climatology." Journal of Geophysical Research, Oceans 109. doi: 10.1029/2004JC002378

De Cáceres, M., and P. Legendre. 2009. "Associations Between Species and Groups of Sites: Indices and Statistical Inference." Ecology 90: 3566–3574. doi: 10.1890/08-1823.1

Dupont, C. L., D. B. Rusch, S. Yooseph, et al. 2012. "Genomic Insights to SAR86, an Abundant and Uncultivated Marine Bacterial Lineage." ISME Journal 6: 1186–1199. doi: 10.1038/ismej.2011.189

Fernández de Puelles, M. L., M. Gazá, M. Cabanellas-Reboredo, et al. 2021. "Abundance and Structure of the Zooplankton Community During a Post-Eruptive Process: The Case of the Submarine Volcano Tagoro (El Hierro; Canary Islands), 2013–2018." Frontiers in Marine Science 8: 923. doi: 10.3389/fmars.2021.692885

Ferrera, I., J. Arístegui, J. M. González, M. F. Montero, E. Fraile-Nuez, and J. M. Gasol. 2015. "Transient Changes in Bacterioplankton Communities Induced by the Submarine Volcanic Eruption of El Hierro (Canary Islands)." PLoS One 10. doi: 10.1371/journal.pone.0118136

Fraile-Nuez, E., M. González-Dávila, J. M. Santana-Casiano, et al. 2012. "The Submarine Volcano Eruption at the Island of El Hierro: Physical-Chemical Perturbation and Biological Response." Scientific Reports 2. doi: 10.1038/srep00486

Fraile-Nuez, E., J. M. Santana-Casiano, M. González-Dávila, et al. 2023. "Ten Years of Intense Physical–Chemical, Geological and Biological Monitoring Over the Tagoro Submarine Volcano Marine Ecosystem (Eruptive and Degassing Stages)." In El Hierro Island, edited by P. J. González. Springer International Publishing.

Fraile-Nuez, E., J. M. Santana-Casiano, M. González-Dávila, et al. 2018. "Cyclic Behavior Associated With the Degassing Process at the Shallow Submarine Volcano Tagoro, Canary Islands, Spain." Geosciences 8. doi: 10.3390/geosciences8120457

Getz, E. W., V. C. Lanclos, C. Y. Kojima, et al. 2023. "The AEGEAN-169 Clade of Bacterioplankton Is Synonymous With SAR11 Subclade V (HIMB59) and Metabolically Distinct." mSystems 8. doi: 10.1128/msystems.00179-23

Gómez-Letona, M., J. Arístegui, A. G. Ramos, M. F. Montero, and J. Coca. 2018. "Lack of Impact of the El Hierro (Canary Islands) Submarine Volcanic Eruption on the Local Phytoplankton Community." Scientific Reports 8. doi: 10.1038/s41598-018-22967-6

González, F. J., B. Rincón-Tomás, L. Somoza, et al. 2020. "Low-Temperature, Shallow-Water Hydrothermal Vent Mineralization Following the Recent Submarine Eruption of Tagoro Volcano (El Hierro, Canary Islands)." Marine Geology 430. doi: 10.1016/j.margeo.2020.106333

González, P. J., ed. 2023. El Hierro Island. Springer International Publishing.

González-Vega, A., J. M. Arrieta, M. Santana-Casiano, et al. 2023. "Tagoro Submarine Volcano as a Natural Source of Significant Dissolved Inorganic Nutrients." In El Hierro Island, edited by P. J. González, 185–201. Springer International Publishing.

González-Vega, A., I. Callery, J. M. Arrieta, J. M. Santana-Casiano, J. F. Domínguez-Yanes, and E. Fraile-Nuez. 2022. "Severe Deoxygenation Event Caused by the 2011 Eruption of the Submarine Volcano Tagoro (El Hierro, Canary Islands)." Frontiers in Marine Science 9: 834691. doi: 10.3389/fmars.2022.834691

González-Vega, A., E. Fraile-Nuez, J. M. Santana-Casiano, et al. 2020. "Significant Release of Dissolved Inorganic Nutrients From the Shallow Submarine Volcano Tagoro (Canary Islands) Based on Seven-Year Monitoring." Frontiers in Marine Science 6. doi: 10.3389/fmars.2019.00829

Guérin, N., M. Ciccarella, E. Flamant, et al. 2022. "Genomic Adaptation of the Picoeukaryote Pelagomonas Calceolata to Iron-Poor Oceans Revealed by a Chromosome-Scale Genome Sequence." Communications Biology 5: 1–14. doi: 10.1038/s42003-022-03939-z

Guieu, C., S. Bonnet, A. Petrenko, et al. 2018. "Iron From a Submarine Source Impacts the Productive Layer of the Western Tropical South Pacific (WTSP)." Scientific Reports 8. doi: 10.1038/s41598-018-27407-z

Guillou, L., D. Bachar, S. Audic, et al. 2013. "The Protist Ribosomal Reference Database (PR2): A Catalog of Unicellular Eukaryote Small Sub-Unit rRNA Sequences With Curated Taxonomy." Nucleic Acids Research 41. doi: 10.1093/nar/gks1160

Guillou, L., M. Viprey, A. Chambouvet, et al. 2008. "Widespread Occurrence and Genetic Diversity of Marine Parasitoids Belonging to Syndiniales (Alveolata)." Environmental Microbiology 10. doi: 10.1111/j.1462-2920.2008.01731.x

Hoarfrost, A., S. Nayfach, J. Ladau, et al. 2020. "Global Ecotypes in the Ubiquitous Marine Clade SAR86." ISME Journal 14: 178–188. doi: 10.1038/s41396-019-0516-7

Holm-Hansen, O., C. J. Lorenzen, R. W. Holmes, and J. D. H. Strickland. 1965. "Fluorometric Determination of Chlorophyll." Journal of Conservation and Perennial Integrative Exploration of the Marine Environment 30: 3–15. doi: 10.1093/icesjms/30.1.3

Hu, S. K., E. L. Herrera, A. R. Smith, et al. 2021. "Protistan Grazing Impacts Microbial Communities and Carbon Cycling at Deep-Sea Hydrothermal Vents." Proceedings of

the National Academy of Sciences of the United States of America 118. doi: 10.1073/pnas.2102674118

Hu, S. K., A. R. Smith, R. E. Anderson, et al. 2023. "Globally-Distributed Microbial Eukaryotes Exhibit Endemism at Deep-Sea Hydrothermal Vents." Molecular Ecology 32: 6580–6598. doi: 10.1111/mec.16745

Kassambara, A. 2021. "rstatix: Pipe-Friendly Framework for Basic Statistical Tests." R Package Version 0.7.0.

Klevenz, V., S. G. Sander, M. Perner, and A. Koschinsky. 2012. "Amelioration of Free Copper by Hydrothermal Vent Microbes as a Response to High Copper Concentrations." Chemistry and Ecology 28: 405–420. doi: 10.1080/02757540.2012.666531

Leblanc, K., B. Quéguiner, F. Diaz, et al. 2018. "Nanoplanktonic Diatoms Are Globally Overlooked but Play a Role in Spring Blooms and Carbon Export." Nature Communications 9: 953. doi: 10.1038/s41467-018-03376-9

Lemieux, C., M. Turmel, C. Otis, and J.-F. Pombert. 2019. "A Streamlined and Predominantly Diploid Genome in the Tiny Marine Green Alga Chloropicon Primus." Nature Communications 10: 4061. doi: 10.1038/s41467-019-12014-x

Lilley, M. D., R. A. Feely, and J. H. Trefry. 1995. "Chemical and Biochemical Transformations in Hydrothermal Plumes." In Seafloor Hydrothermal Systems: Physical, Chemical, Biological, and Geological Interactions, edited by E. Humphris, R. A. Zierenberg, L. S. Mullineaux, and R. E. Thomsom, 369–391. American Geophysical Union (AGU).

Lopes dos Santos, A., T. Pollina, P. Gourvil, et al. 2017. "Chloropicophyceae, A New Class of Picophytoplanktonic Prasinophytes." Scientific Reports 7: 14019. doi: 10.1038/s41598-017-12412-5

Lorbacher, K., D. Dommenget, P. P. Niiler, and A. Köhl. 2006. "Ocean Mixed Layer Depth: A Subsurface Proxy of Ocean-Atmosphere Variability." Journal of Geophysical Research, Oceans 111: C07010. doi: 10.1029/2003JC002157

Lozano-Bilbao, E., G. Lozano, Á. J. Gutiérrez, et al. 2022. "The Influence of the Degassing Phase of the Tagoro Submarine Volcano (Canary Islands) on the Metal Content of Three Species of Cephalopods." Marine Pollution Bulletin 182. doi: 10.1016/j.marpolbul.2022.113964

Marie, D., F. Partensky, S. Jacquet, and D. Vaulot. 1997. "Enumeration and Cell Cycle Analysis of Natural Populations of Marine Picoplankton by Flow Cytometry Using the Nucleic Acid Stain SYBR Green I." Applied and Environmental Microbiology 63. doi: 10.1128/aem.63.1.186-193.1997

Martín-Díaz, J. P., A. González-Vega, T. Barreyre, et al. 2024. "Unveiling the Inherent Physical-Chemical Dynamics: Direct Measurements of Hydrothermal Fluid Flow, Heat, and Nutrient Outflow at the Tagoro Submarine Volcano (Canary Islands, Spain)." Science of the Total Environment 918: 170565. doi: 10.1016/j.scitotenv.2024.170565

Maugeri, T. L., G. Bianconi, F. Canganella, et al. 2010. "Shallow Hydrothermal Vents in the Southern Tyrrhenian Sea." Chemistry and Ecology 26: 285–298. doi: 10.1080/02757541003693250

McMurdie, P. J., and S. Holmes. 2013. "phyloseq: An R Package for Reproducible Interactive Analysis and Graphics of Microbiome Census Data." PLoS One 8. doi: 10.1371/journal.pone.0061217

Mériguet, Z., M. Vilain, A. Baudena, et al. 2023. "Plankton Community Structure in Response to Hydrothermal Iron Inputs Along the Tonga-Kermadec Arc." Frontiers in Marine Science 10. doi: 10.3389/fmars.2023.1232923

Morel, F. M. M., and N. M. Price. 2003. "The Biogeochemical Cycles of Trace Metals in the Oceans." Science 300: 944–947. doi: 10.1126/science.1083545

Oksanen, J., F. G. Blanchet, M. Friendly, et al. 2019. "vegan: Community Ecology Package." v2.6.4.

Olins, H. C., D. R. Rogers, K. L. Frank, C. Vidoudez, and P. R. Girguis. 2013. "Assessing the Influence of Physical, Geochemical and Biological Factors on Anaerobic Microbial Primary Productivity Within Hydrothermal Vent Chimneys." Geobiology 11: 279–293. doi: 10.1111/gbi.12034

Parada, A. E., D. M. Needham, and J. A. Fuhrman. 2016. "Every Base Matters: Assessing Small Subunit rRNA Primers for Marine Microbiomes With Mock Communities, Time Series and Global Field Samples." Environmental Microbiology 18: 1403–1414. doi: 10.1111/1462-2920.13023

Park, M. G., W. Yih, and D. W. Coats. 2004. "Parasites and Phytoplankton, With Special Emphasis on Dinoflagellate Infections." Journal of Eukaryotic Microbiology 51: 145–155. doi: 10.1111/j.1550-7408.2004.tb00539.x

Price, R. E., and D. Giovannelli. 2017. "A Review of the Geochemistry and Microbiology of Marine Shallow-Water Hydrothermal Vents." In Reference Module in Earth Systems and Environmental Sciences. Elsevier.

Price, R. E., I. Savov, B. Planer-Friedrich, S. I. Bühring, J. Amend, and T. Pichler. 2013. "Processes Influencing Extreme as Enrichment in Shallow-Sea Hydrothermal Fluids of Milos Island, Greece." Chemical Geology 348: 15–26. doi: 10.1016/j.chemgeo.2012.06.007

R Core Team. 2021. R: A Language and Environment for Statistical Computing. R Foundation for Statistical Computing.

Roda-Garcia, J. J., J. M. Haro-Moreno, L. A. Huschet, F. Rodriguez-Valera, and M. López-Pérez. 2021. "Phylogenomics of SAR116 Clade Reveals Two Subclades With Different Evolutionary Trajectories and an Important Role in the Ocean Sulfur Cycle." mSystems 6, no. 5: e0094421. doi: 10.1128/msystems.00944-21

Sambrook, J., and D. W. Russell. 2001. Molecular Cloning: A Laboratory Manual. 3rd ed. Cold Spring Harbor Laboratory Press.

Santana-Casiano, J. M., E. Fraile-Nuez, M. González-Dávila, E. T. Baker, J. A. Resing, and S. L. Walker. 2016. "Significant Discharge of CO2 From Hydrothermalism Associated With the Submarine Volcano of El Hierro Island." Scientific Reports 6: 25686. doi: 10.1038/srep25686

Santana-Casiano, J. M., M. González-Dávila, E. Fraile-Nuez, et al. 2013. "The Natural Ocean Acidification and Fertilization Event Caused by the Submarine Eruption of El Hierro." Scientific Reports 3: 1140. doi: 10.1038/srep01140

Santana-Casiano, J. M., M. González-Dávila, and E. Fraile-Nuez. 2017. The Emissions of the Tagoro Submarine Volcano (Canary Islands, Atlantic Ocean): Effects on the Physical and Chemical Properties of the Seawater.

Santana-González, C., J. M. Santana-Casiano, M. González-Dávila, and E. Fraile-Nuez. 2017. "Emissions of Fe(II) and Its Kinetic of Oxidation at Tagoro Submarine Volcano, El Hierro." Marine Chemistry 195: 129–137.

Schine, C. M. S., A.-C. Alderkamp, G. van Dijken, et al. 2021. "Massive Southern Ocean Phytoplankton Bloom Fed by Iron of Possible Hydrothermal Origin." Nature Communications 12: 1211. doi: 10.1038/s41467-021-21339-5

Serôdio, J., and J. Lavaud. 2020. "Diatoms and Their Ecological Importance." In Life Below Water. Encyclopedia of the UN Sustainable Development Goals, edited by W. Leal Filho, A. M. Azul, L. Brandli, A. Lange Salvia, and T. Wall, 1–9. Springer International Publishing.

Skovgaard, A., S. Karpov, and L. Guillou. 2012. "The Parasitic Dinoflagellates Blastodinium spp. Inhabiting the Gut of Marine, Planktonic Copepods: Morphology, Ecology, and Unrecognized Species Diversity." Frontiers in Microbiology 3. doi: 10.3389/fmicb.2012.00305

Sotomayor-García, A., J. L. Rueda, O. Sánchez-Guillamón, et al. 2023. "Impact of Tagoro Volcano Formation on Benthic Habitats and Associated Biota: A Review." In El Hierro Island, edited by P. J. González, 217–239. Springer International Publishing.

Sotomayor-García, A., J. L. Rueda, O. Sánchez-Guillamón, et al. 2020. "Chapter 51 – Geomorphic Features, Main Habitats and Associated Biota on and Around the Newly Formed Tagoro Submarine Volcano, Canary Islands." In Seafloor Geomorphology as Benthic Habitat, edited by P. T. Harris and E. Baker, Second ed., 835–846. Elsevier.

Stoeck, T., D. Bass, M. Nebel, et al. 2010. "Multiple Marker Parallel Tag Environmental DNA Sequencing Reveals a Highly Complex Eukaryotic Community in Marine Anoxic Water." Molecular Ecology 19: 21–31. doi: 10.1111/j.1365-294X.2009.04480.x

Suzuki, R., Y. Terada, and H. Shimodaira. 2019. "pvclust: Hierarchical Clustering With P-Values via Multiscale Bootstrap Resampling." v.2.

Tarasov, V. G. 2006. "Effects of Shallow-Water Hydrothermal Venting on Biological Communities of Coastal Marine Ecosystems of the Western Pacific." Advances in Marine Biology 50: 267–421. doi: 10.1016/S0065-2881(05)50004-X

Tarasov, V. G., A. V. Gebruk, A. N. Mironov, and L. I. Moskalev. 2005. "Deep-Sea and Shallow-Water Hydrothermal Vent Communities: Two Different Phenomena?" Chemical Geology 224: 5–39. doi: 10.1016/j.chemgeo.2005.07.021

Tilliette, C., F. Gazeau, G. Portlock, et al. 2023. "Influence of Shallow Hydrothermal Fluid Release on the Functioning of Phytoplankton Communities." Frontiers in Marine Science 10: 1082077. doi: 10.3389/fmars.2023.1082077

Vázquez, J.-T., O. Sánchez Guillamón, D. Palomino, et al. 2023. "Geomorphology of Tagoro Volcano Along Eruptive and Posteruptive Phases." In El Hierro Island, edited by P. J. González, 131–158. Springer International Publishing.

Wankel, S. D., L. N. Germanovich, M. D. Lilley, et al. 2011. "Influence of Subsurface Biosphere on Geochemical Fluxes From Diffuse Hydrothermal Fluids." Nature Geoscience 4: 461–468. doi: 10.1038/ngeo1183

Weinstein, M. M., A. Prem, M. Jin, S. Tang, and J. M. Bhasin. 2019. "FIGARO: An Efficient and Objective Tool for Optimizing Microbiome rRNA Gene Trimming Parameters." doi: 10.1101/610394

Wickham, H., M. Averick, J. Bryan, et al. 2019. "Welcome to the Tidyverse." Journal of Open Source Software 4: 1686. doi: 10.21105/joss.01686

Yu, G. 2020. "Using Ggtree to Visualize Data on Tree-Like Structures." Current Protocols in Bioinformatics 69. doi: 10.1002/cpbi.96

Yücel, M., S. M. Sievert, C. Vetriani, D. I. Foustoukos, D. Giovannelli, and N. Le Bris. 2013. "Eco-Geochemical Dynamics of a Shallow-Water Hydrothermal Vent System at Milos Island, Aegean Sea (Eastern Mediterranean)." Chemical Geology 356: 11–20. doi: 10.1016/j.chemgeo.2013.07.020

Zhou, Z., P. Q. Tran, K. Kieft, and K. Anantharaman. 2020. "Genome Diversification in Globally Distributed Novel Marine Proteobacteria Is Linked to Environmental Adaptation." ISME Journal 14: 2060–2077. doi: 10.1038/s41396-020-0669-4

CHAPTER 4

SPATIAL DISTRIBUTION AND DIVERSITY OF PROKARYOTIC COMMUNITIES ACROSS EPIPELAGIC AND BENTHIC HABITATS IN THE TAGORO SHALLOW HYDROTHERMAL SYSTEM (CANARY ISLANDS, SPAIN)

Manuscript

The shallow hydrothermal system of the Tagoro submarine volcano (Canary Islands, Spain) has been actively discharging nutrient-rich fluids with low temperature and pH, and high concentrations of CO_2 and H_2S, since entering a degassing phase in March 2012. While these hydrothermal emissions are known to influence local microbial communities, their impact on community structure, diversity and function across spatial gradients remains poorly understood. Using 16S rRNA gene sequencing, this study revealed significant differences in prokaryotic community structure and diversity across epipelagic seawater to benthic habitats (including microbial mats, volcanic rocks, sediments and chimney fragments) affected by hydrothermal activity. Prokaryotic richness and diversity decreased with proximity to sources of hydrothermal discharge, yet novel taxa were highly prominent across all hydrothermally influenced habitats. Archaeal diversity was low and primarily dominated by ammonia-oxidizing *Nitrosopumilaceae*, whereas the predominant and diverse bacterial communities were largely composed of iron-oxidizing *Mariprofundaceae*, methane-oxidizing *Methylomonadaceae* and metabolically versatile *Rhodobacteraceae* families. Molecular analyses further demonstrated the ecological versatility of several species within

these families, providing insights into microbial specialization within the Tagoro hydrothermal system. Scanning electron microscopy further revealed active bacterial biomineralization, mainly linked to *Mariprofundus* members, within chimney fragments from the active vent field. Altogether, our findings advance our understanding of the ecology and functionality of key microbes inhabiting the Tagoro hydrothermal system, which are mainly involved in marine nitrogen, iron, sulfur and methane cycling. This study provides valuable information on microbial distribution and potential ecological functions in shallow-sea hydrothermal fields, while highlighting the high prevalence of novel taxa with promising biotechnological applications in these extreme habitats.

4.1 Introduction

Marine shallow-water hydrothermal systems (<200 mbsl) are dynamic environments where geothermal activity interacts with the surrounding marine ecosystem. The simultaneous presence of light and geothermally reduced compounds makes these systems high-energy environments where both photosynthesis and chemosynthesis take place (Tarasov et al., 2005; Price and Giovannelli, 2017), contributing to enhance primary production in the surface layer (e.g., Buck et al., 2018; Bonnet et al., 2023; Tilliette et al., 2023; Pérez-Barrancos et al., 2025). These unique environments harbor diverse microbial communities adapted to extreme conditions (Caramanna et al., 2021) and play essential roles in sustaining the food web by enhancing organic matter (Gomez-Saez et al., 2017). Additionally, microorganisms often develop new habitats (e.g., microbial mats and biofilms) (Danovaro et al., 2024) and establish potential symbiotic relationships with biota colonizing these newly formed ecosystems (Dubilier et al., 2008).

While shallow-water vents have been documented on seamount summits, volcanic island flanks, and other near-shore environments with high heat flow, they remain significantly less explored than their deep-sea (>1000 mbsl) counterparts (Price and Giovannelli, 2017). The submarine volcanic eruption that took place just 1.8 km off the coast of El Hierro (Canary Islands) in October 2011, of relatively easy access, provided a unique opportunity to expand our understanding of underwater volcanism and the subsequent shallow hydrothermal activity.

The submarine eruption lasted 5 months and formed the Tagoro underwater volcano (Fraile-Nuez et al., 2012; Álvarez-Valero et al., 2023; Vázquez et al., 2023). Its degassing period began in March 2012, with the affected area concentrated within 0.5 km of the main crater, extending from approximately 127 mbsl (main crater) to 88 mbsl (summit) (Santana-Casiano et al., 2016; Martín-Díaz et al., 2024). The eruption led to the development of a 7600 m^2 shallow hydrothermal system covered with iron (Fe)-oxide deposits (González et al., 2020; Martín-Díaz et al., 2024) and characterized by thousands of irregularly distributed vent orifices discharging low-temperature (21–33.3ºC) low-pH (–1.37 average anomaly) fluids (Martín-Díaz et al., 2024), together with CO_2 and reduced sulfur species (such as S^0 and H_2S) degassing (Santana-Casiano et al., 2013, 2016). The vents exhibit diverse morphologies, including fissures, fractures and delicate chimney-like structures, with venting areas often covered by microbial mats (Danovaro et al., 2017; Sotomayor-García et al., 2023; Martín-Díaz et al., 2024).

Diffuse hydrothermal emissions from Tagoro have significantly altered the physical and chemical properties of seawater and marine sediments (Santana-Casiano et al., 2013; Santana-González et al., 2017; Fraile-Nuez et al., 2018; González et al., 2020; González-Vega et al., 2020). Hydrothermal discharge creates persistent positive potential temperature anomalies, as well as low salinity and density values in the water column (Fraile-Nuez et al., 2018). Vertical profiles further revealed positive Fe^{2+} concentration anomalies, coinciding with a significant pH reduction, apparently limited to an area and depth close to the main cone (Santana-González et al., 2017). However, significant inorganic nutrient enrichments have been constantly observed not only near the vents but also in the water column (González-Vega et al., 2020; Martín-Díaz et al., 2024; Pérez-Barrancos et al., 2025), with anomalies detected up to 50 m above the seabed and occasionally reaching the mixed layer and surface waters. Higher concentrations of dissolved PO_4^{3-} and $Si(OH)_4$ were detected in samples collected directly from the vents, whereas dissolved $NO_2^- + NO_3^-$ was highest in the water column and decreased with proximity to active venting (González-Vega et al., 2020). In fact, González-Vega et al. (2020) suggest that nitrogen is mainly emitted as NH_4^+ rather than NO_2^- or NO_3^- in the Tagoro hydrothermal system. These features create a complex shallow-water vent field with ongoing active discharge, which likely influences the biogeochemistry and mineralization patterns of the surrounding marine environment.

Despite its ecological significance and potential biotechnological relevance (García-Davis et al., 2021), research on microbial communities associated with the Tagoro ecosystem in the post-eruptive stage remains limited. One of the most remarkable discoveries in the area was the identification of a novel filamentous bacterium, *Candidatus* Thiolava veneris, in microbial mats attached to rock substrates (Danovaro et al., 2017). This species appears to have played a pioneering role in recolonizing areas affected by the eruption, yet it remains uncultured, and its complete genetic sequence is still unknown. While macrofaunal colonization of this newly formed benthic habitat has been more extensively documented (Sotomayor-García et al., 2019, 2020, 2023), potential symbiotic relationships with microbial communities remain unexplored. Furthermore, certain microbes involved in Fe, S and CH_4 cycles have been detected in Fe-rich sediments and mineral deposits from Tagoro (González et al., 2020). However, these earlier studies were based on limited microbiological data, demonstrating the need for a more comprehensive study in the area.

Experimental approaches have shown that nutrient-rich hydrothermal discharge from Tagoro enhances primary production in surface seawater, primarily mediated by phototrophic microbes (Pérez-Barrancos et al., 2025). Furthermore, geothermal compounds released by Tagoro are thought to serve as a source of energy for chemosynthetic microbes inhabiting the water column after the eruptive episode (Ferrera et al., 2015; Pérez-Barrancos et al., 2025). Thus, Tagoro supports the development of diverse microbial communities, potentially enhancing the transfer of matter and energy to higher trophic levels. Similarly, direct observations of the abundance, diversity and isotopic composition of zooplankton affected by hydrothermal activity highlighted the significant impact of Tagoro on pelagic communities (Fernández de Puelles et al., 2021; Herrera et al., 2024).

This study characterizes epipelagic and benthic prokaryotic communities inhabiting distinct hydrothermal habitats within the Tagoro shallow-water hydrothermal field, including seawater, microbial mat, rock, sediment and chimney habitats. The community structure and diversity of both bacteria and archaea were determined using 16S rRNA gene amplicon sequencing data. The analysis of prokaryotic communities in background seawater further allowed the identification of specific microbial taxa unique to the Tagoro hydrothermal field. Comparative phylogenetic analyses provided a deeper understanding of the taxonomic diversity and metabolic potential of prokaryotic microorganisms in the area. Additionally, bacterial biomineralization was examined through

SEM analyses. These findings are essential to better understand the role of microbes in benthic and epipelagic marine habitats affected by shallow hydrothermal activity, as well as their contribution to local biogeochemical cycles.

4.2 Material and methods

Seawater, microbial mat, sediment, rock and chimney samples were collected to characterize the prokaryotic communities inhabiting the active hydrothermal vent system at Tagoro (**Figure 1**), and to evaluate their plausible contribution to biomineralization and local biogeochemical cycles. In this study, we analyzed a total of 37 discrete biological samples obtained over 6 oceanographic cruises conducted between April 2017 and February 2022 onboard the R/V *Ramón Margalef* and R/V *Ángeles Alvariño* (**Table S1**).

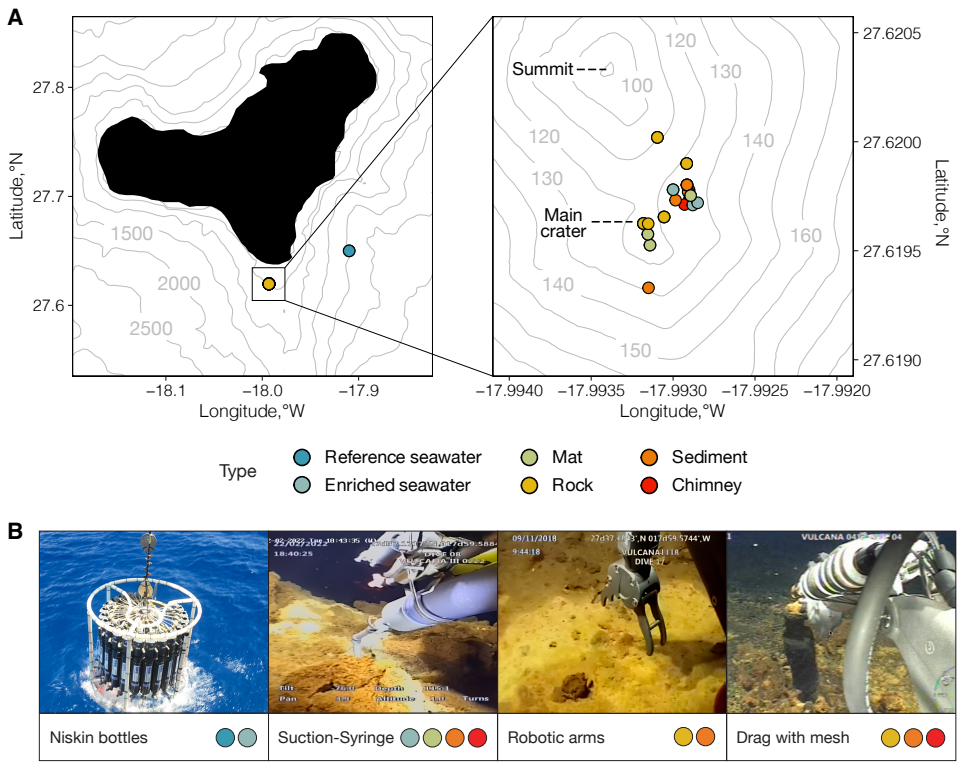

Figure 1. (A) Maps showing the location of the reference station (southeast of El Hierro island) and stations above the main hydrothermal field of Tagoro. Colored points indicate the sampled habitats. **(B)** Photographs of the oceanographic instrumentation used to collect each sample.

4.2.1 Microbial and geological sampling

Discrete hydrothermally enriched seawater samples were collected from ~127 mbsl at two vertical hydrographic stations located above the main crater of the Tagoro shallow submarine volcano (**Figure 1A**). Seawater sampling was conducted using a rosette frame equipped with 24 12-L Niskin bottles. Bottles were closed when real-time anomalies in temperature, pH or ORP (indicators of active hydrothermal activity) were detected by an SBE 911-plus CTD coupled with pH/ORP sensors. All sensors were calibrated before each oceanographic cruise- For comparison, reference seawater samples were also collected at ~127 mbsl from a control station located east of El Hierro, outside the influence of the Tagoro hydrothermal system (**Figure 1A**).

Additional hydrothermally enriched seawater, along with microbial mats, rocks, sediments and chimneys samples were obtained directly from visually active hydrothermal vents and areas adjacent the main active crater using a remotely operated vehicle (ROV; *Liropus 2000*, IEO-CSIC) (**Figure 1B**). The ROV was equipped with a range of marine sampling instruments specifically designed for each sampling purpose. Vent fluids, microbial mat, sediment and rock samples were obtained using a suction system, which was upgraded in 2021 to a piston-driven suction system known as syringe. Chimney samples were collected using a drag mesh, as well as some sediment samples. The ROV was also equipped with robotic arms to collect additional sediment and rock samples. All samples were preserved at –20ºC until analysis.

In this study, sample types serve as proxy for proximity to active hydrothermal sources, ranging from the most distant to the nearest habitat: reference seawater, enriched seawater, microbial mat, sediment, rock and chimney.

4.2.2 DNA extraction, amplification and sequencing

Genomic DNA isolation and sequencing library preparation for 16S V4 gene sequencing were conducted at the Oceanographic Center of the Canary Islands (IEO-CSIC, Tenerife, Spain). The OmniPrep™ Soil DNA kit (G-Biosciences) was used following the provided guidelines to extract DNA from microbial mat, sediment, volcanic rocks and chimney samples. Seawater samples were filtered through a 0.20 μm pore-size filter before DNA extraction using the phenol-chloroform method (Sambrook and Russell, 2001). Sequencing libraries were prepared following the methods described by Pérez-Barrancos et al.

(2025). The cleaned and indexed samples were pooled in equal molar proportions and paired-end sequenced (2x300) on an Illumina MiSeq platform (Macrogen, Korea).

4.2.3 Sequencing processing

Analyses were conducted in R v4.3.1 (R Core Team, 2021) using tidyverse v2.0 (Wickham et al., 2019). Amplicons were processed with DADA2 v1.28 (Callahan et al., 2016) after primer removal using cutadapt v1.18. Sequence reads were trimmed using optimal parameters (*truncLen* 216,143 and *maxEE* 1) estimated using the FIGARO package (Weinstein et al., 2019). Sequences were pooled together for sample inference and chimeras were removed following the consensus approach. This process resulted in an amplicon sequence variant (ASV) table containing 84% of the original reads. Taxonomic assignment of prokaryotic sequences (including species level assignment) was performed according to Silva SSU version 138.1. About 5% sequences were removed as they were classified as eukaryotes, mitochondria, or chloroplasts. The amplicon dataset was then rarefied to a sample size of 22,944 reads to minimize library size differences using phyloseq v.1.44 (McMurdie and Holmes, 2013). This rarefaction resulted in the loss of two samples (S41 and S44, **Table S1**) and the removal of 313 ASVs after random subsampling.

Sequences unassigned at the genus level in the rarefied dataset using Silva were subjected to BLAST searches (Sayers et al., 2025) against the NCBI Nucleotide collection (nr/nt) to check for members of poorly studied groups not present in curated datasets like Silva but found elsewhere. Additionally, these unassigned sequences were compared against the NCBI 16S ribosomal RNA sequences (Bacteria and Archaea) database to assess their potential relationship with cultured bacteria. To ensure the robustness of the results, the statistical significance (E-value) and sequence similarity (Max Ident) of each match were evaluated. The results of the BLAST analyses are temporarily available in the Shared Organizational Storage Service (SACO) of CSIC (https://saco.csic.es/s/sjqnLEb9zz89Ar5). They were further interpreted using the approximate taxonomic thresholds for bacteria and archaea defined by Yarza et al. (2014): 94.5% for genus level, 86.5% for family level and 82% for order level.

A phylogenetic tree was constructed for some of the most abundant taxonomic families in the rarified dataset using DECIPHER v2.24 (Wright, 2016). For this

purpose, sequences from each family were extracted from the rarefied dataset and visually inspected. Selected Silva sequences were incorporated into the respective datasets to serve as references, along with an outgroup bacterial or archaeal sequence that constituted the root of the phylogenetic tree (**Table S2**). After aligning the sequences, Silva pure sequences were shortened to match the length of the region sequenced in our study. The phylogenetic tree was constructed on phangorn v2.11.1 (Schliep, 2011). Several substitution models were tested using a neighbor-joining tree as a starting point, with the GTR+G+I maximum likelihood model consistently showing the best fit. Gamma distribution $k = 4$ and invariant sites $inv = 0.2$ parameters were applied before optimizing each tree without rearrangement. Bootstrapping was conducted to estimate the maximum likelihood (ML) tree up to 1,000 times, ensuring the robustness of the phylogenetic analysis.

Diversity metrics, Chao1 (species richness) and Inverse Simpson (species diversity), were estimated using phyloseq v.1.44 (McMurdie and Holmes, 2013). The statistical significance of alpha diversity differences between habitats was assessed using Games-Howell *post-hoc* tests following Welch's ANOVA. These statistical tests were chosen because data consistently met normality, but not always homogeneity of variances. Analyses were performed with rstatix v.0.7.2 (Kassambara, 2021) and visualized using ggpubr v.0.6.0 (Kassambara, 2020).

Variations in microbial community structure among samples were evaluated through hierarchical clustering based on Bray-Curtis dissimilarities using pvclust v2.2 (Suzuki et al., 2019). To quantify the uncertainty associated with clustering, multiscale bootstrap resampling was conducted up to 1,000 times, providing approximately unbiased (au) values for each identified cluster. The results were visualized using ggtree v3.8.2 (Yu, 2020).

The associations between species and specific habitats were assessed using the Indicator Value (IndVal) index, calculated through an indicator species analysis with indicspecies v1.7.15 (De Cáceres and Legendre, 2009). This statistical index combines relative abundance and frequency of occurrence data to identify species strongly associated with particular habitats or environmental conditions (hereafter referred to as 'indicator taxa'). To ensure the robustness of our results, we set a threshold of 75% or higher for the association value (*stat*) and a statistical significance (p) of 0.001. This approach allows the identification of prokaryotic species that may serve as biological markers of

shallow submarine hydrothermal activity, providing insights into the ecological processes and dynamics of local microbial communities.

4.2.4 Petrographic microscopy

A chimney fragment (S41, **Table S1**) was embedded in epoxy, and a thin section was prepared following standard procedures at the University of La Laguna. The thin section was studied under a Nikon Eclipse LV100N Pol polarization optical microscope located at the Oceanographic Center of the Canary Islands (IEO-CSIC, Tenerife, Spain). Images were acquired using a Pixelink camera and were processed with NIS-Elements BR v5.42.06 software. Areas exhibiting dendritic features were photographed under 20X and 10X magnification in plane-polarized light and selected for subsequent microanalyses.

4.2.5 Scanning electron microscopy

Textures and detailed morphology of individual filaments and globular structures were studied using a Zeiss EVO 15 Scanning Electron Microscope (SEM) with 2 nm resolution equipped with 50 mm^2 Oxford X-max X-ray scattering energy microanalyzer (EDX) from the General Research Support Service (SEGAI) of the University of La Laguna (Tenerife, Spain). Prior to analysis, the thin section was sputter-coated with carbon in the first analytical session and with gold in the second session using a Quorum Q150R ES Plus system at a thickness of 15 nm. Additionally, a chimney fragment (also from sample S41) attached to an aluminum stub was coated with gold following the same procedure. Microanalyses were performed at a voltage of 20 kV and a working distance of 8.5 mm. Images of both the thin section and the chimney fragment were examined using the secondary electron (SE) detector at 20 kV and an average working distance of 7 mm.

4.3 Results

4.3.1 Prokaryotic alpha diversity

Alpha diversity estimates revealed significant differences among the different habitats (Welch ANOVA, $p < 0.001$), indicating a marked decline in prokaryotic richness and diversity as proximity to hydrothermal vent emissions increased (**Figure 2**). Microbial mats exhibited the highest richness (i.e., the

number of prokaryotic ASVs), but had lower diversity compared to seawater samples. Specifically, hydrothermally enriched seawater displayed greater richness and diversity than reference seawater. In contrast, rock samples exhibited lower richness than reference seawater and lower diversity relative to microbial mats. Sediment samples followed this decreasing trend, showing further declines in both richness and diversity, while chimney samples presented the lowest values overall. These contrasting variations in alpha diversity were particularly significant between microbial mat and chimney samples (Games-Howell *post-hoc*, $p \leq 0.01$).

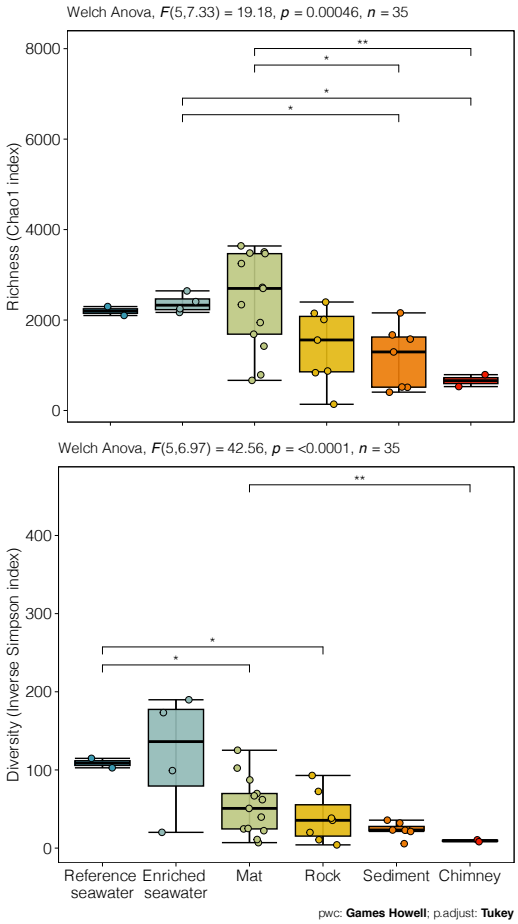

Figure 2. Prokaryotic Chao1 richness and Inverse Simpson diversity estimates across habitats, ordered by increasing proximity to hydrothermal sources: reference seawater, hydrothermally enriched seawater, microbial mat, rocks, sediments and chimney samples. Statistically significant differences between habitats, based on Welch ANOVA followed by Games-Howell pairwise *post-hoc* tests, are stated at the top of each panel or indicated with brackets and asterisks (* for $p \leq 0.05$ and ** for $p \leq 0.01$) for each pairwise comparison.

4.3.2 Prokaryotic community structure

Distinct prokaryotic communities were observed between habitats based on hierarchical clustering of Bray-Curtis dissimilarities (**Figure 3**). Seawater samples clustered separately from those samples collected in benthic habitats (microbial mats, rocks, sediments and chimneys), indicating a singular prokaryotic community in seawater. For instance, the archaeal class Nitrososphaeria, composed exclusively of the family *Nitrosopumilaceae* (**Figure S1**), was particularly abundant in seawater samples. This archaeal group accounted for 13% of the median relative abundance in reference seawater and 6% in hydrothermally enriched seawater (**Figure 4**). Specifically, the genus *Candidatus* Nitrosopelagicus was consistently observed (**Figure S2**) (see **Section 4.3.3**).

4.3.2.1 Epipelagic seawater

Reference and hydrothermally enriched seawater samples shared similar dominant taxonomic groups, yet their community structures exhibited some differences. Gammaproteobacteria were more abundant in enriched seawater (37%) than reference seawater (15%) (**Figure 3**), whereas Alphaproteobacteria were more prevalent in reference seawater (31%) compared to enriched seawater (22%) (**Figure 3**). Nonetheless, Pseudomonadales remained the predominant Gammaproteobacteria order in seawater (Figure 4), with notable contributions from the families *SAR86 clade*, *Pseudomonadaceae* and *Moraxellaceae* (**Figure S1**). Similarly, the orders SAR11 clade and Rhodospirillales were consistently observed in both reference and enriched seawater (**Figure 4**), with *Clade I* and *II*, and *AEGEAN-169 marine group* driving their relative abundances (**Figure S1**). Furthermore, indicator species analysis identified *Rhodospirillaceae*, a low-abundance family (<1%) within Rhodospirillales (**Figure S1**), as a strong indicator taxa of reference seawater ($stat \geq 0.92$ and $p \leq 0.001$; **Table S3**). Meanwhile, enriched seawater was particularly associated with several low-abundance families within Alphaproteobacteria and other classes like Bacteroidia and Desulfobacteria ($stat \geq 0.82$ and $p \leq 0.001$; **Table S3**).

4.3.2.2 Volcanic rocks

In contrast to seawater samples, rock samples exhibited high variability in their prokaryotic composition (**Figure 3**). Notably, no ASVs were identified as

indicators of rock habitats (*stat* < 0.75 and $p > 0.001$; **Table S3**). While some rock samples clustered closely with microbial mats, others differed significantly.

Two rock samples, S43 and S50, formed a separate cluster that was significantly differentiated from all other benthic samples (**Figure 3**). These samples were characterized by a high abundance of Alphaproteobacteria, particularly within the orders Rhizobiales (~12-22%), Parvibaculales (~5-9.5%) and Rhodobacterales (~4-6.5%) (**Figure 4** and **Figure S1**). The order Steroidobacterales of Gammaproteobacteria were also notably present (up to 8%). These rock samples were also visually described as bland, with orange precipitates attached, during on-board sampling. In contrast, rock sample S42 showed greater similarity to sediment and chimney samples. This sample was predominantly composed of Gammaproteobacteria (**Figure 3**), with a high relative abundance of the order Enterobacterales (up to 70%) (**Figure 4**) and the *Pseudoalteromonadaceae* family (**Figure S1**). Lastly, the remaining rock samples clustered with or near microbial mats, displaying a notable presence of Zetaproteobacteria (30%) (**Figure 3**), which in our dataset was exclusively composed of the genus *Mariprofundus* within the order Mariprofundales (**Figure 4** and **Figure S2**). However, the highest relative abundances of Zetaproteobacteria were observed in microbial mat samples (~32%) (**Figure 3**), where 14 *Mariprofundus* ASVs were significant indicators (*stat* ≥ 0.84 and $p \leq 0.001$; **Table S3** and **Figure S2**).

4.3.2.3 Microbial mats

Microbial mats exhibited the highest number of ASVs serving as indicators, including members from 15 phyla, 22 classes and 32 orders (**Table S3**). In addition to Zetaproteobacteria, 15 Alphaproteobacterial ASVs were identified as indicators of this habitat (*stat* ≥ 0.76 and $p \leq 0.001$; **Table S3**). Among these, 10 ASVs belonged to the family *Rhodobacteraceae*, which accounted for ~6% of the median relative abundance in microbial mats (**Figure S1**). Notably, the genus *Roseobacter* clade NAC11-7 lineage was the most prevalent within this family and habitat (**Figure S2**). Several members of Gammaproteobacteria were also associated with microbial mats, with 18 ASVs highlighted as indicators (*stat* ≥ 0.79 and $p \leq 0.001$; **Table S3**). The orders Enterobacterales and Pseudomonadales were the most consistent among these, comprising 5% and 2% of the median relative abundance in microbial mat samples, respectively (**Figure 4**). In this particular habitat, Enterobacterales was mostly represented by the family *Colwelliaceae*, while Pseudomonadales by *Halieaceae* (**Figure S1**).

Additionally, 8 Bacteroidia ASVs were associated with microbial mats (*stat* ≥ 0.78 and $p \leq 0.001$; **Table S3**), including 5 ASVs classified as Flavobacteriales (~1%). The class Bdellovibrionia (~1%) also exhibited 10 ASVs as indicators (*stat* ≥ 0.78 and $p \leq 0.001$; **Table S3**), along with several other low-abundance taxa (<1%), such as members of the phyla Desulfobacterota, Campylobacterota, Firmicutes, Myxococcota and Patescibacteria (*stat* > 0.75 and $p \leq 0.001$; **Table S3**).

4.3.2.4 Sediment and chimney fragments

Sediment and chimney samples shared similarities in prokaryotic community composition that significantly set them apart from other benthic samples (**Figure 3**). Both habitats were characterized by the presence of Gammaproteobacteria (28-51%), Thermoanaerobaculia (2-13%), Thermodesulfovibrionia (2-18%), Alphaproteobacteria (7.5-10%), Calditrichia (3-4%), Anaerolineae (3-4%) and Desulfobulbia (<2%). However, as observed in other habitats, differences at lower taxonomic levels (**Figure 4**, **Figure S1 and S2**) and the identification of indicator taxa (T**able S3**) revealed unique microbial features specific to these habitats.

Sediment samples were particularly characterized by Thermodesulfovibrionia class, with notably higher relative abundances (18%) compared to chimney samples (2%). Among 19 ASVs classified within this class, 3 ASVs were significantly indicative of hydrothermally influenced sediments (*stat* ≥ 0.90 and $p \leq 0.001$; **Table S3**), including one classified as the genus *Thermodesulfovibrio*. This ASV was the only one classified to the genus level, while the other 18 ASVs remained at the Thermodesulfovibrionia class level. Sediments also featured Desulfobulbia (~2%), which was exclusively composed of the order Desulfobulbales, with 5 ASVs acting as indicators (*stat* ≥ 0.90 and $p \leq 0.001$; **Table S3**). Four of these ASVs were classified as the family *Desulfobulbaceae*, including two identified as the genus *Desulfobulbus*. Furthermore, 2 ASVs from low-abundance orders (<1%) within Anaerolineae (~2%), such as Anaerolineales (**Figure S1**), were identified as significant indicators of sediment (*stat* ≥ 0.97 and $p \leq 0.001$; **Table S3**). Nonetheless, the order SJA-15 predominated within this class in both sediment and chimney samples (~2%) (**Figure 4**).

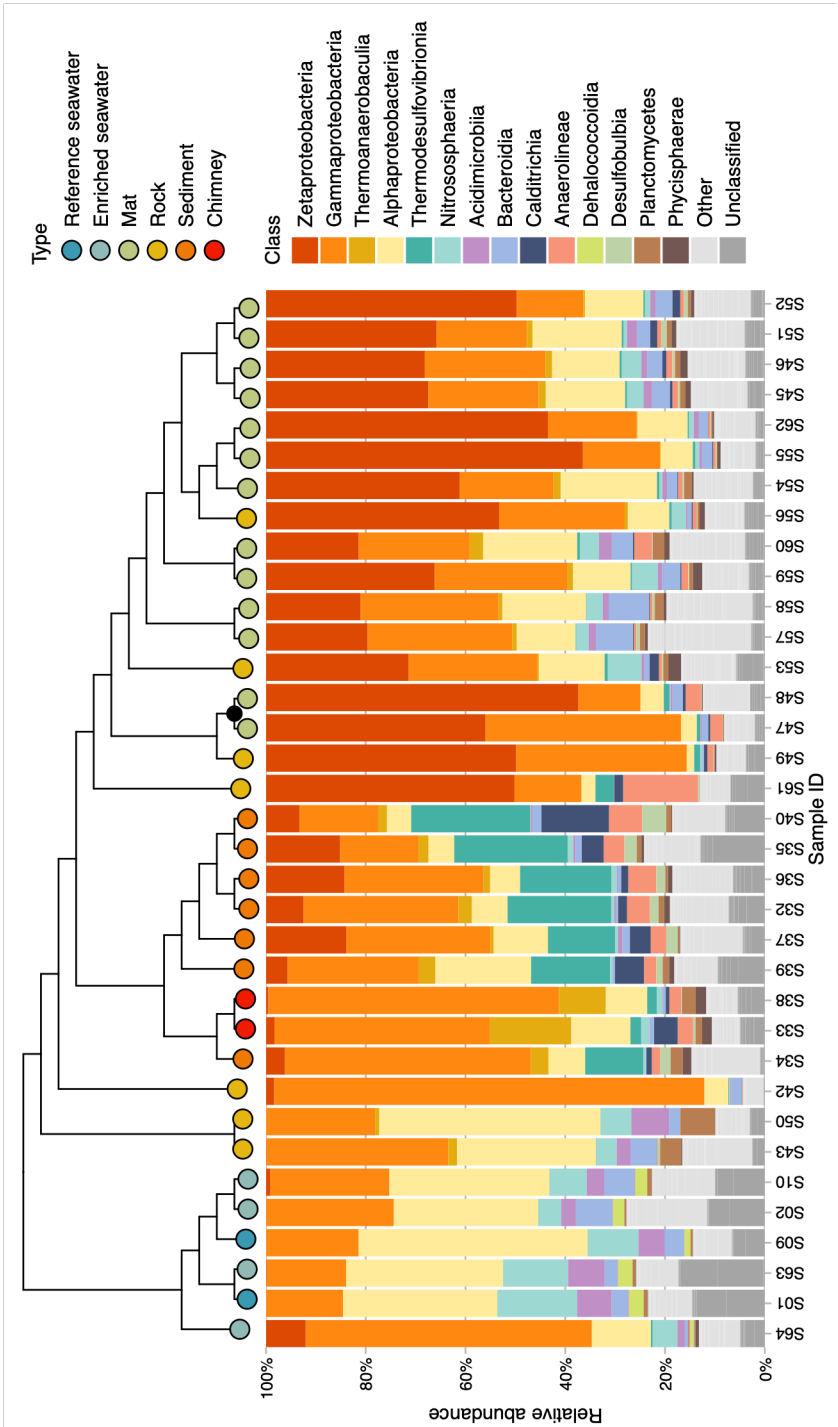

Figure 3. Hierarchical clustering of prokaryotic communities based on Bray-Curtis dissimilarities and relative abundance of class-classified prokaryotes. Color points on the dendrogram represent habitats, while black points indicate clusters with approximately unbiased (au) values below 75%. Classes are arranged in decreasing order of median relative abundance across each habitat, with those contributing <2% grouped as "Other.".

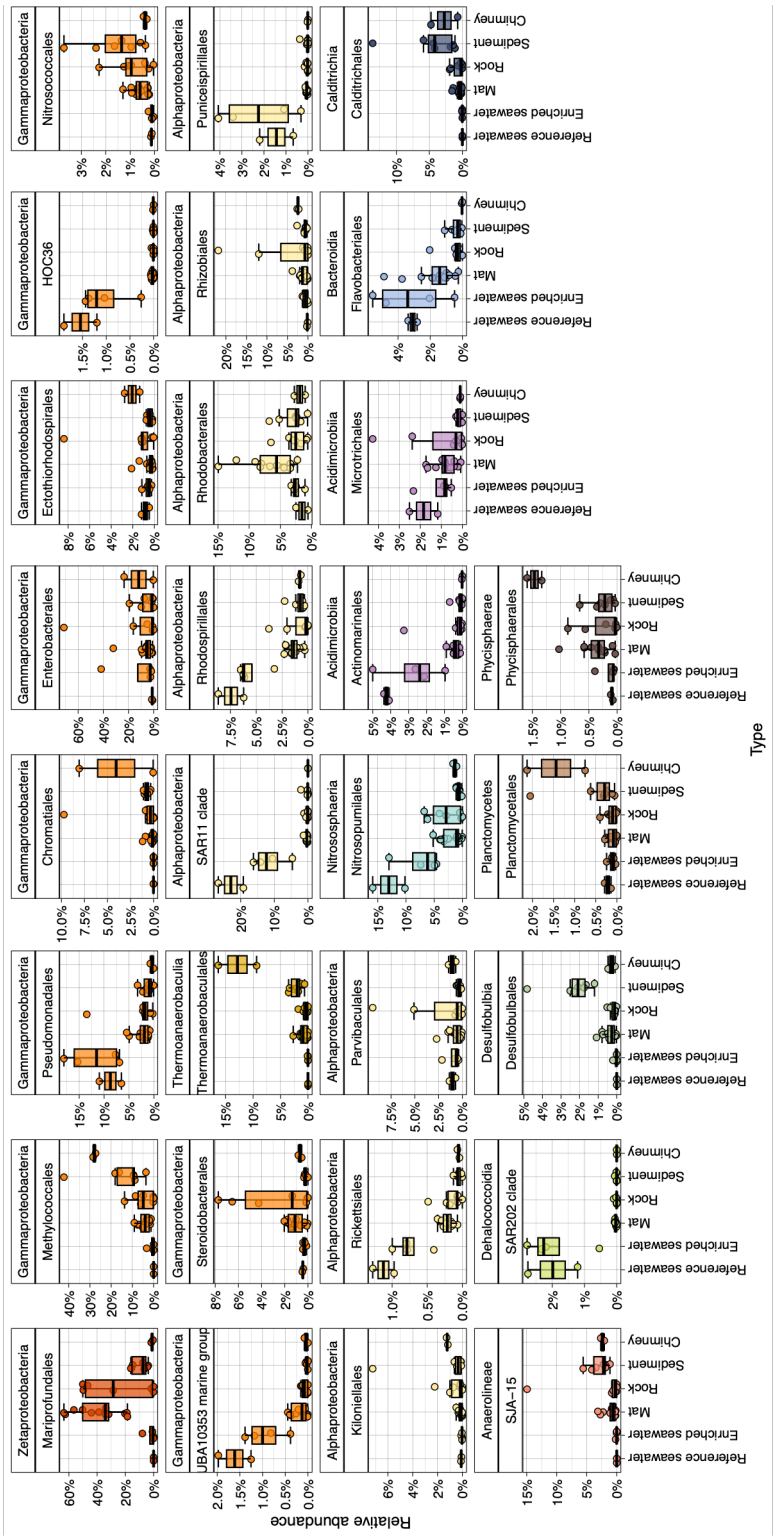

Figure 4. Boxplots showing the median, first and third quartiles, and error bars for prokaryotic orders with ≥ 1% median relative abundance in each habitat. Individual data points are overlaid. Colors correspond to the taxonomic class of each order, following the same color scheme used in **Figure 3**.

Chimneys, on the other hand, were characterized by the dominance of the class Thermoanaerobaculia (~13%) (**Figure 3**), with the family *Thermoanaerobaculaceae* being the unique representative (**Figure S1**) and almost entirely represented by the genus *Subgroup 10* (**Figure S2**). However, no Thermoanaerobaculia ASVs were found indicative of chimney samples (*stat* < 0.75 and $p > 0.001$; **Table S3**). In contrast, 1 ASV from the genus *Subgroup 23* (<1%) was indicative of sediment samples (*stat* ≥ 0.93 and $p \leq 0.001$; **Table S3**), where this family constituted only 2% of the relative abundance (**Figure S1**). Similarly, the order Methylococcales of Gammaproteobacteria exhibited higher relative abundances in chimney (28%) than sediment (9%) samples (**Figure 4**), yet an ASV classified as the low-abundance *Methylomarinum* genus (<1%) was found to be a sediment indicator (*stat* ≥ 0.95 and $p \leq 0.001$; **Table S3**). The gammaproteobacterial Nitrosococcales was also higher in sediment samples (~1%). Chimney samples were further distinguished by the order Chromatiales (4%) within Gammaproteobacteria (Figure 4), which was rare in other habitats (<1%), particularly by the genus *Candidatus* Thiobios (**Figure S2**). Additionally, 2 ASVs from Alphaproteobacteria were also identified as indicative of chimney samples (*stat* ≥ 0.90 and $p \leq 0.001$; **Table S3**), with 1 ASV classified under the family *Rhodobacteraceae* (~2%). However, the median relative abundance of Alphaproteobacteria in chimney samples was relatively low (10%) compared to other hydrothermally influenced habitats (**Figure 3**). Additionally, chimney samples exhibited the highest median relative abundances of Planctomycetales and Phycisphaerales (~1.5%) (**Figure 4**), which were the relatively most abundant orders of the Planctomycetota phylum. Although each of these classes comprised a small proportion of the overall prokaryotic community (<1%), one ASV from the order Phycisphaerales, classified as the genus *SM1A02*, was found to be indicative of chimney samples (*stat* ≥ 0.88 and $p \leq 0.001$; **Table S3**).

Few other ASVs, typically belonging to low-abundance phyla (<1%), such as Acidobacteriota, Myxococcota, SAR 324 clade (Marine group B), were also found to be indicative of either sediment or chimney samples (*stat* ≥ 0.85 and $p \leq 0.001$; **Table S3**), yet none were classified beyond the order level.

4.3.3 Phylogenetic overview of dominant prokaryotic families

Four prokaryotic families predominated across the hydrothermally influenced habitats at the Tagoro submarine volcano: *Mariprofundaceae* (16% of median relative abundance), *Methylomonadaceae* (5%) and *Rhodobacteraceae* (3%), and

Nitrosopumilaceae (1%) (**Figure S1**). Phylogenetic trees constructed for selected families (**Figure 5**) showed the evolutionary relationships among ASVs, accompanied by heatmaps and bar plots displaying the median and maximum relative abundances of each ASV across habitats. *Rhodobacteraceae* were excluded from the analysis due to the high diversity within the family and substantial metabolic differences among its groups. Altogether, the results suggest potential metabolic specialization within the analyzed families and their association with distinct ecological niches, consistent with trends described in **Section 4.3.2**.

4.3.3.1 *Mariprofundaceae* family (Zetaproteobacteria)

Mariprofundaceae was the most abundant family in the dataset, comprising 16% of the median relative abundance. In terms of median relative abundances, members of this family were particularly prevalent in microbial mats (see **Section 4.3.2**).

However, *Mariprofundaceae* exhibited substantial ASV richness, with 66 ASVs classified as *Mariprofundus* and most detected at low relative abundances (≤1%) across multiple habitats affected by hydrothermal activity (**Figure 5A**). For instance, ASV_4, ASV_3 and ASV_2 were present in all hydrothermal habitats and accounted for the majority of relative abundances (≥ 5%) (**Figure 5A**). These ASVs were particularly associated with *Mariprofundus* cultured species, such as *M. ferrooxydans*, *M. ferrooxydans* PV-1, *M. micogutta* and *M. aestuarium*.

Only ASV_11 was classified at the species level as *M. micogutta*. Among all hydrothermally influenced habitats, this species had the highest median relative abundance in chimney samples (~9%), with individual observations reaching up to ~16%.

Phylogenetic analysis showed no distinct associations between *Mariprofundus* ASVs and specific habitats at Tagoro, in contrast to the numerous low-abundance ASVs (≤1%) identified as microbial mat indicators through indicator species analysis (see **Section 4.3.2**). Among these 14 indicator ASVs, ASV_10 stood out with a median relative abundance of 6% in microbial mat samples and was closely related to the cultured species *M. ferrinatatus*. Meanwhile, 7 of the 14 indicator ASVs formed a distinct cluster, significantly differing from other *Mariprofundus* ASVs and cultured species in the dataset. These findings evidence the high species diversity within this genus and suggest the presence of novel species.

4.3.3.2 *Methylomonadaceae* family (Gammaproteobacteria)

Methylomonadaceae comprised ~5% of median relative abundance in the dataset and included 29 ASVs (**Figure 5B**). Although no species were identified and 10 ASVs remained unclassified at genus level, most ASVs were associated with cultured species (**Table S2**) or classified taxa belonging to genera *IheB2-23*, *Methylomonas* and *Methylomarinum*.

The ASVs classified as *IheB2-23* formed a distinct cluster, predominantly associated with chimney samples, accounting for ~5% of the median relative abundance. However, certain ASVs were also detected in hydrothermally enriched seawater, rock and sediment samples, reaching values up to 38%.

The *Methylomonas* ASV exhibited a maximum abundance of 4% in a rock sample and was closely related to *Methylomonas koyamae* and *Methylomonas methanica* MC09. Yet, its overall median relative abundance remained low (e.g., 0.5% in microbial mats and 0.02% in chimneys).

Among the *Methylomarinum* ASVs, ASV_259 was the only indicator ASV within the *Methylomonadaceae* family. It was significantly associated with sediment samples, where it was exclusively found, reaching relative abundances up to ~8%. In contrast, the remaining *Methylomarinum* ASVs exhibited peak abundances in rock samples (~10%) and hydrothermally enriched seawater (40%).

Lastly, ASVs classified as *Marine Methylotrophic Group 2* and *pItb-vmat-59* formed a cluster closely related to Methylomarinum vadi and *Methylomonas rubra*. The *Marine Methylotrophic Group 2* ASVs were particularly associated with microbial mats, with median and maximum relative abundances up to ~23% and 73%, respectively. Similarly, *pItb-vmat-59* ASVs were most prevalent in microbial mats, accounting for ~2% of the median relative abundance, although they reached higher relative abundances in chimney and rock samples (2–8%).

Our findings therefore highlighted the potential ecological flexibility of Methylomonadaceae, as members of this family were detected in multiple habitats across Tagoro.

4.3.3.3 *Nitrosopumilaceae* family (Nitrososphaeria)

The family *Nitrosopumilaceae* represented 1% of the median relative abundance and was found in all habitats affected by hydrothermal activity at Tagoro, with

particularly high abundance in seawater (~6%) (**Section 4.3.2**). This family exhibited substantial ASV richness, with 147 ASVs identified, including 40 ASVs classified as *Candidatus* Nitrosopelagicus, 29 ASVs as *Candidatus* Nitrosopumilus, 2 ASVs as *Cenarchaeum* and 76 ASVs as unclassified *Nitrosopumilaceae* taxa (**Figure 5D**). None of these ASVs were classified at the species level or identified as significant indicators of specific habitats (**Table S3**). However, phylogenetic analyses revealed two major clusters associated with habitat-specific distributions (**Figure 5D**).

The first cluster primarily included benthic ASVs classified as *Candidatus* Nitrosopumilus and *Cenarchaeum*, with median relative abundances up to ~57% and ~2.5%, respectively. Within this group, ASV_2403 was closely related to *Candidatus* Nitrosopumilus piranensis and *Candidatus* Nitrosopumilus adriaticus, yet exhibited low abundances (≤1%). Additionally, both ASV_16 and ASV_6770 were associated with *Candidatus* Nitrosopumilus maritimus, *Candidatus* Nitrosopumilus koreensis and *Candidatus* Nitrosopumilus sediminis. ASV_16 was widespread across all habitats, showing median relative abundances of 35–57% in benthic samples and of 9–15% in seawater, while ASV_6770 was low-abundant (≤0.5%) and confined to microbial mats and rocks.

The second major cluster comprised all ASVs classified as *Candidatus* Nitrosopelagicus and most unclassified *Nitrosopumilaceae*, being overall predominant in seawater samples. For instance, ASV_12 was associated with *Candidatus* Nitrosopelagicus brevis, displayed a median relative abundance of ~37–41% in seawater samples, and reached a maximum relative abundance of 60% in a sample of hydrothermally enriched seawater.

Altogether, differences between clusters highlighted the ecological versality and adaptation of *Nitrosopumilaceae* members to distinct benthic and pelagic habitats.

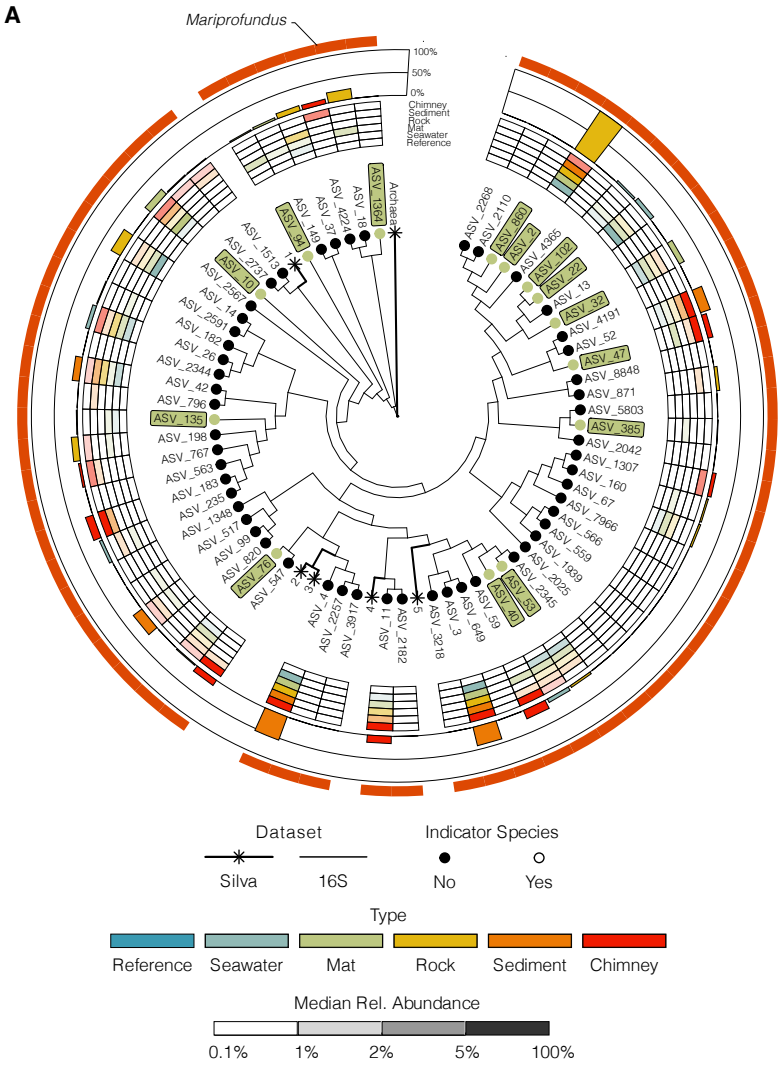

Figure 5. Phylogenetic trees, habitat-specific distributions and relative abundances of ASVs across some of the dominant microbial families in our rarefied dataset. The families (class) shown are **(A)** *Mariprofundaceae* (Zetaproteobacteria), **(B)** *Methylomonadaceae* (Gammaproteobacteria), and **(C)** *Nitrosopumilaceae* (Nitrososphaeria). For each family, the phylogenetic tree (center) illustrates evolutionary relationships among ASVs. Branch points (nodes) are shaped to distinguish data sources, including referenced cultured species retrieved from the Silva dataset (asterisk, detailed in **Table S2**) and sequenced species from our 16S rRNA analysis (circle). Nodes are colored to indicate ASVs identified as specific to a habitat through Indicator Species Analyses. A consistent color palette is used across all visual elements to represent habitats. The heatmap (first outer layer) displays the median relative abundance (%) of ASVs across habitats. The bar plot (second outer layer) highlights the maximum relative abundance (%) of each ASV, with bars colored by the habitat where the highest relative abundance was observed. Genera are annotated directly in the plot and distinguished using a separate color palette.

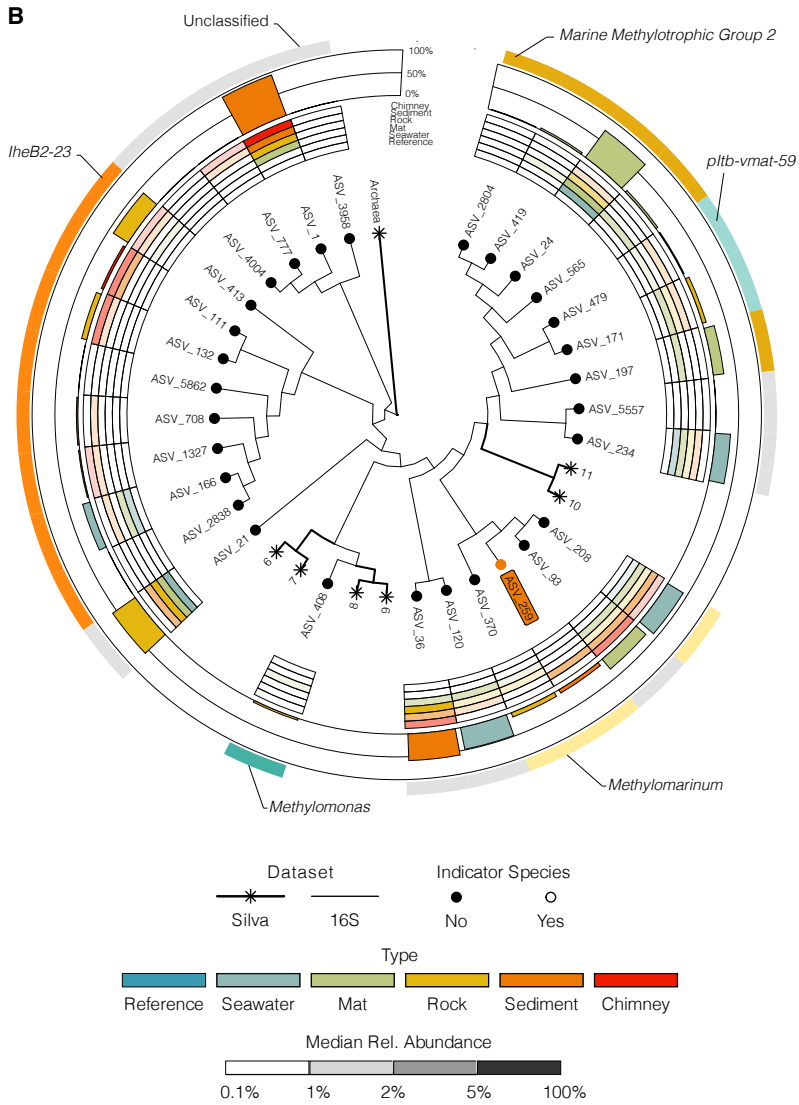

Figure 5. Continued.

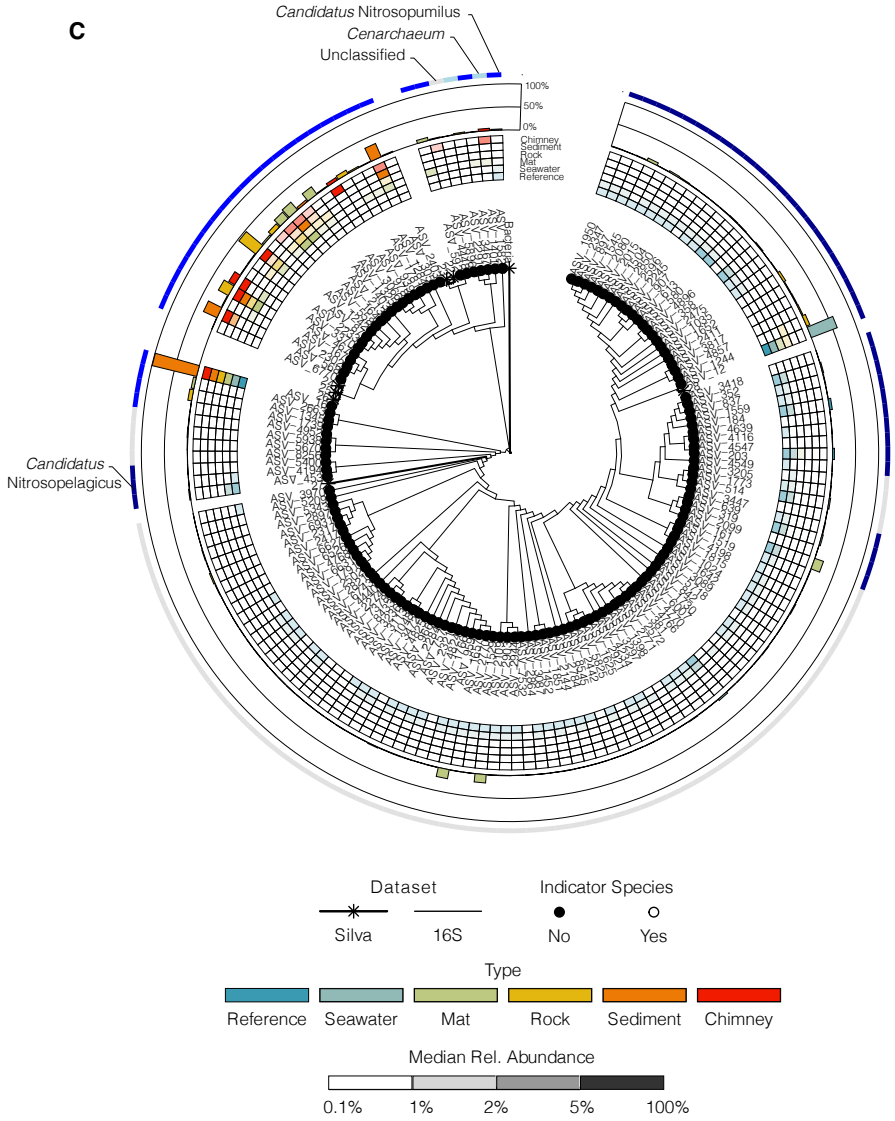

Figure 5. Continued.

4.3.4 Unexplored prokaryotic diversity

Approximately 66% of the sequences in the rarefied dataset remained unassigned at genus level, with 37% unclassified at family level, 22% at order level and 10% at class level. Notably, nearly half (around 48%) of the robust ASVs identified as indicators of specific habitats were unassigned to a known genus (**Table S4**). Direct BLAST analysis against the NCBI Nucleotide collection (nr/nt) showed that 99.9% of unassigned sequences matched sequences corresponding to uncultured prokaryotes from diverse environments around the world (see **Section 4.2.3**). The highest percentage of identity between each of our sequences and its best database match (i.e, their closest GenBank relative) was ≥94.5% for ~89% of the sequences, suggesting genus level similarity based on published thresholds (see **Section 4.2.3**). An additional ~11% had identities between 86.5% and <94.5% (family level), and only ~0.1% fell between 83% and <86.5% (order level). Meanwhile, BLAST searches against the NCBI 16S ribosomal RNA sequences database showed that all unassigned sequences were distantly related to formally described prokaryotes, as the highest identity values were on average below 90% ± 4%, highlighting the novelty of these unassigned sequences. In both databases expectation values were low (E-value ≤ 4e-51), indicating that the matches were reliable and highly significant. These results indicate that, although most sequences share high similarity with other environmental sequences, they remain taxonomically unassigned, highlighting the extent of novel diversity at Tagoro and particularly of novel prokaryotic genera yet to be formally described.

The class Thermodesulfovibrionia, characteristic of our sediment samples (**Table S3**), exemplifies this unexplored diversity. Among the 19 ASVs classified within this class, only one was classified to the genus *Thermodesulfovibrio* (ASV_170), while the remaining ASVs were classified only at class level. Direct BLAST of these 18 unassigned Thermodesulfovibrionia sequences against the NCBI nucleotide collection confirmed their presence in aquatic environments elsewhere (**Table S4**). These closest GenBank relatives of these sequences presented maximum identities ranging from 96 to 100%, suggesting a close relationship at the level of genus or species with our unidentified Thermodesulfovibrionia ASVs. However, BLAST against the NCBI 16S ribosomal RNA sequences database yielded lower identity matches (83–87%), further indicating that these sequences are highly different from

those of formally described organisms available in pure culture (**Table S4**). All BLAST results showed extremely low expectation values, indicating that the matches were reliable and highly significant. These findings indicate that vast, unexplored microbial diversity awaits discovery in unique environments such as the Tagoro hydrothermal system.

4.3.5 Chimney textures and morphology

Directional dendritic features were frequently observed throughout the thin section using optical microscopy (**Figure S3A–B**), along with Fe-rich bands forming stacked, dome-shaped structures (**Figure S3C**). SEM images of these dendritic areas revealed complex structures and diverse morphologies, occasionally embedded within the Si-Fe chimney matrix (**Figure S3D–F** and **Figure S4**).

At higher magnifications, the chimney fragment exhibited mineralized surfaces with intricate textures, including twisted stalks and globular precipitates indicative of bacterial biomineralization (**Figure 6**). Filamentous structures were often observed interwoven within the mineral matrix, especially those with irregular and straight morphologies (**Figure 6C**). Twisted stalks were also individually identified throughout the chimney fragment (**Figure 6D–F**) and were sometimes partially covered by crystalline salt deposits (**Figure 6F** and **Figure S5**).

EDX analyses showed that twisted stalks were primarily composed of silicon (Si) and Fe, with a lower Si:Fe ratio (higher Fe content relative to Si) compared to the surrounding chimney matrix (**Figure S4** and **Table S5**). Additionally, both regions contained calcium (Ca), magnesium (Mg), titanium (Ti) and potassium (K), with manganese (Mn) uniquely present in the filaments.

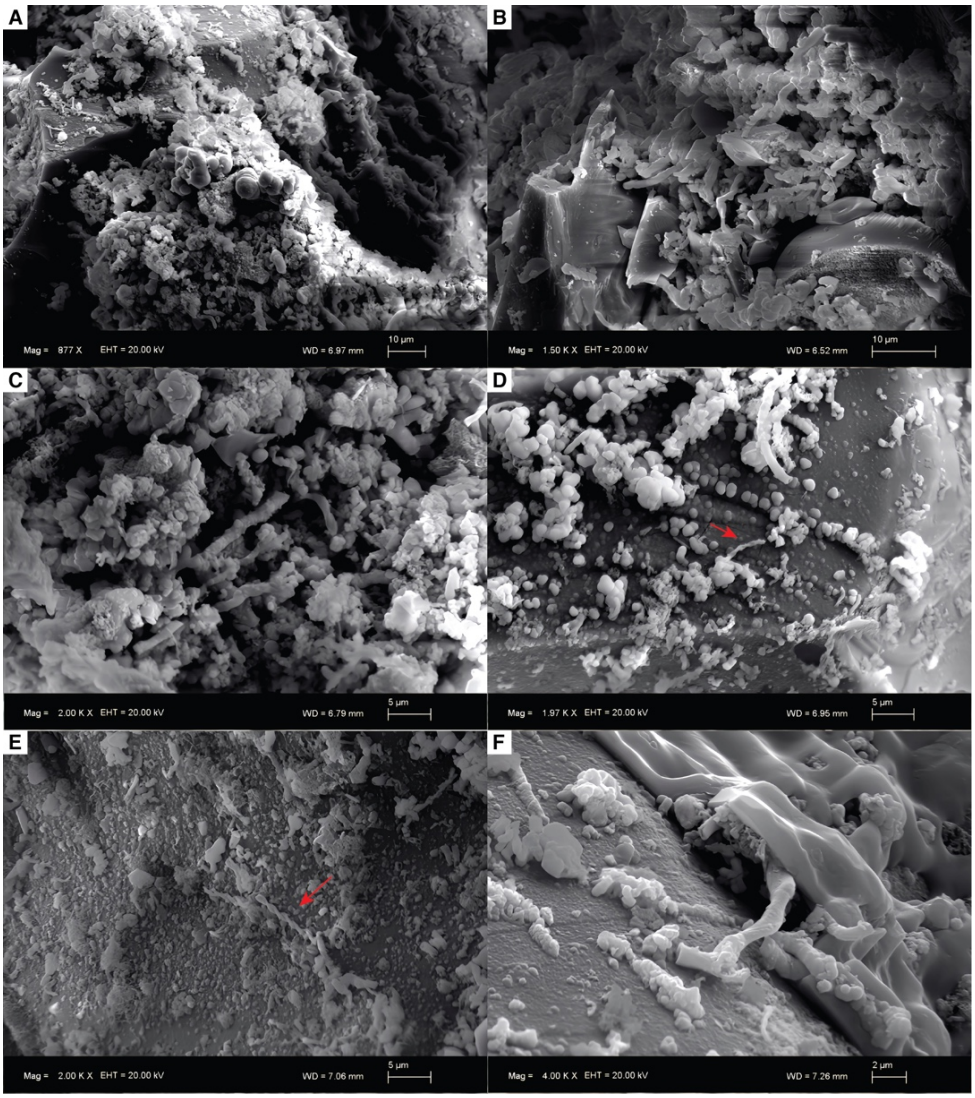

Figure 6. SEM images of **(A, B)** textures, filamentous and globular structures in the chimney fragment. **(C)** Interwoven straight filaments within the Si-Fe chimney matrix. **(D, E)** Examples of ribbon-like twisted stalks (red arrows). **(F)** Twisted stalk partially covered by crystalline salt deposits (see **Figure S4** and **Table S5** for detailed chemical composition).

4.4 Discussion

The shallow-water hydrothermal field of Tagoro, located at depths of 88–127 mbsl and just 1.8 km off the southern coast of El Hierro (Canary Islands, Spain), has been intensely monitored by the Spanish Institute of Oceanography (IEO-CSIC) since its underwater eruption in October 2011 (Fraile-Nuez et al., 2023). Still, research on microbial communities during the current degasification phase remains limited. The role of geothermally reduced compounds in shaping local microbial communities is still poorly understood, although recent experimental studies evidence their significant impact on surface seawater microorganisms (Pérez-Barrancos et al., 2025). Additionally, studies on seawater, microbial mats and mineral deposits at Tagoro detected both novel and typical taxa associated with hydrothermal processes (Ferrera et al., 2015; Danovaro et al., 2017; González et al., 2020; García-Davis et al., 2021). However, most of these field studies were based on a limited number of microbiological samples, often derived from only a few samples or even a single sample, highlighting the need for more extensive research. By analyzing 16S rRNA amplicon sequencing of 37 samples (including seawater, microbial mats, sediments, rocks and chimney fragments), our study enhances our understanding of the epipelagic and benthic prokaryotic community structure and composition at the Tagoro hydrothermal field. Furthermore, our findings provide new insights into the biogeochemical processes mediated by prokaryotes shaping this dynamic ecosystem.

4.4.1 Prokaryotic alpha diversity

Prokaryotic alpha diversity estimates were significantly different between habitats. Species richness and diversity decreased with proximity to hydrothermal vents from Tagoro, in accordance with observations in hydrothermal diffuse flow environments worldwide (Huber et al., 2003; Campbell et al., 2013).

The complex geochemistry of these ecosystems may account for the comparatively low richness and diversity in the Tagoro vent field. The variability of upper ocean processes (e.g., tidal and wind forcing, surface currents and vertical mixing, weather patterns, etc.) may also influence alpha diversity estimates. Previous research highlighted that the hydrothermal system of Tagoro exhibited a stationary cyclic degassing behavior with a strong peak of a 140-min period centered on a significant interval of 130–170 min at 99.9%

confidence (Fraile-Nuez et al., 2018). The consistency of this cyclic behavior provides a highly stable environment as compared to the water column, which may explain the low diversity in those environments most affected by the hydrothermal emissions.

In addition, phylogenetic assignments based on average nucleotide identity of 16S rRNA sequences against NCBI sequence databases (Nucleotide collection and 16S ribosomal RNA sequences) revealed that most bacterial populations in the Tagoro environment are genetically distant from formally described species, but closely related to sequences previously found in other hydrothermal settings. These findings suggest that shallow-water hydrothermal systems harbor a substantial proportion of novel microbial lineages waiting to be discovered. This also underscores the urgent need to improve diversity assessments in these often overlooked but ecologically significant ecosystems, as current estimates may be biased due to limited microbial data.

4.4.2 Prokaryotic community structure and habitat specificity

4.4.2.1 Epipelagic seawater

Seawater enriched with hydrothermal fluids from Tagoro exhibited a distinct prokaryotic community structure compared to unaffected waters, consistent with previous studies in the area showing that even small hydrothermal emissions can significantly reshape surface microbial communities (Pérez-Barrancos et al., 2025). Enriched and reference seawater samples shared similar dominant taxonomic groups, yet their overall community structure differed significantly. Furthermore, distinct low-abundance taxa were associated with each environment, underscoring how hydrothermal activity promotes niche differentiation even among less abundant microbial populations.

Alpha- and Gammaproteobacteria were dominant in hydrothermally enriched seawater samples, consistent with observations from shallow and deep-sea hydrothermal vents worldwide (Price and Giovannelli, 2017; Zeng et al., 2021). Alphaproteobacteria included groups typically prevalent in oceanic bacterioplankton communities, such as the SAR11 *Clade I* and *II* (Giovannoni, 2017). Among Gammaproteobacteria, the order Pseudomonadales was notably abundant, suggesting that these bacteria benefit significantly from hydrothermal inputs at Tagoro. Families such as *SAR86 clade*, *Pseudomonadaceae* and *Moraxellaceae* contributed substantially to this gammaproteobacterial order.

The *SAR86 clade*, along with photoheterotrophic microbes with genes for proteorhodopsin-based phototrophy, were in fact previously linked to Tagoro (Pérez-Barrancos et al., 2025). The availability of sunlight, combined with natural sources of inorganic and organic compounds, likely supply these organisms with the necessary energy sources to support their proliferation in shallow-water hydrothermal systems.

The archaeal class Nitrososphaeria was also abundant in our seawater samples, with the genus *Candidatus* Nitrosopelagicus consistently observed. The notable presence of these aerobic ammonia-oxidizing archaea (Santoro et al., 2021) highlights their potential role in nitrogen cycling in hydrothermally enriched seawater, which will be further discussed in **Section 4.4.3**.

Several low-abundance families were also characteristic of the prokaryotic community in seawater affected by the hydrothermal activity of Tagoro, including *Oligoflexaceae* (Oligoflexia), *NS7 marine group* (Bacteroidia), *OCS116 clade* (Alphaproteobacteria) and *Desulfosarcinaceae* (Desulfobacteria). Notably, the genus *SEEP-SRB1*, an anaerobic sulfate-reducing bacterial group within the *Desulfosarcinaceae* family associated with methane oxidation in deep-sea environments (Knittel et al., 2003; Schreiber et al., 2010), was detected. *SEEP-SRB1* has been found in methane seeps, hydrothermal vents and cold seep ecosystems, all characterized by low-temperature, hydrocarbon-rich fluid emissions. This group couples sulfate reduction with the anaerobic oxidation of methane and other non-methane hydrocarbons (Boetius et al., 2000; Kleindienst et al., 2012; Vigneron et al., 2017), often in syntrophy with anaerobic methanotrophic archaea (Boetius et al., 2000). The environmental conditions at Tagoro, involving the active discharge of diffuse low-temperature vent fluids, presumably rich in reduced sulfur compounds (Santana-Casiano et al., 2013), may favor the presence of sulfate-reducing microbes. Additionally, these findings suggest the potential availability of methane in the area, although its presence has not yet been documented at Tagoro, possibly because methane-oxidation rates at shallow vents are typically low compared to their deep-sea counterparts (Tarasov et al., 2005).

Additionally, our study highlighted the presence of microbes with industrial and biotechnological potential in the water column of Tagoro, such as the gammaproteobacterial genera *Acinetobacter* and *Psychrobacter* (Teixeira and Merquior, 2014). This finding aligns with previous discoveries of bacterial taxa with antiproliferative properties in deep-sea algae, invertebrates and volcanic

sediments at Tagoro (García-Davis et al., 2021), and further confirms that shallow-water hydrothermal systems may serve as hotspots for biotechnologically valuable microbes.

4.4.2.2 Microbial mats

Zetaproteobacteria, a group of obligate autotrophs capable of oxidizing ferrous iron (Fe^{2+}) to ferric iron (Fe^{3+}), were the main prokaryotes in our microbial mat samples. These bacteria were first discovered in hydrothermal vents at the Loihi Seamount in Hawaii (Emerson and Moyer, 2002), where distinct rust-colored Fe oxides suggested high concentrations of CO_2 and Fe^{2+} (see **Section 4.4.4**). Notably, they are known to produce highly reactive Fe-oxyhydroxides that can adsorb or precipitate nutrients and metals (McAllister et al., 2019). In our study, Zetaproteobacteria were exclusively represented by the lithotrophic iron-oxidizing genus *Mariprofundus* (McAllister et al., 2019). Approximately 22% of *Mariprofundus* ASVs were identified as strong indicators of microbial mat samples, highlighting their ecological significance in this benthic habitat. The presence of orange precipitates in rock samples, which resemble ferric hydroxide ($Fe(OH)_3$) deposits found in seamounts influenced by active hydrothermal venting (e.g., Boyd and Scott, 2001), reinforces our observations of iron-oxidizing bacteria contributing to mineral precipitation (see **Section 4.4.4**). At iron-dominated vents, Zetaproteobacteria can significantly shape the environment through the production of mineral precipitates and exopolysaccharides, which contribute to the formation of microbial mats, impact the local geochemistry and enhance microbial diversity. Our findings therefore indicate that dissolved iron concentration is a major factor influencing the prokaryotic community structure at Tagoro, consistent with observations in hydrothermal vents worldwide (Hager et al., 2017; Fullerton et al., 2024). The role of bacterial iron oxidizers in iron cycling and biomineralization processes at the Tagoro submarine volcano is further discussed in **Sections 4.4.3 and 4.4.4**.

Our study also documented the high microbial diversity characterizing microbial mats at Tagoro, with 21 bacterial classes, including Alphaproteobacteria, Gammaproteobacteria and Bacteroidia, identified as indicators of this habitat alongside Zetaproteobacteria. Within Alphaproteobacteria, the *Roseobacter* clade NAC11-7 lineage was particularly associated with microbial mats, being the most abundant genus within the family *Rhodobacteraceae*. This lineage has been frequently linked to algae and algal

blooms in surface seawater environments (Buchan et al., 2005; Teeling et al., 2012), suggesting that it thrives at relatively high concentrations of organic matter. Similarly, members of Gammaproteobacteria and Bacteroidia that are frequently associated with a copiotrophic lifestyle and the utilization of organic matter were consistently detected in our microbial mat samples. For instance, the ubiquitous genus *Thalassotalea* (*Colwelliaceae* family) and the cosmopolitan *OM60/NOR5* clade (*Halieaceae* family) are well known for their polysaccharide-degrading abilities (Taylor et al., 2014; Kim et al., 2020; Li et al., 2023). Their prevalence in the Tagoro hydrothermal system suggests that the region maintains high productivity rates, sustaining bacterial groups highly adapted to the utilization of biogenic organic material inputs and contributing to biogeochemical nutrient cycling (e.g, Buchan et al., 2014). Notably, Rhodobacterales and Flavobacteriales have been shown to increase in response to the accumulation of transparent exopolymer particles (TEPs) produced by phytoplankton (Taylor et al., 2014). These findings align with previous experimental evidence at Tagoro, where hydrothermal inputs fueled phytoplankton biomass, thereby increasing organic matter availability ready for microbial utilization (Pérez-Barrancos et al., 2025).

Furthermore, indicator species analysis revealed that microbial mats at the Tagoro hydrothermal system contained specific bacterial groups linked to sulfur and nitrogen cycles, consistent with previous studies in the area (Danovaro et al., 2017; González et al., 2020). Notably, one of the most remarkable discoveries at Tagoro has been *Candidatus* Thiolava veneris, a novel bacterium belonging to the order Thiotrichales capable of utilizing sulfur and nitrogen compounds, as well as organic and inorganic carbon, forming massive microbial mats of long, white filaments attached to the rock substrate (Danovaro et al., 2017). However, since the 16S rRNA gene sequence of *Ca.* Thiolava veneris was not retrieved from the metagenomic assembled sequences and the bacterium has not been isolated in pure culture (Danovaro et al., 2017), we were unable to confirm its presence in our samples. Instead, 10 Thiotrichales ASVs were detected with low relative abundances (<1%) across our benthic samples (data not shown). Notably, our analysis also identified the genus *Desulfoconvexum* (Desulfobacterota) in microbial mats, which was unexpected given that only one species, *D. algidum*, has been isolated so far from permanently cold marine sediments in Norway (Könneke et al., 2013). This psychrophilic, sulfate-reducing bacterium plays a crucial role in reducing sulfate (SO_4^{2-}) to hydrogen sulfide (H_2S) in strictly anaerobic environments.

Likewise, the microaerophilic genus *Sulfurospirillum* (Campylobacterota) was strongly associated with microbial mats at Tagoro, including physiologically versatile species capable of sulfur oxidation and reduction, dissimilatory nitrate reduction, indirect Fe^{3+} reduction and utilization of toxic compounds (Goris and Diekert, 2016).

These findings demonstrate that microbial mats at Tagoro harbor a complex microbial network shaped by the unique physical and chemical properties of this shallow-water hydrothermal system. For instance, González et al. (2020) already discussed that sulfur-oxidizing bacterial mats are typically associated with higher-temperature vents and chimney conduits, whereas iron-rich bacterial mats tend to form in lower-temperature, more diffuse venting areas (Vander Roost et al., 2017). At Tagoro, vent temperatures range from approximately 26–29 ºC (Martín-Díaz et al., 2024), and while these differences are subtle, they may contribute to variations in microbial mat structure. Previous analyses also described a gradual increase in hydrothermal fluid temperatures from diffuse (~26.8 ºC) to transitional (~27.2 ºC) and rocky-focused (~28.7 ºC) venting areas (Martín-Díaz et al., 2024), similar to temperature trends observed at the Lucky Strike hydrothermal field (Barreyre et al., 2012). This temperature gradient was particularly evident in the eastern region of the main crater of Tagoro, characterized by extensive areas of diffuse venting and low vent densities, where most of our microbial mat samples were collected. Therefore, the environmental conditions likely contributed to the bacterial heterogeneity observed in microbial mats at Tagoro and emphasize the need for more comprehensive geochemical studies of the benthic compartment in the current degassing stage.

4.4.2.3 Rocks, sediments and chimney fragments

Several bacterial taxa frequently associated with ammonia oxidation were also found in rocks, sediments and chimneys influenced by the hydrothermal activity at Tagoro, in addition to the archaea Nitrososphaeria. For instance, the order Nitrosococcales was identified in rocks and sediments, while Planctomycetales and Phycisphaerales were more abundant in chimney fragments. Notably, the genus *SM1A02*, a potential anammox bacterium of the order Phycisphaerales, was significantly associated with chimneys at the Tagoro hydrothermal field. Planctomycetes have previously been linked to iron hydroxide deposits at deep-sea vents in the southwestern Pacific, where *SM1A02* was also detected (Storesund et al., 2018). These findings provide

evidence of diverse ammonia oxidation processes at Tagoro, including aerobic ammonia oxidization by archaea (such as Nitrososphaeria) and bacteria (Nitrosococcales), as well as anaerobic ammonium oxidation by annamox bacteria (Planctomycetales and Phycisphaerales) in low-oxygen environments like hydrothermal vent chimneys.

Sediment samples were particularly characterized by strictly anaerobic sulfate-reducing bacteria, such as members of Thermodesulfovibrionia and Desulfobulbia commonly isolated from hot springs. Thermodesulfovibrionia was among the most abundant taxa in the sediments from Tagoro, with several ASVs identified as significant indicators of sediment habitats influenced by hydrothermal activity. This class mostly encompasses thermophilic sulfate reducers that also oxidize organic compounds or hydrogen, producing hydrogen sulfide (H_2S) as by-product (e.g., Henry et al., 1994; Haouari et al., 2008). Even though they remain uncultured, these bacteria have gained increasing interest not only in microbial ecology but also in biotechnology due to their role in sulfur cycling and their potential applications in bioenergy or bioremediation. Notably, our study highlights Thermodesulfovibrionia as an example of yet undescribed bacterial diversity in this shallow-water hydrothermal field. About 19 ASVs were classified within this class, but only one was identified beyond the class level as the genus *Thermodesulfovibrio*. Consistently, most strains within this genus have been isolated from hot springs in vent fluids, microbial mats and sediments (e.g., Henry et al., 1994; Sonne-Hansen and Ahring, 1999; Haouari et al., 2008; Sekiguchi et al., 2008). These findings indicate that active hydrothermal fluid entrainment, rich in sulfur compounds, may be prevalent in the benthic habitats of Tagoro and highlight the need for further research on sulfate availability on the area.

In addition to the sulfate-reducing bacteria detected in sediments, chimney samples also exhibited a notable presence of sulfur-oxidizing bacteria, like the gammaproteobacterial order Chromatiales (Imhoff, 2014). The genus *Candidatus* Thiobios, a chemolithoautotrophic sulfide-oxidizing ectosymbiont, was particularly abundant within this order. This genus is typically associated with *Zoothamnium niveum*, a sessile, giant, colonial marine ciliate from sulfide-rich habitats that is consistently covered with chemoautotrophic, sulfide-oxidizing bacteria (Rinke et al., 2006). These bacteria, including *Candidatus* Thiobios, are responsible for the brilliant white color of *Z. niveum*. These observations indicate that the potential sulfur-rich conditions across the Tagoro shallow-water hydrothermal ecosystem promote symbiotic

relationships between bacteria and eukaryotes. This finding underscores Tagoro as a hotspot for studying microbial symbiosis in sulfur-rich environments and its potential contribution to marine eukaryotic evolution.

Furthermore, aerobic methane-oxidizing bacteria commonly found at shallow submarine hot springs were also detected in sediments and chimney samples, especially members of Methylococcales (e.g., Hirayama et al., 2013). This is consistent with previous studies in Tagoro that identified methane-related microbes (methanogenic archaea, and methanotrophic archaea and bacteria) in mineralized samples (González et al., 2020), emphasizing the need for direct methane measurements in the area. The co-occurrence of sulfate-reducing bacteria and methane-related microbes in Tagoro suggests potential microbial mutualism, similar to the syntrophic relationships observed in seawater. For instance, certain species of *Thermodesulfovibrio* have been shown to degrade lactate in association with hydrogenotrophic methanogens in the absence of external electron acceptors (Sekiguchi et al., 2008). This further enhances the diverse and interconnections between microbial communities in hydrothermal environments.

The benthic habitats of Tagoro also harbor highly diverse microbial assemblages capable of expressing a wide variety of metabolic pathways. One such group is Anaerolineae bacteria, which can oxidize a broad range of carbon compounds, from simple sugars to complex organic molecules, and express both fermentation and carbon fixation pathways (Payne et al., 2024). Among Anaerolineae, the heterotrophic genus *Thermomarinilinea* was significantly associated with hydrothermally influenced sediments at Tagoro. The only cultured species within this genus was isolated from the Taketomi submarine hot spring field in Japan, where it relies on fermentation in anaerobic, high-temperature (37–65 ºC), low-pH (5.5–7.3) environments (Nunoura et al., 2013), similar to those conditions observed in Tagoro sediments.

Other abundant thermophilic, strictly anaerobic microbes involved in organic matter utilization, such as Thermoanaerobaculia, were also detected, especially in sediments and chimneys at Tagoro. Thermoanaerobaculia strains are typically found in hot springs and exhibit great metabolic flexibility, from carbohydrate fermentation to chemolithoautotrophy (Stackebrandt, 2014). In our study, *Subgroup 10* accounted for most of Thermoanaerobaculia abundance and was strongly linked to hydrothermal vent chimneys. This supports previous observations of their adaptation to the extreme temperature and chemical

conditions of vent chimneys, as the first cultivated representative of *Subgroup 10* was an obligate anaerobe, capable of fermentative growth on complex proteinaceous substances, isolated from a deep-sea hydrothermal vent chimney at the Hatoma Knoll in Japan (Izumi et al., 2012). In contrast, *Subgroup 23* was more notably associated with sediment samples, suggesting a preference for slightly cooler or less hydrothermally impacted environments compared to the active chimneys. However, environmental sequences of *Subgroup 23* have been found not only in marine sediments but also in hot spring microbial mats, and even freshwater hot springs, where the first cultivated member of this subgroup was isolated (Losey et al., 2013; Dedysh and Yilmaz, 2018).Altogether, these findings highlight the metabolic diversity of prokaryotic communities in the hydrothermal ecosystem of Tagoro, with specialized prokaryotes capable of utilizing inorganic and/or organic compounds in habitats influenced by hydrothermal activity alongside cosmopolitan taxa. Furthermore, the presence of different microbial groups across these habitats emphasizes the adaptability of these microbes to varying environmental conditions, making them key players in local biogeochemical processes.

4.4.3 Iron, nitrogen, sulfur and methane compounds as main sources of energy

Our study revealed a remarkable presence of prokaryotes associated with iron, nitrogen, sulfur and methane cycling across the Tagoro shallow-water hydrothermal field, expanding on the previous observations in the area (Danovaro et al., 2017; González et al., 2020).

Bacterial taxa involved in iron cycling were consistently identified at Tagoro, with a notable abundance of iron-oxidizing bacteria within the Zetaproteobacteria class. These chemolithoautotrophic bacteria were particularly dominant in hydrothermally influenced benthic habitats, consistent with their known ecological versality and widespread distribution in marine environments (McAllister et al., 2019). Zetaproteobacteria typically inhabit environments characterized by brackish to hypersaline water, abundant Fe^{2+} and predominantly micro-oxic conditions. Therefore, the periodic release of shallow-water vent fluids enriched in CO_2 and Fe^{2+} (Santana-Casiano et al., 2016) likely promotes the proliferation of iron microbial mats and the colonization of Fe-rich mineral deposits at Tagoro.

Given that these conditions are widespread and found globally in diverse habitats, it is thought that the diversification and evolution of Zetaproteobacteria must be prominent. However, Zetaproteobacteria remain largely uncultivated, with only a small fraction of environmental sequences represented by cultured isolates (McAllister et al., 2018). In our study, Zetaproteobacteria sequences were exclusively assigned to the genus *Mariprofundus* within to the family *Mariprofundaceae*. This group exhibited high ASV richness, with most ASVs closely related to cultured species such as *M. ferrinatatus*, *M. ferrooxydans*, *M. ferrooxydans* PV-1, *M. micogutta* and *M. aestuarium*. Only one ASV was classified at the species level as *M. micogutta*, a species originally isolated from deep-sea sediments in the hydrothermal field of Bayonnaise knoll in Japan (Makita et al., 2017). The high relative abundance of *M. micogutta* in Tagoro chimney fragments aligns with its known preference for microaerophilic, Fe^{2+}-rich environments at temperatures around 25 ºC and pH 6.4.

Nevertheless, three ASVs, consistently detected across all of our explored hydrothermal habitats, accounted for most of the relative abundance of *Mariprofundus* sequences. These ASVs were genetically similar to *M. ferrooxydans*, *M. ferrooxydans* PV-1, *M. micogutta* and *M. aestuarium*. *M. aestuarium* and *M. ferrinatatus* were first identified in redox-stratified waters of Chesapeake Bay, the largest estuary in the United States (Chiu et al., 2017). Chiu et al. (2017) reported that these species produce shorter filaments to avoid cell encrustation and, particularly CP strains, possess genes associated with biofilm formation, an adaptation that likely facilitates particle colonization to pelagic Zetaproteobacteria. This may explain why the most abundant *Mariprofundus* ASV identified in our study as a significant indicator taxon of microbial mats in Tagoro, is closely related to *M. ferrinatatus*. Such biofilm-forming traits could provide an advantage in benthic habitats of Tagoro, where notable rates of particle suspension and flux occur (Martín-Díaz et al., 2024).

Phylogenetic analyses also revealed a consistent presence of ammonia-oxidizing archaea in seawater samples collected both directly from hydrothermal vents and throughout the water column at Tagoro. The detection of Nitrososphaeria, particularly members of the family *Nitrosopumilaceae*, in both pelagic and benthic habitats supports the hypothesis that ammonium (NH_4^+) is the primary form of dissolved inorganic nitrogen released at Tagoro (González-Vega et al., 2020). However, this ammonium may be rapidly oxidized to nitrite

and nitrate by these archaea, explaining the enhanced concentrations of nitrate observed in the vicinity of Tagoro as compared to the surrounding waters.

Moreover, we observed habitat-specific patterns in the distribution of Nitrosopumilaceae genera across Tagoro. *Candidatus* Nitrosopumilus and *Cenarchaeum* were more prevalent in hydrothermally influenced benthic habitats, while *Candidatus* Nitrosopelagicus and unclassified *Nitrosopumilaceae* sequences were consistently observed in epipelagic waters unaffected by hydrothermal discharge. These distinctions likely reflect adaptations to local physiochemical conditions. For instance, *Ca.* Nitrosopelagicus is known to dominate ammonia oxidation in epipelagic and upper mesopelagic waters of low and mid-latitude open oceans, where it correlates with nitrification rates. Its low biomass nitrogen requirements, facilitated by a small genome and a higher molar growth efficiency, likely contributes to their ecological success in open oceans (Santoro et al., 2015). In contrast, *Ca.* Nitrosopumilus exhibits greater tolerance to elevated ammonium and nitrite concentrations, as well as higher temperatures and growth rates, factors that may provide a competitive advantage in the dynamic, warm, nutrient-rich benthic habitats near hydrothermal vents.

In addition to iron and nitrogen cycling, our data suggest a potential role for methane-based metabolisms within the Tagoro hydrothermal system, particularly in chimney and sediment habitats. Several taxa associated with methane and one-carbon compound metabolism were detected, highlighting the need for further research to confirm both the availability of biogenic and/or thermogenic methane in this environment. Aerobic methane-oxidizing bacteria from the family *Methylomonadaceae* were the only methanotrophs identified, with 5 genera detected, including *Methylomonas* and *Methylomarinum*, which have cultured representatives (e.g., Boden et al., 2011; Ogiso et al., 2012; Hirayama et al., 2013).

In our analysis, *Methylomarinum* was primarily detected in rock, sediment and hydrothermally influenced seawater samples, rather than in microbial mats where other methylotrophic taxa, such as *Marine Methylotrophic Group 2* and *pItb-vmat-59*, were observed. However, *Methylomarinum vadi*, the only described species within the genus, was firstly isolated from a microbial mat in a shallow hydrothermal system off Okinawa, Japan (Hirayama et al., 2013). These observations highlight the ecological diversity of methane-related microbes at Tagoro and other hydrothermal fields. In contrast, the uncultured clade *IheB2-23* was predominantly found in chimney samples, consistent with previous

reports of its presence in methane seeps and plumes off the coast of Taiwan, in the northern South China Sea (Mau et al., 2020). Nevertheless, the presence of methanotrophic taxa across multiple habitats at Tagoro, including low-oxygen sediments rich in organic matter, suggests that methane could be microbially consumed before being released into the water column, potentially contributing to greenhouse gas mitigation.

Additionally, the detection of methanogenic archaea such as *Methanosarcina* sp. and *Methanoccoides* sp. in bedrock samples from Tagoro (González et al., 2020) suggests a possible biogenic source of methane resulting from anaerobic microbial activity. This hypothesis aligns with our findings of abundant microbes capable of utilizing organic matter, indicating that sediments at Tagoro are rich in organic material and thus underscore the high biological productivity at the hydrothermal system (Pérez-Barrancos et al., 2025). Sulfur-cycling microbes, including sulfate-reducing and sulfur-oxidizing bacteria, were also detected in our study, and some likely rely on organic matter degradation and/or syntrophic associations (discussed in **Section 4.4.2**). Still, further studies are needed to clarify the presence, origin and metabolic fate of such compounds in the area.

The geochemistry of shallow-water hydrothermal systems therefore supports diverse microbial taxa with distinct metabolic strategies (Price and Giovannelli, 2017), as demonstrated in our study. In contrast to deep-sea vents, which predominantly rely on chemosynthesis, shallow-water vents also exhibit phototrophic primary production. Recent studies indicate that chemoautotrophy plays a significant role in primary production within hydrothermally influenced coastal environments (Gomez-Saez et al., 2017). The contribution of chemosynthesis to total primary production at shallow-water vents has been reported to range from 1% to 50% (Tarasov et al., 1999), with experimental assessments suggesting even higher contributions (Gomez-Saez et al., 2017). These findings highlight the potential importance of vent microorganisms in producing significant amounts of newly synthesized organic matter, using the energy derived from the oxidation of chemical compounds such as H_2S, CH_4, or Fe^{2+}. Similar to their deep-sea counterparts, these organic compounds may sustain higher trophic levels (Dick, 2019). Given its potential impact on primary production, further research on chemosynthesis in shallow-water hydrothermal environments is essential to better constrain its ecological implications.

4.4.4 Bacterial biomineralization

The identification of diverse biogenic structures, including twisted stalks and globular precipitates, in a chimney fragment collected in 2017 provides direct evidence of ongoing microbial Fe biomineralization in the active hydrothermal field of Tagoro. Twisted stalks are a characteristic vestige of *Mariprofundus ferrooxydans* (Emerson et al., 2007; Singer et al., 2013; McAllister et al., 2019), a Zetaproteobacterium that regulates Fe mineral growth near the cell surface while preventing encrustation (Chan et al., 2011). These structures also anchor cells to surfaces, promoting bacterial motility within Fe^{2+} and O_2 gradients (Krepski et al., 2013), which may facilitate their proliferation in hydrothermal environments. Sheaths, another biomineralization structure, have also been linked to Zetaproteobacteria members and may function similarly to stalks (Fleming et al., 2013; Chan et al., 2016).

Our microbial analyses consistently identified Zetaproteobacteria as one of the most abundant taxa in microbial mat, rock and sediment samples from active hydrothermal areas over 5 years (2017–2022) (see **Section 4.4.2**). These findings suggest that Zetaproteobacteria play a key role in driving Fe-oxyhydroxide precipitation within this shallow-water hydrothermal system. This contrasts with a 2014 survey, which reported a low relative abundance of Zetaproteobacteria alongside a high prevalence of twisted stalks and empty sheaths in mineralized samples from the summit and secondary vents of Tagoro (González et al., 2020). González et al. (2020) suggested that biogenic Fe oxidation may have occurred during past hydrothermal events and that hydrothermal fluid emissions through the sediments had ceased at the analyzed locations. However, evidence of ongoing deposition of Fe-rich precipitates on oceanographic instruments deployed at the site and the substantial abundance of DNA from iron-oxidizing microbes indicates that hydrothermal iron emissions are still taking place. Microbial activity likely contributes to the extensive Fe-rich deposits in the Tagoro hydrothermal field, consistent with observations from diffuse low-temperature hydrothermal vents worldwide (e.g., Johannessen et al., 2017).

4.5 Conclusions

Our study demonstrates that hydrothermal venting at the Tagoro submarine volcano significantly shapes the microbial diversity and functional potential of both epipelagic and benthic prokaryotic communities. Prokaryotic richness and diversity consistently decreased with proximity to hydrothermal vent sources. Meanwhile, novel taxa were prevalent across all hydrothermally influenced habitats, unveiling an extensive, unexplored microbial diversity in the vicinity of this shallow submarine hydrothermal system. Closest GenBank relatives matched at taxonomic levels from order to genus, highlighting the vast unknown microbial diversity and the strong potential for discovering new metabolic capabilities in these unique hydrothermal areas. In hydrothermally enriched epipelagic seawater, Alpha- and Gammaproteobacteria were dominant, with several groups with potential biotechnological applications identified for the first time in the area. Both pelagic and benthic compartments harbored photoautotrophic and chemoautotrophic populations, confirming our previous finding that sufficient light reaches all the way down to the surface of the main crater. Microbial mats were notably characterized by iron-oxidizing Zetaproteobacteria, which directly contribute to Fe-oxyhydroxide precipitation. In benthic habitats (including volcanic rocks, sediments and vent chimneys), nitrogen- and sulfur-cycling microbes, such as the ammonia-oxidizing archaea Nitrososphaeria, were particularly abundant. This confirms previous hypotheses suggesting that nitrogen at Tagoro is emitted as hydrothermal ammonium and is rapidly oxidized to nitrite and nitrate by microbes, explaining the high nitrate concentrations reported in the area. Sediments were also enriched with bacteria involved in organic matter utilization, indicating high organic availability and supporting earlier observations of increased productivity in the Tagoro marine ecosystem. Together, these findings emphasize the key role of prokaryotic communities in local biogeochemical processes at this unique environment and provide preliminary evidence of the importance of yet unexplored carbon and energy sources in the area, such as methane. Complex microbial interactions were also observed, including potential syntropic relationships between microbial groups and symbiotic associations with microfauna in benthic environments. The Tagoro submarine volcano thus stands as a valuable natural laboratory for studying microbial diversity, biogeochemical cycling and intricate microbial relationships in underexplored shallow-water hydrothermal systems.

Supplementary material

Supplementary figures

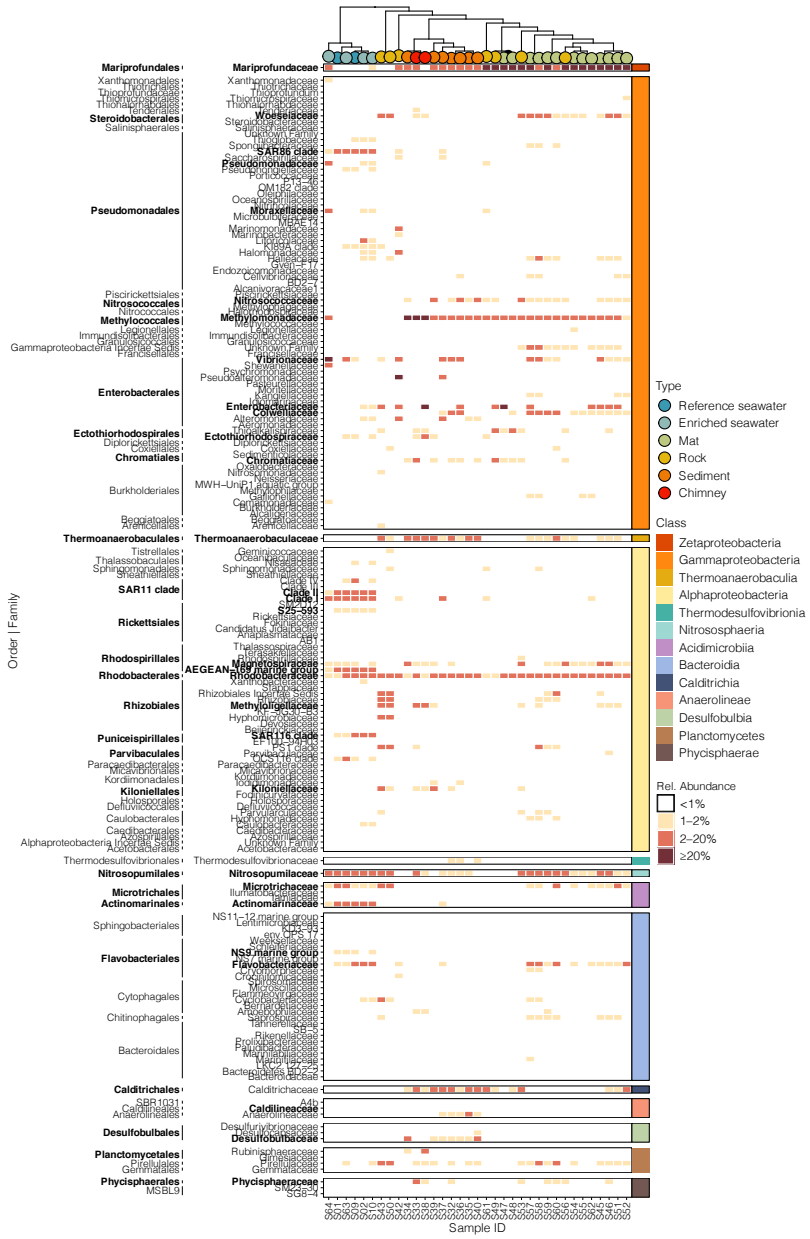

Figure S1. Hierarchical clustering of prokaryotic communities based on Bray-Curtis dissimilarities and heatmap of relative abundance of family-classified prokaryotes belonging to classes with median relative abundance ≥2%. Color points on the dendrogram represent habitats, while black points indicate clusters with approximately unbiased (au) values below 75%. Prokaryotic classes are arranged in decreasing order of median relative abundance across habitats. Bold labels indicate orders and families with at least median relative abundance ≥1% in some habitat.

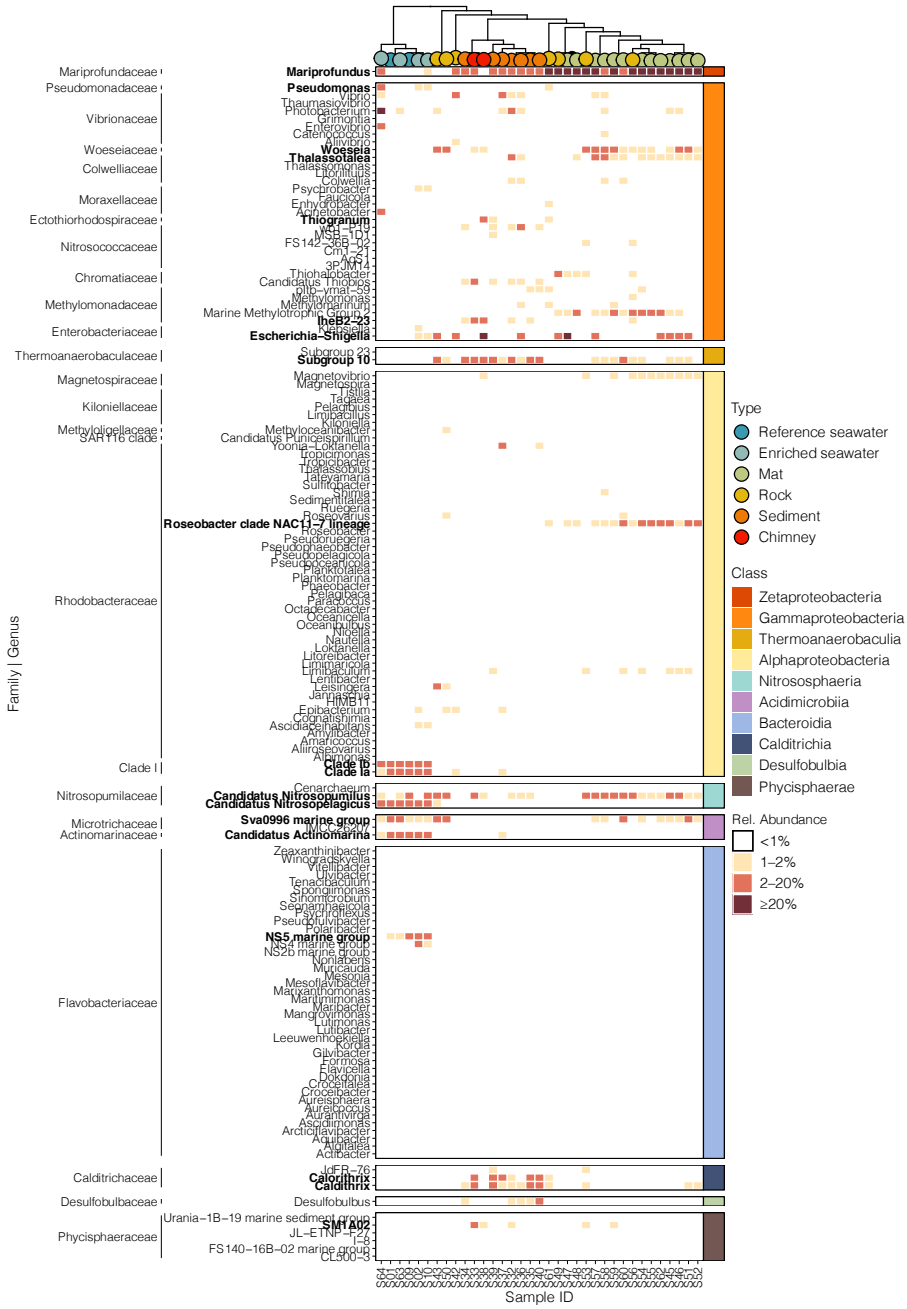

Figure S2. Hierarchical clustering of prokaryotic communities based on Bray-Curtis dissimilarities and heatmap of relative abundance of genus-classified prokaryotes belonging to classes and families with median relative abundance >2% and >1%, respectively. Color points on the dendrogram represent habitats, while black points indicate clusters with approximately unbiased (au) values below 75%. Prokaryotic classes are arranged in decreasing order of median relative abundance across habitats. Bold labels indicate prokaryotic genus with median relative median relative abundance ≥1%.

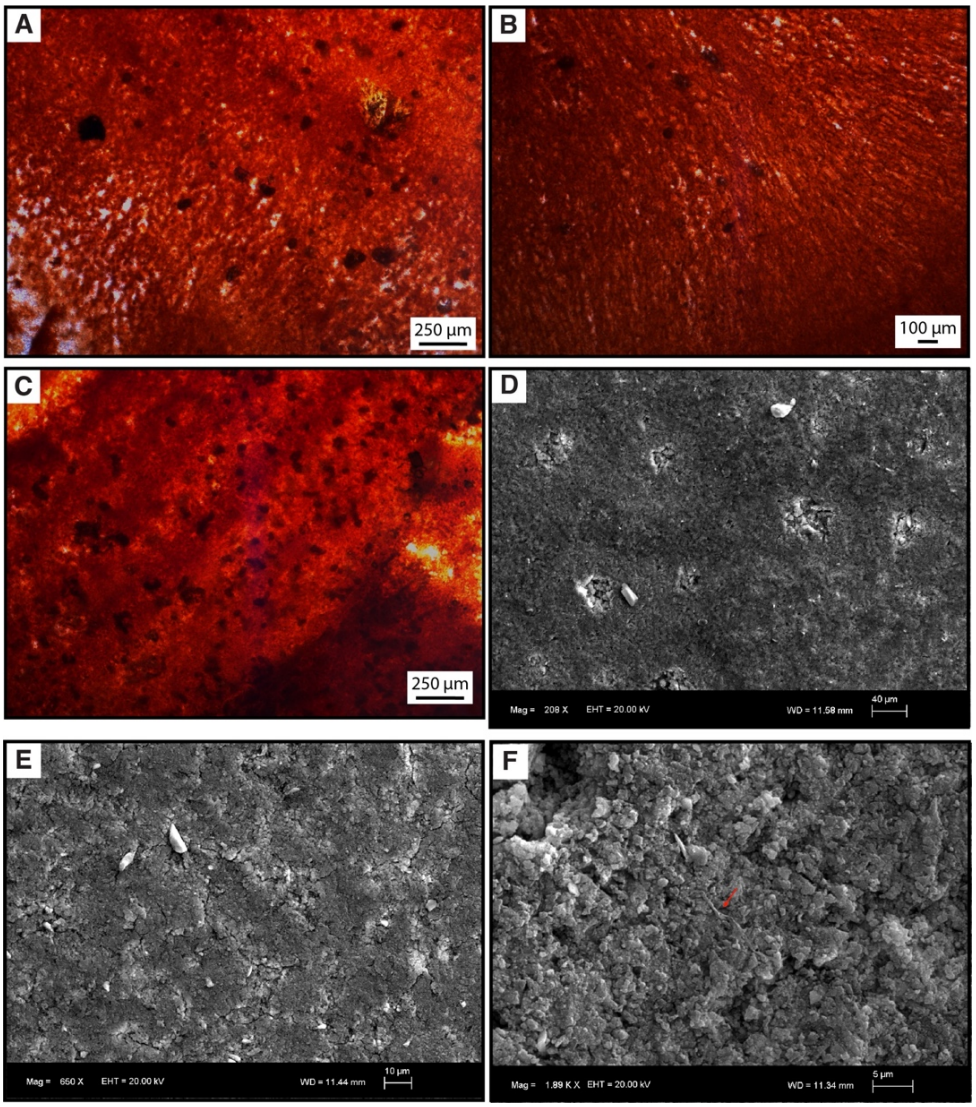

Figure S3. Optical images (10x) of a thin section from a chimney fragment showing **(A, B)** dendritic features and **(C)** dome-shaped, Fe-rich bands. **(D, E, F)** SEM images of dendritic areas at higher magnification evidencing complex textures embedded in the Si-Fe chimney. The red arrow indicates an example of a filament with twisted morphology.

Figure S4. SEM image showing the locations of Spectrum 2 (twisted filament) and Spectrum 3 (chimney surface) used for chemical composition analyses (see **Table S5**).

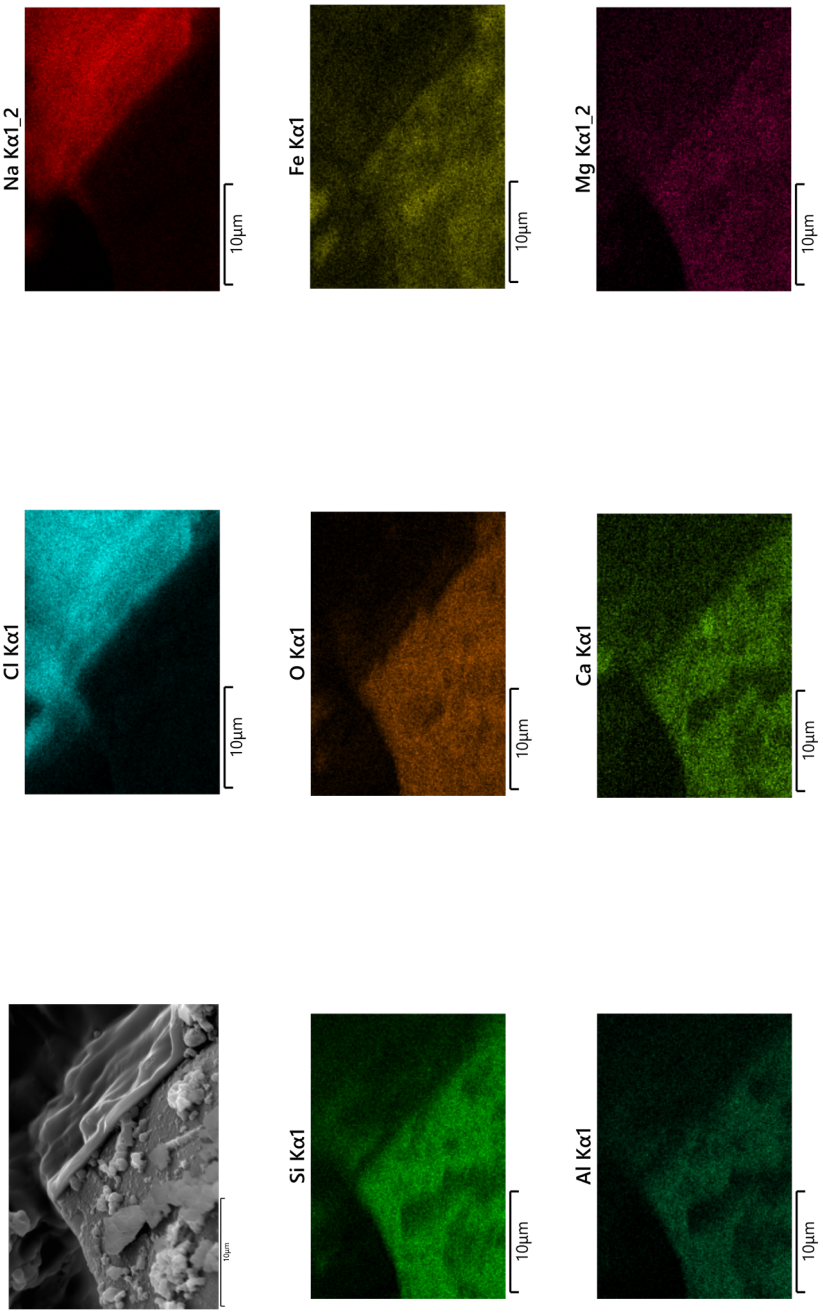

Figure S5. SEM image and elemental mapping of a region exhibiting salt precipitation in a chimney fragment.

Supplementary Tables

Table S1. Sample properties. Asterisk * indicates the chimney sample used for microscope-imagery and microanalyses.

Cruise date	Dive or Station	Sample ID	Latitude (°N)	Longitude (°W)	Depth (m)	Vehicle	Instrument	Type
Apr-17	2	S42	27.619743	-17.992898	122	ROV	Arm	Rock
Apr-17	4	S33	27.619712	-17.992930	122	ROV	Drag mesh	Chimney
Apr-17	4	S32	27.619778	-17.992903	122	ROV	Drag mesh	Sediment
Apr-17	4	S36	27.619778	-17.992903	122	ROV	Drag mesh	Sediment
Apr-17	4	S34	27.619770	-17.992908	122	ROV	Suction	Sediment
Apr-17	5	S38	27.619802	-17.992915	128	ROV	Drag mesh	Chimney
Apr-17	5	S41*	27.619802	-17.992915	128	ROV	Drag mesh	Chimney
Apr-17	5	S35	27.619802	-17.992915	128	ROV	Drag mesh	Sediment
Apr-17	5	S40	27.619802	-17.992915	128	ROV	Drag mesh	Sediment
Apr-17	5	S37	27.619330	-17.993150	128	ROV	Suction	Sediment
Apr-17	6	S39	27.619732	-17.992985	115	ROV	Arm	Sediment
Nov-18	18	S43	27.619900	-17.992917	124	ROV	Arm	Rock
Nov-18	18	S44	27.619900	-17.992917	124	ROV	Arm	Rock
Nov-18	18	S50	27.619900	-17.992917	124	ROV	Arm	Rock

Table S1. Continued.

Cruise date	Dive or Station	Sample ID	Latitude (°N)	Longitude (°W)	Depth (m)	Vehicle	Instrument	Type
Nov-19	31	S02	27.619780	-17.993000	127	Rosette	Niskin	Seawater
Nov-19	901	S01	27.650020	-17.909800	127	Rosette	Niskin	Seawater
Apr-21	31	S10	27.619780	-17.993000	129	Rosette	Niskin	Seawater
Apr-21	901	S09	27.650020	-17.909800	127	Rosette	Niskin	Seawater
Oct-21	61	S63	27.619710	-17.992880	129	Rosette	Niskin	Seawater
Oct-21	3	S64	27.619720	-17.992850	122	ROV	Syringe	Seawater
Feb-22	2	S45	27.619753	-17.992893	122	ROV	Syringe	Mat
Feb-22	2	S46	27.619753	-17.992893	122	ROV	Syringe	Mat
Feb-22	4	S47	27.619655	-17.993055	122	ROV	Syringe	Mat
Feb-22	4	S48	27.619655	-17.993055	122	ROV	Syringe	Mat
Feb-22	4	S49	27.619655	-17.993055	122	ROV	Arm	Rock
Feb-22	5	S51	27.620020	-17.993096	112	ROV	Syringe	Mat
Feb-22	5	S52	27.620020	-17.993096	112	ROV	Syringe	Mat
Feb-22	5	S53	27.620020	-17.993096	112	ROV	Arm	Rock
Feb-22	7	S54	27.619625	-17.993181	115	ROV	Syringe	Mat

Table S1. Continued.

Cruise date	Dive or Station	Sample ID	Latitude (ºN)	Longitude (ºW)	Depth (m)	Vehicle	Instrument	Type
Feb-22	7	S55	27.619625	-17.993181	115	ROV	Syringe	Mat
Feb-22	7	S62	27.619625	-17.993181	115	ROV	Syringe	Mat
Feb-22	7	S56	27.619625	-17.993181	115	ROV	Arm	Rock
Feb-22	8	S57	27.619526	-17.993141	115	ROV	Syringe	Mat
Feb-22	8	S58	27.619526	-17.993141	115	ROV	Syringe	Mat
Feb-22	9	S59	27.619576	-17.993154	116	ROV	Syringe	Mat
Feb-22	9	S60	27.619576	-17.993154	116	ROV	Syringe	Mat

Table S2. Silva sequences added to their respective family dataset to serve as references. Each set of reference sequences was extracted from the Silva v138.1 database.

Root/Family	ID* in Fig.4	Silva ID
Archaea	Root	Archaea;Halobacterota;Halobacteria;Halobacterales; Halomicrobiaceae;Haloarcula;
Bacteria	Root	AB001445.1.1538 *Pseudomonas amygdali pv. morsprunorum*
Mariprofundaceae	1	CP018800.1916659.1918196 *Mariprofundus ferrinatatus*
	2	EF493244.1.1528 *Mariprofundus ferrooxydans*
	3	AATS01000005.157233.158763 *Mariprofundus ferrooxydans* PV-1
	4	LC107871.1.1500 *Mariprofundus micogutta*
	5	CP018799.352707.354246 *Mariprofundus aestuarium*
Methylomonadaceae	6	AF304196.1.1499 *Methylomonas methanica*
	7	CP014476.2704053.2705588 *Methylomonas denitrificans*
	8	AB538964.1.1458 *Methylomonas koyamae*
	9	CP002738.850441.851961 *Methylomonas methanica* MC09
	10	AB301717.1.1464 *Methylomarinum vadi*
	11	AF304194.1.1498 *Methylomonas rubra*
Nitrosopumilaceae	22	*Nitrosopumilus piranensis*
	23	*Nitrosopumilus adriaticus*
	24	*Nitrosopumilus maritimus*
	25	*Nitrosopumilus koreensis*
	26	*Nitrosopumilus sediminis*
	27	*Cenarchaeum symbiosum*
	28	*Nitrosopelagicus brevis*

Table S3. Indicator species showing robust statistics (Indicator Species test, *stat* ≥ 0.75 and $p \leq 0.001$) for each habitat. The dash symbol (–) indicates unclassified taxa. Results are ordered by decreasing *stat* and Phylum.

ASV	*stat*	Phylum	Class	Order	Family	Genus
Reference seawater						
ASV_4023	0.92	Proteobacteria	Alphaproteobacteria	Rhodospirillales	*Rhodospirillaceae*	–
Enriched seawater						
ASV_4284	1.00	Bdellovibrionota	Oligoflexia	Oligoflexales	*Oligoflexaceae*	–
ASV_5728	1.00	Bdellovibrionota	Oligoflexia	Oligoflexales	*Oligoflexaceae*	–
ASV_5910	1.00	Bacteroidota	Bacteroidia	Flavobacteriales	*NS7 marine group*	–
ASV_5999	1.00	Proteobacteria	Alphaproteobacteria	Parvibaculales	*OCS116 clade*	–
ASV_6000	1.00	Margulisbacteria	–	–	–	–
ASV_6420	1.00	Acidobacteriota	Vicinamibacteria	Vicinamibacterales	–	–
ASV_3652	0.82	Desulfobacterota	Desulfobacteria	Desulfobacterales	*Desulfosarcinaceae*	*SEEP-SRB1*
Microbial mat						
ASV_369	0.98	Bacteroidota	Bacteroidia	Bacteroidales	–	–
ASV_439	0.97	Bacteroidota	Bacteroidia	Chitinophagales	*Saprospiraceae*	*Aureispira*
ASV_574	0.95	Bacteroidota	Bacteroidia	Flavobacteriales	*Cryomorphaceae*	–
ASV_238	0.94	Bacteroidota	Bacteroidia	Bacteroidales	–	–

Table S3. Continued.

ASV	*stat*	Phylum	Class	Order	Family	Genus
ASV_64	0.93	Bacteroidota	Bacteroidia	Flavobacteriales	*Flavobacteriaceae*	–
ASV_707	0.89	Bacteroidota	Bacteroidia	Flavobacteriales	*Flavobacteriaceae*	–
ASV_968	0.88	Bacteroidota	Bacteroidia	Chitinophagales	*Saprospiraceae*	*Portibacter*
ASV_716	0.88	Bacteroidota	Bacteroidia	Flavobacteriales	–	–
ASV_321	0.85	Bacteroidota	Bacteroidia	Chitinophagales	*Saprospiraceae*	*Phaeodactylibacter*
ASV_451	0.84	Bacteroidota	Ignavibacteria	Ignavibacteriales	*Melioribacteraceae*	*IheB3-7*
ASV_1334	0.84	Bacteroidota	Bacteroidia	Flavobacteriales	*Crocinitomicaceae*	*Crocinitomix*
ASV_81	0.82	Bacteroidota	Rhodothermia	Rhodothermales	*Rhodothermaceae*	–
ASV_1267	0.78	Bacteroidota	Bacteroidia	Bacteroidales	*Marinifilaceae*	–
ASV_45	0.98	Firmicutes	Clostridia	Peptostreptococcales-Tissierellales	*Fusibacteraceae*	*Fusibacter*
ASV_434	0.96	Bdellovibrionota	Oligoflexia	053A03-B-DI-P58	–	–
ASV_810	0.95	Bdellovibrionota	Bdellovibrionia	Bdellovibrionales	*Bdellovibrionaceae*	*OM27 clade*
ASV_252	0.94	Bdellovibrionota	Bdellovibrionia	Bacteriovoracales	*Bacteriovoracaceae*	–
ASV_90	0.94	Bdellovibrionota	Bdellovibrionia	Bacteriovoracales	*Bacteriovoracaceae*	*Peredibacter*
ASV_616	0.94	Bdellovibrionota	Bdellovibrionia	Bacteriovoracales	*Bacteriovoracaceae*	*Peredibacter*
ASV_689	0.94	Bdellovibrionota	Bdellovibrionia	Bdellovibrionales	*Bdellovibrionaceae*	*OM27 clade*

Table S3. Continued.

ASV	*stat*	Phylum	Class	Order	Family	Genus
ASV_519	0.93	Bdellovibrionota	Bdellovibrionia	Bdellovibrionales	*Bdellovibrionaceae*	*OM27 clade*
ASV_246	0.92	Bdellovibrionota	Bdellovibrionia	Bdellovibrionales	*Bdellovibrionaceae*	*OM27 clade*
ASV_386	0.91	Bdellovibrionota	Bdellovibrionia	Bacteriovoracales	*Bacteriovoracaceae*	–
ASV_701	0.87	Bdellovibrionota	Bdellovibrionia	Bdellovibrionales	*Bdellovibrionaceae*	*OM27 clade*
ASV_1189	0.78	Bdellovibrionota	Bdellovibrionia	Bacteriovoracales	*Bacteriovoracaceae*	–
ASV_879	0.96	Proteobacteria	Gammaproteobacteria	Pseudomonadales	*Halieaceae*	*Halioglobus*
ASV_23	0.95	Proteobacteria	Alphaproteobacteria	Rhodobacterales	*Rhodobacteraceae*	–
ASV_102	0.95	Proteobacteria	Zetaproteobacteria	Mariprofundales	*Mariprofundaceae*	*Mariprofundus*
ASV_385	0.95	Proteobacteria	Zetaproteobacteria	Mariprofundales	*Mariprofundaceae*	*Mariprofundus*
ASV_61	0.94	Proteobacteria	Gammaproteobacteria	–	–	–
ASV_509	0.94	Proteobacteria	Alphaproteobacteria	Rhodobacterales	*Rhodobacteraceae*	–
ASV_194	0.93	Proteobacteria	Alphaproteobacteria	Rhodobacterales	*Rhodobacteraceae*	*Roseobacter* clade NAC11-7
ASV_28	0.93	Proteobacteria	Alphaproteobacteria	Rhodobacterales	*Rhodobacteraceae*	–
ASV_178	0.93	Proteobacteria	Gammaproteobacteria	Gammaproteobacteria Incertae Sedis	–	–
ASV_135	0.92	Proteobacteria	Zetaproteobacteria	Mariprofundales	*Mariprofundaceae*	*Mariprofundus*
ASV_947	0.91	Proteobacteria	Gammaproteobacteria	Pseudomonadales	*Halieaceae*	–

Table S3. Continued.

ASV	*stat*	Phylum	Class	Order	Family	Genus
ASV_241	0.91	Proteobacteria	Gammaproteobacteria	Gammaproteobacteria Incertae Sedis	–	*Marinicella*
ASV_82	0.91	Proteobacteria	Gammaproteobacteria	Enterobacterales	*Kangiellaceae*	*Aliikangiella*
ASV_254	0.91	Proteobacteria	Gammaproteobacteria	Pseudomonadales	*Oleiphilaceae*	*Oleiphilus*
ASV_619	0.91	Proteobacteria	Alphaproteobacteria	Rhodobacterales	*Rhodobacteraceae*	*Octadecabacter*
ASV_32	0.91	Proteobacteria	Zetaproteobacteria	Mariprofundales	*Mariprofundaceae*	*Mariprofundus*
ASV_1142	0.90	Proteobacteria	Gammaproteobacteria	Pseudomonadales	*Halieaceae*	*Haliea*
ASV_250	0.90	Proteobacteria	Gammaproteobacteria	eub62A3	–	–
ASV_17	0.90	Proteobacteria	Alphaproteobacteria	Rhodobacterales	*Rhodobacteraceae*	*Roseobacter* clade NAC11-7
ASV_175	0.89	Proteobacteria	Gammaproteobacteria	Thiomicrospirales	*Thiomicrospiraceae*	*endosymbionts*
ASV_670	0.89	Proteobacteria	Gammaproteobacteria	Pseudomonadales	*Spongiibacteraceae*	*BD1-7 clade*
ASV_288	0.89	Proteobacteria	Alphaproteobacteria	Rhodobacterales	*Rhodobacteraceae*	*Shimia*
ASV_94	0.89	Proteobacteria	Zetaproteobacteria	Mariprofundales	*Mariprofundaceae*	*Mariprofundus*
ASV_53	0.89	Proteobacteria	Zetaproteobacteria	Mariprofundales	*Mariprofundaceae*	*Mariprofundus*
ASV_928	0.88	Proteobacteria	Alphaproteobacteria	Rhodobacterales	*Rhodobacteraceae*	*Yoonia-Loktanella*
ASV_40	0.88	Proteobacteria	Zetaproteobacteria	Mariprofundales	*Mariprofundaceae*	*Mariprofundus*
ASV_420	0.88	Proteobacteria	Gammaproteobacteria	Enterobacterales	*Kangiellaceae*	*Aliikangiella*

Table S3. Continued.

ASV	*stat*	Phylum	Class	Order	Family	Genus
ASV_251	0.88	Proteobacteria	Alphaproteobacteria	Rhodobacterales	*Rhodobacteraceae*	–
ASV_173	0.88	Proteobacteria	Gammaproteobacteria	Burkholderiales	*Gallionellaceae*	*Candidatus* Nitrotoga
ASV_22	0.88	Proteobacteria	Zetaproteobacteria	Mariprofundales	*Mariprofundaceae*	*Mariprofundus*
ASV_10	0.87	Proteobacteria	Zetaproteobacteria	Mariprofundales	*Mariprofundaceae*	*Mariprofundus*
ASV_76	0.87	Proteobacteria	Zetaproteobacteria	Mariprofundales	*Mariprofundaceae*	*Mariprofundus*
ASV_950	0.86	Proteobacteria	Gammaproteobacteria	–	–	–
ASV_860	0.86	Proteobacteria	Zetaproteobacteria	Mariprofundales	*Mariprofundaceae*	*Mariprofundus*
ASV_311	0.86	Proteobacteria	Gammaproteobacteria	Pseudomonadales	*Halieaceae*	*OM60(NOR5) clade*
ASV_1295	0.86	Proteobacteria	Gammaproteobacteria	Pseudomonadales	*Halieaceae*	*Parahaliea*
ASV_2	0.86	Proteobacteria	Zetaproteobacteria	Mariprofundales	*Mariprofundaceae*	*Mariprofundus*
ASV_1006	0.86	Proteobacteria	Alphaproteobacteria	Rhodospirillales	*Terasakiellaceae*	–
ASV_1364	0.85	Proteobacteria	Zetaproteobacteria	Mariprofundales	*Mariprofundaceae*	*Mariprofundus*
ASV_724	0.85	Proteobacteria	Alphaproteobacteria	Rickettsiales	*Rickettsiaceae*	–
ASV_103	0.85	Proteobacteria	Gammaproteobacteria	Enterobacterales	*Colwelliaceae*	*Thalassotalea*
ASV_312	0.84	Proteobacteria	Alphaproteobacteria	Rhodobacterales	*Rhodobacteraceae*	*Limibaculum*
ASV_47	0.84	Proteobacteria	Zetaproteobacteria	Mariprofundales	*Mariprofundaceae*	*Mariprofundus*

Table S3. Continued.

ASV	*stat*	Phylum	Class	Order	Family	Genus
ASV_316	0.82	Proteobacteria	Alphaproteobacteria	Sphingomonadales	*Sphingomonadaceae*	*Erythrobacter*
ASV_1797	0.81	Proteobacteria	Alphaproteobacteria	Rickettsiales	*Candidatus* Jidaibacter	–
ASV_27	0.79	Proteobacteria	Gammaproteobacteria	Enterobacterales	*Colwelliaceae*	*Thalassotalea*
ASV_412	0.77	Proteobacteria	–	–	–	–
ASV_542	0.77	Proteobacteria	Alphaproteobacteria	Rhodospirillales	*Magnetospiraceae*	*Magnetovibrio*
ASV_487	0.95	Chloroflexi	Anaerolineae	Anaerolineales	*Anaerolineaceae*	*Thermomarinilinea*
ASV_657	0.95	Patescibacteria	Gracilibacteria	JGI 0000069-P22	–	–
ASV_540	0.93	Patescibacteria	Gracilibacteria	JGI 0000069-P22	–	–
ASV_156	0.90	Patescibacteria	Gracilibacteria	JGI 0000069-P22	–	–
ASV_802	0.88	Patescibacteria	Gracilibacteria	JGI 0000069-P22	–	–
ASV_1868	0.86	Patescibacteria	Gracilibacteria	JGI 0000069-P22	–	–
ASV_1742	0.86	Patescibacteria	ABY1	*Candidatus* Kerfeldbacteria	–	–
ASV_359	0.94	Planctomycetota	OM190	–	–	–
ASV_416	0.83	Planctomycetota	Planctomycetes	Pirellulales	*Pirellulaceae*	–
ASV_758	0.91	Nanoarchaeota	Nanoarchaeia	Woesearchaeales	*SCGC AAA286-E23*	–
ASV_1104	0.90	Spirochaetota	Leptospirae	Leptospirales	*Leptospiraceae*	*Turneriella*

Table S3. Continued.

ASV	*stat*	Phylum	Class	Order	Family	Genus
ASV_1890	0.90	Desulfobacterota	Desulfobacteria	Desulfobacterales	*Desulfobacteraceae*	*Desulfoconvexum*
ASV_555	0.90	Desulfobacterota	Desulfuromonadia	PB19	–	–
ASV_442	0.89	Myxococcota	Polyangia	Polyangiales	*Sandaracinaceae*	*Sandaracinus*
ASV_525	0.87	Myxococcota	Myxococcia	Myxococcales	*Myxococcaceae*	*P3OB-42*
ASV_33	0.84	Actinobacteriota	Acidimicrobiia	Microtrichales	*Microtrichaceae*	*Sva0996 marine group*
ASV_1429	0.79	Latescibacterota	–	–	–	–
ASV_645	0.79	SAR324 clade (Marine group B)	–	–	–	–
ASV_41	0.77	Campylobacterota	Campylobacteria	Campylobacterales	*Sulfurospirillaceae*	*Sulfurospirillum*
Sediment						
ASV_206	1.00	Desulfobacterota	Desulfobulbia	Desulfobulbales	*Desulfobulbaceae*	*Desulfobulbus*
ASV_297	0.98	Desulfobacterota	Desulfobulbia	Desulfobulbales	*Desulfobulbaceae*	–
ASV_286	0.95	Desulfobacterota	Desulfobulbia	Desulfobulbales	*Desulfobulbaceae*	–
ASV_248	0.93	Desulfobacterota	Desulfobulbia	Desulfobulbales	*Desulfobulbaceae*	*Desulfobulbus*
ASV_151	0.90	Desulfobacterota	Desulfobulbia	Desulfobulbales	–	–
ASV_722	0.99	SAR324 clade (Marine group B)	–	–	–	–

Table S3. Continued.

ASV	*stat*	Phylum	Class	Order	Family	Genus
ASV_7	0.98	Nitrospirota	Thermodesulfovibrionia	–	–	–
ASV_6	0.90	Nitrospirota	Thermodesulfovibrionia	–	–	–
ASV_170	0.96	Nitrospirota	Thermodesulfovibrionia	Thermodesulfovibrionales	*Thermodesulfovibrionaceae*	*Thermodesulfovibrio*
ASV_70	0.98	Actinobacteriota	Thermoleophilia	Gaiellales	–	–
ASV_518	0.97	Chloroflexi	Anaerolineae	Anaerolineales	*Anaerolineaceae*	*Thermomarinilinea*
ASV_527	0.97	Chloroflexi	Anaerolineae	Ardenticatenales	–	–
ASV_391	0.95	Myxococcota	–	–	–	–
ASV_259	0.95	Proteobacteria	Gammaproteobacteria	Methylococcales	*Methylomonadaceae*	*Methylomarinum*
ASV_1010	0.93	Acidobacteriota	Thermoanaerobaculia	Thermoanaerobaculales	*Thermoanaerobaculaceae*	*Subgroup 23*
ASV_69	0.85	Acidobacteriota	Subgroup 22	–	–	–
Chimney						
ASV_1235	0.95	Proteobacteria	Alphaproteobacteria	Rhodobacterales	*Rhodobacteraceae*	–
ASV_148	0.90	Proteobacteria	Alphaproteobacteria	–	–	–
ASV_1621	0.94	Myxococcota	Polyangia	UASB-TL25	–	–
ASV_888	0.88	Planctomycetota	Phycisphaerae	Phycisphaerales	*Phycisphaeraceae*	*SM1A02*
ASV_363	0.85	SAR324 clade (Marine group B)	–	–	–	–

Table S4. Direct BLAST results of unassigned Thermodesulfovibrionia sequences from the rarefied dataset against the NCBI Nucleotide collection (nr/nt) and NCBI 16S ribosomal RNA sequences (Bacteria and Archaea) databases. The parameter E-value indicates the statistical significance of the sequence match (with lower values suggesting more significant matches), while Max Ident (Maximum Identity) measures the similarity between our sequence and the best-matching sequence in the database (with higher values ≥ 97% indicating close relatedness, and lower values < 90% suggesting more distant or novel relationships).

ASV	NCBI Nucleotide Collection				NCBI 16S Ribosomal RNA Sequences		
	GenBank ID	E-value	Max Ident	Isolation Source (Location)	GenBank ID	E-value	Max Ident
ASV_6	EU181863.1	1e-113	97%	Seawater and sediment (South China Sea)	NR_181964.1	2e-64	85%
ASV_7	MG638459.1	6e-122	99%	Sediment (Aarhus Bay Site M5, Denmark)	NR_040795.1	1e-76	87%
ASV_92	KX100095.1	6e-122	99%	Sediment (Cochin transect, Arabian Sea)	NR_118216.1	8e-73	87%
ASV_308	KU370774.1	1e-119	98%	Soil (Qinghai Lake, China)	NR_181964.1	2e-69	86%
ASV_609	FJ351343.1	6e-122	99%	Sediment (Lake Pontchartrain, USA)	NR_181964.1	8e-58	83%
ASV_624	MT175495.1	4e-123	99%	Seawater (Bedford Basin, Nova Scotia, Atlantic coast)	NR_118216.1	8e-68	86%
ASV_949	KP292505.1	3e-125	100%	Sediment (Jiaojiang Estuary, China)	NR_118216.1	2e-69	86%
ASV_1020	MF364253.1	3e-125	100%	Wastewater and groundwater (Mexico)	NR_118216.1	2e-64	85%
ASV_1075	KY518677.1	3e-120	98%	Lake water (Ontario, Canada)	NR_044075.1	5e-75	87%

Table S4. Continued.

ASV	NCBI Nucleotide Collection				NCBI 16S Ribosomal RNA Sequences		
	GenBank ID	E-value	Max Ident	Isolation Source (Location)	GenBank ID	E-value	Max Ident
ASV_1217	KX100095.1	3e-120	98%	Sediment (Cochin transect, Arabian Sea)	NR_118216.1	4e-71	86%
ASV_1948	EU181863.1	1e-108	96%	Seawater and sediment (South China Sea)	NR_181964.1	2e-64	85%
ASV_2880	OW752444.1	4e-123	99%	Desert soil (Taklimakan Desert, China)	NR_181964.1	8e-68	86%
ASV_4935	KT018547.1	1e-123	99%	Heavy metal contaminated soil (China)	NR_118216.1	8e-63	84%
ASV_6052	KC631532.1	3e-125	98%	Sediment (Finfish aquaculture farm, southern coast of Korea)	NR_040795.1	5e-80	87%
ASV_6243	EU181863.1	6e-117	97%	Seawater and sediment (South China Sea)	NR_118216.1	1e-66	84%
ASV_6845	JN884987.1	1e-123	99%	Sediment (Deep-sea methane seeps at Hikurangi continental margin, New Zealand)	NR_134169.1	2e-64	85%
ASV_7218	KC925127.1	3e-115	97%	Sediment (Jiulongjiang and Minjiang Rivers, Fujian province of China)	NR_040795.1	1e-71	86%
ASV_8811	MG638459.1	7e-86	99%	Marine sediment (Aarhus Bay Site M5, Denmark)	No Match	No Match	No Match

Table S5. Chemical composition of Spectrum 2 (filament) and Spectrum 3 (chimney surface) shown in **Figure S4**. Results include weight percent (Wt%), standard deviation (Wt% Sigma) and atomic percent (Atomic%) for each detected element.

Element	Spectrum 2: Filament			Spectrum 3: Chimney surface		
	Wt%	Wt% Sigma	Atomic%	Wt%	Wt% Sigma	Atomic%
O	41.98	0.37	48.43	45.42	0.39	51.07
C	21.11	0.59	32.44	20.23	0.59	30.3
Fe	15.08	0.15	4.98	9.18	0.11	2.96
Si	7.52	0.08	4.94	11.5	0.11	7.37
Na	4.58	0.08	3.67	2.42	0.06	1.89
Cl	3.13	0.04	1.63	0.36	0.02	0.18
Al	2.01	0.04	1.37	4.17	0.06	2.78
Ca	1.78	0.04	0.82	3.08	0.04	1.38
Mg	1.57	0.04	1.19	1.76	0.04	1.3
Ti	0.58	0.03	0.22	1.16	0.04	0.44
K	0.53	0.03	0.25	0.73	0.03	0.34
Mn	0.14	0.04	0.05	–	–	–
Total	100	–	100	100	–	100

References

Álvarez-Valero, A. M., Sánchez-Guillamón, O., Navarro, I., Albert, H., Sánchez, A. P., Rodríguez, J. A. L., et al. (2023). "From Magma Source to Volcanic Sink Under Tagoro Volcano (El Hierro, Canary Islands): Petrologic, Geochemical and Physiographic Evolution of the 2011–2012 Submarine Eruption," in El Hierro Island, ed. P. J. González (Cham: Springer International Publishing), 61–89. doi: 10.1007/978-3-031-35135-8_4

Barreyre, T., Escartín, J., Garcia, R., Cannat, M., Mittelstaedt, E., and Prados, R. (2012). Structure, temporal evolution, and heat flux estimates from the Lucky Strike deep-sea hydrothermal field derived from seafloor image mosaics. Geochemistry, Geophysics, Geosystems 13. doi: 10.1029/2011GC003990

Boden, R., Cunliffe, M., Scanlan, J., Moussard, H., Kits, K. D., Klotz, M. G., et al. (2011). Complete genome sequence of the aerobic marine methanotroph Methylomonas methanica MC09. J Bacteriol 193, 7001–7002. doi: 10.1128/JB.06267-11

Boetius, A., Ravenschlag, K., Schubert, C. J., Rickert, D., Widdel, F., Gieseke, A., et al. (2000). A marine microbial consortium apparently mediating anaerobic oxidation of methane. Nature 407, 623–626. doi: 10.1038/35036572

Bonnet, S., Guieu, C., Taillandier, V., Boulart, C., Bouruet-Aubertot, P., Gazeau, F., et al. (2023). Natural iron fertilization by shallow hydrothermal sources fuels diazotroph blooms in the ocean. Science 380, 812–817. doi: 10.1126/science.abq4654

Boyd, T. D., and Scott, S. D. (2001). Microbial and hydrothermal aspects of ferric oxyhydroxides and ferrosic hydroxides: the example of Franklin Seamount, Western Woodlark Basin, Papua New Guinea. Geochem. Trans. 2, 45–56. doi: 10.1039/B105277M

Buchan, A., González, J. M., and Moran, M. A. (2005). Overview of the Marine Roseobacter Lineage. Appl Environ Microbiol 71, 5665–5677. doi: 10.1128/AEM.71.10.5665-5677.2005

Buchan, A., LeCleir, G. R., Gulvik, C. A., and González, J. M. (2014). Master recyclers: features and functions of bacteria associated with phytoplankton blooms. Nat Rev Microbiol 12, 686–698. doi: 10.1038/nrmicro3326

Buck, N. J., Resing, J. A., Baker, E. T., and Lupton, J. E. (2018). Chemical Fluxes From a Recently Erupted Shallow Submarine Volcano on the Mariana Arc. Geochemistry, Geophysics, Geosystems 19, 1660–1673. doi: 10.1029/2018GC007470

Callahan, B. J., McMurdie, P. J., Rosen, M. J., Han, A. W., Johnson, A. J. A., and Holmes, S. P. (2016). DADA2: High-resolution sample inference from Illumina amplicon data. Nat Methods 13, 581–583. doi: 10.1038/nmeth.3869

Campbell, B., Polson, S., Zeigler Allen, L., Williamson, S., Lee, C., Wommack, K., et al. (2013). Diffuse flow environments within basalt- and sediment-based hydrothermal vent

ecosystems harbor specialized microbial communities. Frontiers in Microbiology 4. doi: 10.3389/fmicb.2013.00182

Caramanna, G., Sievert, S. M., and Bühring, S. I. (2021). Submarine Shallow-Water Fluid Emissions and Their Geomicrobiological Imprint: A Global Overview. Frontiers in Marine Science 8. doi: 10.3389/fmars.2021.727199

Chan, C. S., Fakra, S. C., Emerson, D., Fleming, E. J., and Edwards, K. J. (2011). Lithotrophic iron-oxidizing bacteria produce organic stalks to control mineral growth: implications for biosignature formation. ISME J 5, 717–727. doi: 10.1038/ismej.2010.173

Chan, C. S., McAllister, S. M., Leavitt, A. H., Glazer, B. T., Krepski, S. T., and Emerson, D. (2016). The Architecture of Iron Microbial Mats Reflects the Adaptation of Chemolithotrophic Iron Oxidation in Freshwater and Marine Environments. Front. Microbiol. 7. doi: 10.3389/fmicb.2016.00796

Chiu, B. K., Kato, S., McAllister, S. M., Field, E. K., and Chan, C. S. (2017). Novel Pelagic Iron-Oxidizing Zetaproteobacteria from the Chesapeake Bay Oxic–Anoxic Transition Zone. Front. Microbiol. 8. doi: 10.3389/fmicb.2017.01280

Danovaro, R., Canals, M., Tangherlini, M., Dell'Anno, A., Gambi, C., Lastras, G., et al. (2017). A submarine volcanic eruption leads to a novel microbial habitat. Nat Ecol Evol 1, 1–9. doi: 10.1038/s41559-017-0144

Danovaro, R., Levin, L. A., Fanelli, G., Scenna, L., and Corinaldesi, C. (2024). Microbes as marine habitat formers and ecosystem engineers. Nat Ecol Evol 8, 1407–1419. doi: 10.1038/s41559-024-02407-7

De Cáceres, M., and Legendre, P. (2009). Associations between species and groups of sites: indices and statistical inference. Ecology 90, 3566–3574. doi: 10.1890/08-1823.1

Dedysh, S. N., and Yilmaz, P. (2018). Refining the taxonomic structure of the phylum Acidobacteria. International Journal of Systematic and Evolutionary Microbiology 68, 3796–3806. doi: 10.1099/ijsem.0.003062

Dick, G. J. (2019). The microbiomes of deep-sea hydrothermal vents: distributed globally, shaped locally. Nat Rev Microbiol 17, 271–283. doi: 10.1038/s41579-019-0160-2

Dubilier, N., Bergin, C., and Lott, C. (2008). Symbiotic diversity in marine animals: the art of harnessing chemosynthesis. Nat Rev Microbiol 6, 725–740. doi: 10.1038/nrmicro1992

Emerson, D., and Moyer, C. L. (2002). Neutrophilic Fe-Oxidizing Bacteria Are Abundant at the Loihi Seamount Hydrothermal Vents and Play a Major Role in Fe Oxide Deposition. Applied and Environmental Microbiology 68, 3085–3093. doi: 10.1128/AEM.68.6.3085-3093.2002

Emerson, D., Rentz, J. A., Lilburn, T. G., Davis, R. E., Aldrich, H., Chan, C., et al. (2007). A Novel Lineage of Proteobacteria Involved in Formation of Marine Fe-Oxidizing Microbial Mat Communities. PLOS ONE 2, e667. doi: 10.1371/journal.pone.0000667

Fernández de Puelles, M. L., Gazá, M., Cabanellas-Reboredo, M., González-Vega, A., Herrera, I., Presas-Navarro, C., et al. (2021). Abundance and Structure of the Zooplankton Community During a Post-eruptive Process: The Case of the Submarine Volcano Tagoro (El Hierro; Canary Islands), 2013-2018. Frontiers in Marine Science 8, 923. doi: 10.3389/fmars.2021.692885

Ferrera, I., Arístegui, J., González, J. M., Montero, M. F., Fraile-Nuez, E., and Gasol, J. M. (2015). Transient Changes in Bacterioplankton Communities Induced by the Submarine Volcanic Eruption of El Hierro (Canary Islands). PLOS ONE 10, e0118136. doi: 10.1371/journal.pone.0118136

Fleming, E. J., Davis, R. E., McAllister, S. M., Chan, C. S., Moyer, C. L., Tebo, B. M., et al. (2013). Hidden in plain sight: discovery of sheath-forming, iron-oxidizing Zetaproteobacteria at Loihi Seamount, Hawaii, USA. FEMS Microbiology Ecology 85, 116–127. doi: 10.1111/1574-6941.12104

Fraile-Nuez, E., M. González-Dávila, J. M. Santana-Casiano, et al. (2012). "The Submarine Volcano Eruption at the Island of El Hierro: Physical-Chemical Perturbation and Biological Response." Scientific Reports 2. doi: 10.1038/srep00486

Fraile-Nuez, E., Santana-Casiano, J. M., González-Dávila, M., Vázquez, J. T., Fernández-Salas, L. M., Sánchez-Guillamón, O., et al. (2018). Cyclic Behavior Associated with the Degassing Process at the Shallow Submarine Volcano Tagoro, Canary Islands, Spain. Geosciences 8, 457. doi: 10.3390/geosciences8120457

Fraile-Nuez, E., Santana-Casiano, J. M., González-Dávila, M., González-Vega, A., Vázquez, J. T., Sotomayor-García, A., et al. (2023). "Ten Years of Intense Physical–Chemical, Geological and Biological Monitoring Over the Tagoro Submarine Volcano Marine Ecosystem (Eruptive and Degassing Stages)," in El Hierro Island, ed. P. J. González (Cham: Springer International Publishing). doi: 10.1007/978-3-031-35135-8_8

Fullerton, H., Smith, L., Enriquez, A., Butterfield, D., Wheat, C. G., and Moyer, C. L. (2024). Seafloor incubation experiments at deep-sea hydrothermal vents reveal distinct biogeographic signatures of autotrophic communities. FEMS Microbiology Ecology 100, fiae001. doi: 10.1093/femsec/fiae001

García-Davis, S., Reyes, C. P., Lagunes, I., Padrón, J. M., Fraile-Nuez, E., Fernández, J. J., et al. (2021). Bioprospecting Antiproliferative Marine Microbiota From Submarine Volcano Tagoro. Frontiers in Marine Science 8. doi: 10.3389/fmars.2021.687701

Giovannoni, S. J. (2017). SAR11 Bacteria: The Most Abundant Plankton in the Oceans. Annual Review of Marine Science 9, 231–255. doi: 10.1146/annurev-marine-010814-015934

Gomez-Saez, G. V., Pop Ristova, P., Sievert, S. M., Elvert, M., Hinrichs, K.-U., and Bühring, S. I. (2017). Relative Importance of Chemoautotrophy for Primary Production in a Light Exposed Marine Shallow Hydrothermal System. Front. Microbiol. 8. doi: 10.3389/fmicb.2017.00702

González, F. J., Rincón-Tomás, B., Somoza, L., Santofimia, E., Medialdea, T., Madureira, P., et al. (2020). Low-temperature, shallow-water hydrothermal vent mineralization

following the recent submarine eruption of Tagoro volcano (El Hierro, Canary Islands). Marine Geology 430, 106333. doi: 10.1016/j.margeo.2020.106333

González-Vega, A., Fraile-Nuez, E., Santana-Casiano, J. M., González-Dávila, M., Escánez-Pérez, J., Gómez-Ballesteros, M., et al. (2020). Significant Release of Dissolved Inorganic Nutrients From the Shallow Submarine Volcano Tagoro (Canary Islands) Based on Seven-Year Monitoring. Frontiers in Marine Science 6, 829. doi: 10.3389/fmars.2019.00829

Goris, T., and Diekert, G. (2016). "The Genus Sulfurospirillum," in Organohalide-Respiring Bacteria, eds. L. Adrian and F. E. Löffler (Berlin, Heidelberg: Springer), 209–234. doi: 10.1007/978-3-662-49875-0_10

Hager, K. W., Fullerton, H., Butterfield, D. A., and Moyer, C. L. (2017). Community Structure of Lithotrophically-Driven Hydrothermal Microbial Mats from the Mariana Arc and Back-Arc. Front. Microbiol. 8. doi: 10.3389/fmicb.2017.01578

Haouari, O., Fardeau, M.-L., Cayol, J.-L., Fauque, G., Casiot, C., Elbaz-Poulichet, F., et al. (2008). Thermodesulfovibrio hydrogeniphilus sp. nov., a new thermophilic sulphate-reducing bacterium isolated from a Tunisian hot spring. Systematic and Applied Microbiology 31, 38–42. doi: 10.1016/j.syapm.2007.12.002

Henry, E. A., Devereux, R., Maki, J. S., Gilmour, C. C., Woese, C. R., Mandelco, L., et al. (1994). Characterization of a new thermophilic sulfate-reducing bacterium. Arch. Microbiol. 161, 62–69. doi: 10.1007/BF00248894

Herrera, I., Fraile-Nuez, E., and González-Ortegón, E. (2024). Exploring marine zooplankton dynamics through carbon stable isotope signatures in a recently marine submarine volcano. Estuarine, Coastal and Shelf Science 310, 109005. doi: 10.1016/j.ecss.2024.109005

Hirayama, H., Fuse, H., Abe, M., Miyazaki, M., Nakamura, T., Nunoura, T., et al. (2013a). Methylomarinum vadi gen. nov., sp. nov., a methanotroph isolated from two distinct marine environments. International Journal of Systematic and Evolutionary Microbiology 63, 1073–1082. doi: 10.1099/ijs.0.040568-0

Hirayama, H., Fuse, H., Abe, M., Miyazaki, M., Nakamura, T., Nunoura, T., et al. (2013b). Methylomarinum vadi gen. nov., sp. nov., a methanotroph isolated from two distinct marine environments. International Journal of Systematic and Evolutionary Microbiology 63, 1073–1082. doi: 10.1099/ijs.0.040568-0

Huber, J. A., Butterfield, D. A., and Baross, J. A. (2003). Bacterial diversity in a subseafloor habitat following a deep-sea volcanic eruption. FEMS Microbiology Ecology 43, 393–409. doi: 10.1111/j.1574-6941.2003.tb01080.x

Imhoff, J. F. (2014). "The Family Chromatiaceae," in The Prokaryotes: Gammaproteobacteria, eds. E. Rosenberg, E. F. DeLong, S. Lory, E. Stackebrandt, and F. Thompson (Berlin, Heidelberg: Springer), 151–178. doi: 10.1007/978-3-642-38922-1_295

Izumi, H., Nunoura, T., Miyazaki, M., Mino, S., Toki, T., Takai, K., et al. (2012). Thermotomaculum hydrothermale gen. nov., sp. nov., a novel heterotrophic

thermophile within the phylum Acidobacteria from a deep-sea hydrothermal vent chimney in the Southern Okinawa Trough. Extremophiles 16, 245–253. doi: 10.1007/s00792-011-0425-9

Johannessen, K. C., Vander Roost, J., Dahle, H., Dundas, S. H., Pedersen, R. B., and Thorseth, I. H. (2017). Environmental controls on biomineralization and Fe-mound formation in a low-temperature hydrothermal system at the Jan Mayen Vent Fields. Geochimica et Cosmochimica Acta 202, 101–123. doi: 10.1016/j.gca.2016.12.016

Kassambara, A. (2020). ggpubr: "ggplot2" Based Publication Ready Plots. R package version 0.4.0. Available at: https://CRAN.R-project.org/package=ggpubr

Kassambara, A. (2021). rstatix: Pipe-Friendly Framework for Basic Statistical Tests. R package version 0.7.0. Available at: https://CRAN.R-project.org/package=rstatix

Kim, M., Cha, I.-T., Lee, K.-E., Lee, E.-Y., and Park, S.-J. (2020). Genomics Reveals the Metabolic Potential and Functions in the Redistribution of Dissolved Organic Matter in Marine Environments of the Genus Thalassotalea. Microorganisms 8, 1412. doi: 10.3390/microorganisms8091412

Kleindienst, S., Ramette, A., Amann, R., and Knittel, K. (2012). Distribution and in situ abundance of sulfate-reducing bacteria in diverse marine hydrocarbon seep sediments. Environmental Microbiology 14, 2689–2710. doi: 10.1111/j.1462-2920.2012.02832.x

Knittel, K., Boetius, A., Lemke, A., Eilers, H., Lochte, K., Pfannkuche, O., et al. (2003). Activity, distribution, and diversity of sulfate reducers and other bacteria in sediments above gas hydrate (Cascadia margin, Oregon). Geomicrobiology Journal 20, 269–294.

Könneke, M., Kuever, J., Galushko, A., and Jørgensen, B. B. (2013). Desulfoconvexum algidum gen. nov., sp. nov., a psychrophilic sulfate-reducing bacterium isolated from a permanently cold marine sediment. International Journal of Systematic and Evolutionary Microbiology 63, 959–964. doi: 10.1099/ijs.0.043703-0

Krepski, S. T., Emerson, D., Hredzak-Showalter, P. L., Luther III, G. W., and Chan, C. S. (2013). Morphology of biogenic iron oxides records microbial physiology and environmental conditions: toward interpreting iron microfossils. Geobiology 11, 457–471. doi: 10.1111/gbi.12043

Li, S.-H., Kang, I., and Cho, J.-C. (2023). Metabolic Versatility of the Family Halieaceae Revealed by the Genomics of Novel Cultured Isolates. Microbiol Spectr 11, e0387922. doi: 10.1128/spectrum.03879-22

Losey, N. A., Stevenson, B. S., Busse, H.-J., Damsté, J. S. S., Rijpstra, W. I. C., Rudd, S., et al. (2013). Thermoanaerobaculum aquaticum gen. nov., sp. nov., the first cultivated member of Acidobacteria subdivision 23, isolated from a hot spring. International Journal of Systematic and Evolutionary Microbiology 63, 4149–4157. doi: 10.1099/ijs.0.051425-0

Makita, H., Tanaka, E., Mitsunobu, S., Miyazaki, M., Nunoura, T., Uematsu, K., et al. (2017). Mariprofundus micogutta sp. nov., a novel iron-oxidizing zetaproteobacterium

isolated from a deep-sea hydrothermal field at the Bayonnaise knoll of the Izu-Ogasawara arc, and a description of Mariprofundales ord. nov. and Zetaproteobacteria classis nov. Arch Microbiol 199, 335–346. doi: 10.1007/s00203-016-1307-4

Martín-Díaz, J. P., González-Vega, A., Barreyre, T., Cornide, B., Arrieta, J. M., Vázquez, J.-T., et al. (2024). Unveiling the inherent physical-chemical dynamics: Direct measurements of hydrothermal fluid flow, heat, and nutrient outflow at the Tagoro submarine volcano (Canary Islands, Spain). Science of The Total Environment, 170565. doi: 10.1016/j.scitotenv.2024.170565

Mau, S., Tu, T.-H., Becker, M., dos Santos Ferreira, C., Chen, J.-N., Lin, L.-H., et al. (2020). Methane Seeps and Independent Methane Plumes in the South China Sea Offshore Taiwan. Front. Mar. Sci. 7. doi: 10.3389/fmars.2020.00543

McAllister, S. M., Moore, R. M., and Chan, C. S. (2018). ZetaHunter, a Reproducible Taxonomic Classification Tool for Tracking the Ecology of the Zetaproteobacteria and Other Poorly Resolved Taxa. Microbiol Resour Announc 7, e00932-18. doi: 10.1128/MRA.00932-18

McAllister, S. M., Moore, R. M., Gartman, A., Luther, G. W., III, Emerson, D., and Chan, C. S. (2019). The Fe(II)-oxidizing Zetaproteobacteria: historical, ecological and genomic perspectives. FEMS Microbiology Ecology 95, fiz015. doi: 10.1093/femsec/fiz015

McMurdie, P. J., and Holmes, S. (2013). phyloseq: An R Package for Reproducible Interactive Analysis and Graphics of Microbiome Census Data. PLOS ONE 8, e61217. doi: 10.1371/journal.pone.0061217

Nunoura, T., Hirai, M., Miyazaki, M., Kazama, H., Makita, H., Hirayama, H., et al. (2013). Isolation and characterization of a thermophilic, obligately anaerobic and heterotrophic marine Chloroflexi bacterium from a Chloroflexi-dominated microbial community associated with a Japanese shallow hydrothermal system, and proposal for Thermomarinilinea lacunofontalis gen. nov., sp. nov. Microbes Environ 28, 228–235. doi: 10.1264/jsme2.me12193

Ogiso, T., Ueno, C., Dianou, D., Huy, T. V., Katayama, A., Kimura, M., et al. (2012). Methylomonas koyamae sp. nov., a type I methane-oxidizing bacterium from floodwater of a rice paddy field. Int J Syst Evol Microbiol 62, 1832–1837. doi: 10.1099/ijs.0.035261-0

Payne, P. E., Knobbe, L. N., Chanton, P., Zaugg, J., Mortazavi, B., and Mason, O. U. (2024). Uncovering novel functions of the enigmatic, abundant, and active Anaerolineae in a salt marsh ecosystem. mSystems 10, e01162-24. doi: 10.1128/msystems.01162-24

Pérez-Barrancos, C., Fraile-Nuez, E., Martín-Díaz, J. P., González-Vega, A., Escánez-Pérez, J., Díaz-Durán, M. I., et al. (2025). Shallow Hydrothermal Fluids Shape Microbial Dynamics at the Tagoro Submarine Volcano (Canary Islands, Spain). Environmental Microbiology 27, e70052. doi: 10.1111/1462-2920.70052

Price, R. E., and Giovannelli, D. (2017). "A Review of the Geochemistry and Microbiology of Marine Shallow-Water Hydrothermal Vents," in Reference Module in Earth Systems and Environmental Sciences, (Elsevier). doi: 10.1016/B978-0-12-409548-9.09523-3

R Core Team (2021). R: A language and environment for statistical computing. R Foundation for Statistical Computing, Vienna, Austria. Available at: https://www.R-project.org/

Rinke, C., Schmitz-Esser, S., Stoecker, K., Nussbaumer, A. D., Molnár, D. A., Vanura, K., et al. (2006). "Candidatus Thiobios zoothamnicoli," an Ectosymbiotic Bacterium Covering the Giant Marine Ciliate Zoothamnium niveum. Applied and Environmental Microbiology 72, 2014–2021. doi: 10.1128/AEM.72.3.2014-2021.2006

Sambrook, J., and Russell, D. W. (2001). Molecular Cloning: A Laboratory Manual., 3rd Edn. Cold Spring Harbor Laboratory Press.

Santana-Casiano, J. M., Fraile-Nuez, E., González-Dávila, M., Baker, E. T., Resing, J. A., and Walker, S. L. (2016). Significant discharge of CO2 from hydrothermalism associated with the submarine volcano of El Hierro Island. Sci Rep 6, 25686. doi: 10.1038/srep25686

Santana-Casiano, J. M., González-Dávila, M., Fraile-Nuez, E., de Armas, D., González, A. G., Domínguez-Yanes, J. F., et al. (2013). The natural ocean acidification and fertilization event caused by the submarine eruption of El Hierro. Sci Rep 3, 1140. doi: 10.1038/srep01140

Santana-González, C., Santana-Casiano, J. M., González-Dávila, M., and Fraile-Nuez, E. (2017). Emissions of Fe(II) and its kinetic of oxidation at Tagoro submarine volcano, El Hierro. Marine Chemistry 195, 129–137. doi: 10.1016/j.marchem.2017.02.001

Santoro, A. E., Bayer, B., Elling, F. J., and Pearson, A. (2021). "Candidatus Nitrosopelagicus," in Bergey's Manual of Systematics of Archaea and Bacteria, (John Wiley & Sons, Ltd), 1–13. doi: 10.1002/9781118960608.gbm01969

Santoro, A. E., Dupont, C. L., Richter, R. A., Craig, M. T., Carini, P., McIlvin, M. R., et al. (2015). Genomic and proteomic characterization of "Candidatus Nitrosopelagicus brevis": An ammonia-oxidizing archaeon from the open ocean. Proceedings of the National Academy of Sciences 112, 1173–1178. doi: 10.1073/pnas.1416223112

Sayers, E. W., Beck, J., Bolton, E. E., Brister, J. R., Chan, J., Connor, R., et al. (2025). Database resources of the National Center for Biotechnology Information in 2025. Nucleic Acids Res 53, D20–D29. doi: 10.1093/nar/gkae979

Schliep, K. P. (2011). phangorn: phylogenetic analysis in R. Bioinformatics 27, 592–593. doi: 10.1093/bioinformatics/btq706

Schreiber, L., Holler, T., Knittel, K., Meyerdierks, A., and Amann, R. (2010). Identification of the dominant sulfate-reducing bacterial partner of anaerobic methanotrophs of the ANME-2 clade. Environmental Microbiology 12, 2327–2340. doi: 10.1111/j.1462-2920.2010.02275.x

Sekiguchi, Y., Muramatsu, M., Imachi, H., Narihiro, T., Ohashi, A., Harada, H., et al. (2008). Thermodesulfovibrio aggregans sp. nov. and Thermodesulfovibrio thiophilus sp. nov., anaerobic, thermophilic, sulfate-reducing bacteria isolated from thermophilic methanogenic sludge, and emended description of the genus Thermodesulfovibrio. International Journal of Systematic and Evolutionary Microbiology 58, 2541–2548. doi: 10.1099/ijs.0.2008/000893-0

Singer, E., Heidelberg, J., Dhillon, A., and Edwards, K. (2013). Metagenomic insights into the dominant Fe(II) oxidizing Zetaproteobacteria from an iron mat at Lō´ihi, Hawai´I. Frontiers in Microbiology 4. doi: 10.3389/fmicb.2013.00052

Sonne-Hansen, J., and Ahring, B. K. (1999). Thermodesulfobacterium hveragerdense sp.nov., and Thermodesulfovibrio islandicus sp.nov., Two Thermophilic Sulfate Reducing Bacteria Isolated from a Icelandic Hot Spring. Systematic and Applied Microbiology 22, 559–564. doi: 10.1016/S0723-2020(99)80009-5

Sotomayor-García, A., Rueda, J. L., Sánchez-Guillamón, O., Urra, J., Martín-Arjona, A., González-Porto, M., et al. (2023). "Impact of Tagoro Volcano Formation on Benthic Habitats and Associated Biota: A Review," in El Hierro Island, ed. P. J. González (Cham: Springer International Publishing), 217–239. doi: 10.1007/978-3-031-35135-8_11

Sotomayor-García, A., Rueda, J. L., Sánchez-Guillamón, O., Urra, J., Vázquez, J. T., Palomino, D., et al. (2019). First Macro-Colonizers and Survivors Around Tagoro Submarine Volcano, Canary Islands, Spain. Geosciences 9, 52. doi: 10.3390/geosciences9010052

Sotomayor-García, A., Rueda, J. L., Sánchez-Guillamón, O., Vázquez, J. T., Palomino, D., Fernández-Salas, L. M., et al. (2020). "Chapter 51 - Geomorphic features, main habitats and associated biota on and around the newly formed Tagoro submarine volcano, Canary Islands," in Seafloor Geomorphology as Benthic Habitat (Second Edition), eds. P. T. Harris and E. Baker (Elsevier), 835–846. doi: 10.1016/B978-0-12-814960-7.00051-8

Stackebrandt, E. (2014). "The Family Thermoanaerobacteraceae," in The Prokaryotes: Firmicutes and Tenericutes, eds. E. Rosenberg, E. F. DeLong, S. Lory, E. Stackebrandt, and F. Thompson (Berlin, Heidelberg: Springer), 413–419. doi: 10.1007/978-3-642-30120-9_367

Storesund, J. E., Lanzèn, A., García-Moyano, A., Reysenbach, A.-L., and Øvreås, L. (2018). Diversity patterns and isolation of Planctomycetes associated with metalliferous deposits from hydrothermal vent fields along the Valu Fa Ridge (SW Pacific). Antonie van Leeuwenhoek 111, 841–858. doi: 10.1007/s10482-018-1026-8

Suzuki, R., Terada, Y., and Shimodaira, H. (2019). pvclust: Hierarchical Clustering with P-Values via Multiscale Bootstrap Resampling. Available at: https://CRAN.R-project.org/package=pvclust

Tarasov, V. G., Gebruk, A. V., Mironov, A. N., and Moskalev, L. I. (2005). Deep-sea and shallow-water hydrothermal vent communities: Two different phenomena? Chemical Geology 224, 5–39. doi: 10.1016/j.chemgeo.2005.07.021

Tarasov, V. G., Gebruk, A. V., Shulkin, V. M., Kamenev, G. M., Fadeev, V. I., Kosmynin, V. N., et al. (1999). Effect of shallow-water hydrothermal venting on the biota of Matupi Harbour (Rabaul Caldera, New Britain Island, Papua New Guinea). Continental Shelf Research 19, 79–116. doi: 10.1016/S0278-4343(98)00073-9

Taylor, J. D., Cottingham, S. D., Billinge, J., and Cunliffe, M. (2014). Seasonal microbial community dynamics correlate with phytoplankton-derived polysaccharides in surface coastal waters. The ISME Journal 8, 245–248. doi: 10.1038/ismej.2013.178

Teeling, H., Fuchs, B. M., Becher, D., Klockow, C., Gardebrecht, A., Bennke, C. M., et al. (2012). Substrate-Controlled Succession of Marine Bacterioplankton Populations Induced by a Phytoplankton Bloom. Science 336, 608–611. doi: 10.1126/science.1218344

Teixeira, L. M., and Merquior, V. L. C. (2014). "The Family Moraxellaceae," in The Prokaryotes: Gammaproteobacteria, eds. E. Rosenberg, E. F. DeLong, S. Lory, E. Stackebrandt, and F. Thompson (Berlin, Heidelberg: Springer), 443–476. doi: 10.1007/978-3-642-38922-1_245

Tilliette, C., Gazeau, F., Portlock, G., Benavides, M., Bonnet, S., Guigue, C., et al. (2023). Influence of shallow hydrothermal fluid release on the functioning of phytoplankton communities. Frontiers in Marine Science 10. doi: 10.3389/fmars.2023.1082077

9/19/25 12:03:00 PMVander Roost, J., Thorseth, I. H., and Dahle, H. (2017). Microbial analysis of Zetaproteobacteria and co-colonizers of iron mats in the Troll Wall Vent Field, Arctic Mid-Ocean Ridge. PLOS ONE 12, e0185008. doi: 10.1371/journal.pone.0185008

Vázquez, J.-T., Sánchez Guillamón, O., Palomino, D., Fernández Salas, L. M., Bárcenas, P., Gómez-Ballesteros, M., et al. (2023). "Geomorphology of Tagoro Volcano Along Eruptive and Posteruptive Phases," in El Hierro Island, ed. P. J. González (Cham: Springer International Publishing), 131–158. doi: 10.1007/978-3-031-35135-8_7

Vigneron, A., Alsop, E. B., Cruaud, P., Philibert, G., King, B., Baksmaty, L., et al. (2017). Comparative metagenomics of hydrocarbon and methane seeps of the Gulf of Mexico. Sci Rep 7, 16015. doi: 10.1038/s41598-017-16375-5

Weinstein, M. M., Prem, A., Jin, M., Tang, S., and Bhasin, J. M. (2019). FIGARO: An efficient and objective tool for optimizing microbiome rRNA gene trimming parameters. 610394. doi: 10.1101/610394

Wickham, H., Averick, M., Bryan, J., Chang, W., McGowan, L., François, R., et al. (2019). Welcome to the Tidyverse. JOSS 4, 1686. doi: 10.21105/joss.01686

Wright, E. S. (2016). Using DECIPHER v2.0 to Analyze Big Biological Sequence Data in R. The R Journal 8, 352–359. doi: 10.32614/RJ-2016-025

Yarza, P., Yilmaz, P., Pruesse, E., Glöckner, F. O., Ludwig, W., Schleifer, K.-H., et al. (2014). Uniting the classification of cultured and uncultured bacteria and archaea using 16S rRNA gene sequences. Nat Rev Microbiol 12, 635–645. doi: 10.1038/nrmicro3330

Yu, G. (2020). Using ggtree to Visualize Data on Tree-Like Structures. Current Protocols in Bioinformatics 69, e96. doi: 10.1002/cpbi.96

Zeng, X., Alain, K., and Shao, Z. (2021). Microorganisms from deep-sea hydrothermal vents. Mar Life Sci Technol 3, 204–230. doi: 10.1007/s42995-020-00086-4

CHAPTER 5
CONCLUSIONS AND FUTURE PERSPECTIVES

5.1 General conclusions

This thesis set out to investigate how surface marine microbial communities respond to natural geochemical fertilization events in the subtropical Northeast Atlantic Ocean, focusing on two nutrient sources found in the region: Saharan dust deposition and shallow submarine hydrothermal emissions.

The two main hypotheses guiding this research were:

- Natural fertilization events, including Saharan dust deposition and shallow submarine hydrothermal activity, provide essential nutrients and trace elements to surface waters that can significantly enhance microbial productivity in marine ecosystems.
- These nutrient inputs promote distinct responses among microbial taxa, leading to changes in cell abundance, metabolic activity and community structure.

Throughout this work, a series of specific questions were addressed regarding the influence of these fertilization processes on microbial abundance and activity, microbial food-web dynamics, taxonomic shifts, and their broader implications for biogeochemical cycles and regional productivity. The outcomes of this research resulted in the following conclusions:

i. Experimental and observational evidence clearly demonstrated that both atmospheric dust deposition and submarine hydrothermal activity significantly influence the growth of microbial communities in the

subtropical Northeast Atlantic. These nutrient-enriched inputs consistently set off dynamic ecological cascades in microbial communities, shaping microbial diversity, community structure and metabolic activity, with important implications for surface productivity and ecosystem functioning.

ii. Dust deposition effects on surface microbial communities were strongest under nutrient-limited, oligotrophic conditions, where bacterial production rapidly increased more than primary production. These metabolic responses were primarily driven by the bioavailability of phosphorus and organic carbon, as well as by microbial competition following dust deposition. Future scenarios involving increased dust input and weakened upwelling in the Mauritanian-Senegalese region may favor a more heterotrophic microbial system, potentially reducing carbon sequestration efficiency through the biological carbon pump.

iii. Specific microbial taxa were favored by dust enrichment according to their nutrient requirements and ecological traits. Raphid-pennate diatoms, copiotrophic bacteria (e.g., *Hyphomonas* and *Alteromonas*) and smaller phytoplankton (picoeukaryotes and *Synechococcus*) particularly benefited from dust-derived nutrients, especially under oligotrophic conditions. This taxon-specific reorganization of microbial assemblages highlights the complexity of ecological interactions under changing nutrient regimes.

iv. Prokaryotic alpha diversity showed little response to dust addition, while eukaryotic alpha diversity significantly increased under low-nutrient conditions. However, alpha diversity was mainly modulated by the initial nutrient and productivity conditions.

v. Diffuse hydrothermal emissions at the Tagoro submarine volcano reached sunlit surface waters for the most part of the year and extended up to hundreds of meters from active vent sources. These inputs rich in phosphate and silicate notably stimulated phytoplankton biomass and growth, particularly among green algae and diatoms. This demonstrates that shallow hydrothermal systems can enhance local primary production in surface waters exposed to both nutrient enrichment and sunlight.

vi. In addition to phototrophic responses, hydrothermal activity supported the proliferation of heterotrophic and chemotrophic prokaryotes. The structure of surface microbial communities was further shaped by

complex trophic interactions, including parasitism (e.g., by Syndiniales dinoflagellates) and protistan grazing, which likely modulated nutrient cycling and carbon export. Our results emphasize the need to consider top-down and bottom-up controls in future assessments of oceanic responses to natural perturbations.

vii. Even though prokaryotic diversity decreased with proximity to vent sources, taxa involved in the active cycling of iron (Zetaproteobacteria), nitrogen (Nitrososphaeria), sulfur (Desulfobacterota) and methane (Methylomonadaceae) remained prevalent across pelagic and benthic habitats. The simultaneous presence of both chemo- and photoautotrophic populations reflects a unique combination of energy sources and ecological niches in shallow hydrothermal systems. Moreover, the presence of microbial groups linked to still uncharacterized energy sources like methane, together with the high abundance of novel and uncultured taxa observed at Tagoro, reveals a largely unexplored microbial niche with potential new metabolic functions. These findings underscore the ecological richness and complexity of shallow hydrothermal ecosystems, further supported by evidence of syntrophic microbial interactions and symbioses with benthic fauna.

viii. Altogether, this thesis demonstrates that both geochemical perturbations–Saharan dust deposition and shallow hydrothermal activity–shape microbial community dynamics and biogeochemical cycling in the subtropical Northeast Atlantic. While dust inputs predominantly affect oligotrophic surface waters by promoting heterotrophic activity (ii-iv), shallow hydrothermal emissions enhance primary production and sustain unique pelagic and benthic microbial assemblages (v-vii). These findings highlight the importance of considering the distinct characteristics of each nutrient source and their impacts to microbial ecology. Moreover, the combined results emphasize the need for further research into how microbial communities may respond to these natural fertilization processes in the context of a changing climate.

5.2 Future perspectives

This thesis advances our understanding of the response of microbial communities to natural geochemical perturbations–particularly dust deposition and shallow hydrothermal activity–in the subtropical Northeast Atlantic Ocean. Nonetheless, some of our findings raised new questions that require further research to fully comprehend the microbial processes and the biogeochemical impacts triggered by these external events.

Experimental bioassays have proven valuable for assessing short-term microbial responses to episodic fertilization events like dust deposition and hydrothermal emissions. Indeed, many previous studies have successfully employed bioassays to explore the effects of dust inputs on local surface microbial communities (e.g., Bonnet et al., 2005; Herut et al., 2005, 2016; Duarte et al., 2006; Ridame et al., 2011; Rahav et al., 2018) and of hydrothermal emissions (e.g., Bonnet et al. 2023; Tilliette et al. 2023). However, this thesis emphasized several methodological limitations that should be addressed. For instance, microbial responses to dust enrichment, particularly changes in cell abundance and metabolic activity, occurred rapidly within the first 24 hours (**Chapter 2**), indicating that future experiments would benefit from a more frequent and earlier sampling to fully capture microbial changes. Additionally, while bioassays are effective for assessing immediate microbial responses, they might miss long-term ecological processes.

Simulating natural inputs also carry intrinsic uncertainties when trying to mimic complex natural conditions. In dust deposition experiments, for example, estimates of deposition rates often rely on theoretical constants such as particle deposition velocities and atmospheric dust solubility in seawater, which may not adequately reflect local environmental variability. Physical parameters like temperature, salinity and pH, which influence the dissolution and bioavailability of both dust and hydrothermal inputs, vary locally and temporally due to dynamic ocean processes and thus should be taken into account. Similarly, assumptions such as homogenous seawater mixing or constant emission rates simplify the complex, heterogeneous nature of these processes. Despite these limitations, experimental studies remain useful complements to in situ field observations.

In that sense, the Tagoro submarine volcano represents an exceptional long-term dataset with high-resolution oceanographic and geochemical data that

strongly supports the experimental findings presented in this thesis. Since its eruption in 2011, its shallow hydrothermal system has been intensively monitored, especially by the Spanish Institute of Oceanography (IEO-CSIC), using high-precision physical and biochemical instrumentation deployed using ROVs, rosette samplers and seabed mooring systems (e.g., Fraile-Nuez et al., 2012, 2018, 2023; González-Vega et al., 2022; Martín-Díaz et al., 2024). This sustained effort has provided a detailed physical and geochemical characterization of an active venting area covering approximately 7600 m^2 and comprising thousands of diverse hydrothermal vents (Martín-Díaz et al., 2024). Most chemical characterizations have focused on identifying the composition of hydrothermal emissions (Santana-Casiano et al., 2013, 2016, 2017; Santana-González et al., 2017; González-Vega et al., 2020), revealing that nutrient fluxes from Tagoro are comparable in magnitude to major regional inputs like the NW-African upwelling. Importantly, our microbial data revealed that biological observations can help resolve uncertainties in geochemical processes. For example, chemical studies have suggested that nitrogen is predominantly released as ammonium and subsequently transformed into nitrate and nitrite (González-Vega et al., 2020). This is now supported by our detection of persistent ammonia-oxidizing microbes in benthic habitats of Tagoro (**Chapter 4**). Likewise, evidence of biomineralization and geomicrobiological interactions documented in **Chapter 4** demonstrate the critical role microbes play in shaping the chemical environment. Expanding microbial observations in hydrothermal systems like Tagoro will thus be essential to better constrain key chemical dynamics that remain unresolved.

Despite the advances, several important chemicals with direct microbial relevance, such as methane and reduced iron and sulfur, remain understudied or only partially characterized at Tagoro (Santana-Casiano et al., 2013; Santana-González et al., 2017). However, microbial analyses indicated active microbial cycling of these compounds in benthic habitats (**Chapters 3 and 4**). While sulfur has been detected in vent fluids (Santana-Casiano et al., 2013), specific species like thiosulfate or sulfide have yet to be resolved. Future work employing iodometric titration or photometric methods (Volkov and Kokryatskaya, 2004; Reyna Robelo, 2023) could better characterize sulfur pools and link them to microbial metabolic pathways. Methane also appears to be relevant for local microbial activity at Tagoro (**Chapter 4**), yet direct measurements of its concentrations and isotopic signatures are still lacking. Methane could be quantified using gas chromatography (GC) and isotope-ratio

mass spectrometry (IRMS) or monitored in real time with infrared (IR)-based sensors, which have been successfully applied to map hydrothermal plumes in the past (e.g., Schmidt et al., 2013; Preston et al., 2022). Such scientific instrumentation would be particularly valuable if active methane-release is confirmed at Tagoro.

Future research at Tagoro also should prioritize comprehensive studies of both prokaryotic and eukaryotic microbes. Although high-throughput sequencing has substantially improved our understanding of bacterial diversity, the diversity and ecological roles of eukaryotic microbes remain underexplored. In addition, approaches like metagenomics and metatranscriptomics are needed to elucidate the metabolic capabilities and active processes of microbial communities affected by either dust deposition or hydrothermal activity, complementing the taxonomic insights provided in **Chapters 2 to 4**.

Understanding the microbial interactions that regulate community responses also requires more attention. Our studies indicated that protistan grazing and parasitism, among others, exert significant top-down controls on microbial populations, influencing community composition and biogeochemical cycling (**Chapter 2 and 3**). In hydrothermal settings, parasitism may play a substantial but understudied role (Hu et al., 2021; Pérez-Barrancos et al., 2024). Similarly, during dust deposition events, these biotic interactions likely modulate microbial dynamics (Pitta et al., 2017).

Lastly, hydrothermally influenced environments harbor novel microbial assemblages with potential biotechnological applications (e.g., García-Davis et al., 2021) that remain largely undescribed (**Chapter 4**). The case of *Candidatus* Thiolava veneris, a filamentous organism discovered after the Tagoro eruption (Danovaro et al., 2017), illustrates the challenges of taxonomic identification in such systems. Despite its ecological relevance, its formal description remains pending due to the lack of cultured isolates, and the absence of a 16S rRNA gene in the partially assembled genome makes its taxonomic placement even more uncertain. This highlights the need for greater efforts in microbial taxonomy using complementary approaches, such as gene-targeted methods and cultivation techniques, to confirm the identity and function of novel taxa. Moreover, syntrophic relationships among microbes both in dust deposition and hydrothermally affected environments (**Chapter 2 to 4**) may influence ecosystem functioning. Future research integrating microbial ecology, physiology, and genomics will be key to uncover the ecological significance and

biotechnological potential of the novel microbial taxa inhabiting these unique environments. Protecting the vast diversity of marine microbes yet to be discovered requires ambitious conservation strategies and regulatory frameworks, such as the Kunming-Montreal Global Biodiversity Framework (GBF) and the Biodiversity Beyond National Jurisdiction Agreement (BBNJ), which aim to preserve large areas of the ocean. However, the rich and largely unexplored microbial diversity found in smaller, unique environments like the Tagoro submarine volcano stresses the need to implement conservation policies that also protect these smaller but ecologically significant environments.

References

Bonnet, S., Guieu, C., Chiaverini, J., Ras, J., and Stock, A. (2005). Effect of atmospheric nutrients on the autotrophic communities in a low nutrient, low chlorophyll system. Limnol. Oceanogr. 50, 1810–1819. doi: 10.4319/lo.2005.50.6.1810

Bonnet, S., C. Guieu, V. Taillandier, et al. 2023. "Natural Iron Fertilization by Shallow Hydrothermal Sources Fuels Diazotroph Blooms in the Ocean." Science 380: 812–817. doi: 10.1126/science.abq4654

Danovaro, R., Canals, M., Tangherlini, M., Dell'Anno, A., Gambi, C., Lastras, G., et al. (2017). A submarine volcanic eruption leads to a novel microbial habitat. Nat Ecol Evol 1, 1–9. doi: 10.1038/s41559-017-0144

Duarte, C. M., Dachs, J., Llabrés, M., Alonso-Laita, P., Gasol, J. M., Tovar-Sánchez, A., et al. (2006). Aerosol inputs enhance new production in the subtropical northeast Atlantic. J. Geophys. Res. 111. doi: 10.1029/2005JG000140

Fraile-Nuez, E., González-Dávila, M., Santana-Casiano, J. M., Arístegui, J., Alonso-González, I. J., Hernández-León, S., et al. (2012). The submarine volcano eruption at the island of El Hierro: physical-chemical perturbation and biological response. Sci Rep 2, 486. doi: 10.1038/srep00486

Fraile-Nuez, E., Santana-Casiano, J. M., González-Dávila, M., Vázquez, J. T., Fernández-Salas, L. M., Sánchez-Guillamón, O., et al. (2018). Cyclic Behavior Associated with the Degassing Process at the Shallow Submarine Volcano Tagoro, Canary Islands, Spain. Geosciences 8, 457. doi: 10.3390/geosciences8120457

Fraile-Nuez, E., Santana-Casiano, J. M., González-Dávila, M., González-Vega, A., Vázquez, J. T., Sotomayor-García, A., et al. (2023). "Ten Years of Intense Physical–Chemical, Geological and Biological Monitoring Over the Tagoro Submarine Volcano Marine Ecosystem (Eruptive and Degassing Stages)," in El Hierro Island, ed. P. J. González (Cham: Springer International Publishing). doi: 10.1007/978-3-031-35135-8_8

García-Davis, S., Reyes, C. P., Lagunes, I., Padrón, J. M., Fraile-Nuez, E., Fernández, J. J., et al. (2021). Bioprospecting Antiproliferative Marine Microbiota From Submarine Volcano Tagoro. Frontiers in Marine Science 8. doi: 10.3389/fmars.2021.687701

González-Vega, A., Fraile-Nuez, E., Santana-Casiano, J. M., González-Dávila, M., Escánez-Pérez, J., Gómez-Ballesteros, M., et al. (2020). Significant Release of Dissolved Inorganic Nutrients From the Shallow Submarine Volcano Tagoro (Canary Islands) Based on Seven-Year Monitoring. Frontiers in Marine Science 6, 829. doi: 10.3389/fmars.2019.00829

Herut, B., Rahav, E., Tsagaraki, T. M., Giannakourou, A., Tsiola, A., Psarra, S., et al. (2016). The Potential Impact of Saharan Dust and Polluted Aerosols on Microbial Populations in the East Mediterranean Sea, an Overview of a Mesocosm Experimental Approach. Front. Mar. Sci. 3. doi: 10.3389/fmars.2016.00226

Herut, B., Zohary, T., Krom, M. D., Mantoura, R. F. C., Pitta, P., Psarra, S., et al. (2005). Response of East Mediterranean surface water to Saharan dust: On-board microcosm experiment and field observations. Deep Sea Research Part II: Topical Studies in Oceanography 52, 3024–3040. doi: 10.1016/j.dsr2.2005.09.003

Hu, S. K., E. L. Herrera, A. R. Smith, et al. 2021. "Protistan Grazing Impacts Microbial Communities and Carbon Cycling at Deep-Sea Hydrothermal Vents." Proceedings of the National Academy of Sciences of the United States of America 118. doi: 10.1073/pnas.2102674118

Martín-Díaz, J. P., González-Vega, A., Barreyre, T., Cornide, B., Arrieta, J. M., Vázquez, J.-T., et al. (2024). Unveiling the inherent physical-chemical dynamics: Direct measurements of hydrothermal fluid flow, heat, and nutrient outflow at the Tagoro submarine volcano (Canary Islands, Spain). Science of The Total Environment, 170565. doi: 10.1016/j.scitotenv.2024.170565

Pérez-Barrancos, C., Fraile-Nuez, E., Martín-Díaz, J. P., González-Vega, A., Escánez-Pérez, J., Díaz-Durán, M. I., et al. (2025). Shallow Hydrothermal Fluids Shape Microbial Dynamics at the Tagoro Submarine Volcano (Canary Islands, Spain). Environmental Microbiology 27, e70052. doi: 10.1111/1462-2920.70052

Pitta, P., Kanakidou, M., Mihalopoulos, N., Christodoulaki, S., Dimitriou, P. D., Frangoulis, C., et al. (2017). Saharan Dust Deposition Effects on the Microbial Food Web in the Eastern Mediterranean: A Study Based on a Mesocosm Experiment. Front. Mar. Sci. 4, 117. doi: 10.3389/fmars.2017.00117

Preston, V., Flaspohler, G., Kapit, J., Pardis, W., Youngs, S., Martocello, D. E., et al. (2022). Discovering hydrothermalism from Afar: In Situ methane instrumentation and change-point detection for decision-making. Front. Earth Sci. 10. doi: 10.3389/feart.2022.984355

Rahav, E., Belkin, N., Paytan, A., and Herut, B. (2018). Phytoplankton and Bacterial Response to Desert Dust Deposition in the Coastal Waters of the Southeastern Mediterranean Sea: A Four-Year In Situ Survey. Atmosphere 9, 305. doi: 10.3390/atmos9080305

Reyna Robelo, M. J. (2023). Determinación de especies sulfuradas mediante titulación aplicado a procesos minero-metalúrgicos. Available at: http://www.ptolomeo.unam.mx:8080/xmlui/handle/RepoFi/18574.

Ridame, C., Le Moal, M., Guieu, C., Ternon, E., Biegala, I. C., L'Helguen, S., et al. (2011). Nutrient control of N2 fixation in the oligotrophic Mediterranean Sea and the impact of Saharan dust events. Biogeosciences 8, 2773–2783. doi: 10.5194/bg-8-2773-2011

Santana-Casiano, J. M., Fraile-Nuez, E., González-Dávila, M., Baker, E. T., Resing, J. A., and Walker, S. L. (2016). Significant discharge of CO2 from hydrothermalism associated with the submarine volcano of El Hierro Island. Sci Rep 6, 25686. doi: 10.1038/srep25686

Santana-Casiano, J. M., Fraile-Nuez, M. G.-D. and E., Santana-Casiano, J. M., and Fraile-Nuez, M. G.-D. and E. (2017). The Emissions of the Tagoro Submarine Volcano (Canary

Islands, Atlantic Ocean): Effects on the Physical and Chemical Properties of the Seawater. IntechOpen. doi: 10.5772/intechopen.70422

Santana-Casiano, J. M., González-Dávila, M., Fraile-Nuez, E., de Armas, D., González, A. G., Domínguez-Yanes, J. F., et al. (2013). The natural ocean acidification and fertilization event caused by the submarine eruption of El Hierro. Sci Rep 3, 1140. doi: 10.1038/srep01140

Santana-González, C., Santana-Casiano, J. M., González-Dávila, M., and Fraile-Nuez, E. (2017). Emissions of Fe(II) and its kinetic of oxidation at Tagoro submarine volcano, El Hierro. Marine Chemistry 195, 129–137. doi: 10.1016/j.marchem.2017.02.001

Schmidt, M., Linke, P., and Esser, D. (2013). Recent Development in IR Sensor Technology for Monitoring Subsea Methane Discharge. Marine Technology Society Journal 47, 27–36. doi: 10.4031/MTSJ.47.3.8

Tilliette, C., F. Gazeau, G. Portlock, et al. 2023. "Influence of Shallow Hydrothermal Fluid Release on the Functioning of Phytoplankton Communities." Frontiers in Marine Science 10: 1082077. doi: 10.3389/fmars.2023.1082077

Volkov, I. I., and Kokryatskaya, N. M. (2004). Compounds of Reduced Inorganic Sulfur in the Waters of the White Sea and the Northern Dvina Mouth. Water Resources 31, 423–430. doi: 10.1023/B:WARE.0000035682.21728.87

CHAPTER 6
RESUMEN

6.1 Introducción

6.1.1 Funciones microbianas en la productividad oceánica superficial

Los microorganismos se encuentran en todo el océano y constituyen uno de los componentes más abundantes y diversos de la vida marina (Sunagawa et al., 2015; Bar-On y Milo, 2019). Estos conjuntos microscópicos incluyen una amplia variedad de organismos, como bacterias, arqueas, protistas, hongos y virus, que en su conjunto representan aproximadamente el 68% de la biomasa marina total (Bar-On et al., 2018; Bar-On y Milo, 2019). La mayor parte de esta biomasa es planctónica, se transporta mediante las corrientes oceánicas y contribuye de manera significativa a procesos biogeoquímicos clave, como la fijación de carbono, la degradación de la materia orgánica y el ciclo de nutrientes. En conjunto, estos procesos favorecen la exportación y el secuestro a largo plazo de carbono en las aguas profundas del océano y en sus sedimentos mediante la bomba biológica, lo que repercute significativamente en el clima global.

En la capa superficial del océano iluminada por el sol, conocida como zona epipelágica (0–200 m), el fitoplancton actúa como principal productor primario, determinando la estructura y la productividad de los ecosistemas marinos. Este grupo diverso de organismos unicelulares fotosintéticos incluye tanto algas eucariotas (como dinoflagelados y diatomeas) como procariotas fotoautótrofas como las cianobacterias *Synechococcus* y *Prochlorococcus*. Aunque representa menos del 1% de la biomasa autótrofa total del planeta (Field et al.,

1998; Bar-On et al., 2018), el fitoplancton es responsable de cerca de la mitad de la producción primaria neta global, estimada en aproximadamente 50 Gt C $año^{-1}$ (Falkowski et al., 1998; Field et al., 1998). Su éxito ecológico se atribuye, en gran medida, al pequeño tamaño de sus células (~0,2–200 μm) y a su elevada relación superficie-volumen, que facilitan la absorción de nutrientes, especialmente en ambientes oligotróficos donde la disponibilidad de nutrientes es limitada (Litchman et al., 2010; Marañón, 2015; Hillebrand et al., 2022).

A través de la liberación de compuestos orgánicos y de la depredación ejercida por el zooplancton, el fitoplancton no solo sustenta los niveles tróficos superiores, sino que también alimenta la actividad de bacterias y arqueas heterótrofas (Azam et al., 1983; Ducklow et al., 2001; Pomeroy et al., 2015). Como productores primarios, impulsan el ciclo del carbono marino al convertir el CO_2 en biomasa mediante la fotosíntesis. Sin embargo, gran parte de este carbono fijado es rápidamente utilizado y reciclado por los consumidores microbianos. Los microorganismos heterótrofos desempeñan un papel clave en la degradación y remineralización de la materia orgánica, transformándola en componentes inorgánicos como carbono, nitrógeno y fósforo. Al utilizar la materia orgánica particulada y disuelta (POM y DOM, por sus siglas en inglés) como fuentes de energía y carbono (Azam y Malfatti, 2007; Buchan et al., 2014), estos microorganismos reciclan nutrientes esenciales que sustentan el crecimiento autótrofo en las capas superficiales del océano (Levitus et al., 1993) y mantienen la productividad en regiones con un aporte limitado de nutrientes nuevos. Además, parte de la materia orgánica se transforma en biomasa microbiana, que regresa a las redes tróficas marinas mediante procesos de predación (Azam et al., 1983; Kirchman, 1994). Esta vía trófica, conocida como el bucle microbiano (Pomeroy et al., 2015), desempeña un papel fundamental en las aguas epipelágicas, especialmente en ambientes oligotróficos, al retener la energía y los nutrientes en el océano superficial y sostener el funcionamiento general del ecosistema.

La diversidad microbiana marina abarca múltiples dominios de la vida e incluye miles de grupos taxonómicos con diversas estrategias metabólicas, funciones ecológicas y nichos ambientales. A pesar de los avances significativos en las técnicas de secuenciación y los esfuerzos de muestreo a escala global, una gran parte de esta diversidad microbiana sigue sin cultivarse ni describirse (Giovannoni y Stingl, 2005). Esta fracción no caracterizada contiene un enorme potencial ecológico y biotecnológico, incluyendo nuevas enzimas y compuestos bioactivos (Paoli et al., 2022). Las estimaciones más conservadoras indican que

sólo se ha identificado formalmente alrededor del 1% de los taxones procariotas marinos, suponiendo una diversidad total de aproximadamente $\sim 2 \times 10^6$ especies (Curtis et al., 2002). Sin embargo, estimaciones más recientes sugieren que la diversidad procariota en los océanos podría alcanzar $\sim 10^{10}$ especies (Lennon y Locey, 2020), lo que implica que las especies descritas representarían apenas el 0,0002% del total. No obstante, ambas estimaciones ponen de manifiesto el grado en que la vida microbiana ha sido subestimada o ignorada en evaluaciones globales de biodiversidad, especialmente en entornos extremos (Shu y Huang, 2022). Además, estudios taxonómicos más amplios indican que entre un tercio y dos tercios de todas las especies marinas permanecen sin describir (Appeltans et al., 2012). Por lo tanto, comprender la diversidad y función de los microorganismos marinos es esencial para evaluar las respuestas microbianas y la resistencia de los ecosistemas frente al cambio climático y las presiones antropogénicas (Doney et al., 2012).

6.1.2 La disponibilidad de nutrientes limita el crecimiento microbiano

El crecimiento microbiano y la productividad en el océano superficial están determinados por una compleja interacción de factores físicos, químicos y biológicos, como la disponibilidad de luz, la estratificación estacional, los pulsos de nutrientes, la competencia y las interacciones tróficas (Moreno y Martiny, 2018). Entre estos múltiples factores, la disponibilidad de nutrientes desempeña un papel central, ya que la mayoría de las aguas superficiales oceánicas presentan concentraciones limitadas de nitrógeno inorgánico, fósforo, hierro y/o silicio (Bristow et al., 2017).

Los microorganismos marinos requieren una amplia gama de elementos químicos para mantener el crecimiento y las funciones celulares (Arrigo, 2005; Moore et al., 2013; Bristow et al., 2017). Los macronutrientes, como el nitrógeno (N), el fósforo (P) y el silicio (Si), son necesarios en concentraciones relativamente altas, ya que son componentes estructurales fundamentales de proteínas, ácidos nucleicos y membranas celulares; por ejemplo, el silicio es esencial para la formación de las frústulas silíceas de las diatomeas. Por otra parte, los micronutrientes como el hierro (Fe), el cobalto (Co) y el zinc (Zn), aunque requeridos en menores concentraciones, son indispensables para funciones clave como la actividad enzimática, el transporte de electrones y la fotosíntesis. El hierro, en particular, actúa como cofactor en proteínas implicadas en la fijación del nitrógeno, la respiración y la transferencia de electrones.

La disponibilidad de estos nutrientes varía tanto espacial como temporalmente, generando importantes contrastes en la productividad de las regiones oceánicas superficiales. Un factor determinante de esta variabilidad es el equilibrio entre el suministro de nutrientes y la demanda biológica, lo cual se refleja en los requerimientos estequiométricos de las comunidades microbianas (Moore et al., 2013). Las proporciones elementales del plancton pueden variar considerablemente de la relación de Redfield (106C:16N:1P) (Redfield, 1934; Martiny et al., 2014; Moreno y Martiny, 2018), dependiendo del taxón y del entorno, lo que da lugar a distintos patrones de limitación de nutrientes. Según la Ley del Mínimo de Liebig, el crecimiento está condicionado por el nutriente disponible en menor proporción respecto a la demanda. No obstante, investigaciones recientes destacan la importancia de la co-limitación, en la que múltiples nutrientes limitan simultáneamente el crecimiento microbiano (Browning y Moore, 2023). Por ejemplo, el nitrógeno suele ser el principal factor limitante en gran parte del océano superficial de baja latitud y en los giros subtropicales estratificados, mientras que el hierro es más a menudo limitante en los principales sistemas de afloramiento oceánico. El fósforo, el silicio y otras vitaminas y micronutrientes también pueden co-limitar el crecimiento microbiano bajo condiciones ecológicas específicas. Además, Moreno y Martiny (2018) observaron que, en ambientes ricos en nutrientes, los rasgos fisiológicos de las comunidades planctónicas tienen una mayor influencia en su estequiometría, mientras que en giros oligotróficos dominan las interacciones biogeoquímicas a gran escala.

La producción primaria en aguas superficiales depende en gran medida del aporte de nutrientes a través de la mezcla vertical de aguas profundas ricas en nutrientes y mediante la remineralización de materia orgánica por microorganismos descomponedores. Sin embargo, los aportes externos de nutrientes son esenciales para sostener la productividad a largo plazo y el secuestro de carbono en el océano profundo (Bristow et al., 2017). El suministro externo de nutrientes como fósforo, hierro y silicio proviene principalmente de la deposición atmosférica y de los aportes costeros y fluviales. Mientras tanto, el nitrógeno también puede incorporarse biológicamente mediante la fijación microbiana del nitrógeno atmosférico. Aunque estos aportes alternativos han sido estudiados en menor detalle, desempeñan un papel relevante en la modulación de la productividad superficial, especialmente en regiones oceánicas dinámicas como el océano Atlántico Nororiental, donde los aportes externos como la deposición

atmosférica representan una fuente significativa de nutrientes (Jickells et al., 2016). En esta región, estudios emergentes también ponen de relieve la importancia de las emisiones volcánicas e hidrotermales submarinas como fuentes puntuales de nutrientes capaces de influir en la productividad en aguas superficiales (por ejemplo, Santana-Casiano et al., 2013; González-Vega et al., 2020). En conjunto, el ciclo de los nutrientes, a través de los reservorios atmosféricos, terrestres, oceánicos y bióticos, impulsa la producción biológica y determina la dinámica biogeoquímica del océano superficial (Arrigo, 2005). No obstante, comprender la relación entre los procesos microbianos y el ciclo de nutrientes sigue siendo uno de los principales retos en la biogeoquímica oceánica.

6.1.3 Posibles fuentes de nutrientes en el Océano Atlántico Nororiental subtropical: deposición de polvo atmosférico y actividad volcánica e hidrotermal

El océano Atlántico Nororiental subtropical constituye uno de los mayores receptores de polvo atmosférico a escala global. Debido a su proximidad a las extensas zonas áridas del norte de África, el océano Atlántico recibe aproximadamente el 43% de las 450 Tg año^{-1} de polvo atmosférico que es depositado en los océanos superficiales (Jickells, 2005). Transportados hacia el oeste por la capa de aire sahariano, principalmente desde el Sáhara y el Sahel (Prospero y Lamb, 2003; Jickells, 2005), estos aportes minerales suministran de fosfato, hierro y otros oligoelementos esenciales al océano superficial (Guieu et al., 2002; Jickells et al., 2016). Como se expuso anteriormente, estos nutrientes pueden influir en la productividad marina global al modular el crecimiento microbiano y las tasas de fijación de nitrógeno (Jickells y Moore, 2015), especialmente en aguas oligotróficas, donde el suministro de nutrientes es limitado (Mills et al., 2008; Moore et al., 2008).

Si bien la importancia del polvo sahariano en esta región es reconocida desde hace tiempo, estudios recientes han documentado aumentos sin precedentes tanto en la frecuencia como en la intensidad de los eventos de deposición de polvo sahariano. Entre 2020 y 2022, grandes cantidades de polvo fueron transportadas desde el noroeste de África hacia el Atlántico y Europa, con concentraciones de partículas que en algunos casos superaron los 6000 μm m^{-3} (Rodríguez y López-Darias, 2024). Comprender estas tendencias resulta fundamental en esta región, ya que las proyecciones climáticas anticipan una

expansión hacia el noroeste de las tierras áridas del norte de África, acompañada de un aumento en la carga de aerosoles minerales (Liu et al., 2024).

Estos eventos intensos de deposición de polvo son especialmente relevantes para los sistemas marinos, ya que pueden provocar incrementos a corto plazo de la productividad superficial y una mayor exportación vertical de partículas (Neuer et al., 2004). Sin embargo, la interpretación de las respuestas microbianas y biogeoquímicas en esta región sigue siendo un reto debido al elevado transporte lateral y a la variabilidad mesoescala, factores característicos de los ecosistemas de afloramiento del margen oriental (Chávez y Messié, 2009; Nowald et al., 2015).

Por otro lado, aproximadamente el 85% de la actividad volcánica mundial ocurre bajo la superficie oceánica (Crisp, 1984), de la cual cerca del ~75% está vinculada a sistemas de dorsales oceánicas medias. Aunque históricamente la mayoría de las investigaciones se han centrado en el hidrotermalismo situado en el océano profundo, el vulcanismo submarino poco profundo e intraplaca ha despertado recientemente un creciente interés científico (por ejemplo, Buck et al., 2018; Esposito et al., 2018; Bellec et al., 2020; Rizzo et al., 2022; Barosa et al., 2023). A diferencia de las fuentes hidrotermales de aguas profundas, que suelen encontrarse a profundidades de 1–4 km, las fuentes hidrotermales de aguas someras se producen a profundidades por encima de los ~200 m, lo que permite una interacción directa con la luz solar, las aguas superficiales y las comunidades microbianas superficiales (Price y Giovannelli, 2017). Estos entornos combinan la energía química de los compuestos reducidos con la disponibilidad de luz, lo que favorece la presencia de metabolismos microbianos tanto fototróficos como quimiotróficos (Tarasov et al., 2005; Price y Giovannelli, 2017). La emisión de macro- y micronutrientes biodisponibles, como amonio, silicato y hierro, desde fuentes hidrotermales someras hacia las aguas superficiales, puede estimular el crecimiento microbiano e influir en la estructura de la comunidad (por ejemplo, Ardyna et al., 2019; Bonnet et al., 2023; Tilliette et al., 2023).

El Atlántico Nororiental subtropical constituye como una región de creciente interés para el estudio del hidrotermalismo somero. Cadenas de islas volcánicas como las Islas Canarias y Cabo Verde, junto con miles de montes submarinos posiblemente aún no identificados (Gevorgian et al., 2023), sugieren un alto potencial de actividad hidrotermal submarina en esta cuenca. Un ejemplo destacado es la erupción submarina de 2011–2012 frente a la isla de El Hierro,

que originó el volcán submarino Tagoro y su sistema hidrotermal somero situado entre los 88 y 127 m de profundidad. Este entorno representa un laboratorio natural único para investigar los procesos hidrotermales someros y sus comunidades microbianas, las cuales probablemente albergan una gran diversidad de microorganismos con un alto valor ecológico y biotecnológico (p. ej., García-Davis et al., 2021; Rizzo et al., 2022).

6.2 Objetivos y estructura de la tesis

El objetivo de esta tesis es investigar la respuesta de las comunidades microbianas marinas superficiales, concretamente el fitoplancton y las bacterias, frente a eventos naturales de fertilización geoquímica en el Océano Atlántico Nororiental subtropical. En particular, se centra en los efectos de los aportes de nutrientes derivados de la deposición de polvo sahariano y de la actividad hidrotermal submarina somera sobre la ecología microbiana. Esta investigación se articula en torno a las siguientes hipótesis:

- Los eventos de fertilización natural, como la deposición de polvo sahariano y la actividad hidrotermal submarina poco profunda, proporcionan nutrientes esenciales y oligoelementos a las aguas superficiales que pueden aumentar significativamente la productividad microbiana en los ecosistemas marinos.
- Estos aportes de nutrientes promueven respuestas diferenciales entre los distintos grupos microbianos, dando lugar a variaciones en la abundancia celular, la actividad metabólica y la estructura de la comunidad.

Para evaluar el impacto ecológico de estos procesos de fertilización natural bajo condiciones oceanográficas variables y en el contexto del cambio climático, el enfoque experimental de la tesis abarca una serie de escenarios que reflejan la variabilidad natural del medio marino. Entre estos escenarios se contemplan las diferencias en la productividad superficial, patrones estacionales y variaciones en la magnitud y frecuencia de los eventos de deposición atmosférica y actividad hidrotermal.

A partir del marco general definido por las dos hipótesis principales, esta tesis pretende responder a las siguientes preguntas de investigación:

i. ¿Cómo afectan los aportes de nutrientes procedentes de la deposición de polvo y de la actividad hidrotermal a las comunidades microbianas

marinas superficiales en términos de abundancia celular y actividad metabólica?

ii. ¿En qué medida los gradientes tróficos o la variabilidad estacional modulan la producción microbiana?

iii. ¿Influyen estos aportes de nutrientes de manera diferenciada en los componentes autótrofos y heterótrofos de la red trófica microbiana?

iv. ¿Favorecen estos aportes el desarrollo de taxones microbianos específicos con funciones ecológicas y biogeoquímicas relevantes, alterando la diversidad microbiana de los hábitats?

v. ¿Pueden las respuestas microbianas observadas influir en los ciclos biogeoquímicos locales o regionales y en la productividad superficial?

Estas cuestiones se exploraron mediante una combinación de bioensayos experimentales y observaciones in situ, desarrolladas a lo largo de tres capítulos de investigación.

El **Capítulo 2** aborda las cuatro primeras preguntas de investigación analizando los efectos de la deposición de polvo sahariano en las comunidades microbianas superficiales de la zona costera de transición entre Mauritania y Senegal. Se realizaron experimentos de enriquecimiento con polvo a lo largo de un gradiente de productividad superficial con el fin de evaluar los cambios en la abundancia celular, las tasas metabólicas y la composición de la comunidad microbiana bajo diferentes condiciones ambientales. Asimismo, este capítulo incorpora un análisis de más de 20 años de seguimiento de la deposición de polvo atmosférico en las Islas Canarias (España), que incluye análisis de gravimetría, caracterización química y estudios de retrotrayectoria. Estos datos ofrecen un marco contextual más amplio para comprender el papel del polvo en la productividad microbiana y en los ciclos biogeoquímicos regionales, contribuyendo así también a responder la quinta pregunta de investigación.

> Este estudio dio lugar a la siguiente publicación:
> Pérez-Barrancos, C., Gelado-Caballero, M. D., Hernández-Hernández, N., Baños, I., Gómez-Letona, M., Montero, M. F., Arrieta, J.M., and Arístegui, J. (2022). *Uneven response of microbial communities to intense dust deposition across the coastal transition zone off Mauritania. Front. Mar. Sci.* 9, 999729. doi: 10.3389/fmars.2022.999729

Los **Capítulos 3 y 4** exploran la influencia de las emisiones hidrotermales difusas del volcán submarino Tagoro (Islas Canarias) sobre las comunidades

microbianas. Estos estudios integran más de una década de monitorización ambiental, desde la erupción de Tagoro en 2011 hasta su actual fase de desgasificación, proporcionando una visión integrada del alcance espacial y temporal de la influencia hidrotermal en la columna de agua y en los hábitats bentónicos adyacentes.

El **Capítulo 3** investiga la respuesta del fitoplancton y las bacterias en aguas superficiales mediante experimentos que simulan gradientes de dilución natural de fluidos hidrotermales. Se analizaron los cambios en abundancia celular, metabolismo y estructura de la comunidad, en conjunto con perfiles hidrográficos y concentraciones de silicato disuelto, un trazador de actividad hidrotermal en la región. Además, se consideró el posible efecto de la variación estacional en aguas superficiales integrando datos hidrográficos de la última década. Este capítulo contribuye principalmente a las preguntas i, ii, iii y v, y sienta las bases para la caracterización de la comunidad microbiana que se desarrolla con más detalle en el capítulo siguiente.

> Este estudio dio lugar a la siguiente publicación:
> Pérez-Barrancos, C., Fraile-Nuez, E., Martín-Díaz, J.P., González-Vega, A., Escánez-Pérez, J., Díaz-Durán, M.I., Presas-Navarro, C., Nieto-Cid, M., and Arrieta, J.M. (2025). *Shallow hydrothermal fluids shape microbial dynamics at the Tagoro submarine volcano (Canary Islands, Spain). Environmental Microbiology* 27, e70052. doi: 10.1111/1462-2920.70052

El **Capítulo 4** se centra en la identificación de los principales taxones procariotas que habitan los distintos hábitats hidrotermales del volcán Tagoro, tanto en ambientes pelágicos como bentónicos. En particular, se analizaron sus posibles contribuciones a los procesos biogeoquímicos locales. Este capítulo responde directamente las tres últimas preguntas de investigación.

Finalmente, el **Capítulo 5** sintetiza los principales resultados de la tesis y analiza sus implicaciones en un contexto más amplio, ofreciendo también perspectivas para futuras líneas de investigación.

En conjunto, esta tesis aporta una visión multidisciplinar sobre cómo distintos eventos de fertilización natural moldean las comunidades microbianas marinas y los procesos biogeoquímicos en una región oceánica climáticamente sensible y ecológicamente relevante como es el Océano Atlántico Nororiental subtropical.

6.3 Síntesis de resultados y conclusiones

Esta tesis se propuso investigar cómo responden las comunidades microbianas marinas superficiales a eventos naturales de fertilización geoquímica en el Océano Atlántico Nororiental subtropical, centrándose en dos fuentes de nutrientes que se encuentran en la región: la deposición de polvo sahariano y las emisiones hidrotermales submarinas poco profundas.

Las dos hipótesis principales que guiaron esta investigación fueron:

- Los eventos de fertilización natural, como la deposición de polvo sahariano y la actividad hidrotermal submarina poco profunda, proporcionan nutrientes esenciales y oligoelementos a las aguas superficiales que pueden aumentar significativamente la productividad microbiana en los ecosistemas marinos.
- Estos aportes de nutrientes promueven respuestas diferenciales entre los distintos grupos microbianos, dando lugar a variaciones en la abundancia celular, la actividad metabólica y la estructura de la comunidad.

A lo largo de este trabajo se abordaron varias cuestiones específicas relacionadas con la influencia de estos procesos de fertilización natural sobre la abundancia y actividad microbiana, la dinámica de las redes tróficas microbianas, los cambios taxonómicos y sus implicaciones más amplias en los ciclos biogeoquímicos y la productividad regional. Los resultados de esta investigación dieron lugar a las siguientes conclusiones:

i. Las evidencias experimentales y observacionales demuestran claramente que tanto la deposición de polvo atmosférico como la actividad hidrotermal submarina influyen significativamente en el crecimiento de las comunidades microbianas en el Atlántico Nororiental subtropical. Estos aportes enriquecidos en nutrientes desencadenan cascadas ecológicas dinámicas que configuran la diversidad microbiana, la estructura de la comunidad y la actividad metabólica, con importantes implicaciones para la productividad superficial y el funcionamiento del ecosistema.

ii. Los efectos de la deposición de polvo sobre las comunidades microbianas superficiales fueron más intensos en condiciones oligotróficas limitadas por nutrientes, donde la producción bacteriana

aumentó rápidamente, superando las tasas de producción primaria. Estas respuestas metabólicas se relacionaron principalmente con la biodisponibilidad de fósforo y carbono orgánico, así como la competencia entre microorganismos tras los eventos de deposición atmosférica. Escenarios futuros que impliquen un aumento en la entrada de polvo y un debilitamiento del afloramiento en la región Mauritano-Senegalesa podrían favorecer un sistema microbiano más heterótrofo, reduciendo potencialmente la eficiencia del secuestro de carbono mediante la bomba biológica.

iii. El enriquecimiento por polvo atmosférico favoreció a determinados taxones microbianos en función de sus necesidades nutricionales y rasgos ecológicos. Las diatomeas pennadas con rafe, las bacterias copiotróficas (p. ej., *Hyphomonas* y *Alteromonas*) y el fitoplancton más pequeño (picoeucariotas y *Synechococcus*) se beneficiaron especialmente de los nutrientes derivados del polvo, sobre todo en condiciones oligotróficas. Esta reorganización específica de los ensamblajes microbianos pone de manifiesto la complejidad de las interacciones ecológicas bajo regímenes cambiantes de nutrientes.

iv. La diversidad alfa procariota mostró poca respuesta a la adición de polvo, mientras que la diversidad alfa eucariota aumentó significativamente en condiciones de baja disponibilidad de nutrientes. No obstante, la diversidad alfa estuvo modulada principalmente por las condiciones iniciales de nutrientes y productividad.

v. Las emisiones hidrotermales difusas del volcán submarino Tagoro alcanzaron la zona fótica durante la mayor parte del año y se extendieron hasta cientos de metros desde las fuentes de emisión activas. Estos aportes, ricos en fosfato y silicato, estimularon notablemente la biomasa y el crecimiento del fitoplancton, en particular de algas verdes y diatomeas. Esto demuestra que los sistemas hidrotermales poco profundos pueden aumentar la producción primaria local en aguas superficiales expuestas tanto a la luz solar como al enriquecimiento en nutrientes de forma natural.

vi. Además de las respuestas fototróficas, la actividad hidrotermal favoreció la proliferación de procariotas heterótrofos y quimiotróficos. La estructura de las comunidades microbianas superficiales estuvo también condicionada por interacciones tróficas complejas, incluido el

parasitismo (p. ej., por dinoflagelados Syndiniales) y la depredación por protistas, que probablemente influyeron en el reciclaje de nutrientes y la exportación de carbono. Nuestros resultados subrayan la necesidad de considerar conjuntamente los controles ascendentes y descendentes en futuras evaluaciones de las respuestas oceánicas a perturbaciones naturales.

vii. Aunque la diversidad procariota disminuyó con la proximidad a las fuentes de emisión hidrotermal, taxones implicados en el ciclo activo del hierro (Zetaproteobacteria), nitrógeno (Nitrososphaeria), azufre (Desulfobacterota) y metano (Methylomonadaceae) prevalecieron en diversos hábitats pelágicos y bentónicos. La coexistencia de poblaciones quimio- y fotoautótrofas refleja una combinación singular de fuentes de energía y nichos ecológicos en los sistemas hidrotermales someros. Asimismo, la presencia de grupos microbianos asociados a fuentes de energía aún no caracterizadas como el metano, junto con la gran abundancia de taxones nuevos y no cultivados observados en Tagoro, revela un nicho microbiano en gran medida inexplorado, con posibles funciones metabólicas novedosas. Estos hallazgos subrayan la riqueza ecológica y la complejidad funcional de los ecosistemas hidrotermales someros, respaldadas además por evidencias de interacciones microbianas sintróficas y simbióticas con la fauna bentónica.

viii. En conjunto, esta tesis demuestra que ambas perturbaciones geoquímicas –la deposición de polvo sahariano y la actividad hidrotermal somera– influyen significativamente en la dinámica de las comunidades microbianas y en el ciclo biogeoquímico del Atlántico Nororiental subtropical. Mientras que los aportes de polvo atmosférico afectan predominantemente a las aguas superficiales oligotróficas promoviendo la actividad heterotrófica (ii-iv), las emisiones hidrotermales someras aumentan la producción primaria y sustentan conjuntos microbianos pelágicos y bentónicos únicos (v-vii). Estos resultados destacan la importancia de considerar las características distintivas de cada fuente de nutrientes y su impacto diferencial sobre la ecología microbiana. Además, subrayan la necesidad de continuar investigando cómo pueden responder las comunidades microbianas a estos procesos naturales de fertilización en el contexto de un clima cambiante.

6.4 Trabajo futuro

Esta tesis profundiza en la comprensión de las respuestas de las comunidades microbianas a perturbaciones geoquímicas naturales –en particular, la deposición de polvo y la actividad hidrotermal somera– en el Océano Atlántico Nororiental subtropical. No obstante, varios de nuestros hallazgos plantean nuevas cuestiones que requieren más investigación para comprender plenamente los procesos microbianos y los impactos biogeoquímicos desencadenados por estos fenómenos externos.

Los estudios experimentales han demostrado ser herramientas eficaces para evaluar las respuestas microbianas a corto plazo ante episodios de fertilización como los asociados a la deposición de polvo o a emisiones hidrotermales. De hecho, numerosos trabajos previos han empleado bioensayos para investigar los efectos de los aportes de polvo (p. ej., Bonnet et al., 2005; Herut et al., 2005, 2016; Duarte et al., 2006; Ridame et al., 2011; Rahav et al., 2018) y de las emisiones hidrotermales sobre comunidades microbianas superficiales (p. ej., Bonnet et al. 2023; Tilliette et al. 2023). Sin embargo, esta tesis también pone de relieve varias limitaciones metodológicas que es necesario abordar. Por ejemplo, en los experimentos con enriquecimiento por aportes de polvo (**Capítulo 2**), los cambios en abundancia celular y actividad metabólica ocurrieron rápidamente en las primeras 24 horas, lo que indica que futuros experimentos se beneficiarían de muestreos más frecuentes y tempranos para captar con mayor precisión la dinámica microbiana. Asimismo, aunque los estudios experimentales permiten explorar respuestas microbianas inmediatas, podrían subestimar procesos ecológicos de mayor escala temporal.

La simulación experimental de eventos naturales también conlleva incertidumbres intrínsecas cuando se intenta imitar entornos naturales complejos. En los experimentos de deposición de polvo, por ejemplo, las estimaciones de las tasas de deposición suelen basarse en constantes teóricas, como las velocidades de deposición de las partículas y la solubilidad del polvo atmosférico en el agua de mar, los cuales no siempre reflejan la variabilidad local. Factores físicos como la temperatura, la salinidad y el pH, que influyen en la disolución y biodisponibilidad tanto del polvo como de los aportes hidrotermales, varían espacial y temporalmente debido a los procesos oceánicos dinámicos en superficie, por lo que debe considerarse al interpretar los resultados. Del mismo modo, suposiciones como la mezcla homogénea del agua de mar o tasas constantes de emisión simplifican la naturaleza heterogénea

de estos procesos. A pesar de estas limitaciones, los estudios experimentales siguen siendo un complemento valioso a las observaciones in situ.

En este contexto, el volcán submarino Tagoro representa un caso excepcional, con un conjunto único de datos oceanográficos y geoquímicos de alta resolución, que refuerzan y contextualizan los resultados experimentales de esta tesis. Desde su erupción en 2011, el sistema hidrotermal somero de Tagoro ha sido intensamente monitorizado, principalmente por el Instituto Español de Oceanografía (IEO-CSIC), mediante instrumentación de alta precisión desplegada a través de ROVs, rosetas de muestreo y sistemas de fondeo (p. ej.., Fraile-Nuez et al., 2012, 2018, 2023; González-Vega et al., 2022; Martín-Díaz et al., 2024). Este esfuerzo sostenido ha permitido caracterizar detalladamente el área de emisión activa que cubre aproximadamente 7600 m^2, compuesta por centenares de fuentes hidrotermales (Martín-Díaz et al., 2024). Si bien gran parte de los estudios químicos se han centrado en identificar la composición de las emisiones hidrotermales (Santana-Casiano et al., 2013, 2016, 2017; Santana-González et al., 2017; González-Vega et al., 2020), los resultados muestran que los flujos de nutrientes de Tagoro son comparables en magnitud a los aportes del afloramiento costero del noroeste africano. Cabe destacar que nuestras observaciones microbiológicas han contribuido a reducir las incertidumbres asociadas a la interpretación de los procesos geoquímicos en Tagoro. Por ejemplo, estudios químicos previos propusieron que el nitrógeno se libera principalmente en forma de amonio, que posteriormente se transforma en nitrato y nitrito (González-Vega et al., 2020). Esta hipótesis se ve ahora respaldada por nuestra evidencia biológica, a partir de la detección de microorganismos oxidadores de amonio persistentes en los hábitats bentónicos de Tagoro (**Capítulo 4**). Asimismo, las observaciones de biomineralización y las interacciones geomicrobiológicas documentadas en el **Capítulo 4** demuestran el papel esencial de los microorganismos en la configuración del entorno geoquímico. Por tanto, una caracterización microbiológica más detallada será fundamental para restringir mejor los procesos químicos en sistemas hidrotermales como Tagoro.

A pesar de los avances, varios compuestos químicos con relevancia para la ecología microbiana, como el metano, y el hierro y azufre reducidos, permanecen escasamente caracterizados en Tagoro (Santana-Casiano et al., 2013; Santana-González et al., 2017). Mientras tanto, nuestros análisis microbianos indicaron una utilización microbiana de estos compuestos en hábitats bentónicos (**Capítulos 3 y 4**). Si bien se ha detectado la presencia de

azufre en los fluidos hidrotermales de Tagoro (Santana-Casiano et al., 2013), especies específicas como el tiosulfato o el sulfuro aún no se han cuantificado. Métodos analíticos como la valoración yodométrica o fotométrica (Volkov y Kokryatskaya, 2004; Reyna Robelo, 2023) podrían utilizarse en futuros estudios para mejorar la caracterización de esta reserva de azufre y asociarlas a rutas metabólicas microbianas. En cuanto al metano, su papel en la actividad microbiana bentónica de Tagoro parece ser relevante (**Capítulo 4**), aunque todavía faltan mediciones directas de sus concentraciones y su fracción isotópica. Herramientas como la cromatografía de gases (GC), la espectrometría de masas de relación isotópica (IRMS) o sensores infrarrojos (IR) de detección in situ (p. ej., Schmidt et al., 2013; Preston et al., 2022), podrían ser claves para confirmar la emisión activa de metano en Tagoro.

También se requieren esfuerzos adicionales para describir en mayor detalle la diversidad y funciones de los microorganismos procariotas y eucariotas. Aunque la secuenciación masiva ha mejorado sustancialmente nuestra comprensión de la diversidad procariótica, el conocimiento sobre el grupo de eucariotas es aún limitado. En este sentido, técnicas como la metagenómica y la metatranscriptómica podrían proporcionar información valiosa sobre las capacidades metabólicas y los procesos activos de las comunidades microbianas afectadas tanto por la deposición de polvo atmosférico como por la actividad hidrotermal, complementando los conocimientos taxonómicos presentados en los **Capítulos 2 a 4**.

Otro aspecto que requiere mayor atención es el papel de las interacciones microbianas en la regulación de las respuestas comunitarias a eventos de fertilización natural. Los resultados de esta tesis sugieren que la depredación por protistas y el parasitismo, entre otros, ejercen controles importantes sobre las poblaciones microbianas, con implicaciones en la estructura de las comunidades y en los ciclos biogeoquímicos locales (**Capítulos 2 y 3**). En ambientes hidrotermales, el parasitismo podría tener un impacto ecológico relevante pero escasamente explorado (Hu et al., 2021; Pérez-Barrancos et al., 2024). Del mismo modo, durante los eventos de deposición de polvo, estas interacciones tróficas probablemente modulan la dinámica microbiana (Pitta et al., 2017).

Por último, los entornos influenciados por hidrotermalismo activo, albergan comunidades microbianas únicas con potenciales aplicaciones biotecnológicas (p. ej., García-Davis et al., 2021) que permanecen en gran parte inexploradas

(**Capítulo 4**). El caso de *Candidatus* Thiolava veneris, un organismo filamentoso descubierto tras la erupción del Tagoro (Danovaro et al., 2017), ejemplifica los retos de la identificación taxonómica en estos tipos de ecosistemas. A pesar de su presuntamente relevancia ecológica, su descripción formal sigue pendiente debido a la falta de cultivos aislados y la ausencia de un gen 16S rRNA en el genoma parcialmente ensamblado. Este tipo de limitaciones pone de relieve la necesidad de integrar métodos complementarios para confirmar la identidad y el papel ecológico de posibles nuevos taxones. Además, las relaciones sintróficas entre microorganismos que se establecen en entornos afectados por la deposición de polvo o el hidrotermalismo somero (**Capítulos 2 a 4**) pueden ser determinantes para el funcionamiento del ecosistema. Avanzar en el conocimiento de esta biodiversidad microbiana emergente, así como su potencial biotecnológico, requerirá estudios que integren análisis de ecología, fisiología y genómica microbiana. Asimismo, la conservación y protección de esta gran diversidad de microorganismos marinos aún por descubrir debe ser una prioridad científica y política. Si bien marcos globales como el Marco Mundial para la Biodiversidad (GBF) de Kunming-Montreal o el Acuerdo sobre la Biodiversidad fuera de las Jurisdicciones Nacionales (BBNJ) pretenden proteger grandes regiones oceánicas, es necesario estrategias de conservación y marcos normativos ambiciosos también en entornos singulares y localizados – como el volcán submarino Tagoro– dada su extraordinaria singularidad ecológica y su contribución al patrimonio microbiano global.

Referencias

Achterberg, E. P., Moore, C. M., Henson, S. A., Steigenberger, S., Stohl, A., Eckhardt, S., et al. (2013). Natural iron fertilization by the Eyjafjallajökull volcanic eruption. Geophysical Research Letters 40, 921–926. doi: 10.1002/grl.50221

Appeltans, W., Ahyong, S. T., Anderson, G., Angel, M. V., Artois, T., Bailly, N., et al. (2012). The Magnitude of Global Marine Species Diversity. Current Biology 22, 2189–2202. doi: 10.1016/j.cub.2012.09.036

Ardyna, M., Lacour, L., Sergi, S., d'Ovidio, F., Sallée, J.-B., Rembauville, M., et al. (2019). Hydrothermal vents trigger massive phytoplankton blooms in the Southern Ocean. Nat Commun 10, 2451. doi: 10.1038/s41467-019-09973-6

Arrigo, K. R. (2005). Marine microorganisms and global nutrient cycles. Nature 437, 349–355. doi: 10.1038/nature04159

Azam, F., Fenchel, T., Field, J. G., Gray, J. S., Meyer-Reil, L. A., and Thingstad, F. (1983). The Ecological Role of Water-Column Microbes in the Sea. Marine Ecology Progress Series 10, 257–263.

Azam, F., and Malfatti, F. (2007). Microbial structuring of marine ecosystems. Nat Rev Microbiol 5, 782–791. doi: 10.1038/nrmicro1747

Bar-On, Y. M., and Milo, R. (2019). The Biomass Composition of the Oceans: A Blueprint of Our Blue Planet. Cell 179, 1451–1454. doi: 10.1016/j.cell.2019.11.018

Bar-On, Y. M., Phillips, R., and Milo, R. (2018). The biomass distribution on Earth. Proceedings of the National Academy of Sciences 115, 6506–6511. doi: 10.1073/pnas.1711842115

Barosa, B., Ferrillo, A., Selci, M., Giardina, M., Bastianoni, A., Correggia, M., et al. (2023). Mapping the microbial diversity associated with different geochemical regimes in the shallow-water hydrothermal vents of the Aeolian archipelago, Italy. Front. Microbiol. 14. doi: 10.3389/fmicb.2023.1134114

Bellec, L., Cambon-Bonavita, M.-A., Durand, L., Aube, J., Gayet, N., Sandulli, R., et al. (2020). Microbial Communities of the Shallow-Water Hydrothermal Vent Near Naples, Italy, and Chemosynthetic Symbionts Associated With a Free-Living Marine Nematode. Front. Microbiol. 11. doi: 10.3389/fmicb.2020.02023

Bonnet, S., Guieu, C., Chiaverini, J., Ras, J., and Stock, A. (2005). Effect of atmospheric nutrients on the autotrophic communities in a low nutrient, low chlorophyll system. Limnol. Oceanogr. 50, 1810–1819. doi: 10.4319/lo.2005.50.6.1810

Bonnet, S., Benavides, M., Le Moigne, F. A. C., Camps, M., Torremocha, A., Grosso, O., et al. (2023). Diazotrophs are overlooked contributors to carbon and nitrogen export to the deep ocean. ISME J 17, 47–58. doi: 10.1038/s41396-022-01319-3

Bristow, L. A., Mohr, W., Ahmerkamp, S., and Kuypers, M. M. M. (2017). Nutrients that limit growth in the ocean. Current Biology 27, R474–R478. doi: 10.1016/j.cub.2017.03.030

Browning, T. J., Bouman, H. A., Henderson, G. M., Mather, T. A., Pyle, D. M., Schlosser, C., et al. (2014). Strong responses of Southern Ocean phytoplankton communities to volcanic ash. Geophysical Research Letters 41, 2851–2857. doi: 10.1002/2014GL059364

Browning, T. J., and Moore, C. M. (2023). Global analysis of ocean phytoplankton nutrient limitation reveals high prevalence of co-limitation. Nat Commun 14, 5014. doi: 10.1038/s41467-023-40774-0

Buchan, A., LeCleir, G. R., Gulvik, C. A., and González, J. M. (2014). Master recyclers: features and functions of bacteria associated with phytoplankton blooms. Nat Rev Microbiol 12, 686–698. doi: 10.1038/nrmicro3326

Buck, N. J., Resing, J. A., Baker, E. T., and Lupton, J. E. (2018). Chemical Fluxes From a Recently Erupted Shallow Submarine Volcano on the Mariana Arc. Geochemistry, Geophysics, Geosystems 19, 1660–1673. doi: 10.1029/2018GC007470

Chavez, F. P., and Messié, M. (2009). A comparison of Eastern Boundary Upwelling Ecosystems. Progress in Oceanography 83, 80–96. doi: 10.1016/j.pocean.2009.07.032

Crisp, J. A. (1984). Rates of magma emplacement and volcanic output. Journal of Volcanology and Geothermal Research 20, 177–211. doi: 10.1016/0377-0273(84)90039-8

Curtis, T. P., Sloan, W. T., and Scannell, J. W. (2002). Estimating prokaryotic diversity and its limits. Proceedings of the National Academy of Sciences 99, 10494–10499. doi: 10.1073/pnas.142680199

Danovaro, R., Canals, M., Tangherlini, M., Dell'Anno, A., Gambi, C., Lastras, G., et al. (2017). A submarine volcanic eruption leads to a novel microbial habitat. Nat Ecol Evol 1, 1–9. doi: 10.1038/s41559-017-0144

Doney, S. C., Ruckelshaus, M., Duffy, J. E., Barry, J. P., Chan, F., English, C. A., et al. (2012). Climate change impacts on marine ecosystems. Ann Rev Mar Sci 4, 11–37. doi: 10.1146/annurev-marine-041911-111611

Ducklow, H., Steinberg, D., and Buesseler, K. (2001). Upper Ocean Carbon Export and the Biological Pump. oceanog 14, 50–58. doi: 10.5670/oceanog.2001.06

Duarte, C. M., Dachs, J., Llabrés, M., Alonso-Laita, P., Gasol, J. M., Tovar-Sánchez, A., et al. (2006). Aerosol inputs enhance new production in the subtropical northeast Atlantic. J. Geophys. Res. 111. doi: 10.1029/2005JG000140

Esposito, V., Andaloro, F., Canese, S., Bortoluzzi, G., Bo, M., Bella, M. D., et al. (2018). Exceptional discovery of a shallow-water hydrothermal site in the SW area of Basiluzzo islet (Aeolian archipelago, South Tyrrhenian Sea): An environment to preserve. PLOS ONE 13, e0190710. doi: 10.1371/journal.pone.0190710

Falkowski, P. G., Barber, R. T., and Smetacek, V. (1998). Biogeochemical Controls and Feedbacks on Ocean Primary Production. Science 281, 200–206. doi: 10.1126/science.281.5374.200

Field, C. B., Behrenfeld, M. J., Randerson, J. T., and Falkowski, P. (1998). Primary Production of the Biosphere: Integrating Terrestrial and Oceanic Components. Science 281, 237–240. doi: 10.1126/science.281.5374.237

Fraile-Nuez, E., González-Dávila, M., Santana-Casiano, J. M., Arístegui, J., Alonso-González, I. J., Hernández-León, S., et al. (2012). The submarine volcano eruption at the island of El Hierro: physical-chemical perturbation and biological response. Sci Rep 2, 486. doi: 10.1038/srep00486

Fraile-Nuez, E., Santana-Casiano, J. M., González-Dávila, M., Vázquez, J. T., Fernández-Salas, L. M., Sánchez-Guillamón, O., et al. (2018). Cyclic Behavior Associated with the Degassing Process at the Shallow Submarine Volcano Tagoro, Canary Islands, Spain. Geosciences 8, 457. doi: 10.3390/geosciences8120457

Fraile-Nuez, E., Santana-Casiano, J. M., González-Dávila, M., González-Vega, A., Vázquez, J. T., Sotomayor-García, A., et al. (2023). "Ten Years of Intense Physical–Chemical, Geological and Biological Monitoring Over the Tagoro Submarine Volcano Marine Ecosystem (Eruptive and Degassing Stages)," in El Hierro Island, ed. P. J. González (Cham: Springer International Publishing). doi: 10.1007/978-3-031-35135-8_8

García-Davis, S., Reyes, C. P., Lagunes, I., Padrón, J. M., Fraile-Nuez, E., Fernández, J. J., et al. (2021). Bioprospecting Antiproliferative Marine Microbiota From Submarine Volcano Tagoro. Frontiers in Marine Science 8. Available at: https://www.frontiersin.org/articles/10.3389/fmars.2021.687701 (Accessed November 3, 2022).

Gevorgian, J., Sandwell, D. T., Yu, Y., Kim, S.-S., and Wessel, P. (2023). Global Distribution and Morphology of Small Seamounts. Earth and Space Science 10, e2022EA002331. doi: 10.1029/2022EA002331

Giovannoni, S. J., and Stingl, U. (2005). Molecular diversity and ecology of microbial plankton. Nature 437, 343–348. doi: 10.1038/nature04158

González-Vega, A., Fraile-Nuez, E., Santana-Casiano, J. M., González-Dávila, M., Escánez-Pérez, J., Gómez-Ballesteros, M., et al. (2020). Significant Release of Dissolved Inorganic Nutrients From the Shallow Submarine Volcano Tagoro (Canary Islands) Based on Seven-Year Monitoring. Frontiers in Marine Science 6, 829. doi: 10.3389/fmars.2019.00829

Guieu, C., Loÿe-Pilot, M.-D., Ridame, C., and Thomas, C. (2002). Chemical characterization of the Saharan dust end-member: Some biogeochemical implications for the western Mediterranean Sea. Journal of Geophysical Research: Atmospheres 107, ACH 5-1-ACH 5-11. doi: 10.1029/2001JD000582

Herut, B., Rahav, E., Tsagaraki, T. M., Giannakourou, A., Tsiola, A., Psarra, S., et al. (2016). The Potential Impact of Saharan Dust and Polluted Aerosols on Microbial Populations in the East Mediterranean Sea, an Overview of a Mesocosm Experimental Approach. Front. Mar. Sci. 3. doi: 10.3389/fmars.2016.00226

Herut, B., Zohary, T., Krom, M. D., Mantoura, R. F. C., Pitta, P., Psarra, S., et al. (2005). Response of East Mediterranean surface water to Saharan dust: On-board microcosm experiment and field observations. Deep Sea Research Part II: Topical Studies in Oceanography 52, 3024–3040. doi: 10.1016/j.dsr2.2005.09.003

Hillebrand, H., Acevedo-Trejos, E., Moorthi, S. D., Ryabov, A., Striebel, M., Thomas, P. K., et al. (2022). Cell size as driver and sentinel of phytoplankton community structure and functioning. Functional Ecology 36, 276–293. doi: 10.1111/1365-2435.13986

Hu, S. K., E. L. Herrera, A. R. Smith, et al. 2021. "Protistan Grazing Impacts Microbial Communities and Carbon Cycling at Deep-Sea Hydrothermal Vents." Proceedings of the National Academy of Sciences of the United States of America 118. doi: 10.1073/pnas.2102674118

Jickells, T. D. (2005). Global Iron Connections Between Desert Dust, Ocean Biogeochemistry, and Climate. Science 308, 67–71. doi: 10.1126/science.1105959

Jickells, T. D., Baker, A. R., and Chance, R. (2016). Atmospheric transport of trace elements and nutrients to the oceans. Phil. Trans. R. Soc. A 374, 20150286. doi: 10.1098/rsta.2015.0286

Jickells, T., and Moore, C. M. (2015). The Importance of Atmospheric Deposition for Ocean Productivity. Annual Review of Ecology, Evolution, and Systematics 46, 481–501. doi: 10.1146/annurev-ecolsys-112414-054118

Kirchman, D. L. (1994). The uptake of inorganic nutrients by heterotrophic bacteria. Microb Ecol 28, 255–271. doi: 10.1007/BF00166816

Lennon, J. T., and Locey, K. J. (2020). More support for Earth's massive microbiome. Biology Direct 15, 5. doi: 10.1186/s13062-020-00261-8

Levitus, S., Conkright, M. E., Reid, J. L., Najjar, R. G., and Mantyla, A. (1993). Distribution of nitrate, phosphate and silicate in the world oceans. Progress in Oceanography 31, 245–273. doi: 10.1016/0079-6611(93)90003-V

Litchman, E., de Tezanos Pinto, P., Klausmeier, C. A., Thomas, M. K., and Yoshiyama, K. (2010). Linking traits to species diversity and community structure in phytoplankton. Hydrobiologia 653, 15–28. doi: 10.1007/s10750-010-0341-5

Liu, J., Wang, X., Wu, D., Wei, H., Li, Y., and Ji, M. (2024). Historical footprints and future projections of global dust burden from bias-corrected CMIP6 models. npj Clim Atmos Sci 7, 1. doi: 10.1038/s41612-023-00550-9

Marañón, E. (2015). Cell size as a key determinant of phytoplankton metabolism and community structure. Ann Rev Mar Sci 7, 241–264. doi: 10.1146/annurev-marine-010814-015955

Martín-Díaz, J. P., González-Vega, A., Barreyre, T., Cornide, B., Arrieta, J. M., Vázquez, J.-T., et al. (2024). Unveiling the inherent physical-chemical dynamics: Direct measurements of hydrothermal fluid flow, heat, and nutrient outflow at the Tagoro

submarine volcano (Canary Islands, Spain). Science of The Total Environment, 170565. doi: 10.1016/j.scitotenv.2024.170565

Martiny, A. C., Vrugt, J. A., and Lomas, M. W. (2014). Concentrations and ratios of particulate organic carbon, nitrogen, and phosphorus in the global ocean. Sci Data 1, 140048. doi: 10.1038/sdata.2014.48

Mélançon, J., Levasseur, M., Lizotte, M., Delmelle, P., Cullen, J., Hamme, R. C., et al. (2014). Early response of the northeast subarctic Pacific plankton assemblage to volcanic ash fertilization. Limnology and Oceanography 59, 55–67. doi: 10.4319/lo.2014.59.1.0055

Mills, M. M., Moore, C. M., Langlois, R., Milne, A., Achterberg, E., Nachtigall, K., et al. (2008). Nitrogen and phosphorus co-limitation of bacterial productivity and growth in the oligotrophic subtropical North Atlantic. Limnol. Oceanogr. 53, 824–834. doi: 10.4319/lo.2008.53.2.0824

Moore, C. M., Mills, M. M., Arrigo, K. R., Berman-Frank, I., Bopp, L., Boyd, P. W., et al. (2013). Processes and patterns of oceanic nutrient limitation. Nature Geosci 6, 701–710. doi: 10.1038/ngeo1765

Moore, C. M., Mills, M. M., Langlois, R., Milne, A., Achterberg, E. P., La Roche, J., et al. (2008). Relative influence of nitrogen and phosphorous availability on phytoplankton physiology and productivity in the oligotrophic sub-tropical North Atlantic Ocean. Limnol. Oceanogr. 53, 291–305. doi: 10.4319/lo.2008.53.1.0291

Moreno, A. R., and Martiny, A. C. (2018). Ecological Stoichiometry of Ocean Plankton. Ann. Rev. Mar. Sci. 10, 43–69. doi: 10.1146/annurev-marine-121916-063126

Neuer, S., Torres-Padrón, M. E., Gelado-Caballero, M. D., Rueda, M. J., Hernández-Brito, J., Davenport, R., et al. (2004). Dust deposition pulses to the eastern subtropical North Atlantic gyre: Does ocean's biogeochemistry respond?: Dust deposition in the eastern subtropic. Global Biogeochem. Cycles 18, n/a-n/a. doi: 10.1029/2004GB002228

Nowald, N., Iversen, M. H., Fischer, G., Ratmeyer, V., and Wefer, G. (2015). Time series of in-situ particle properties and sediment trap fluxes in the coastal upwelling filament off Cape Blanc, Mauritania. Prog. Oceanogr. 137, 1–11. doi: 10.1016/j.pocean.2014.12.015

Paoli, L., Ruscheweyh, H.-J., Forneris, C. C., Hubrich, F., Kautsar, S., Bhushan, A., et al. (2022). Biosynthetic potential of the global ocean microbiome. Nature 607, 111–118. doi: 10.1038/s41586-022-04862-3

Pérez-Barrancos, C., Fraile-Nuez, E., Martín-Díaz, J. P., González-Vega, A., Escánez-Pérez, J., Díaz-Durán, M. I., et al. (2025). Shallow Hydrothermal Fluids Shape Microbial Dynamics at the Tagoro Submarine Volcano (Canary Islands, Spain). Environmental Microbiology 27, e70052. doi: 10.1111/1462-2920.70052

Pitta, P., Kanakidou, M., Mihalopoulos, N., Christodoulaki, S., Dimitriou, P. D., Frangoulis, C., et al. (2017). Saharan Dust Deposition Effects on the Microbial Food Web in the

Eastern Mediterranean: A Study Based on a Mesocosm Experiment. Front. Mar. Sci. 4, 117. doi: 10.3389/fmars.2017.00117

Pomeroy, L. R., Williams, P. J. leB, Azam, F., and Hobbie, J. E. (2015). The Microbial Loop. Oceanography 20, 28–33. doi: 10.5670/oceanog.2007.45

Preston, V., Flaspohler, G., Kapit, J., Pardis, W., Youngs, S., Martocello, D. E., et al. (2022). Discovering hydrothermalism from Afar: In Situ methane instrumentation and change-point detection for decision-making. Front. Earth Sci. 10. doi: 10.3389/feart.2022.984355

Price, R. E., and Giovannelli, D. (2017). "A Review of the Geochemistry and Microbiology of Marine Shallow-Water Hydrothermal Vents," in Reference Module in Earth Systems and Environmental Sciences, (Elsevier). doi: 10.1016/B978-0-12-409548-9.09523-3

Prospero, J. M., and Lamb, P. J. (2003). African Droughts and Dust Transport to the Caribbean: Climate Change Implications. Science 302, 1024–1027. doi: 10.1126/science.1089915

Rahav, E., Belkin, N., Paytan, A., and Herut, B. (2018). Phytoplankton and Bacterial Response to Desert Dust Deposition in the Coastal Waters of the Southeastern Mediterranean Sea: A Four-Year In Situ Survey. Atmosphere 9, 305. doi: 10.3390/atmos9080305

Redfield, A. C. (1934). On the Proportions of Organic Derivatives in Sea Water and Their Relation to the Composition of Plankton. James Johnstone Memorial Volume, University Press of Liverpool.

Reyna Robelo, M. J. (2023). Determinación de especies sulfuradas mediante titulación aplicado a procesos minero-metalúrgicos. Available at: http://www.ptolomeo.unam.mx:8080/xmlui/handle/RepoFi/18574.

Ridame, C., Le Moal, M., Guieu, C., Ternon, E., Biegala, I. C., L'Helguen, S., et al. (2011). Nutrient control of N2 fixation in the oligotrophic Mediterranean Sea and the impact of Saharan dust events. Biogeosciences 8, 2773–2783. doi: 10.5194/bg-8-2773-2011

Rizzo, C., Arcadi, E., Calogero, R., Sciutteri, V., Consoli, P., Esposito, V., et al. (2022). Ecological and Biotechnological Relevance of Mediterranean Hydrothermal Vent Systems. Minerals 12, 251. doi: 10.3390/min12020251

Rodríguez, S., and López-Darias, J. (2024). Extreme Saharan dust events expand northward over the Atlantic and Europe, prompting record-breaking PM10 and PM2.5 episodes. Atmospheric Chemistry and Physics 24, 12031–12053. doi: 10.5194/acp-24-12031-2024

Santana-Casiano, J. M., Fraile-Nuez, E., González-Dávila, M., Baker, E. T., Resing, J. A., and Walker, S. L. (2016). Significant discharge of CO2 from hydrothermalism associated with the submarine volcano of El Hierro Island. Sci Rep 6, 25686. doi: 10.1038/srep25686

Santana-Casiano, J. M., Fraile-Nuez, M. G.-D. and E., Santana-Casiano, J. M., and Fraile-Nuez, M. G.-D. and E. (2017). The Emissions of the Tagoro Submarine Volcano (Canary

Islands, Atlantic Ocean): Effects on the Physical and Chemical Properties of the Seawater. IntechOpen. doi: 10.5772/intechopen.70422

Santana-Casiano, J. M., González-Dávila, M., Fraile-Nuez, E., de Armas, D., González, A. G., Domínguez-Yanes, J. F., et al. (2013). The natural ocean acidification and fertilization event caused by the submarine eruption of El Hierro. Sci Rep 3, 1140. doi: 10.1038/srep01140

Santana-González, C., Santana-Casiano, J. M., González-Dávila, M., and Fraile-Nuez, E. (2017). Emissions of Fe(II) and its kinetic of oxidation at Tagoro submarine volcano, El Hierro. Marine Chemistry 195, 129–137. doi: 10.1016/j.marchem.2017.02.001

Schmidt, M., Linke, P., and Esser, D. (2013). Recent Development in IR Sensor Technology for Monitoring Subsea Methane Discharge. Marine Technology Society Journal 47, 27–36. doi: 10.4031/MTSJ.47.3.8

Shu, W.-S., and Huang, L.-N. (2022). Microbial diversity in extreme environments. Nat Rev Microbiol 20, 219–235. doi: 10.1038/s41579-021-00648-y

Sunagawa, S., Coelho, L. P., Chaffron, S., Kultima, J. R., Labadie, K., Salazar, G., et al. (2015). Structure and function of the global ocean microbiome. Science 348, 1261359. doi: 10.1126/science.1261359

Tarasov, V. G., Gebruk, A. V., Mironov, A. N., and Moskalev, L. I. (2005). Deep-sea and shallow-water hydrothermal vent communities: Two different phenomena? Chemical Geology 224, 5–39. doi: 10.1016/j.chemgeo.2005.07.021

Tilliette, C., Gazeau, F., Portlock, G., Benavides, M., Bonnet, S., Guigue, C., et al. (2023). Influence of shallow hydrothermal fluid release on the functioning of phytoplankton communities. Frontiers in Marine Science 10. doi: 10.3389/fmars.2023.1082077

Volkov, I. I., and Kokryatskaya, N. M. (2004). Compounds of Reduced Inorganic Sulfur in the Waters of the White Sea and the Northern Dvina Mouth. Water Resources 31, 423–430. doi: 10.1023/B:WARE.0000035682.21728.87

Data availability

Raw sequencing datasets produced during this thesis are available online in public repositories as detailed below:

Chapter 2

Raw 16S and 18S rRNA gene sequencing datasets are deposited in the Sequence Read Archive (SRA) at NCBI (https://www.ncbi.nlm.nih.gov/sra) under accession number PRJNA862364.

Chapter 3

Raw 16S and 18S rRNA gene sequencing raw datasets are deposited in the Sequence Read Archive (SRA) at NCBI (https://www.ncbi.nlm.nih.gov/sra) under accession number PRJNA1098582.

Chapter 4

Raw microbial sequencing data have not yet been published in a public repository.

BLAST results are temporarily available in the Shared Organizational Storage Service (SACO) of CSIC (https://saco.csic.es/s/sjqnLEb9zz89Ar5) until Chapter 4 and its corresponding Supplementary Material are published in a scientific journal.